Chiral Concepts in s-Block Metal Chemistry

Silvia Zaragoza Calero

A thesis submitted to the Department of Pure and Applied Chemistry, University of Strathclyde, in part fulfilment of the requirements for the degree of Doctor of Philosophy.

March 2016

A mi madre y mi hermana

Acknowledgements

Deciding to complete a PhD in a different country was not an easy choice but now, looking back to these three years that I have spent in Glasgow I am certain that it was the right one. I feel extremely glad that I met Charlie, John and Laia, as they have been an important support for throughout the whole process. I want to thank all those people that shared this time with me because everyone made an impact on my life somehow.

First and foremost, I would like to thank my supervisor Dr Charlie O'Hara for giving me the opportunity of undertaking this PhD. Thank you for always keeping the door open for me for anything I required whether it was advice or a simple a question. Most importantly thank you for trusting me as a scientist and for being a true friend. I really enjoyed working with you, especially when you moved next door. Thank you for allowing me to attend to the ICOMC conference in Japan and all the USIC conferences. There are not many people as nice as you so I have no words to say how lucky I feel for having you as a supervisor.

Secondly, I would like to thank Prof Robert Mulvey, Prof Eva Hevia and Dr Stuart Robertson for the useful suggestions about my project, which have been greatly appreciated. I would also like to thank Dr Alan Kennedy for solving my crystal structures. I also want to welcome to the two newest members of the group who were born during the time that I was writing this Thesis.

I want to thank Dr Javier Francos for his help during this project, solving my crystal structures and synthesising the magnesium derivatives. I also want to thank Dr Antonio Martínez for his help during the last part of my PhD.

Special thanks go to all my *beta*-lab mates, especially Marco, Andy, Sam, Tracy and Lewis. All of you made my experiments more enjoyable and I will miss my time in the lab with all of you.

I want to thank Laia for all those lunches and coffees together, these are moments that I am going to really miss. I will even miss the weekends at the

library! I am sad that we are living far away from each other but both we know what is like being apart from your dearest people and that there is always time to Skype.

I want to thank everybody that I have met in Scotland, Marco Amores, Mayte, Antonio, Maria Ángeles, Jenni, Sarah, Etienne, Ross, Emma, Ana, Alberto, Marina, Donna, Tobi, Ben, Elaine, Markus, Jan, Andoni, Jannie-Anne and Craig.

Quiero dar las gracias a mis amigos, especialmente a Mariah, Marta, Mónica, Adri, Pablo, Vichy, Iker, Jess, Bel, Jorge, Bea, Lois, Pepe, Ana Rodríguez, Pol, Pili, Andrea y Eva. Gracias por hacer que, aunque pase el tiempo y nos veamos poco, nada cambie. Y muchas gracias a Ana González-Rico por alegrarme este último año por sorpresa, por esos cheese & wine y afternoon teas de señoras. Espero que sigamos descubriendo nuevos países y postres juntas.

Quiero dar las gracias a mi madre y a mi hermana por apoyarme en mi decisión de hacer el doctorado a Escocia. Lauri, gracias por estar siempre ahí de una manera que sólo nosotras entendemos y que sólo se puede definir con ¡Hermanación! Me alegro de poder sumar a Jacobo y Guille a la familia. Todos habeis sido de gran ayuda en estos meses en los que he escrito la tesis.

I want to thank my Scottish family. Thanks to Jean for being always nice and kind and offering me more help than I could even ask for. Thanks to Robert for always being there to help me, for all those roll and sausages for breakfast and always making me laugh. Thanks to Thomas, terrible at choosing films but always nice and up for a great conversation. You have been a great support for me and I could not ask for a better family in law.

I want to thank John for his help during my PhD and the writing up of this thesis. Nobody knows better than you how hard and how good this time has been. You have always been there no matter what, both in Glasgow and Madrid, and I could not have done it without you. Thanks for doing anything that takes for making me happy and thank you for sharing your life with me. Looking forward to the next stage of our life.

March 2016

Abstract

Given the nature of the work undertaken in this project, this thesis will be divided into six chapters. The topics discussed within this thesis primarily focus on the study of chiral bimetallic complexes both from a synthetic and a structural approach.

The chemistry of magnesiate complexes will be covered in Chapters 1-3.

Chapter 1 focuses on the synthesis and characterisation of five different adducts of the synthetically important lithium *tris*(*n*-butyl)magnesiate $LiMg(^nBu)_3$ (**1**). Complex **1** has been co-complexed with different ligands to form the complexes $[(TMPDA)\cdot Li(\mu\text{-}^nBu)_2Mg(\mu\text{-}^nBu)]_2$ (**48**), $[(PMDETA)\cdot Li(\mu\text{-}^nBu)(^nBu)Mg(\mu\text{-}^nBu)]_2$ (**49**) $[\{(R,R)\text{-}TMCDA\}\cdot Li(\mu\text{-}^nBu)_2Mg(\mu\text{-}^nBu)]_2$ (**51**), $[(TMEDA)\cdot Li(\mu\text{-}^nBu)(\mu\text{-}O^nBu)Mg(^nBu)]_2$ (**52**) and $[[(dioxane)\cdot Li(\mu\text{-}^nBu)_2Mg(\mu\text{-}^nBu)]_2]_\infty$ (**56**)

In Chapter 2, the reactivity of lithium magnesiates complexes for the asymmetric deprotonation of prochiral ketones is studied. Homoleptic and heteroleptic lithium magnesiate bases have been evaluated and the results highlight that good conversions and enantioselectivities can be achieved when lithium amide LiPEA (lithium (+)-bis-(*R*)-1-phenylethylamide, Li-**57**) and a second organometallic reagent are combined.

The chemistry of chiral sodium magnesiates is studied in Chapter 3. Solid state and solution structural studies of complexes $[NaMg(PEA)_2{}^nBu]_\infty$ (**103**), $[TMEDA\cdot Na(PEA)_2Mg^nBu]$ (**104**) and inverse crown ether $[NaMg(PEA)_4O]$ (**105**) have been performed. Compounds **103** and **104** have also been tested as deprotonating reagents towards 4-*tert*-butylcyclohexanone.

Chapter 4 focuses on the synthesis of chiral homoleptic and heteroleptic lithium zincates and their applications in enantioselective addition reactions towards ketones. Two new lithium zincates have been fully characterised, $TMEDA\cdot Li(\mu\text{-}PEA)(\mu\text{-}Me)ZnMe$ (**147**) and $(R,R)\text{-}TMCDA\cdot Li(\mu\text{-}Me)_2ZnMe$ (**149**).

The alkyl addition to ketones with this monomer is successful although the enantiomeric excess is relatively low.

Chapter 5 describes the synthesis, characterization and reactivity studies of a series of mixed alkali-metal complexes: [LiNa(PEA)$_2$]$_2$ (**168**), [(THF)$_2$LiNaPEA$_2$] (**169**) and [LiK(PEA)$_2$]$_2$ (**170**). A preliminary study on the reactivity of these amides as initiators of the asymmetric rearrangement of epoxides has been performed.

Each chapter contains a self-contained experimental section where the synthesis and solution characterisation of the complexes are included. Chapter 6 summarises the synthetic procedures for starting materials, as well as a description of general experimental techniques.

Finally, an appendix with the crystallographic data for compounds synthesised in this work is included after Chapter 6.

Abbreviations

(*R,R*)-TMCDA	(*R,R*)-N,N,N',N'-tetramethylcyclohexane-1,2-diamine
°C	degrees Celsius
2D	Bidimensional
Å	Angstrom
BIPHEN	(*R*)-5,5',6,6'-Tetramethyl-3,3'-di-t-butyl-1,1'-biphenyl-2,2'-diol
Boc	*tert*-butyloxycarbonyl
br	Broad peak
C_6D_{12}	Deuterated cyclohexane
C_6D_6	Deuterated benzene
CCDC	Cambridge crystallographic database
CIP	Contacted ion pair
cyc	Cyclic
D	Diffusion coefficient
d	Doublet
D_8-THF	Deuterated tetrahydrofuran
D_8-tol	Deuterated toluene
DA	Diisopropylamide
DES	Deep eutectic solvents
DG	Directing group
DME	Dimethylether
DOSY	Diffusion ordered spectroscopy
e. e.	Enantiomeric excess
e. r.	Enantiomeric ratio
E^+	Electrophile
EQ	External Quench
EXSY	Exchange spectroscopy
FID	Flame Ionization Detector
FW	Molecular weight
HMDS	Bis(trimethylsilyl)amide
*i*Pr	Isopropyl
IQ	Internal Quench
kcal	Kilocalories
LIC-KOR	Alkyllithium/potassium alkoxide Superbase
LiPEA	Lithium (+)-bis((*R*)-1-phenylethyl)amide
LiTMP	Lithium 2,2,6,6-tetramethylpiperidide
Log	Logarithm
NaHMDS	Sodium bis(trimethylsilyl)amide
*n*Bu	*n*-Butyl
NMR	Nuclear magnetic resonance
PEA	(+)-bis((*R*)-1-phenylethyl)amide
PEA(H)	(+)-bis((*R*)-1-phenylethyl)amine

Ph	Phenyl
PhN	1-Phenylnaphthalene
PMDETA	N,N,N',N'',N''-pentamethyldiethylenetriamine
ppm	Parts per million
q	Quartet
r. t.	Ambient temperature
rac	Racemic
s	Singlet
SSIP	Solvent separated ion pair
t	Triplet
T	Temperature
^{t}Bu	tert-Butyl
THF	Tetrahydrofuran
TMEDA	N,N,N'N'-tetramethylethylenediamine
TMP	2,2,6,6-tetramethylpiperidide
TMPDA	N,N,N'N'-tetramethylpropanediamine
TMS	Trimethylsilyl
TPhN	1, 2, 3, 4-Tetraphenylnaphthalene

List of Numbered Compounds

1 Tri-*n*-butyllithium magnesiate

2 *N,N,N'N'*-tetramethylpropanediamine

3 *N,N,N',N'',N''*-pentamethyldiethylenetriamine

4 (*R,R*)-*N,N,N',N'*-tetramethylcyclohexane-1,2-diamine]

5 N,N,N',N'-tetramethylethylenediamine

6 1,4-dioxane

7 Phenyllithium

8 Diphenylmagnesium

9 Triphenyllithium magnesiate

10 Benzalacetophenone

11 cis-1,1,3-triphenylprop-2-en-1-olate

12 1,3,3-triphenylprop-2-en-1-olate

13 Lithium chloride

14 Alkylmagnesium chloride lithium chloride

15 Amidomagnesiumchloride lithium chloride

16 Di-n-butyl(isopropyl)lithium magnesiate

17 Methyl methacrylate

18 Acetophenone

19 2-phenylhexan-2-ol

20 3-hydroxy-1,3-diphenylpropan-1-one

21 1-phenylethanol

22 *n*-Butyllithium

23 *n*-Butylmagnesium chloride

24 Di-*n*-butylmagnesium

25 2,2'-dihydroxy- 1,l'-binaphthyl

26 2-iodoazulene

27 2-(2-thiophene)azulene

28 2-iododiazine

29 Lithium tri(quinolinyl)magnesiates

30 (*R,R*)-$\alpha,\alpha,\alpha,\alpha$-tetraphenyl-1,3-dioxolane-4,5- dimethanol

31 (*R*)-5,5',6,6'-Tetramethyl-3,3'-di-t-butyl-1,1'-biphenyl-2,2'-diol

32 3-fluoropyridine

33 [1,2,3]triazolo[1,5-a]pyridines

34 [(TMEDA)·Li(μ-Me)$_2$Mg(μ-Me)$_2$Li·(TMEDA)]

35 [(TMEDA·Li(μ–Ph)$_2$Mg(μ–Ph)]$_2$

36 [(TMEDA)$_2$Li]$^+$[Ph$_2$Mg(μ–Ph)]$^-$

37 [Li(TMEDA)$_2$]$^+$ [(TMEDA)Li(μ–benzyl)$_2$Mg(benzyl)]$^-$

38 [(TMEDA·Li(μ-C≡CPh)$_2$Mg(μ-C≡CPh)$_2$Li·(TMEDA)]

39 [(TMEDA·Li(μ–C≡CPh)$_2$Mg(μ–C≡CPh)]$_2$

40 (THF)Li(μ-iPr-C$_6$H$_5$)$_2$Mg(iPr-C$_6$H$_5$)

41 [(TMEDA)·Li(μ-CH$_2$SiMe$_3$)$_2$Mg(μ-CH$_2$SiMe$_3$)$_2$Li·(TMEDA)]

42 [(dioxane)·Li$_2$Mg$_2$(CH$_2$SiMe$_3$)$_6$]$_\infty$

43 (PMDETA)·Li(μ–CH$_2$SiMe$_3$)$_2$Mg(CH$_2$SiMe$_3$)

44 (dioxane)$_2$·LiMg(CH$_2$SiMe$_3$)$_3$

45 [{Mg$_3$(CH$_2$SiMe$_3$)$_6$$^+$(OR)}$^-$]

46 [(THF)·LiMg(CH$_2$SiMe$_3$)$_3$]$_\infty$

47 [{(TMEDA)Li}$_2$Mg(C$_4$H$_8$)$_2$]

48 [(TMPDA)·Li(μ-^{n}Bu)$_2$Mg(μ-^{n}Bu)$_2$

49 [(PMDETA)·Li(μ-^{n}Bu)(^{n}Bu)Mg(μ-^{n}Bu)]$_2$

50 [PMDETA·(^{n}BuLi)$_2$]$_2$

51 [((R,R)-TMCDA)·Li(μ-^{n}Bu)$_2$Mg(μ-^{n}Bu)]$_2$

52 [TMEDA·Li(μ-^{n}Bu)(μ-O^{n}Bu)Mg(^{n}Bu)]$_2$

53 $[NaMg(^nBu)_2(O^tBu)\cdot(TMEDA)]_2$

54 $[KMg(^nBu)_2(O^tBu)\cdot(TMEDA)]_2$

55 $[TMEDA\cdot LiMg^nBu_3]_x$

56 $[[(dioxane)\cdot Li(\mu-^nBu)_2Mg(\mu-^nBu)]_2]_\infty$

57 ((+)-Bis-[(*R*)-1-phenylethyl]amide

58 (Dimethylaminomethyl)ferrocene

59 (2-((dimethylamino)methyl) ferrocenyl)diphenylmethanol

60 (–)-Sparteine

61 7-oxabicyclo[4.1.0]heptanes

62 Cyclohex-2-enol

63 Lithium ((1*R*,2*S*)-1-oxido-1-phenylpropan-2-yl)amide

64 (1*R*,3*R*,5*S*)-3-(benzyloxy)-6-oxabicyclo [3.1.0]hexane

65 (1*R*,4*S*)-4-(benzyloxy)cyclopent-2-enol

66 (1*R*,3*R*,5*S*)-6-oxabicyclo[3.1.0]hexan-3-ylmethanol

67 (1*S*,4*R*)-4-(hydroxymethyl)cyclopent-2-enol

68 Tricarbonyl(alkyl ether)chromium

69 Tricarbonyl(1-trimethylsilyl-2-alkyl ether)chromium

70 N,N-Diisopropylferrocenecarboxamide

71 N,N-Diisopropyl-2-iodoferrocene carboxamide

72 N-trityl-N-(*R*)-1-phenylethylamide

73 Diisopropylamide

74 (1*R*)-8-methyl-8-azabicyclo[3.2.1]octan-3-one

75 (1*R*,2*S*)-2-((*R*)-hydroxy(phenyl)methyl)-8-methyl-8-azabicyclo[3.2.1]octan-3-one

76 4-*tert*-butylcyclohexanone

77 (*S*)-((4-(*tert*-butyl)cyclohex-1-en-1-yl)oxy)trimethylsilane

78 $[(R,R)\text{-TMCDA}\cdot LiMg(TMP)_2{}^nBu]$

79 2,2,6,6-tetramethylpiperidide

80 $(TMEDA)\cdot LiMg(PEA)_2{}^nBu$

81 $(PMDETA)LiZnMe_3$

82 $[(PMDETA)_2(Li_2Cl)]^+[ZnMe_3]^-$

83 4-(*tert*-butyl)-1-butylcyclohexanol

84 $(TMEDA)\cdot LiMg(PEA)^nBu_2$

85 Bis(2-(piperidin-1-yl)ethyl)amide

86 (*R*)-1-(piperidin-1-yl)-N-(2,2,2-trifluoroethyl)propan-2-amide

87 *tert*-Butyllithium

88 Di-*tert*-butylmagnesium

89 Dineopentylmagnesium

90 Diphenylmagnesium

91 Di(*p*-tolyl)magnesium

92 Di(trimethylsilylmethyl)magnesium

93 Cobalt bromide

94 Magnesium bromide

95 Zinc chloride

96 Dimethyl zinc

97 Di-*tert*-butylzinc

98 Triisobutylaluminium

99 Trimethylaluminium

100 Di(trimethylsilylmethyl)magnesium

101 Di(trimethylsilylmethyl)manganese

102 Tri-*n*-butylsodium magnesiate

103 $[Na(\mu\text{-PEA})_2Mg^nBu]_\infty$

104 [TMEDA]·Na(μ-PEA$_2$)Mg^{n}Bu

105 Na$_2$Mg$_2$(PEA)$_4$O

106 [(PMDETA·Na)$_2$MgPh$_4$]

107 Na$_2$[Mg(C≡C^{t}Bu)$_3$(TMEDA)$_2$]$_2$

108 Diazabicyclo(2,2,2)octane

109 [[Na$_2$(DABCO)$_3$(toluene)]$^{2+}$(MgBu$_4$)$^{2-}$]$_\infty$.

110 Benzophenone

111 Diphenylmethanol

112 1,1-diphenylpentan-1-ol

113 2,2'-dihydroxy-3,3',5,5'-tetra-*tert*-butyl-1,1'-diphenyl

114 L-lactide

115 Polylactic acid

116 Toluene

117 [(TMP)$_6$Na$_4$(2,5-Mg$_2$C$_7$H$_7$)]

118 [(TMP)$_6$Na$_4$(3,5-Mg$_2$C$_7$H$_7$)]

119 [(TMP)$_6$Na$_4$(1,4-Mg$_2$C$_6$H$_4$)]

120 Na$_4$Mg$_2$TMP$_6$^{n}Bu$_2$

121 NaMgTMP$_2$^{n}Bu

122 Na$_2$MgTMP$_3$^{n}Bu

123 Na$_4$Mg$_2$TMP$_6$^{n}Bu$_2$

124 [1,3-bis(2,6-diisopropylphenyl)imidazol-2-ylidene]

125 [{Na$_3$Mg(TMP)$_3$(IPr$_2^-$)}$_2$]

126 LiMg(HMDS)3

127 bis(trimethylsilyl)amide

128 [Li$_2$Mg$_2$(HMDS)4(O$_2$)$_x$(O)$_y$]

129 [Na$_2$Mg$_2$(HMDS)$_4$O]

130 [Na$_2$Mg$_2$(TMP)$_4$O]

131 NaMg(DA)$_3$

132 [Na$_2$Mg$_2$^{i}Pr$_4$(μ-H)$_2$·(tol)$_2$]

133 Bis(benzene)chromium

134 (TMEDA)·Na(μ-TMP)(μ-nBu)Mg(TMP)

135 (TMEDA)$_2$Na$_2$Mg$_2$TMP$_4$

136 (TMEDA)Na(TMP)(CH$_2$SiMe$_3$)Mg(TMP)

137 (TMEDA)$_2$Na$_2$Mg$_2$(C$_4$H$_2$)

138 ((−)-sparteine)Na(μ-TMP)(μ-^{n}Bu)MgTMP

139 (R,R)-TMCDA· Mg^{n}Bu(NaHMDS)$_2$

140 [(PMDETA)Na]$^+$[Mg(TMP)$_3$]$^-$

141 [(TMEDA)Na]$^+$[Mg(HMDS)$_3$]$^-$

142 [((R,R)-TMCDA)Na]$^+$[Mg(HMDS)$_3$]$^-$

143 *cis*-2,6-dimethylpiperidide

144 [Na(HMDS)$_2$Mg(^{n}Bu)]$_\infty$

145 (Et$_2$O)·NaMg{{N(SiMe$_3$)$_2$}$_2$^{t}Bu

146 (TMEDA)NaMg^{n}Bu$_3$

147 [TMEDA]·Li(μ-PEA)(μ-Me)ZnMe

148 [TMEDA]·Li(μ-PEA)(μ-Ph)Zn^{t}Bu

149 (R,R)-TMCDA·Li(μ-Me)$_2$ZnMe

150 (1R, 2S, 3R, 4S)-3-Dimethylamino-1, 7, 7-trimethylbyciclo[2, 2, 1]heptan-2-ol

151 (THF)Li(μ-TMP)Zn^{t}Bu$_2$

152 (PMDETA)·LiZn^{t}Bu$_3$

153 (TMEDA)NaZn(^{t}Bu)$_2$(TMP)

154 [(TMEDA)Na(μ-TMP)(μ-C$_4$H$_7$O)Zn(CH$_2$SiMe$_3$)]

155 [(TMEDA)·Li(μ-^{n}Bu)(μ-TMP)Zn(^{n}Bu)]

156 (Bis(2-methoxyethyl) ether)

157 [(PMDETA)Li(μ-Me)$_2$ZnMe]

158 [(diglyme)$_2$Li]$^+$[ZnMe$_3$]$^-$

159 (TMEDA)$_2$LiZnMe$_4$

160 TMEDA·NaZn(^{t}Bu)$_2${N(CH$_2$Ph)(CH(CH$_3$)Ph)}

161 (TMEDA)·LiZn(*cis*-DMP)^{t}Bu$_2$

162 2,2,2-Trifluoroacetophenone

163 2,2,2-trifluoro-1-phenylethanol

164 1-(Bis((*R*)-1-phenylethyl)amide)-2,2,2-trifluoro-1-phenylethanol

165 Propiophenone

166 2,2-dimethyl-1-phenylpropan-1-one

167 2-Methylcyclohexanone

168 [LiNaPEA$_2$]$_2$

169 [THF]$_2$LiNaPEA$_2$

170 [LiKPEA$_2$]$_2$

171 [Na$_4$(μ-HMDS)$_4$(μ$_4$-OH)]$^-$[Na$_2$(μ-HMDS){(−)-sparteine}$_2$]$^+$

172 [THF·LiPEA]$_2$

173 [LiK(HMDS)$_2$]

174 (PMDETA)·LiPEA

175 [PhC(NCH$_2$)N(H)Na·PMDETA]

176 [(PhK)$_4$(PhLi)(^{t}BuOLi)(THF)$_6$(C$_6$H$_6$)$_2$]

Papers Published

1. *Optimisation of a lithium magnesiate for use in the non-cryogenic asymmetric deprotonation of prochiral ketones*; Javier Francos, <u>Silvia Zaragoza-Calero</u> and Charles O'Hara, *Dalton Trans.*, 2014, **43**, 1408.

2. *Solid state and solution studies of lithium tris(n-butyl)magnesiates stabilised by Lewis donors*; <u>Silvia Zaragoza-Calero</u>, Javier Francos, Alan Kennedy and Charles O'Hara, *Dalton Trans.*, 2015, **44**, 7258.

Conference Presentations

1. *Chiral alkali-metal magnesiates: Structural elucidation and optimisation for the deprotonation of prochiral ketones*. Poster presentation at ICOMC 2014 conference in Sapporo, Japan, July 13th 2014. Poster presentation at the USIC 2015 conference, Edinburgh, 2nd July 2015.

2. *Chiral alkali-metal magnesiates: Structural elucidation and optimisation for the deprotonation of prochiral ketones*. Oral presentation at USIC 2014 conference in Glasgow, September 4th 2014. Oral presentation at the Inorganic and Analytical Section Postgraduate Talks in Glasgow, 11th June 2014.

3. *Structural diversity and utilisation of a series of mixed s-block-metal magnesiates*. Poster presentation at the USIC 2013 conference, Edinburgh, 25th July 2013.

Table of Contents

Chapter 1. Structural studies of homoleptic lithium magnesiates

1.1 Summary

Chapter 1 is focused on enhancing the existing structural knowledge of lithium magnesiates.

Five different adducts of the synthetically important lithium *tris*(*n*-butyl)magnesiate LiMg(^{n}Bu)$_3$ (**1**) have been synthesised and crystallographically characterised.

These complexes adopt a linear structure with general formula [(donor)Li(μ-^{n}Bu)$_2$Mg(μ-^{n}Bu)$_2$Mg(μ-^{n}Bu)$_2$Li(donor)] and they can be described as contacted ion pairs that dimerise through an additional C-Mg interaction. The tetrahedral magnesium atoms, with higher Lewis acidity, occupy the central positions while the lithium atoms are found in the periphery of the structure. The coordination sphere of the lithium atoms are completed by the neutral Lewis donor.

The nitrogen-donor ligands TMPDA (**2**, *N,N,N'N'*-tetramethylpropanediamine), PMDETA (**3**, *N,N,N',N'',N''*-pentamethyldiethylenetriamine), (*R,R*)-TMCDA (**4**, (*R,R*)-*N,N,N',N'*-tetramethylcyclohexane-1,2-diamine) and TMEDA (**5**, TMEDA=*N,N,N'N'*-tetramethylethylendiamine) have been employed, as well as the bidentate ether 1,4-dioxane (**6**).

Solution studies of these magnesiates have been performed in hydrocarbon solution. Monodimensional ^{1}H, ^{7}Li and ^{13}C NMR experiments of all the compounds are detailed in the experimental section. PMDETA-stabilised dimer has been studied by variable temperature and two-dimensional ^{1}H DOSY NMR spectroscopy.

1.2 Introduction

1.2.1 General features of alkali-metal magnesiates

The metalation reaction, i. e., the exchange of a C-H bond for a more reactive, hence more versatile C-Metal bond, is among the most common reactions performed in chemistry. At the turn of the millennium, heterobimetallic reagents have been employed to overcome some of the shortcomings of the traditionally utilised, monometallic reagents. These problems include low selectivity and the need for low temperatures to avoid decomposition (particularly for organolithium compounds[1]) or low reactivity (for diorganomagnesium[2, 3] or diorganozinc[4] compounds).

The combination of a (homo or heteroleptic) diorganomagnesium compound with an organoalkali-metal reagent produces a bimetallic entity. The magnesium centre formally accepts the anionic charge, as its Lewis acidity is greater than that of the alkali metal. This bimetallic mixture is known as *magnesiate*.

1.2.1.1 Synthesis of alkali-metal magnesiates

There are two main ways to synthesise alkyl alkali-metal magnesiates. The first one is by co-complexation, reacting together the organoalkali-metal reagent and the diorganomagnesium compound in 1:1 or 1:2 ratio. Another synthetic route is salt metathesis, reacting three or four equivalents of the alkyl alkali-metal with one equivalent of magnesium dihalide.

$$RM + R'_2Mg \longrightarrow MMgRR'_2 \quad \text{(co-complexation)}$$

$$3\,RM + MgX_2 \longrightarrow MMgR_3 + 2\,MX \quad \text{(salt metathesis)}$$
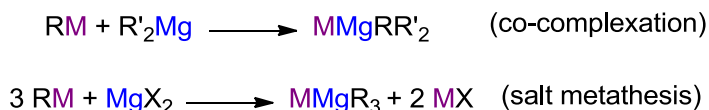
Scheme 1.1 Different pathways for the synthesis alkali-metal magnesiates.

Wittig synthesised the first magnesiate when he reacted together phenyllithium (**7**) and diphenylmagnesium (**8**) to produce **9** and employed the mixture in the addition across benzalacetophenone (**10**).[5] Surprisingly, the bimetallic mixture **9** afforded the 1,4-addition product, instead of the addition to the carbonylic carbon that would be expected if phenyllithium (**7**) was employed (**Scheme 1.2**).
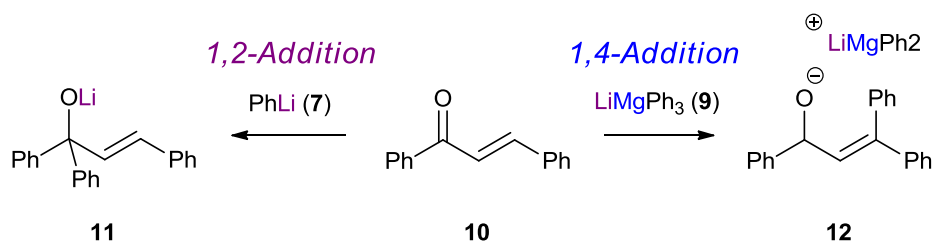
Scheme 1.2 Reaction of benzylacetophenone with PhLi (**7**) and LiMgPh$_3$ (**9**).

Although applications of magnesiates in the 20th century was limited to nucleophilic addition, in recent years interest has focused on halogen/magnesium exchange and deprotonation reactions.

A key player in these areas is Knochel whose work is based on heteroleptic halide alkyl (or amido) magnesiates complexes. He showed that the addition of one equivalent of lithium chloride (**13**) to a Grignard (alkylmagnesium halide) or Hauser (amidomagnesium halide) reagent could enhance their reactivities and selectivities in halogen-magnesium exchange or deprotonation reactions respectively. The lithium magnesiates with general formula RMgCl·LiCl (**14**), coined as "Turbo-Grignards", are useful reagents for inducing halogen-magnesium exchange in unactivated functionalised aryl and heteroaryl bromides in high yields, working at non-cryogenic temperatures with good functional group tolerance.[6-8] The amido containing (TMP)MgCl·LiCl (**15**), coined as a "Turbo-Hauser", is an efficient base for the hydrogen-magnesium exchange (i.e., deprotonation) of aromatic and heteroaromatic substrates.[9-14]

The great synthetic value of magnesiates can be judged by the fact that several reagents including LiMg^{n}Bu$_3$ (**1**) or LiMg^{n}Bu$_2$^{i}Pr (**16**) (as well as Turbo-Grignard and Turbo-Hauser compounds) are commercially available.

1.2.2 Reactivity of alkyllithium magnesiates

Alkyllithium magnesiates have been established as versatile reagents for many reactions.

They have been employed as initiators for the polymerisation of methyl methacrylate (**17**),[15] but they have more commonly been employed in:

nucleophilic addition, halogen-magnesium exchange and deprotonation reactions.

1.2.2.1 Nucleophilic addition

Although the use of lithium magnesiates as nucleophilic reagents is the less common,[5, 16-20] Wittig´s pioneering work showed the "synergic" properties of these bimetallic compounds during the nucleophilic addition of a lithium magnesiate to acetophenone (**18**) (**Scheme 1.2**).[5]

The addition of an organolithium, diorganomagnesium or alkyllithium magnesiate to acetophenone (**18**) was analysed by Ishihara and co-workers (**Scheme 1.3**).[19]
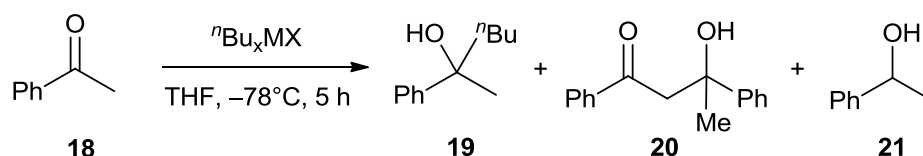
Scheme 1.3 Reactivity of acetophenone.

Table 1.1 Addition to acetophenone with lithium or magnesium reagents.

Complex	^nBu_xMX	Yield (%)		
		19	**20**	**21**
22	^nBuLi	62	7	0
23	^nBuMgCl	50	9	8
24	$^nBu_2Mg$	48	27	20
1	$LiMg^nBu_3$	82	0	0

n-BuLi (**22**) gave the corresponding alcohol (**19**) in 62% yield, but due to its high basicity, it is able to generate the enolate of the acetophenone and give the aldol product (**20**) in 7%. Grignard reagent *n*-BuMgCl (**23**) was similarly ineffective and gave (**19**) in 50% yield. The total conversion of the reaction increased when *n*-Bu₂Mg (**24**) was employed, but the selectivity of the reaction is low as the aldol product (**20**) and the reduction product (**21**) are

present in a 27% and 20% respectively. When the "ate" complex LiMg^{n}Bu$_3$ (**1**) was examined, the reaction gave (**19**) in a 82% yield with no undesired products. The combination of the monometallic species *n*-BuLi (**22**) and *n*-Bu$_2$Mg (**24**) in a 1:1 ratio gave rise to a new reagent that exhibited high nucleophilicity coupled with low basicity.

In 1988, Noyori performed enantioselective nucleophilic addition reactions with chiral multinuclear organometallic compounds, employing 2,2'-dihydroxy- 1,1'-binaphthyl (**25**) as a chiral ligand.[21] The employment of this higher order magnesiate afforded chiral alcohols with enantiomeric excesses up to 92% (**Scheme 1.4**).
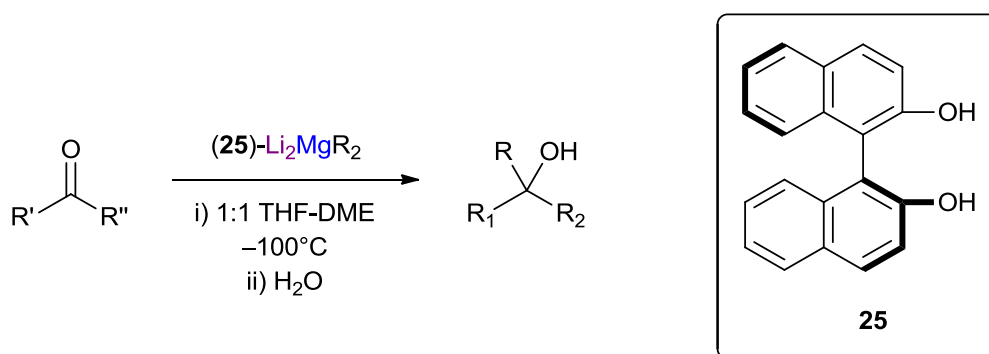
Scheme 1.4 Alkylation of a ketone with Noyori's lithium magnesiate.

1.2.2.2 Halogen-magnesium exchange

While halogen-lithium exchange showed a poor functional group tolerance and the halogen-magnesium exchange reaction with monometallic compounds was slower and thus less useful, lithium magnesiates have demonstrated outright their "synergic" behaviour during this reaction offering both high selectivity and good yields.[22-37]

Oshima reported that the treatment of a series of gem-dibromocyclopropanes with LiMg^{n}Bu$_3$ (**1**) at low temperature and the subsequent treatment with an electrophile, affords the alkylated organomagnesium species via the migration of an alkyl group on magnesium to the α-C of the cyclopropane ring (**Scheme 1.5**).[29] Moreover, he found that the treatment of aryl halides or alkenyl iodides with triakylmagnesiates forms the magnesium derivatives in good yields.[32]
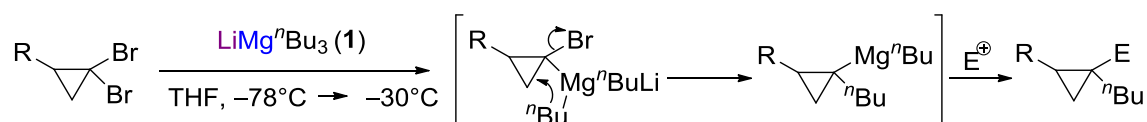
Scheme 1.5 Mechanism proposed by Oshima for the reaction of gem-dibromocyclopropanes with LiMg^{n}Bu$_3$ (**1**).

Shoji, Ito and Morita and co-workers showed how the trialkyllithium magnesiates can be employed for the synthesis of thianylazulenes (**27**) utilising a palladium cross-coupling protocol (**Scheme 1.6**).[34]
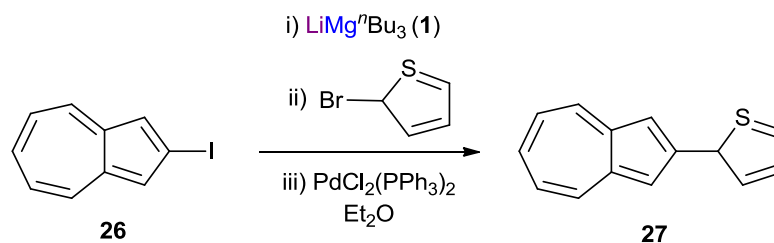
Scheme 1.6 Synthesis of thianylazulenes with tri-n-butyllithium magnesiates.

Turck highlighted how the reaction of a series of diazines (**28**) and tri-*n*-butyllithium butylmagnesiate can be successfully employed in an iodine-magnesium exchange.[22]

Moreover, he proposed an intermediate in which the magnesium coordinates with three equivalents of the substrate so the reaction is performed employing 0.35 equivalents of the alkyllithium magnesiates (**Scheme 1.7**).
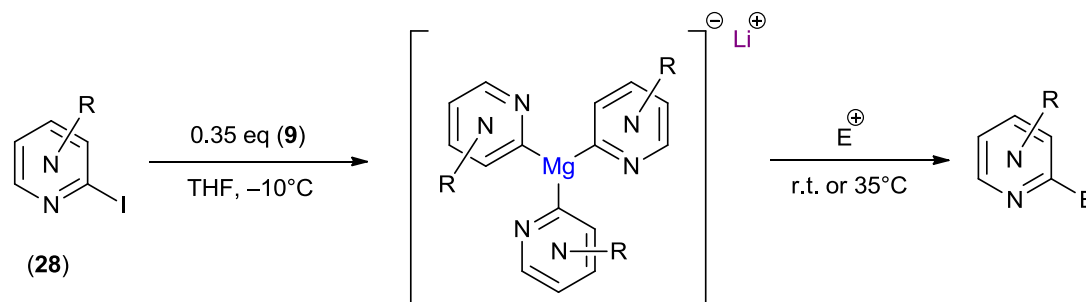
Scheme 1.7 Tri-coordinated intermediate of the halogen-magnesium exchange.

A similar intermediate was presented by Mongin in the bromine-magnesium exchange of 2-, 3- and 4-bromoquinolines to form lithium tri(quinolinyl)magnesiates (**29**).[23]

Inspired by Noyori's work,[21] Gros *et al.* Performed halogen-magnesium exchange reactions with bromopyridines[38] and iodopyrazines[39] obtaining enantioselectivities up to 90% (**Scheme 1.8**).
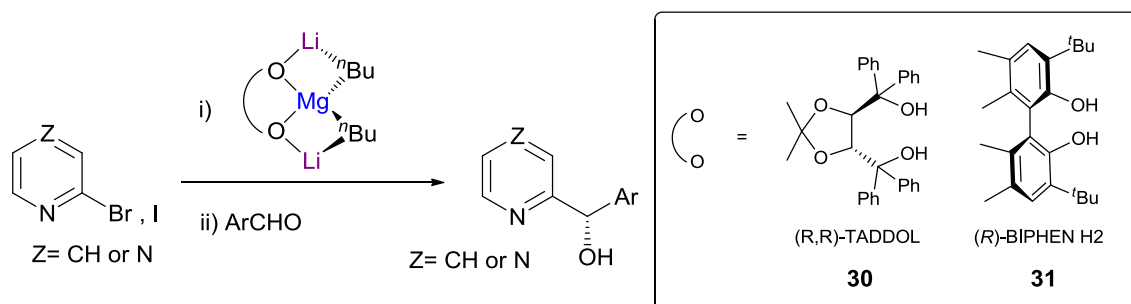
Scheme 1.8 Halogen-magnesium exchange employing chiral lithium magnesiates.

Very recently, O´Hara and co-workers were able to characterise the intermediates of those transformations, employing the achiral version of the BIPHEN ligand (**31**).[40] The structures (**Figure 1.1**) confirm the predictions of Noyori and Gros, where the three metallic centres are bridged by the chiral ligand and the alkyl groups, the magnesium atoms are tetra-coordinated and the coordination spheres of the lithium atoms are completed by binding to solvent molecules. As it will be explained later, this is commonly known as *Weiss motif*.
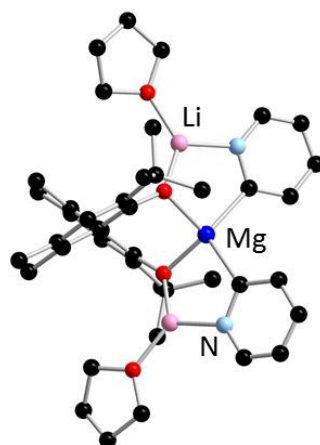
Figure 1.1 X-ray structure of $(THF)_2 \cdot Li_2Mg\{(rac)\text{-BIPHEN}\}(2\text{-pyridyl})_2$.

1.2.2.3 Deprotonation

Deprotonation with alkyllithium magnesiates was firstly reported by Nakata in 1997.[41] Marsais accomplished the deprotonation of several pyridine carboxamides at ambient temperature obtaining quantitative yields when D_2O was used as an electrophile.[42]

Mongin and co-workers have been focusing on the deprotonation reaction of aromatic (sp^2) hydrogen atoms.[43-48] The treatment of 3-fluoropyridine (**32**) with 0.33 equivalents of tri-*n*-butyl lithium magnesiates led to deprotonation taking place at the 4-position[44] (**Scheme 1.9**).
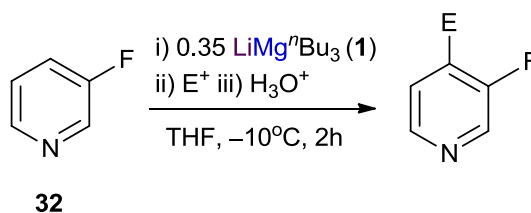
Scheme 1.9 Deprotonation of fluoropyridines with lithium magnesiates.

They have also shown the effectiveness of LiMg^{n}Bu$_3$ (**1**) in the deprotonation of furans, thiophenes and, together with Abarca *et al.*, in the deprotonation of [1,2,3]triazolo[1,5-a]pyridines (**33**).[48]

1.2.3 Structural features of homoleptic lithium magnesiates

Wittig´s magnesiate[5] was crystallographically characterised by Weiss and co-workers. They found that this bimetallic complex crystallises as a dimeric contacted ion pair with formula [(TMEDA·Li(μ–Ph)$_2$Mg(μ–Ph)]$_2$ (**35**).[49] The four metallic centres in **35** are bridged to adjacent metal by Ph rings, the inner region is occupied by magnesium atoms and the outer region by lithium atoms. This kind of motif has been coined as the Weiss motif and it can be found in alkali-metal magnesiates (and other "ate" complexes[50-57]) which depending on their stoichiometry can be grouped as (lower-order) triorganomagnesiates MMgR$_3$ or (higher-order) tetraorganomagnesiates M$_2$MgR$_4$.
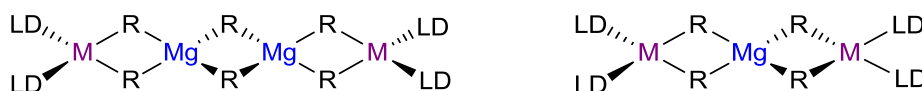
Figure 1.2 ChemDraw representation of a triorganomagnesiate (left) and a tetraorganomagnesiate (right) bearing the typical Weiss motif.

Weiss also characterised two examples of higher-order lithium magnesiates complexes. (**Table 1.2**).

The tetramethyl species [(TMEDA)·Li(μ-Me)$_2$Mg(μ-Me)$_2$Li·(TMEDA)][58] (**34**) crystallise as a monomer with the four methyl groups bridging the metals. The same motif was found when the alkynyl ligand was employed as well as the dimer [(TMEDA)·Li(μ-C$\equiv$CPh)$_2$Mg(μ-C$\equiv$CPh)$_2$Li(TMEDA)][59] (**38**)

Two different dimers were reported by Weiss and co-workers when the phenyl group was employed,[49] namely the contacted pair [[TMEDA·Li(μ–Ph)$_2$Mg(μ–Ph)]$_2$ (**35**) and the solvent separated ion pair

[(TMEDA)$_2$Li]$^+$[Ph$_2$Mg(μ–Ph)$_2$MgPh$_2$]$^-$ (**36**). A solvent separated ion pair is also formed when the benzyl ligand is employed [Li(TMEDA)$_2$]$^+$[(TMEDA)Li(μ-benzyl)$_2$Mg(benzyl)$_2$]$^-$ (**37**)[59].

An extremely curious feature is the coordination of the TMEDA to the magnesium instead of the lithium centres, what makes this metal five-coordinate (**39**).[59]

Power highlighted that a bimetallic monomer is formed when the bulky substituent 2,4,6-^{i}PrC$_6$H$_2$ is used (**40**).[60]

Hevia and co-workers studied a series of lithium magnesiates employing the bulky group CH$_2$SiMe$_3$ as an anionic ligand.[61] The study stresses how the Lewis base which is added to the magnesiate mixture defines their structure, analysing their complexation in presence of ethers and amino ligands.
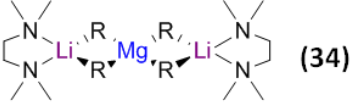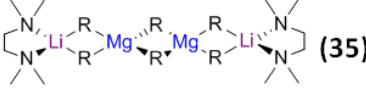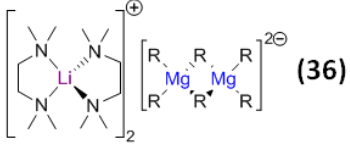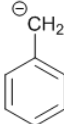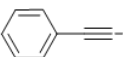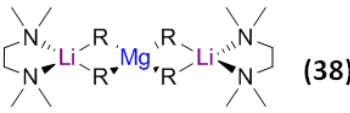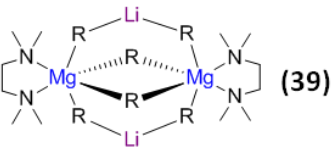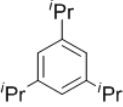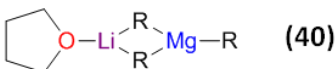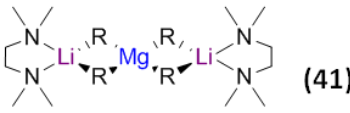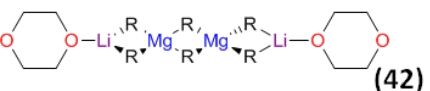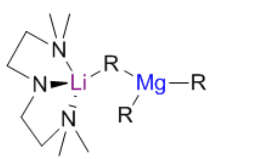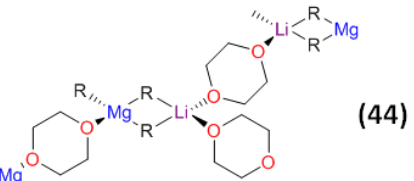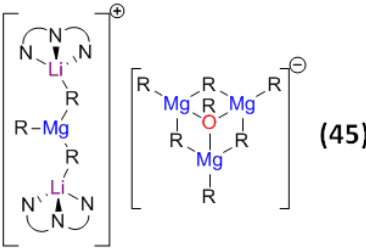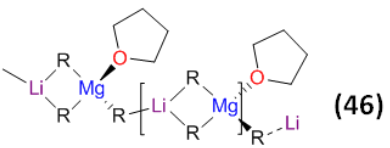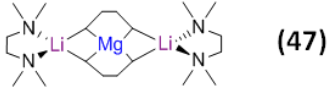
Adducts formed when ethereal solvents are employed are polymer chains with different solvent/monomer compositions in the asymmetric unit. When THF is used as donor the structural motif is the polymer [{(THF)LiMg(CH$_2$SiMe$_3$)$_3$}$_\infty$] (**46**). An unusual feature of **46** is that THF coordinates to Mg rather than Li.

However, when the system is stabilised by the nitrogen donors PMDETA (**43**) or TMEDA (**41**), both complexes crystallise as a monomer which is rich in Li when TMEDA is employed. As discussed earlier this type of magnesiate (where Li:Mg ratio is 2:1) is often referred to as a higher-order magnesiate. The motif of this tetralkyl lithium magnesiate resembles the structures found when the methyl or an alkynyl group is used.

The also characterised an oxygen/containing aryloxo lithium magnesiate (**45**) which crystallises as a solvent separated ion pair.

A higher order magnesiate was found by Westerhausen when he reacted 1,4-dilithiobutane with MgCl$_2$ to achieve the complex [{(TMEDA)Li}$_2$Mg(C$_4$H$_8$)$_2$] (**47**), where the 1,4-dimetallated butyl fragment is acting as a bidentate ligand.[62]

Table 1.2 Structural features of homoleptic lithium magnesiates.

-R	Lithium magnesiate
-CH₃	(34)
(benzene)	(35) (36)
⁻CH₂ (benzyl)	(37)
(phenylacetylide)	(38) (39)
(triisopropylphenyl)	(40)
CH₂SiMe₃	(41) (42) (43) (44) (45) (46)
C₄H₈	(47)

1.3 Results and discussion

Diamines have proven to be a key additive in the field of alkali metal-mediated magnesiation, dramatically modifying both structural pattern and reactivity.[63-65] The disaggregation as a consequence of the addition of a Lewis base such as ethers or amines often makes the complexes more soluble and more reactive, so much so the most of the time the presence of a coordinating solvent is a prerequisite to perform the synthetic transformations.[66]
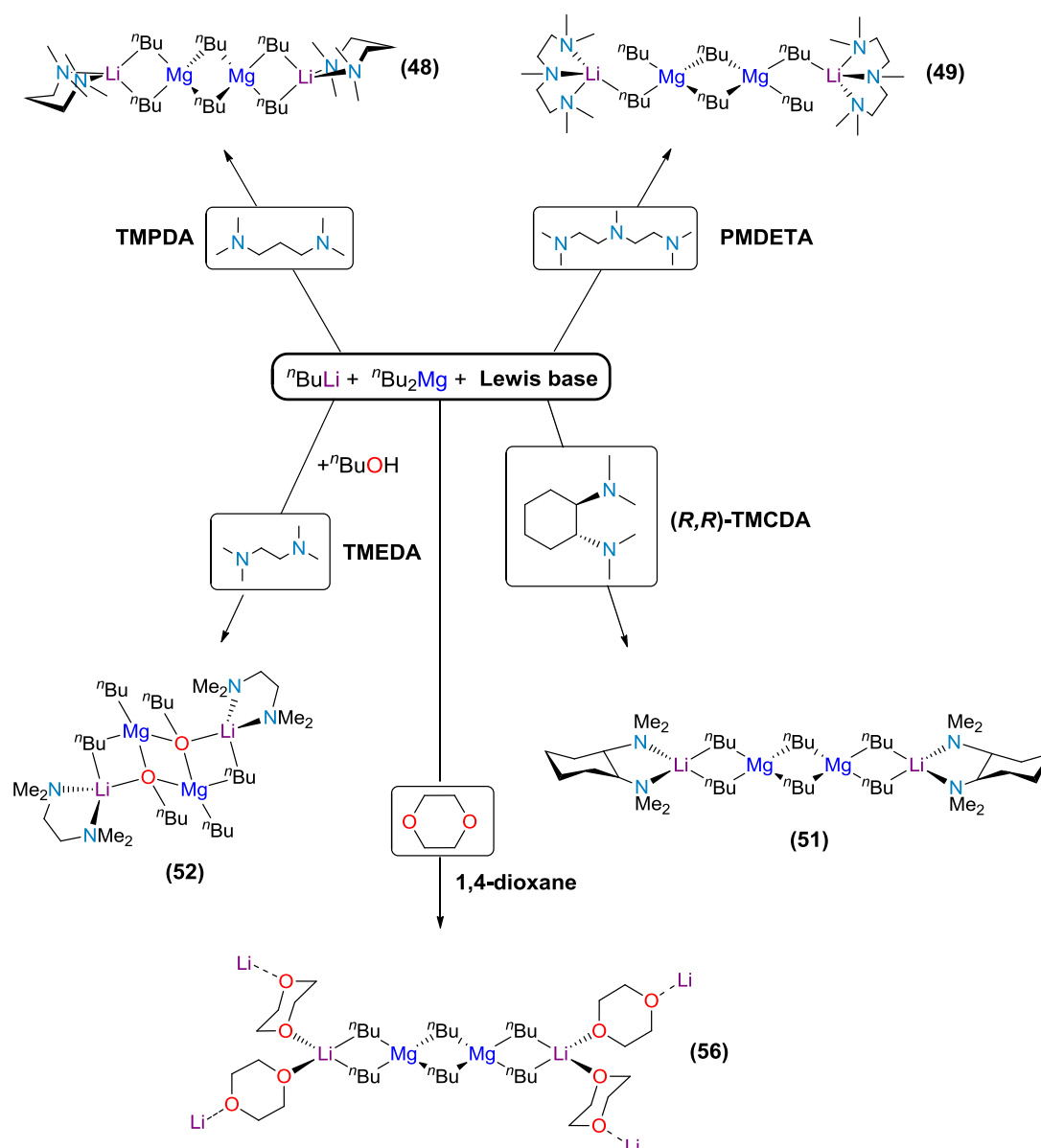
Scheme 1.10 General scheme for the synthesis of lower order magnesiates.

In order to study the different structural patterns caused by a series of ancillary ligands in lithium magnesiates, the bimetallic mixture LiMg^{n}Bu$_3$ has been reacted with five different donors, in a stoichiometric ratio 1:1 (**Scheme 1.10**).[67]

1.3.1 Use of TMPDA (*N,N,N'N'*-tetramethylpropanediamine)

The synthetic pathway employed in these syntheses has been the co-complexation of the monometallic reagents (page 2, **Scheme 1.1**).

The co-complexation reaction of ^{n}BuLi and ^{n}Bu$_2$Mg in hexane solution affords a white suspension of the homoleptic mixture [LiMg^{n}Bu$_3$].

For **48**, one equivalent of freshly distilled TMPDA (*N,N,N'N'*-tetramethylpropanediamine) was added to a hexane solution of LiMg^{n}Bu$_3$, affording a colourless solution. Crystallisation at −35°C resulted in deposition of colourless crystals of dimeric [(TMPDA)·Li(μ-^{n}Bu)$_2$Mg(μ-^{n}Bu)]$_2$ (**48**) in 67% yield.
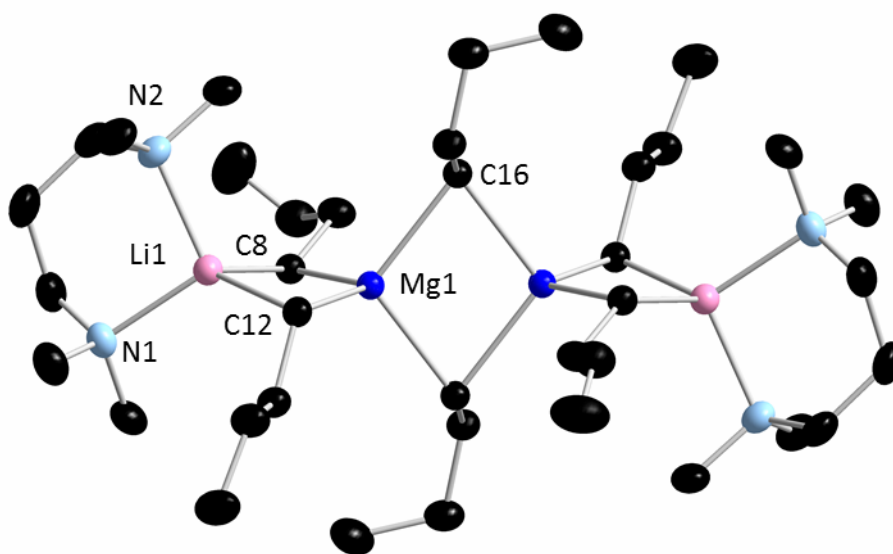
Figure 1.3 Molecular structure of **48**. Hydrogen atoms are omitted for clarity. Selected bond lengths (Å) and angles (°): Li1-N1, 2.092(4); Li1-N2, 2.085(4); Li-C8, 2.348(4); Li1-C12, 2.303(4); Mg1-C8, 2.205(6); Mg1-C12, 2.225(2); Mg1-C16 2.298(2); N1-Li1-N2, 99.8(2); N1-Li1-C8, 106.9(2); N1-Li1-C12, 120.4(2); N2-Li1-C8, 107.4(2); N2-Li1-C12, 117.1(2); C8-Li1-C12, 104.5(1); C8-Mg1-C12, 112.20(8); C8-Mg1-C16, 104.05(7); C8-Mg1-C16*, 112.58(7); C12-Mg1-C16, 110.11(7) Li1-

C8-Mg1, 70.46(1); Li1-C12-Mg1, 70.97(1). Symmetry transformations used to generate equivalent atoms: -x+2,-y+2,-z. Ellipsoids showed at 30% of probability level.

The TMPDA-solvated lithium magnesiate **48** crystallises in the space group P bca (**Figure 1.3**) and it is structurally related to **35**. Lithium magnesiate **48** was found to be a low order dimer with the classical "Weiss-type" motif (**Figure 1.2**) in which the metals are bridged by butyl anions. The structure is completed with two six-membered Li-N-C-C-C-N rings formed by the coordination of the lithium atom and the ancillary ligand. Mg atoms are surrounded by *n*-butyl groups while Li atoms are coordinated to two C and two N atoms of the ancillary ligand. The Li-C distances range from 2.303(4) to 2.348(4) Å and the Mg-C distances from 2.205(6) to 2.298(2) Å are as expected for such species. For example, the average Li-C and Mg-C bond lengths for Weiss's lithium magnesiate TMEDA·LiMgMe$_3$ are 2.284 Å and 2.260 Å respectively.[58]

TMPDA is probably the least frequently used ligand of the ones that have been employed in this study. A search in the Cambridge Structural Database[68] reveals that only four lithium complexes stabilised by TMPDA have been crystallographically characterised, bearing anionic groups such as phenylacetylene,[69] isocyanate,[70] boratabenzene[71] or benzyl.[72] The Li-N bond distances of those complexes are comparable with the Li-N bond distances of **48**, (2.085(4) to 2.092(4) Å).

1.3.2   Use of PMDETA (*N,N,N′,N″,N″*-pentamethyldiethylenetriamine)

Addition of one equivalent of the tridentate ligand PMDETA (*N,N,N′,N″,N″*-pentamethyldiethylenetriamine) to the bimetallic mixture [LiMg^{n}Bu$_3$] affords a yellow oil in bulk hexane. Concentration of the hexane solution and storage at −35°C resulted in the deposition of colourless crystals of [(PMDETA)·Li(μ-^{n}Bu)(^{n}Bu)Mg(μ-^{n}Bu)]$_2$ (**49**) in 35% yield.

Figure 1.4 Molecular structure of **49**. Hydrogen atoms are omitted for clarity. Selected bond lengths (Å) and angles (°): Li-N1, 2.178(5); Li-N2, 2.273(5); Li-N3, 2.161(5); Li-C20, 2.271(5); Li1···C10, 3.161(1); Mg1-C10, 2.186(3); Mg1-C20, 2.237(3); Mg1-C14, 2.321(3); N1-Li-N2, 81.3(2); N1-Li-N3, 120.0(2); N2-Li1-N3, 83.29(17); N1-Li1-C20, 117.3(2); N2-Li1-C20, 108.1(2); N3-Li1-C20, 122.7(2); C10-Mg1-C14, 107.44(1); C10-Mg1-C20, 121.21(1); C14-Mg1-C20, 105.49(1). Symmetry transformations used to generate equivalent atoms: -x+1,-y+1,-z+1. Ellipsoids showed at 30% of probability level.

Tridentate ligand PMDETA has been employed in bimetallic chemistry, being particularly useful to chelate heteroleptic lithium zincates like PMDETA·LiZn(HMDS)Me$_2$,[73] but also homoleptic lithium zincates like PMDETA·LiZn(CH$_2$SiMe$_3$),[74] or PMDETA·LiZnMe$_3$,[75] giving rise to both contacted ion pairs of solvent-separate structures. In these studies, the addition of PMDETA to LiMg^{n}Bu$_3$ causes the lithium magnesiate to crystallise as dimeric [(PMDETA)·Li(μ-^{n}Bu)(^{n}Bu)Mg(μ-^{n}Bu)]$_2$ (**49**) whereby the lithium atoms bind in the usual way to the ancillary ligand crystallising in space group P 2$_1$/n (**Figure 1.4**).

The main difference between **48** and **49** is that the lithium atom in **49** is bridged to a magnesium atom through only one *n*-butyl chain. Compound **49**

can be described as being "open dimeric" whereby the lithium and magnesium atoms are bridged to only one *n*-butyl chain; therefore, the Li atoms are formally linked to one terminal butyl chain otherwise its coordination number would be five. Although that is a less common motif, there are examples in the literature where the coordination number of lithium is higher than four, such as the contact ion pair found by Stalke and co-workers with formula (PMDETA)·LiZnMe$_3$ (**Figure 1.5**).[75]
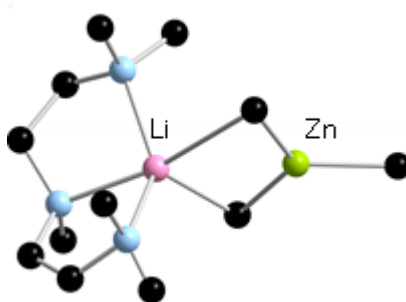
Figure 1.5 X-ray structure of (PMDETA)·LiZnMe$_3$.

Hevia *et al.* employed the same synthetic methodology to produce [(PMDETA)LiMg(CH$_2$SiMe$_3$)$_3$] (**43**),[61] but the steric bulk of the alkyl chain makes this lithium magnesiate crystallise as a monomer. Compound **49**; however, crystallises as a dimer through a Mg-C interaction. As a consequence of the difference of steric bulk of the anionic ligand, the angle Li-C-Mg is dramatically different, being 83.3(2)° for **49** and 149.41(2)° for Hevia's monomer.

Strohmann crystallographically characterised a *n*BuLi adduct stabilised by PMDETA, where the tetranuclear dimer [PMDETA·(*n*BuLi)$_2$]$_2$ (**50**) is produced be interpreted as a dimer with two outer PMDETA·*n*BuLi units linked to a dimeric core of (*n*BuLi)$_2$ for Strohmann's complex or (*n*Bu$_2$Mg)$_2$ for **49**. Strohmann's lithium dimer presents longer Li-C bond distances for the outer unit [2.498(6) Å] than compound **49** [2.271(5) Å] suggesting a stronger interaction between the outer PMDETA·*n*BuLi and the central ring in **49**. The C-Mg distance [2.237(3) Å] is within the range of typical bond lengths in

organomagnesiates as they are similar to those described by Hevia and co-workers.[61, 64]
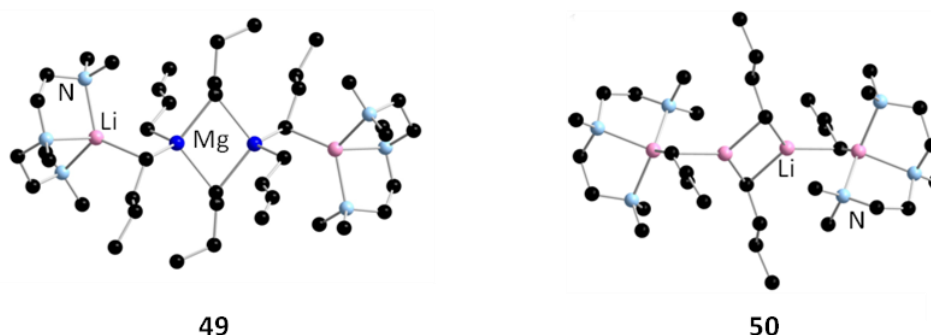
Figure 1.6 Molecular structures of **49** and [PMDETA·(^{n}BuLi)$_2$]$_2$ (**50**).

1.3.3 Use of (*R,R*)-TMCDA ((*R,R*)-*N,N,N',N'*-tetramethylcyclohexane-1,2-diamine)

When the chiral ligand (*R,R*)-TMCDA ((*R,R*)-*N,N,N',N'*-tetramethylcyclohexane-1,2-diamine) was added to an equimolar mixture of *n*-butyllithium and di-*n*-butylmagnesium in hexane, a white suspension was produced which on gentle heating dissolved in the reaction medium. Storage at −35°C for 36 hours deposited dimeric crystalline **51**, [{(*R,R*)-TMCDA}·Li(μ-^{n}Bu)$_2$Mg(μ-^{n}Bu)]$_2$, in high yield (82%).
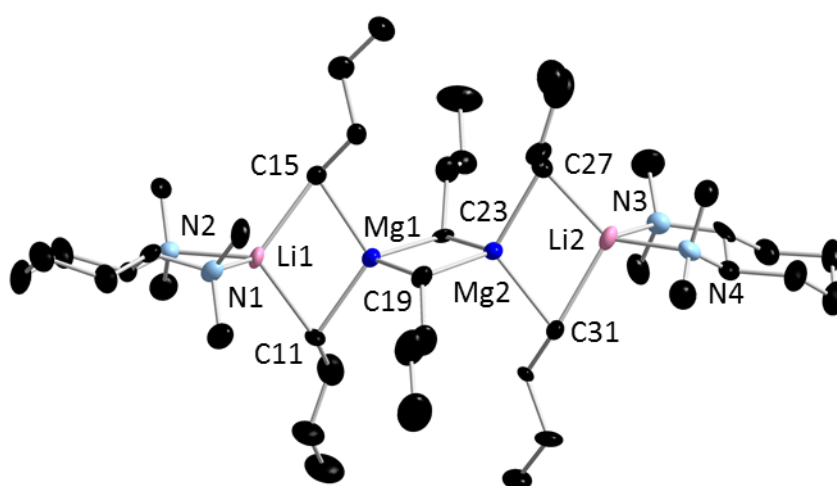
Figure 1.7 Molecular structure of **51**. Hydrogen atoms are omitted for clarity. Ellipsoids showed at 30% of probability level.

Extensive studies have been carried out with the chiral ligand (*R,R*)-TMCDA. Chiral vicinal diamines constitute an important motif commonly employed in asymmetric reactions.[76-78] They are the structural motif of the $\alpha,\beta-$diaminoacids, present in a multitude of natural products and playing a central role in the development of synthetic products that can be therapeutically employed.[79]

This chiral bidentate donor was employed and produced the complex [{(*R,R*)-TMCDA}·Li(μ-^{n}Bu)$_2$Mg(μ-^{n}Bu)]$_2$ (**51**) which crystallises in space group P 2_1 (**Figure 1.7**). (*R,R*)-TMCDA solvates the triorganomagnesiate leading to a contacted ion pair dimer where the atoms in molecule are not related by any symmetry operations. Several alkali-metal magnesium amide complexes stabilised by chiral donors[65, 80, 81] [namely (–)-sparteine and (*R,R*)-TMCDA] have been characterised, but to the best of our knowledge, this is the first example of a chiral alkyllithium magnesiate.

Compound **51** crystallises in space group P 2_1. This space group belongs to the called "Sohncke groups" which characterise because they contain only rotation or screw axes, and are the only space groups in which chiral structures can crystallise.[82] As a consequence, all the atoms of **51** are inequivalent.

1.3.4 Use of TMEDA (*N,N,N′,N′*-tetramethylethylenediamine)

The addition of one equivalent of TMEDA (*N,N,N′,N′*-tetramethylethylenediamine) to LiMg^{n}Bu$_3$ and cooling down to low temperatures afford a crop of crystals (59% yield based on a homoleptic lithium magnesiate) (expected formula TMEDA·LiMg^{n}Bu$_3$, **55**); however, they could not be analysed by X-ray crystallography, even when low temperatures were employed (123 K). The crystals were found to degrade in the X-ray beam.

In one of the attempts to measure one single crystal of this compound, it was possible to collect the data and get the structure of a new compound, [(TMEDA)·Li(μ-^{n}Bu)(μ-O^{n}Bu)Mg(^{n}Bu)]$_2$ (**52**) (**Figure 1.8**). ^{1}H-NMR studies of

the solid revealed that the crop of crystals is composed of a mixture of **52** and the homoleptic lithium magnesiate **55**.

Compound **52**, [(TMEDA)·Li(μ-^{n}Bu)(μ-O^{n}Bu)Mg(^{n}Bu)]$_2$, can be rationally synthesised by the equimolar reaction of *n*-butyllithium and *n*-butanol (in order to synthesise *in-situ* lithium-*n*-butoxide), one equivalent of *n*-butylmagnesium and one equivalent of TMEDA, affording crystalline material in 33% yield.
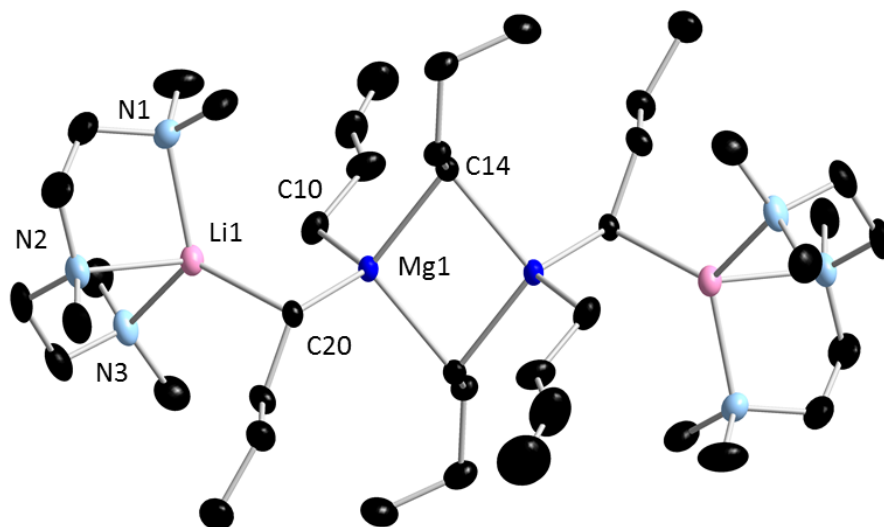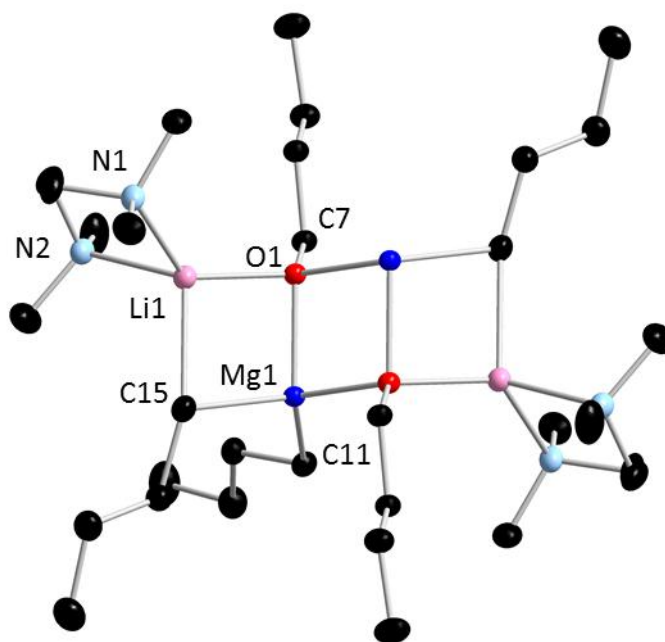

Figure 1.8 Molecular structure of **52**. Hydrogen atoms are omitted for clarity. Selected bond lengths (Å) and angles (°): Li1-N1, 2.114(3); Li1-N2, 2.191(3); Li1-C15, 2.343(3); Li1-O1, 1.946(3); Mg1-C11, 2.156(2); Mg1-C15, 2.211(2); Mg1-O1, 2.044(1); N1-Li1-N2, 86.5(1); N1-Li1-C15, 111.3(1); N1-Li-O1, 125.5(1); N2-Li1-O1, 123.7(1); N2-Li1-C15, 112.4(1); O1-Li1-C15, 98.1(1); C11-Mg1-C15, 118.25(7); C11-Mg1-O1, 115.51(5); C15-Mg1-O1, 99.03(5). Symmetry transformations used to generate equivalent atoms: -x+1,-y+1,-z+2. Ellipsoids showed at 30% of probability level.

Lithium magnesiate **52** crystallises in space group $P2_1/c$. Although the aim of this chapter was to expand the knowledge of homoleptic lithium magnesiates, compound **52** will be explained in detail as it is structurally related to some magnesiates present in the literature.

The main feature of **52** is a Li-C-Mg-O four-membered ring where Mg atoms are binding to one terminal *n*-butyl group and they are connected to Li atoms through a *n*-butyl group and a Othat acts as a bridge. Li atoms complete their coordination sphere with the coordination of TMEDA in order to have tetrahedral (sum of angles 657.44°) coordination. Complex **52** dimerises with another four-membered ring through a Mg-O interaction exhibiting ladder-like features[83, 84] (**Figure 1.8**).

Mulvey *et al.* crystallographically characterised two alkali-metal (sodium and potassium) magnesiates that are closely related to **52** (**Figure 1.9**).[85]
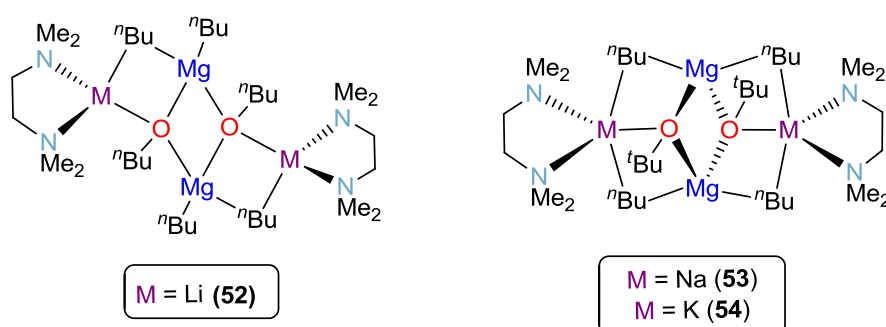
Figure 1.9 ChemDraw representation of **52** and alkali-metal magnesiates of Mulvey.

All the structures have common features as they own an O-Mg-O-Mg core ring and the alkali metal is bonded to one oxygen atom and one molecule of TMEDA.

The main difference between these structures is the coordination sphere of the alkali metal atom. While Mg atoms in **52** are connected to one terminal *n*-butyl group, the magnesium atoms of Mulvey's structures are connected to two alkali-metal so there are not any terminal *n*-butyl groups. The structure could be described as a Lewis acid ring that hosts in its centre a Lewis base,

in this case the *tert*-butoxide groups. Since 1998, this motif has been known as the inverse crown morif.[86, 87]

Accordingly, while lithium atoms in **52** are tetrahedrally-disposed, the complexes described by Mulvey and co-workers have sodium (**53**) or potassium centres (**54**) that are penta-coordinated. These complexes were synthesised by co-complexation of *n*-butylmagnesium and alkali-metal *tert*-butoxide. The difference in the steric hindrance of the *t*-butyl group versus *n*-butyl group may be an explanation for this structural variation; however, the presence of a bulkier group would generally generate more open structures. It seems likely that the presence of the lithium atom is a key factor to get this ladder-like structure instead of the inverse-crown motif.

1.3.5 Use of 1,4-dioxane

As mentioned in paragraph 1.2.2, alkyllithium magnesiates have been employed to perform numerous different reactions. A common reaction condition in most of the reaction is that they are performed in ethereal solution.[19, 42, 44-48] For this reason, it was decided to study the role of oxygen donors such as THF or diethylether when coordinating [LiMg^{n}Bu$_3$]. However, no crystalline material was forthcoming even when the donor was added in stoichiometric, substoichiometric amounts and also in excess.

Next, it was decided to focus on the bidentate ether 1,4-dioxane by addition of one molar equivalent of this donor to an equimolar mixture of *n*-butyllithium and di-*n*-butylmagnesium in bulk benzene. Precipitation of a white solid suggested that a new adduct had formed. Toluene was added to the resultant white solid, which redissolved the complex on strong heating. Cooling the solution slowly to ambient temperature afforded a crop of colourless needles of polymeric magnesiate [[(dioxane)·Li(μ-^{n}Bu)$_2$Mg(μ-^{n}Bu)]$_2$]$_\infty$, **56** (47%).

1,4-dioxane has been previously used to solvate different lithium "ate" complexes,[61, 88, 89] and it is well known that this ligand affords polymeric structures as it is incapable of acting as a chelate.

Lithium magnesiate **56** crystallises in the space group C 2/c (**Figure 1.10**). It can be described as dimeric [(dioxane)LiMg^{n}Bu$_3$]$_2$ units bearing again the typical Weiss motif, with magnesium atoms surrounded by butyl groups and the lithium atoms linked to two butyl chains and two dioxane molecules which act as a bridge between different dimers producing a three-dimensional polymeric structure.

Unfortunately, a large amount of unresolved disorder adversely affects the precision of the *n*-butyl groups, dioxane and benzene molecules (present as crystallisation solvent in the unit cell) and therefore precludes discussion of any geometrical parameters, although its connectivity is unequivocal.
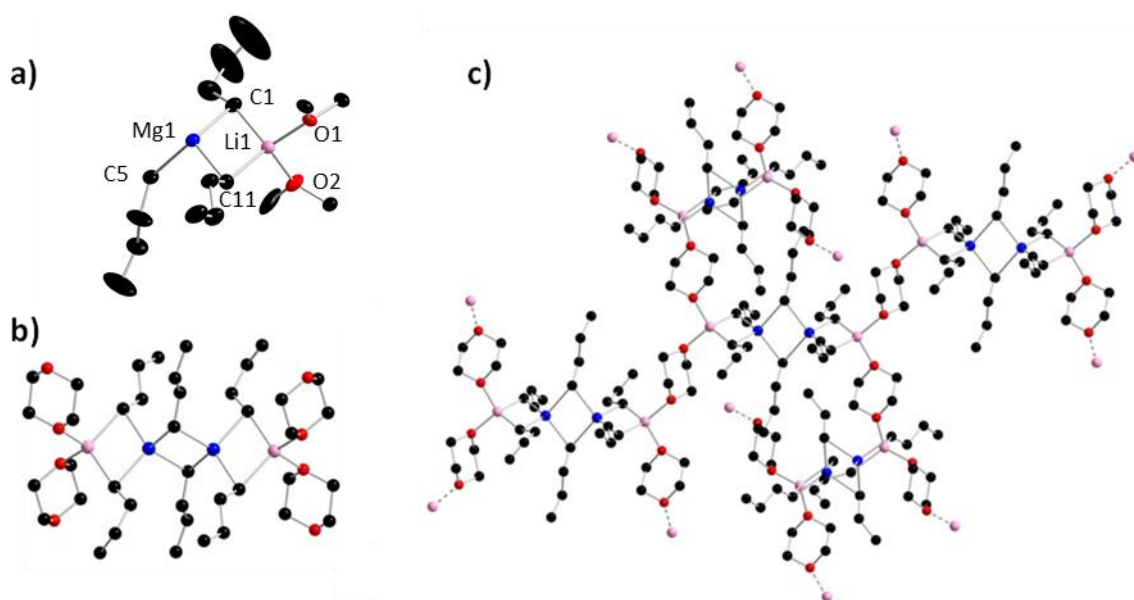
Figure 1.10 Molecular structure of **56**, showing the unit cell (a), the arrangement in the typical Weiss motif (b) and the tridimensional polymerization (c). Ellipsoids on **a)** showed at 30% of probability level.

A close precedent to **56** can be found in the series of lithium magnesiates published by Hevia and co-workers employing (trimethylsilyl)methyl group. The employment of stoichiometric and substoichiometric amounts of dioxane affords two structures (**42** and **44** respectively) which are structurally different to **56**.

Both of them are polymers; compound **42** comprises dimeric (dioxane)LiMgR$_3$ that polymerises through one dioxane molecule bridging lithium atoms while compound **44** is formed by monomers of (dioxane)$_2$LiMgR$_3$ which polymerise through Li-O and Mg-O interactions.

Unlike **56**, every lithium atom in **42** is linked to a single molecule of dioxane and presents an electrostatic interaction with one of the methyl groups of the anionic ligand.

1.3.6 Solution NMR spectroscopic studies

1.3.6.1 One-dimensional studies

Complementing their solid-state characterization, lithium magnesiates **48**, **49**, **51**, **52**, **55** and **56** have also been examined using multinuclear (^{1}H, ^{7}Li and ^{13}C) NMR spectroscopy.

The employment of donor NMR solvents could allow the displacement of the ancillary ligand, so in order to maintain that coordination, the solvent of choice was deuterated cyclohexane for all the complexes except for **56**, which required a more polar solvent, such as deuterated toluene and an elevated acquisition temperature (353K) because of its low solubility.

Therefore, a comparison of the resonances in the ^{1}H and ^{13}C NMR spectra belonging to the ancillary ligands of **48**, **49**, **51** and **52** with those observed for the free Lewis bases suggests that the donors remain coordinated to the metal centres in solution, as the resonances are shifted downfield (**Figure 1.11**).
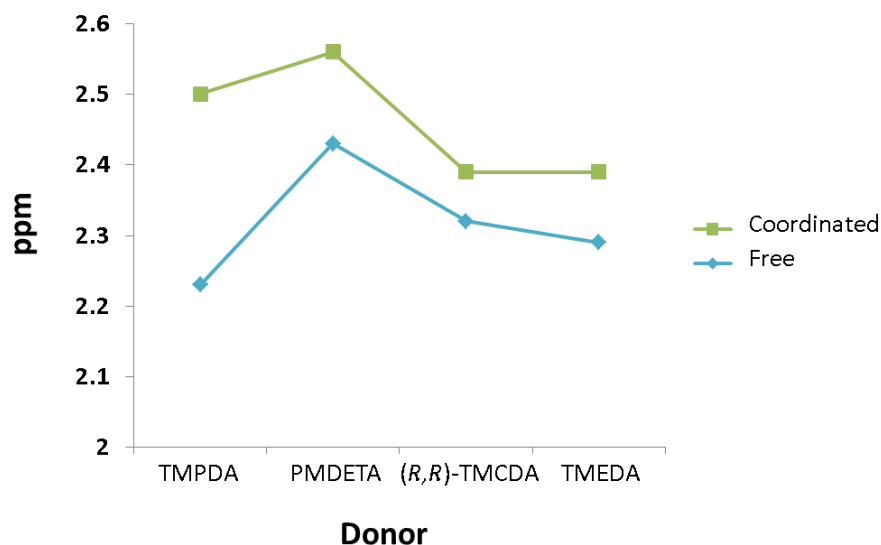
Figure 1.11 Comparison of the ^{1}H NMR spectroscopy resonances of the N-CH_3 group of different nitrogen-ligands when they are coordinated and free.

As a X-ray data acquisition for "[(TMEDA)LiMg(^{n}Bu)$_3$]$_2$" (**55**) was frustratingly not forthcoming, the ^{1}H and ^{13}C spectra of this compound were examined in cyc-C$_6$D$_{12}$. The ^{1}H NMR spectrum shows two singlets at 2.33 and 2.39 ppm while the signals for free TMEDA in cyc-C$_6$D$_{12}$ appear at 2.14 and 2.30 ppm. ^{1}H NMR spectra showed that both TMEDA and ^{n}Bu resonances were present (in an approximate 1 : 3 ratio) which is in agreement with a low order lithium magnesiate.

Compound **52** shows a broad resonance at 3.68 ppm that integrated to four protons. This broad signal belongs to butoxide groups. The ^{1}H NMR spectrum of **55** presents sharp signals and, more importantly, there are no resonances with chemical shift higher than 2.39 ppm, the signal for TMEDA. That appears to suggest that no butoxide groups are present in the crystalline solid.

Turning to ^{7}Li NMR, the resonance for n-butyllithium is shifted upfield from 2.40 ppm to 1.01 ppm when it is co-complexed with the "low polarity" di-n-butylmagnesium (**Table 1.3**). The further shift of this resonance after the addition of the donor also highlights that the Lewis base remains

coordinated to the metallic centre in solution. Tridentate ligand PMDETA causes the most shielded resonance, appearing at 0.77 ppm for **49**.

Table 1.3 Chemical shifts in the ^{7}Li spectrum in C_6D_{12} at 300K.

Complex	^{n}BuLi	LiMg^{n}Bu$_3$	48	49	51	52	56
7Li (ppm)	2.40	1.01	0.79	0.77	1.04	0.87	0.99

Although the X-ray data for these lithium magnesiates show the presence of at least two chemically distinct *n*-butyl chains, the NMR spectroscopic studies at 300 K suggest that only one set of signals for the alkyl groups in hydrocarbon solution is present. This fact implies that rapid exchange of the alkyl positions occurs in solution, causing the signals for the *n*-butyl chains to become equivalent. In all cases the resonance for CH_2-M is broad. As a case study, it was decided to probe further a D^8-toluene solution of **49** using a variable-temperature experiment in an attempt to decipher the three different *n*-butyl groups (one terminal, one bridging Li and Mg centres, and one bridging two Mg centres) which exist in the solid state structure (*N.B.*, *cyc*-C_6D_{12} is solid below 268 K hence was not used as the NMR solvent)..

The temperature was lowered to 240 K and ^{1}H NMR spectroscopic measurements were obtained every 10 K (**Figure 1.12**). At the lowest temperature, the CH_2-M resonance decoalesces into two signals of an approximate integration of 1:2, not the three resonances that were expected.
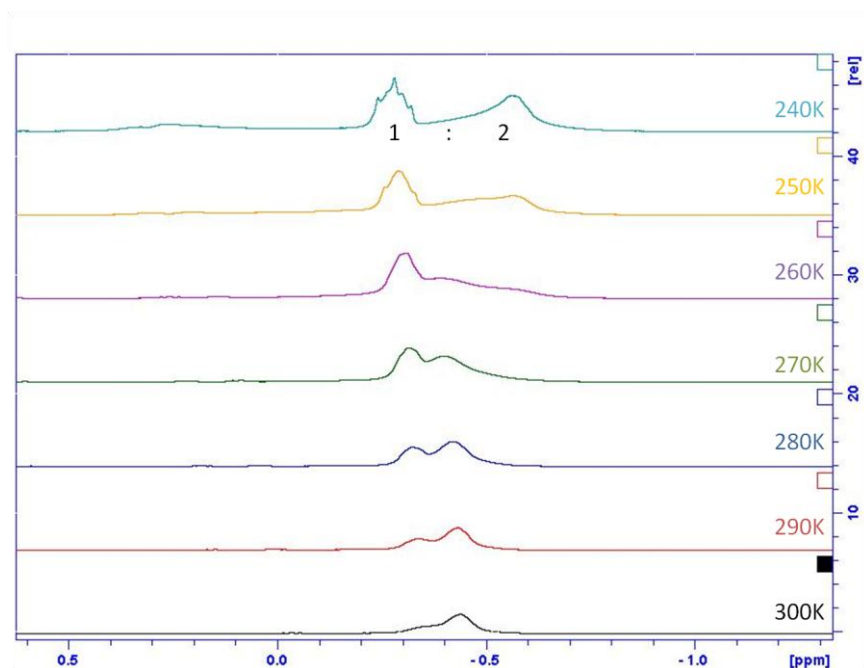
Figure 1.12 Variable-temperature ^{1}H NMR experiment of **49** in D$_8$-toluene.

This seems to point to two possible scenarios (**Scheme 1.11**). Firstly, in arene, the dimer stays intact but the terminal *n*-butyl group now adopts a bridging position (or is in rapid exchange between bridging and terminal with respect to the NMR timescale); or secondly, the dimer dissociates to a monomer in D$_8$-toluene and the resonances therefore correspond to two bridging and one terminal butyl chain. In order to find out whether **49** retains its dimeric structure in solution, it was performed ^{1}H NMR diffusion-ordered nuclear magnetic resonance spectroscopy (^{1}H DOSY) to gain insight into its aggregation in D$_8$-toluene.
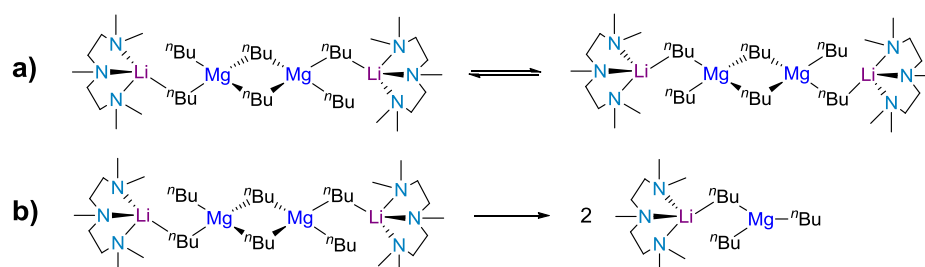
Scheme 1.11 Representation of two different rearangement processes of **49** in solution.

1.3.6.2 DOSY spectroscopy

[1]H Diffusion-ordered nuclear magnetic resonance spectroscopy (DOSY NMR) experiments are useful to estimate molecular weights (and therefore aggregation states) of species in solution.[90-92] Althogh DOSY diffusion constants are not completely shape independent,[93] they can often provide a good approximation of the molecular weight of a molecule, as species with higher molecular weight diffuse more slowly than those with lower molecular weight. A relationship can be established between the diffusion coefficient and molecular weight, which are inversely proportional to each other (**Equation 1**).

$$D = \frac{K_B T}{6\pi\mu r}$$

Equation 1 Stokes-Einstein equation where D is diffusion coefficient, r is radius, K_B is the Boltzmann constant, T is temperature and μ is viscosity.
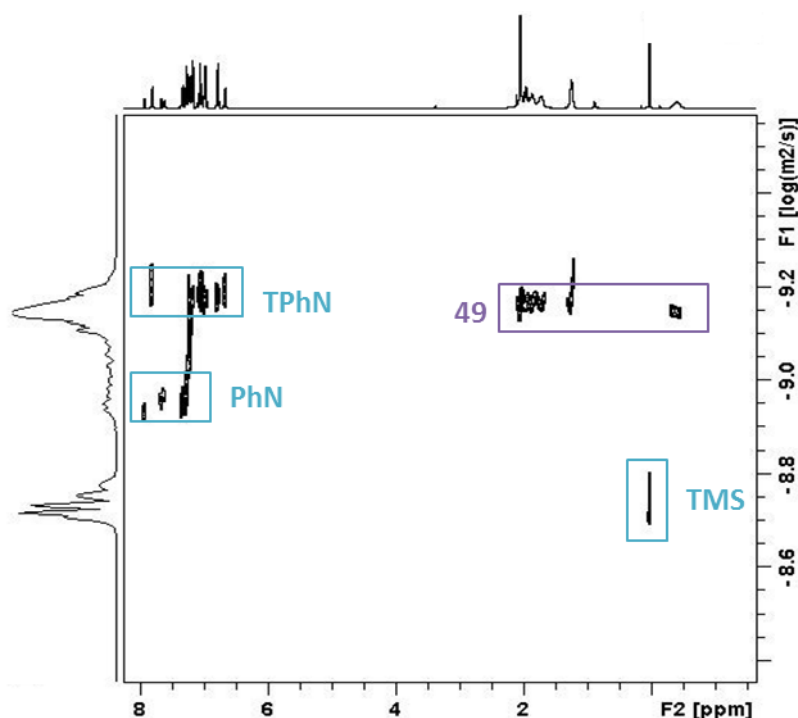
Figure 1.13 ^{1}H DOSY spectrum of **49** in D_8-toluene at 300K.

1,2,3,4-tetraphenylnaphthalene (TPhN), 1-phenylnaphthalene (PhN), and tetramethylsilane (TMS) were chosen as internal standards, as they exhibit good solubility in toluene with minimal overlapping of signals and are inert to magnesiates (**Figure 1.13**).

A correlation between log D (average diffusion value, D, 7.2×10^{-10} m^2 s^{-1}) and log FW (FW = molecular weight) can be established (calibration curve obtained from the internal standards, log D = −0.698 log FW − 7.358; r^2 = 0.997).

Table 1.4 DOSY data for **49.**

Standard	D (m^2s^{-1}) (av)	Log FW	Log D	FW (g/mol)
TPhN	6.43×10^{-10}	2.64	-9.21	432.5
PhN	1.13×10^{-9}	2.31	-8.96	204.3
TMS	1.89×10^{-9}	1.94	-8.72	88.2
49	7.20×10^{-10}	2.57	-9.15	**370.8**
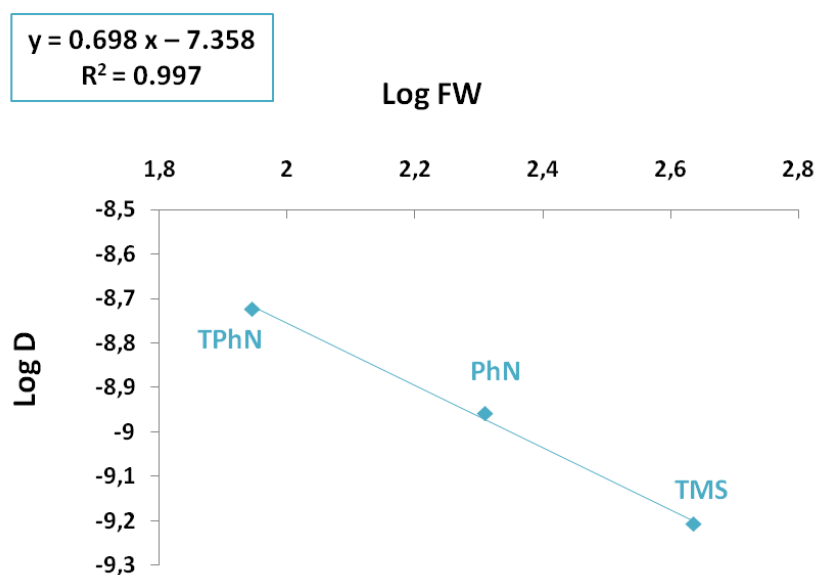
Figure 1.14 Calibration curve for the internal standards added to perform DOSY experiment of **49**.

This correlation gave an experimental molecular weight, estimated to be 370 g/mol, which differs by a 1.23% from the theoretical molecular weight for the monomer [(PMDETA)LiMg^{n}Bu$_3$].

Thus, analysis of this data suggests that the most likely pathway is **b** and the dimeric constitution of **49** in solid state is not retained in solution.

1.4 Conclusions and future work

Five new lithium magnesiates have been crystallographically characterised by combination of the homoleptic lithium magnesiate [LiMg^{n}Bu$_3$] and an ancillary ligand.

All of them invariably crystallise as dimeric complexes where the magnesium atoms are surrounded by the anions and the lithium atoms are coordinated to the ancillary ligand. The employment of the bidentate ligand 1,4-dioxane allows the dimeric lithium magnesiates to polymerise.

Showing the high sensitivity to the air and moisture or this kind of compounds, an oxygen-containing complex (**52**) was found when TMEDA was employed.

Solution NMR spectroscopic studies have been performed for all the compounds in deuterated hydrocarbon solvent and variable temperature and two-dimensional studies has been carried out for lithium magnesiate [(PMDETA)·Li(μ-^{n}Bu)(^{n}Bu)Mg(μ-^{n}Bu)]$_2$ (**49**). These studies prove that the dimeric structure is not maintained in solution, but the compound is present as a monomeric structure.

As a future work and to complement these structural studies, reactivity studies could be undertaken comparing each with monometallic reference compounds and indeed each other.

As detailed in **Scheme 1.1**, two different patterns can be followed to synthesise lithium magnesiates. The main difference is that in salt-metathesis will undergo the presence of metal halide metal halide in the media. As a future work, it would be interesting to perform a study in order to determine if the method of

synthesis of the magnesiates (and therefore the presence of metal halides in the media) affects both, the reactivity and the structure of the "ate" complex.

1.5 Experimental

1.5.1 Synthesis of 48, [TMPDA·Li(μ-^{n}Bu)$_2$Mg(^{n}Bu)]$_2$

^{n}BuLi (0.25 mL, 4 mmol of 1.6 M solution in hexanes) was dissolved in 15 mL of dried hexane in an oven-dried Schlenk tube. 4 mmol of ^{n}Bu$_2$Mg (4 mL of 1 M solution in heptanes) were added, turning the solution slightly turbid. After stirring for 30 minutes, 4 mmol of TMPDA (0.68 mL) were added. Gently heating gave a colourless solution. All volatiles were removed under vacuum and 10 mL of pentane were added. The solution was transferred to a freezer (–80°C) affording colourless crystals after 24 hours. (0.89 g., 67%).

^{1}H NMR (400.13 MHz, 300 K, C$_6$D$_{12}$): δ –0.80--0.42 (12H, br, M-CH_2CH$_2$CH$_2$CH$_3$, Bu), 0.85 (18H, t, $^3J_{HH}$=7.2 Hz, M-CH$_2$CH$_2$CH$_2$CH_3, Bu), 1.22-1.32 (12H, m, M-CH$_2$CH$_2$CH_2CH$_3$, Bu), 1.50-1.58 (12H, m, M-CH$_2$CH_2CH$_2$CH$_3$, Bu), 1.66 (4H, br, N-CH$_2$CH_2CH$_2$-N, TMPDA), 2.25 (24H, s, N-CH$_3$, TMPDA), 2.45-2.47 (8H, t,$^3J_{HH}$=4.8 Hz, N-CH$_2$, TMPDA). ^{13}C{^{1}H} NMR (100.62 MHz, 300 K, C$_6$D$_{12}$): δ 9.9 (M-CH$_2$CH$_2$CH$_2$CH$_3$, Bu), 13.3 (M-CH$_2$CH$_2$CH$_2$$CH_3$, Bu), 23.34 (N-CH$_2$$CH_2CH_2$-N, TMPDA), 31.7 (M-CH$_2$$CH_2CH_2CH_3$, Bu), 32.1, (M-CH$_2CH_2$$CH_2CH_3$, Bu) 46.0 (N-$CH_3$, TMPDA), 60.8 (N-$CH_2CH_2$$CH_2$-N, TMPDA). ^{7}Li NMR (155.50 MHz, 300 K, C$_6$D$_{12}$): δ 0.79.

Elemental Microanalysis calculated for **48**; C, 68.72; H, 12.51; N, 8.90%; found: C, 67.42; H, 14.05; N, 8.72%.

1.5.2 Synthesis of 49, [(PMDETA)·Li(μ-^{n}Bu)(^{n}Bu)Mg(μ-^{n}Bu)]$_2$

^{n}BuLi (2.5 mL, 4 mmol of 1.6 M solution in hexanes) was dissolved in 15 mL of dried hexane in an oven-dried Schlenk tube. 4 mmol of ^{n}Bu$_2$Mg (4 mL of 1 M solution in heptanes) were added and solution turned slightly turbid. After stirring for 30 minutes, 4 mmol of PMDETA (0.84 mL) were added. The solution was gently heated to give a colourless solution with a yellow oil at the bottom of the Schlenk tube. This solution was separated from the oil via

cannula and the solution was concentrated to 5 mL and stored at $-30°C$, affording colourless crystals after 1 day. (0.53 g., 35%).

^{1}H NMR (400.13 MHz, 300 K, C_6D_{12}): δ -0.82--0.62 (12H, br, M-CH_2CH$_2$CH$_2$CH$_3$, Bu), 0.86 (18H, t, $^3J_{HH}$=7.2 Hz, M-CH$_2$CH$_2$CH$_2$CH_3, Bu), 1.23-1.30 (12H, m, M-CH$_2$CH$_2$CH_2CH$_3$, Bu), 1.50-1.56 (m, 12H, M-CH$_2$CH_2CH$_2$CH$_3$, Bu), 2.29 (30H, s, N-CH_3 PMDETA), 2.44-2.53 (16H, br, N-CH_2, PMDETA). The relatively low solubility of **49** over prolonged periods of time in C_6D_{12} solutions precluded the collection of its ^{13}C{^{1}H} spectrum. ^{7}Li NMR (155.50 MHz, 300 K, C_6D_{12}): δ 0.77.

Due to the extreme air- and moisture-sensitivity of this compound, satisfactory elemental microanalysis data could not be obtained.

1.5.3 Synthesis of 51, [((*R,R*)-TMCDA)·Li(μ-*^{n}*Bu)$_2$Mg(μ-*^{n}*Bu)]$_2$

*^{n}*BuLi (2.5 mL, 4 mmol of 1.6 M solution in hexanes) was dissolved in 15 mL of dried hexane in an oven-dried Schlenk tube. 4 mmol of *^{n}*Bu$_2$Mg (4 mL of 1 M solution in heptanes) were added and solution turned slightly turbid. After stirring for 30 minutes, 4 mmol of (*R,R*)-TMCDA (0.76 mL) were added. The mixture was gently heated to yield a transparent colourless solution, which was transferred to a freezer operating at $-30°C$, affording colourless crystals after 24 hours. (1.22 g, 82%).

^{1}H NMR (400.13 MHz, 300 K, C_6D_{12}): δ -0.73--0.71 (12H, br, M-CH_2CH$_2$CH$_2$CH$_3$, Bu), 0.86 (18H, t, $^3J_{HH}$=7.2 Hz, M-CH$_2$CH$_2$CH$_2$CH_3, Bu), 1.07-1.13 (4H, m, γ-CH_2, (*R,R*)-TMCDA), 1.15-1.20 (4H, m, β-CH_2, (*R,R*)-TMCDA), 1.22-1.31 (12H, m, M-CH$_2$CH$_2$CH_2CH$_3$, Bu), 1.50-1.56 (12H, m, M-CH$_2$CH_2CH$_2$CH$_3$, Bu), 1.78-1.80 (4H, m, γ'-CH_2, (*R,R*)-TMCDA), 1.90-1.93 (4H, m, β'-CH_2, (*R,R*)-TMCDA), 2.18 (12H, s, N-CH_3, (*R,R*)-TMCDA), 2.39 (14H, s, N-CH_3 and α-CH, (*R,R*)-TMCDA). ^{13}C{^{1}H} NMR (100.62 MHz, 300 K, C_6D_{12}): δ 10.3 (M-CH$_2$CH$_2$CH$_2$CH$_3$, Bu), 13.3 (M-CH$_2$CH$_2$CH$_2$$CH_3$, Bu), 21.8 (γ-$CH_2$, (*R,R*)-TMCDA), 25.0 (β-CH$_2$, (*R,R*)-TMCDA), 31.6 (M-CH$_2$$CH_2CH_2CH_3$, Bu), 32.2 (M-CH$_2CH_2$$CH_2CH_3$, Bu), 37.1 (N-$CH_3$, (*R,R*)-TMCDA), 44.6 (N-CH$_3$, (*R,R*)-TMCDA), 64.1 (α-CH, (*R,R*)-TMCDA). ^{7}Li NMR (155.50 MHz, 300 K, C6D12): δ 1.04.

Elemental Microanalysis calculated for **51**; C, 71.44; H, 12.54; N, 7.57%; found: C, 67.45; H, 13.22; N, 7.63%.

1.5.4 Synthesis of 52 , [TMEDA·Li(μ-^{n}Bu)(μ-O^{n}Bu)Mg(^{n}Bu)]$_2$

^{n}BuLi (3.35 mL, 5 mmol of 1.6 M solution in hexanes) was dissolved in 15 mL of dried hexane in an oven-dried Schlenk tube. 5 mmol of ^{n}BuOH were added (0.45 mL) at 0°C and white solid immediately precipitates. 5 mmol of ^{n}Bu$_2$Mg (5 mL of 1 M solution in heptanes) were added and solution turned slightly turbid. After stirring for 30 minutes, 5 mmol of TMEDA (0.75 mL) were added. The suspension was stirred for 2 hours and filtered over celite with a filter stick. The resultant solution was concentrated and stored at −35°C, affording a crop of crystals after 24 hours (0.44 g., 33%).

^{1}H NMR (400.13 MHz, 300 K, C$_6$D$_{12}$): δ −0.94-−0.46 (8H, br, M-CH_2CH$_2$CH$_2$CH$_3$, Bu), 0.84-0.93 (18H, m, M-(O)-CH$_2$CH$_2$CH$_2$CH_3,Bu and OBu), 1.26 (12H, br, M-(O)-CH$_2$CH$_2$CH_2CH$_3$,Bu and OBu), 1.53 (12H, br, M-(O)-CH$_2$CH_2CH$_2$CH$_3$,Bu and OBu), 2.25 (24H, s, N-CH_3, TMEDA), 2.35 (8H, m, N-CH_2, TMEDA), 3.63 (8H, br, M-O-CH_2CH$_2$CH$_2$CH$_3$,OBu). The relatively low solubility of **52** over prolonged periods of time in C$_6$D$_{12}$ solutions precluded the collection of its ^{13}C{^{1}H} spectrum. ^{7}Li NMR (155.50 MHz, 300 K, C$_6$D$_{12}$): δ 0.99.

Elemental Microanalysis calculated for **52**; C, 64.58; H, 12.95; N, 8.37%; found: C, 62.19; H, 13.31; N, 8.28%.

1.5.5 Synthesis of 55, [TMEDA·LiMg^{n}Bu$_3$]$_x$

^{n}BuLi (2.5 mL, 4 mmol of 1.6 M solution in hexanes) was dissolved in 15 mL of dried hexane in an oven-dried Schlenk tube. 4 mmol of ^{n}Bu$_2$Mg (4 mL of 1 M solution in heptanes) were ad ded and solution turned slightly turbid. After stirring for 30 minutes, 4 mmol of TMEDA (0.60 mL) were added. The mixture was gently heated to yield a transparent colourless solution. This solution was transferred to a freezer operating at −35°C, affording colourless crystals after 48 hours. (0.75 g, 59%).

^{1}H NMR (400.13 MHz, 300 K, C$_6$D$_{12}$): δ −0.75-−0.31 (6H, br, M-CH_2CH$_2$CH$_2$CH$_3$, Bu), 0.84 (9H, t,^{3}J$_{HH}$=7.3 Hz,M-CH$_2$CH$_2$CH$_2$CH_3, Bu), 1.21-1.30 (6H, m, M-

CH$_2$CH$_2$CH_2CH$_3$, Bu), 1.46-1.54 (6H, m, M-CH$_2$CH_2CH$_2$CH$_3$, Bu), 2.28 (12H, s, N-CH_3, TMEDA), 2.34 (4H, s, N-CH$_2$, TMEDA). ^{13}C{^{1}H} NMR (100.62 MHz, 300 K, C$_6$D$_{12}$): δ 10.8 (M-CH$_2$CH$_2$CH$_2$CH$_3$, Bu), 14.2 (M-CH$_2$CH$_2$CH$_2$$CH_3$, Bu), 32.4 (M-CH$_2CH_2$$CH_2CH_3$, Bu), 33.0 (M-CH$_2$$CH_2CH_2CH_3$, Bu), 46.7 (N-$CH_3$, TMEDA) 57.9 (N-$CH_2$, TMEDA). ^{7}Li NMR (155.50 MHz, 300 K, C$_6$D$_{12}$): δ 0.84.

Elemental Microanalysis calculated for **55**; C, 67.82; H, 13.60; N, 8.79%; found: C, 66.23; H, 12.65; N, 8.71%.

1.5.6 Synthesis of 56, [[(dioxane)·Li(μ-^{n}Bu)$_2$Mg(μ-^{n}Bu)]$_2$]$_\infty$

^{n}BuLi (0.125 mL, 2 mmol of 1.6 M solution in hexanes) was dissolved in 5 mL of dried hexane in an oven-dried Schlenk tube. 2 mmol of ^{n}Bu$_2$Mg (2 mL of 1 M solution in heptanes) were added, turning the solution slightly turbid. After stirring for 30 minutes, 2 mmol of 1,4-dioxane (0.17 mL) were added. All the volatiles are removed under vacuum and the white precipitated was suspended in 5 mL of dried benzene. Addition of 2 mL of dried toluene and vigorously heating afforded a colourless solution. The flask containing the colourless solution was placed in a Dewar flask of hot water and allowed to cool slowly to ambient temperature affording colourless needles. (0.27 g, 47%).

^{1}H NMR (400.13 MHz, 343 K, D$_8$-tol): δ –0.31 (12H, t, ^{3}J$_{HH}$=7.2 Hz M-CH_2CH$_2$CH$_2$CH$_3$, Bu), 1.09 (18H, t, ^{3}J$_{HH}$=7.2 Hz, M-CH$_2$CH$_2$CH$_2$CH_3, Bu), 1.52-1.61 (12H, m, M-CH$_2$CH$_2$CH_2CH$_3$, Bu), 1.71-1.79 (12H, m, M-CH$_2$CH_2CH$_2$CH$_3$, Bu), 3.39 (16H, s, dioxane). ^{13}C{^{1}H} NMR (100.62 MHz, 343 K, D$_8$-tol): δ 4.8 (M-CH$_2$CH$_2$CH$_2$CH$_3$, Bu), 9.6 (M-CH$_2$CH$_2$$CH_2CH_3$, Bu), 26.9 (M-CH$_2$$CH_2CH_2CH_3$, Bu), 62.4 (M-CH$_2CH_2$$CH_2CH_3$, Bu) 132.6 ($CH_2$, dioxane). ^{7}Li NMR (155.50 MHz, 343 K, D$_8$-tol): δ 0.67.

Elemental Microanalysis calculated for **55**; C, 66.11; H, 12.14; found: C, 60.93; H, 13.34%.

Chapter 2. Lithium magnesiates in asymmetric synthesis

2.1 Summary

Chapter 2 focuses on the employment of chiral bimetallic bases to perform asymmetric deprotonation reactions of prochiral ketones.

The employment of (*R,R*)-TMCDA ((*R,R*)-*N,N,N',N'*-tetramethylcyclohexane-1,2-diamine) (**4**) as a chiral centre did not afford any enantiomeric excess. As such efforts turned to building magnesiates derived from the the chiral amine (+)-bis-[(*R*)-1-phenylethyl]amine (PEA(H), **57**-(H)).
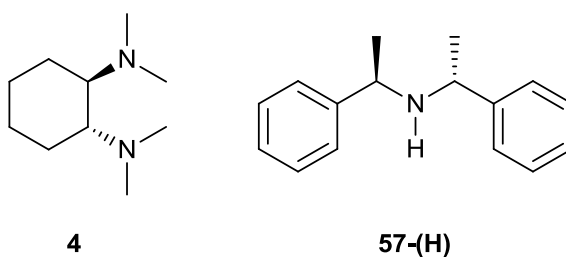
Figure 2.1 ChemDraw representation of (*R,R*)-TMCDA (**4**) and PEA(H) (**57**-(H)).

During the asymmetric deprotonation of 4-*tert*-butylcyclohexanone, the combination of the lithium amide LiPEA (Li-**57**) and a second organometallic compound affords an enhancement in the enantioselectivity of the process from 25% to 46% of enantiomeric excess under the same reaction conditions.

An evaluation of effect of those reaction conditions (such us the solvent, the addition of lithium chloride, the employment of different donors or the use of different amounts of chiral amine) on the outcome of the reaction has been studied.

Solution studies of the bimetallic complex in solution, has been performed in order to gain insights into the equilibrium processes that take place when the chiral lithium magnesiate is synthesised.

2.2 Introduction

2.2.1 Employment of (*R,R*)-TMCDA

Ancillary ligand (*R,R*)-TMCDA (**4**) has been commonly employed in asymmetric synthesis.[94]

For example, Uemura and co-workers performed the enantioselective *ortho-*lithiation of substituted ferrocenes using *n*BuLi/(**4**) with enantiomeric excesses of around 62%.[95] Most recently, Strohmann has shown how these ferrocene derivatives can be lithiated using *i*PrLi and catalytic amounts of (**4**) obtaining enantiomerics ratio up to 99:1.[96] An interesting aspect which must be considered is how altering the solvent mixture dramatically affects the enantioselectivity. Thus, the reaction occurred with no enantioselectivity (e.r.=50:50) when a mixture THF/pentane was employed as solvent.
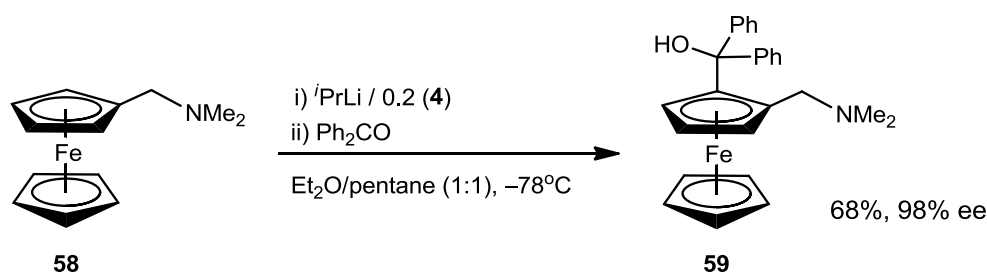
Figure 2.2 Enantioselective metalation of ferrocenes in presence of catalytic amounts of (*R,R*)-TMCDA (**4**).

Although there are exceptions in the literature, (*R,R*)-TMCDA is considered a relatively poor ligand for inducing enantioselectivity. Wiberg and Bailey investigated the divergent behaviour of (–)-sparteine (**60**) and (*R,R*)-TMCDA as chiral auxiliaries for the deprotonation of N-Boc-pyrrolidine with *i*PrLi.[97] They studied the lowest-energy intermediate complexes and transition states forming during the deprotonation of the pro-*S*-hydrogen (namely the transition state that will end up as the *S*-enantiomer) and the pro-*R*-hydrogen by using both chiral ligands. They found that, predominantly due to steric reasons, the difference in the energy of the transition states of the complex formed by (*S,S*)-TMCDA was very small (0.4 Kcal).

Despite multiple applications of organolithium reagents in synthesis, their high reactivity can be problematic during the deprotonation of carbonyl compounds.[98] In these reactions the substrate may also undergo an addition of the alkyl group across the carbonyl carbon affording, after work up, the corresponding tertiary alcohol.

For this reason, synthetic chemists also study the sterically more encumbered lithium amides.

2.2.2 Chiral lithium amides

The main advantage of lithium amides in deprotonation reactions (in comparison with the classical organolithium compounds) is their strong Lowry-Brønsted basicity and relatively low nucleophilic character which allows them to work as efficient deprotonation reagents, generating a lithium enolate from carbonylic compounds. However, lithium amides exhibit similar properties to organolithiums in terms of aggregation and solvation.[99]

Structural features of alkali-metal amides will be covered in Chapter 5 and this section will focus on the reactivity of these complexes.

Chiral lithium amides have been successfully employed hitherto in several different types of reaction[100] which will be reviewed in the following pages. In each of these reactions the chiral base discriminates between a pair of protons in a substrate to produce enantiomerically-enriched chiral product.

2.2.2.1 Asymmetric rearrangement of epoxides

The asymmetric induction with metal amides has been intensively studied since Whitesell and Felman employed for first time a chiral lithium amide to rearrange an epoxide (**61**) to an allylic alcohol (**62**) with a moderately good enantiomeric excess (36%) (**Scheme 2.1**).[101]
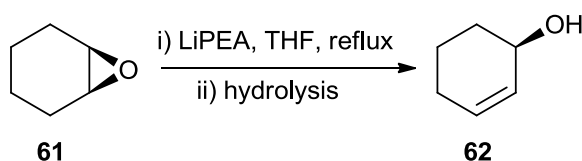
Scheme 2.1. First asymmetric deprotonation with chiral lithium amides.

A notable change in the selectivity of the reaction is observed during the rearrangement of 3-substituted cyclopentene oxides.

Milne and Murphy reacted lithium ((1*R*,2*S*)-1-oxido-1-phenylpropan-2-yl)amide (**63**) with a benzyl protected epoxide (**64**) to produce the corresponding allylic alcohol in 80% of yield (**Scheme 2.2**).[102] Curiously, when Hodgson employed the hydroxy-derivative **66** he found the asymmetric induction was the opposite to that found by Murphy (**Scheme 2.3**).[103]
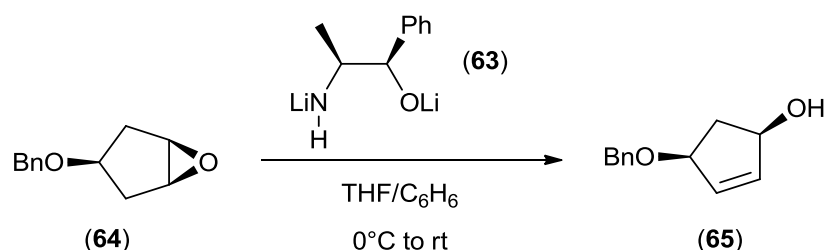
Scheme 2.2. Rearrangement of epoxides to the (*R*)-allylic alcohol.
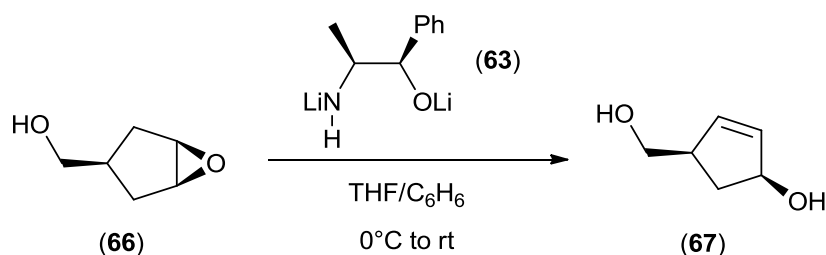
Scheme 2.3. Rearrangement of epoxides to the (*S*)-allylic alcohol.

2.2.2.2 Functionalisation of tricarbonyl(η^6-arene)chromium complexes

Lithium amide LiPEA is a commonly utilised base for the deprotonation of arene-tricarbonylchromium complexes containing directing groups to produce *ortho*-substituted derivatives. Simpkins and co-workers studied the relationship between the size of the directing group and the enantioselectivity of the reaction (**Scheme 2.4**).[104]

-R	Yield	ee(%)
Me	83	84
Et	82	81
^{i}Pr	65	90
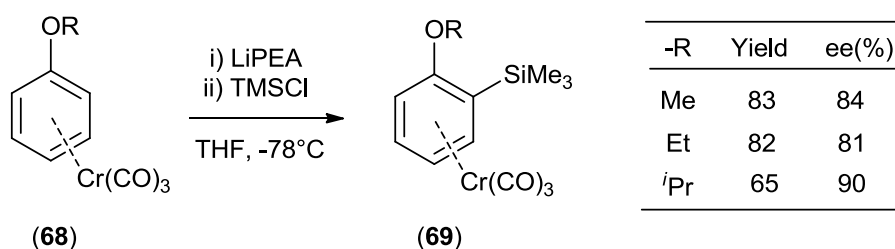
Scheme 2.4 Enantiomeric excess and yield values as a function of the directing group size.

Beside ethers, mono-substituted arenes containing different directing groups such as cyclic amines, carbamates, amides or tertiary amines have been studied in deprotonation reactions.[100] They all exhibit a high selectivity when LiPEA is employed.

However, when the same base is used to deprotonate the benzylic position of the arene complexes, the enantioselectivity notably decreases. Gibson and co-workers performed the deprotonation by adding LiCl (**13**) to the reaction but the optimum enantiomeric excess was only 22%.[105]

Mongin and co-workers combined chiral lithium amide with a second organometallic compound in order to create a chiral bimetallic base capable of deprotonating substituted ferrocenes (**70**) with good enantiomeric excess.[106] They reacted three equivalents of the chiral lithium amide LiPEA with one equivalent of $MgCl_2$ in order to form the lithium magnesiate $[LiMg(PEA)_3 \cdot 2LiCl]$ (**Scheme 2.5**). The employment of this bimetallic complex improves the conversion of the reaction from 19% (obtained when only LiPEA is used as a base) to 80%. However, the enantiomeric excess of the process decreases from 21% to 6%.
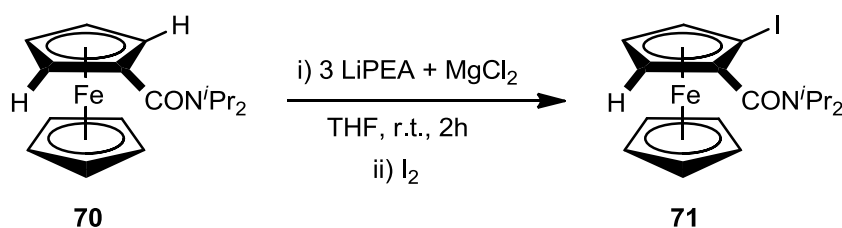
Scheme 2.5 Deprotonation of substituted ferrocenes with 3 LiPEA + $MgCl_2$.

2.2.2.3 Enantioselective deprotonation of prochiral ketones

Deprotonation of 4-substituted cyclohexanones with lithium chiral amides has been widely studied since the pioneering work of Koga[107] and Simpkins.[108]

Koga and co-workers described the first enantioselective deprotonation of prochiral 4-alkyl-cyclohexanones under Corey's internal quench method, finding enantiomeric excesses of up to 97%.[107]

They found that the degree of asymmetric induction is directly related to the bulkiness of the alkyl groups in the cyclohexanones. If the substituent creates a high steric hindrance, only conformers with the substituent in an equatorial disposition are significantly produced.[109] In such systems, there is a stereoelectronic preference for removal of the axial protons and a suitably chosen chiral base should be able to discriminate between the two protons to generate preferentially one enantiomer.[100]
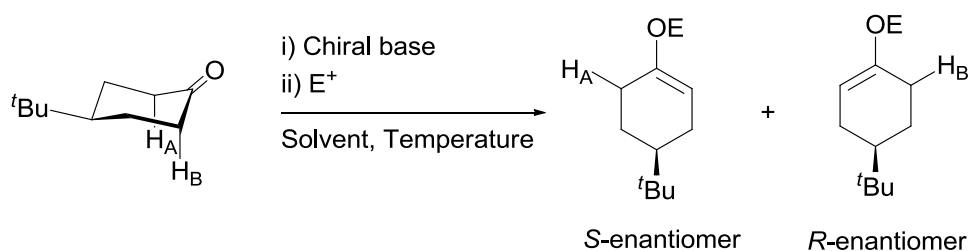
Scheme 2.6 Differentiation of the enantiotopic protons by chiral base.

Examples of chiral lithium amides employed in asymmetric synthesis are numerous.[110] Koga studied the reactivity of different fluorine-containing chiral lithium amides[111] as well as various chelated chiral amines[112] and Corey explored the reactivity of lithium N-trityl-N-(*R*)-1-phenylethylamide (Li-(**72**)).[113]
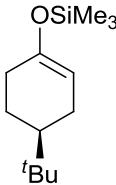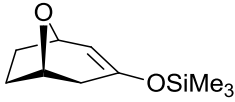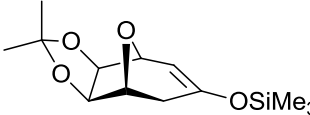
Since LiPEA is an excellent base in asymmetric deprotonation, studies to improve the reactions conditions of the process have been carried out.

Simpkins et al. carried out a study using three different cyclohexanones by comparing the enantioselectivity obtained when internal or external quench protocols were employed (**Table 2.1**).[114]

They found that much lower enantioselectivities were achieved when external quench (EQ) conditions were employed compared when internal quench (IQ), commonly known as Corey's method,[115] is employed. As in the internal quench method, the LiCl (**13**) is liberated as the enolisation proceeds, the next step was to evaluate the enantioselectivity by adding LiCl in external quench conditions and they found higher enantioselectivity than in the absence of LiCl.

Thus, the good enantioselectivity is not limited to the SiMe$_3$Cl-internal quench protocol and can be achieved with a range of different electrophiles.

Table 2.1 The values for the enantiomeric excess of the silyl enol ethers obtained from the deprotonation of the corresponding cyclic ketones with LiPEA in THF at −78°C.

Silylenol ether			
EQ	33%	27%	23%
IQ	82%	70%	69%
EQ + LiCl	82%	58%	83%

Lipshutz et al. studied the interaction in solution between the lithium amide LDA (lithium diisopropylamide, Li-(**73**)) and the electrophile TMSCl.[116] They performed ^{1}H and ^{7}Li NMR spectroscopy experiments at low temperature and they showed that there is a partial generation of LiCl (**13**) as a consequence of the silylation of the lithium amide (**Scheme 2.7**). They also suggested that when similar reactions take place in enantioselective transformations, that small amounts of LiCl can help to improve the enantioselectivity of the processes.
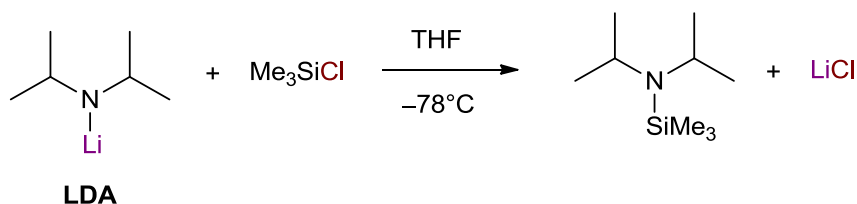
Scheme 2.7 Silylation of LDA by TMSCl.

Mayewski and co-workers deprotonated the tropinone and added different quantities of LiCl (**13**) (**Scheme 2.8**).[117] The most striking result was that the enantioselectivity is even more enhanced when **13** is generated *in situ* by premixing the hydrochloride salt of the chiral amine (HCl·PEA) and ^{n}BuLi.

LiCl (eq)	ee (%)
-	35
0.25	78
0.5	85
1	88
1 (in situ)	95
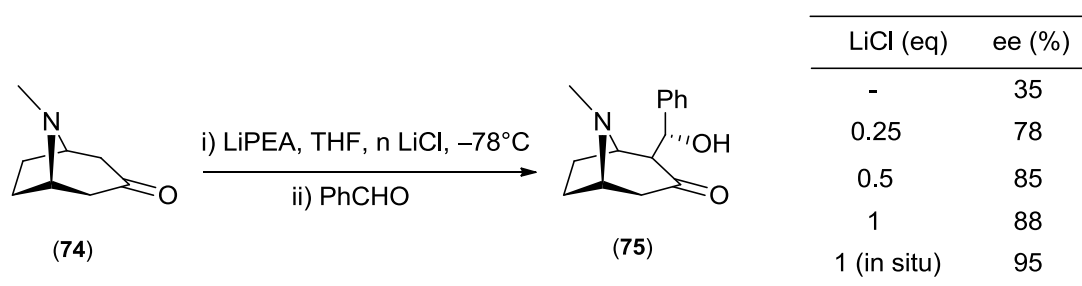
Scheme 2.8 Asymmetric deprotonation of tropinone with LiPEA.

Koga et al. studied by NMR spectroscopy the solution structure of the lithium amide LiPEA upon the addition of LiCl.[118] Their conclusion was that the LiCl changes the structure of the lithium amide in solution and the deprotonation of the ketone takes place through an eight-membered ring.

They also studied the solution structures of the mixed aggregates between LiPEA and LiCl.[119] When LiCl is added to the reaction, they suggested a ladder-like trimer composed of two lithium amides and one LiCl is formed (**Figure 2.3 a**). As the concentration of LiCl unit increases the trinuclear disappears in favour of a dinuclear between the LiPEA and LiCl (**Figure 2.3 b**).
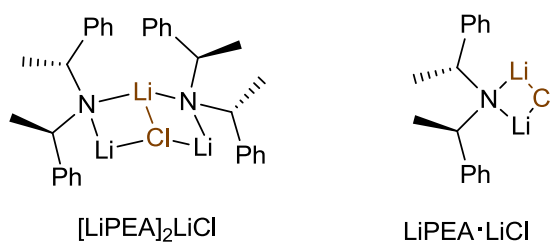
Figure 2.3 Solution structureof the mixed aggregates LiPEA·LiCl.

As it has been seen, asymmetric deprotonation with chiral lithium amides offers good yields and enantioselectivities as long as the reaction is carried out at low temperature and appropiate additives are added.

Therefore, in recent years, the use of chiral magnesium amide bases has been explored.

2.2.3 Deprotonation with chiral magnesium bis(amide) complexes

Magnesium bis(amide) complexes are fast becoming powerful agents for use in organic synthesis.[120] Kerr and co-workers have studied the role of a wide range of magnesium bis(amide) complexes in the asymmetric deprotonation, successfully performing the deprotonation of the prochiral ketones.[121-124] They obtained enantioselectivities up to 80% when the reaction was carried out at temperatures of –20°C (**Scheme 2.9**) using (PEA)$_2$Mg as base.[125]

-R	Conv (%)		ee (%)	
	-20°C	-78°C	-20°C	-78°C
^{t}Bu	93	93	76	86
Me	96	96	80	90
^{n}Pr	96	92	78	88
^{i}Pr	95	96	74	86
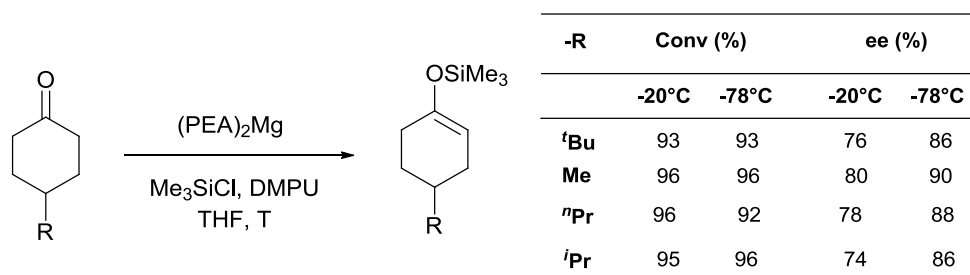
Scheme 2.9 Asymmetric deprotonation with chiral magnesium bis(amide) complexes.

As highlighted in Chapter 1, energy efficiency is becoming a must in modern chemistry, demanding conditions that are incompatible with asymmetric synthesis when simple monometallic reagents are employed.

Over the past years, a new category of bimetallic deprotonating reagents has been investigated[126] and Chapter 2 highlights some of this with respect to the asymmetric deprotonation of prochiral ketones with chiral lithium magnesiates.[127]

The first chiral amine that was evaluated was (*R,R*)-TMCDA, and the results obtained are shown in paragraph 2.3.1.

2.3   Results and discussion

All the reactions were performed in triplicate to ensure the reproducibility of the data.

2.3.1   Utilisation of (*R,R*)-TMCDA as chiral ancillary ligand

Two lithium magnesiates stabilised by (*R,R*)-TMCDA have been employed for the asymmetric deprotonation of 4-tert-butylcyclohexanone (**76**).

The lithium magnesiate [(*R,R*)-TMCDA·Li(μ-^{n}Bu)$_2$Mg(^{n}Bu)]$_2$ (**51**), characterised in Chapter 1, was also employed in the deprotonation of the ketone (**Scheme 2.10**).
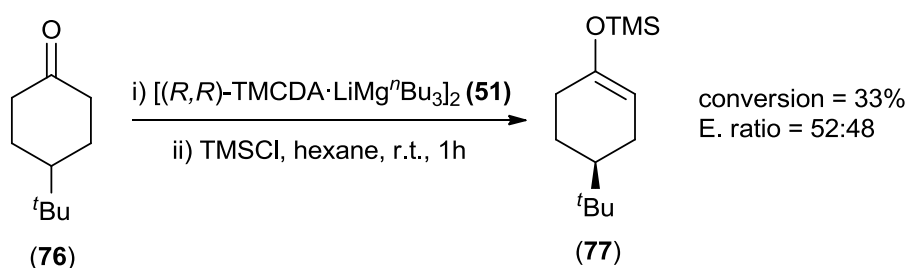
Scheme 2.10 Deprotonation with [(*R,R*)-TMCDA·LiMg(^{n}Bu)$_3$]$_2$ (**51**).

The results from this reaction, when either the crystals of the dimer or the base generated in situ were utilised, were the same. The low conversion to the silyl enol ether is due to several side products being formed in the reaction. When one equivalent of **76** was treated with one lithium magnesiate

51 the conversion of the reaction was 33% with enantiomeric excess of 4%. The main product of the reaction is the nucleophilic addition of the butyl group to the carbonylic carbon (62%). As discussed on page 4, lithium magnesiates can often function as good nucleophiles with respect to ketones.

Chapter 1 has been focused on alkyllithium magnesiates, but there are some examples in the literature of heteroleptic lithium magnesiates which combine amido and alkyl groups.[128, 129]

In order to avoid the alkyl addition and to improve the conversion of the reaction towards the formation of the silyl enol ether, the lithium magnesiate "[(R,R)-TMCDA·LiMg(TMP)$_2$^{n}Bu]" (**78**) was employed as a deprotonation agent (**Scheme 2.11**). Complex **78** was synthesised by the reaction of the homoleptic lithium magnesiate [(R,R)-TMCDA·Li(μ-^{n}Bu)$_2$Mg(^{n}Bu)]$_2$ (**51**) with two equivalents of TMP(H) (2,2,6,6-tetramethylpiperidine, (**79**)-(H)) in hexane.

In this case, the deprotonation affords the silyl enol ether **77** in a 97% of conversion but the enantioselectivity of the process is still very moderate, as the enantiomeric ratio is 52:48 pro the *S*-enantiomer.

i) (R,R)-TMCDA·LiMg(TMP)$_2$^{n}Bu (**78**)

ii) TMSCl, hexane, r.t., 1h

conversion = 97%
E. ratio. = 52:48

76   **77**
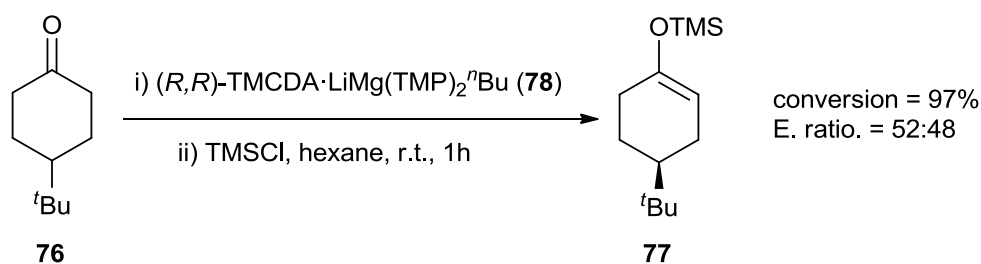
Scheme 2.11 Deprotonation of 4-*tert*-butylcyclohexanone with lithium TMP-magnesiate **78**.

After the good results obtained with respect to conversion with the heteroleptic lithium magnesiate to avoid the formation of the addition product, a new chiral lithium magnesiate has been employed to evaluate the deprotonation of prochiral ketones, but due to the low enantioselectivities

obtained with (*R,R*)-TMCDA (**4**), the next step was to move away from a chiral ancillary and instead use a chiral amine which can be envisaged to link together the two metal centres.

The amine of choice was (+)-bis[(*R*)-1-phenylethyl]amine, PEA(H) (**57**-H) as it has been employed previously in asymmetric transformations providing good values of enantioselectivity, as showed in the introduction.

2.3.2   Utilisation of PEA(H) as chiral centre

Following the synthetic procedure of **78**, two equivalents of the chiral amine PEA(H) were added to the lithium magnesiates **48**, **49**, **51**, and **55** in order to obtain a heteroleptic amido-alkyllithium magnesiate (**Scheme 2.12**).

i) (Donor)·LiMg^{n}Bu$_3$ + 2 PEA(H)

ii) TMSCl, hexane, r.t., 1h

76   **77**
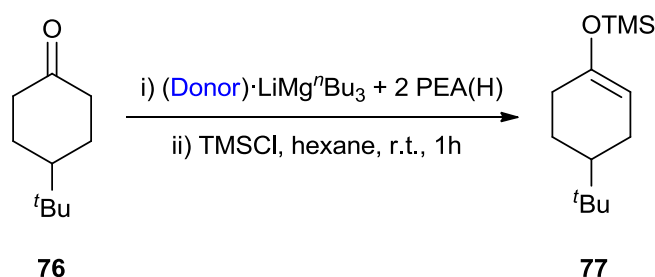
Scheme 2.12 Deprotonation of 4-*tert*-butylcyclohexanone with a chiral lithium magnesiate incorporating the chiral amide **57**, stabilised with different donors.

2.3.2.1 Evaluation of the donor in affecting the outcome of the enantioselective deprotonation.

Table 2.2 summarises the results of the asymmetric deprotonation of 4-*tert*-butylcyclohexanone by diferent lithium magnesiates with general formulae [(Donor)·LiMg(PEA)$_2$^{n}Bu].

Similarly to the results obtained with employment of TMP(H) (**79**-(H)), there is no presence of the 1,2-addition product after the treatment of the ketone with the lithium magnesiates in hexane.

Table 2.2 The effect of adding one equivalent of the donor on the deprotonation of 4-*tert*-butylcyclohexanone.

Compound	Donor	Conversion (%)	E. Ratio
48	TMPDA	84	53 : 47
49	PMDETA	97	62 : 38
51	(*R,R*)-TMCDA	84	66 : 34
55	TMEDA	81	70 : 30

The enantioselectivity of the process was improved when (PEA(H)) was employed as chiral centre as the enantiomeric excess obtained in all the cases is greater than the one obtained when (*R,R*)-TMCDA (**4**) was incorporated to the base.

The highest enantiomeric excess (40%) is found when TMEDA-stabilised complex (**55**) was employed as ancillary ligand, with a conversion of 81%. Both (*R,R*)-TMCDA (**51**) and TMPDA (**48**) complexes afforded a conversion of 84%; however, the lowest enantiomeric excess (6%) was found when TMPDA was employed. When PMDETA-stabilised compound (**49**) was used, the conversion of the reaction was almost quantitative and the enantiomeric ratio of the silyl enol ether was 62:38.

With the aim of getting better enantoselectivities, it was decided to systematically study all the different components of the reaction system of the deprotonation reaction with complex "(TMEDA)·LiMg(PEA)$_2$^{n}Bu" (**80**), as this provided the highest enantiomeric excess.

The next few sections (2.3.2.2 to 2.3.2.4) show the study of the influence of the bulk solvent, the addition of salts or changing the number of equivalents of chiral amine on the outcome of the reaction.

2.3.2.2 Evaluation of the bulk solvent employed during the deprotonation.

The solvent in which an enantioselective reaction is carried out can often dramatically alter its conversion and its selectivity.

Strohmann performed a selective *ortho*-lithiation of a ferrocene derivative in presence of (*R,R*)-TMCDA (**4**) in catalytic amounts, showing that presence of diethyl ether in the media is a prerequisite for the catalytic activity of **4**.[96] When the reaction was performed in pentane, the yield was only 17% while the addition of diethyl ether in a 12:1 ratio with pentane increases the yield to 93%.

Haddad reported that the asymmetric hydrogenation of hydrazones was also highly influenced by the reaction solvent.[130] He discovered that the optimal condition was when methanol was used, giving a conversion of 100% and the enantiomeric excess of 85%. The selectivity and conversion both decrease when other bulkier alcohols like ethanol or 3-pentanol were used. Curiously, the use of non-coordinating solvents such as dichloromethane or 1,2-dichloroethane yielded an inversion of the enantioselectivity.

Zhang had found the same effect in the enantioselectivity during the hydrogenation of itaconates.[131] While both dichloromethane and 2,2,2-trifluoroethane afford the *R*-enantiomer, the use of acetone or ethyl acetate leads to the *S*-enantiomer.

Having a look at achiral systems, another astonishing solvent effect is found in the nucleophilic addition of Grignard and organolithium compounds to ketones using Deep Eutectic solvents (DES).[132] In this case, the solvent reacts with the alkylation agent (**Figure 2.4**), and favouring nucleophilic addition over the competing hydrolysis process, so the reaction can be carried out *in air* at ambient temperature.
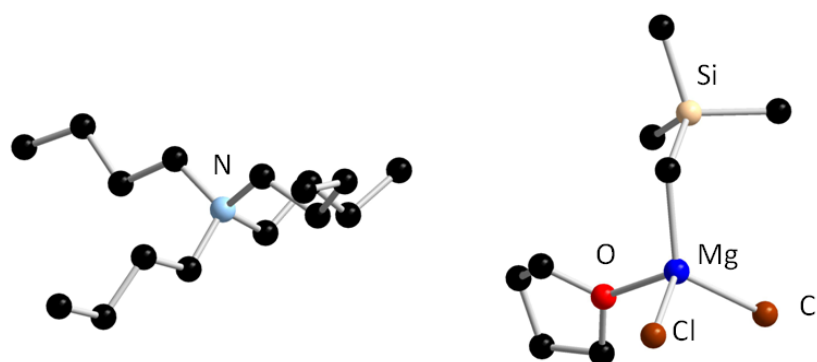
Figure 2.4 Product of the reaction between the deep eutectic solvent $^{n}Bu_4NCl$ and $(Me_3SiCH_2)MgCl$.

Different solvents have been evaluated in this work in order to evaluate if the employment of them could help to improve the enantioselectivity of the synthesis of chiral silyl enol ethers with the lithium magnesiate with "$[(TMEDA)\cdot LiMg(PEA)_2{}^{n}Bu]$" (**80**) (**Scheme 2.13**).
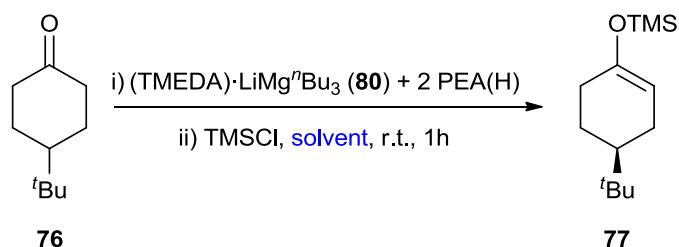
Scheme 2.13 Deprotonation of 4-*tert*-butylcyclohexanone with a lithium magnesiate in different solvents.

The reaction has been carried out in hexane, toluene, diethyl ether, THF and methylcyclohexane. As **Table 2.3** shows, when coordinating solvents are used enantioselectivities are better, the best performing being diethyl ether. With this reaction, 80% of the ketone reacted to form the silyl enol ether with enantiomeric ratio of 73:27. The less effective deprotonation occurs in non-polar methylcyclohexane when the conversion decreases to 45% and the enantiomeric excess diminishes to 20%. Although both, hexane and

methylcyclohexane are aliphatic hydrocarbon solvents, it could be envisaged that both provide similar results.

Table 2.3 Effect of the solvent during the deprotonation of 4-*tert*-butylcyclohexanone.

Solvent	Dielectric constant	Conversion (%)	E. Ratio
Hexane	1.89	81	70 : 30
THF	7.52	76	71 : 29
Toluene	2.38	80	60 : 40
Diethyl ether	4.27	80	73 : 27
Methylcyclohexane	2.02	45	60 : 40

2.3.2.3 Evaluation of the effect of the addition of lithium chloride

As noted in the previous section, solvent can modify the behaviour of the reactions, but equally important is the addition of salts.[133, 134] Especially when reactions occur through a lithium enolate.[102, 135]

As introduced in Chapter 1, Grignard[6-8] and Hauser[9-12] bases dramatically modify its activity when one molar equivalent of lithium chloride is added to the reaction.

Simpkins *et al.* reported that the addition of LiCl (**13**) during the asymmetric deprotonation of cyclic ketones by chiral lithium amides can have a major effect. They found that the enantioselectivity of the reaction under external quench conditions is lower than when an internal quench protocol is carried out. However, a good enantiomeric excess can be achieved under external quench if LiCl is included in the reaction media.[136]

Nevertheless, salt effects are not always beneficial and can lead to a lower selectivity. Maddaluno reported the detrimental effect of the addition of one equivalent of LiCl on the enantioselectivity of the addition of methyllithium on *ortho*-tolualdehyde, in the presence of chiral lithium amides.[137]

To the best of our knowledge, the only structural example of a bimetallic complex that has been reacted with a metal halide is the solvent separated

compound that Merkel included in his PhD Thesis.[138] This complex was found by serendipitious reaction of the lithium zincate (PMDETA)LiZnMe$_3$ (**81**), which crystallises as a contacted ion pair, and LiCl present in the media. The two compounds react to form the trimetallic complex [(PMDETA)$_2$(Li$_2$Cl)]$^+$[ZnMe$_3$]$^-$ (**82**) (**Figure 2.5**), which crystallises as a solvent separated ion pair. The chlorine is encapsulated by two [(PMDETA)·Li] units to form the cation and the anion is the trimethyl [ZnMe$_3$].
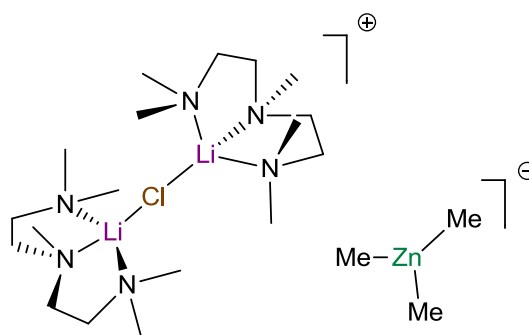
Figure 2.5 ChemDraw representation of [(PMDETA)$_2$(Li$_2$Cl)]$^+$[ZnMe$_3$]$^-$ (**82**).

In this work, the effect of the addition of 0.5, 1, 2 and 4 equivalents of lithium chloride was evaluated. (**Scheme 2.14**)
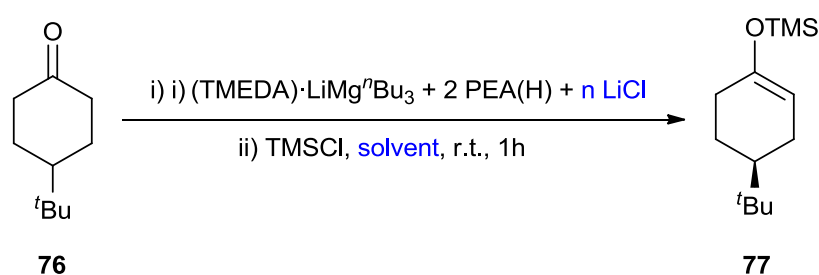
Scheme 2.14 Deprotonation of 4-*tert*-butylcyclohexanone (**76**) with a lithium magnesiate and addition of LiCl (**13**) in different solvents.

Table 2.4 shows the values for the conversion of the achiral ketone into the corresponding silyl enol ether when the reaction is performed in hexane, toluene and diethyl ether.

The addition of lithium chloride (**13**) does not involve a significant change in the conversion. When the reaction is performed in hexane, the conversion diminishes from 81% to 50% when one equivalent of lithium chloride is added to the mixture. In the rest of the solvents the effect of the addition of lithium chloride is smaller; in toluene the conversion is reduced from 80% to 65% when 0.5 or 2 equivalents of LiCl are added while in diethyl ether the lower conversion is found in presence of 0.5 equivalents of salt.

Table 2.4 Conversion (%) of the deprotonation of **76** in presence of LiCl.

Equivalents LiCl	Hexane	Toluene	Diethyl ether
0	81	80	80
0.5	52	65	68
1	50	70	82
2	55	65	74
4	70	88	77
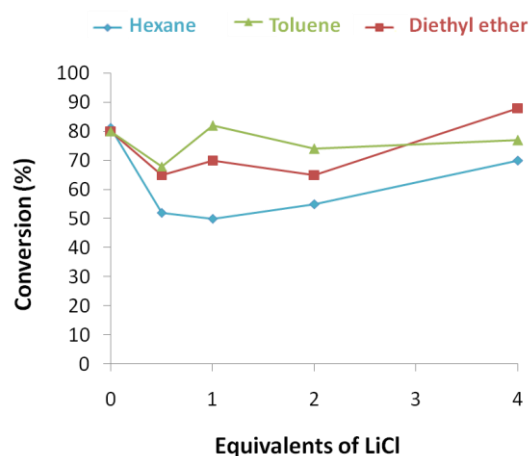
The values for the enantiomeric excesses are displayed in the Table 2.5. The selectivity of the reaction remains practically unchanged, on the addition of one equivalent of lithium chloride, in hexane although; the enantiomeric excess is reduced by 10%. No significant changes in the selectivity of the reaction have been appreciated in the other solvents.

Table 2.5 Selectivity of the deprotonation of **76** in presence of LiCl.

Equivalents LiCl	Hexane	Toluene	Diethyl ether
0	70 : 30	60 : 40	73 : 27
0.5	70 : 30	69 : 31	71 : 29
1	65 : 35	70 : 30	70 : 30
2	66 : 34	70 : 30	70 : 30
4	71 : 29	71 : 29	73 : 27
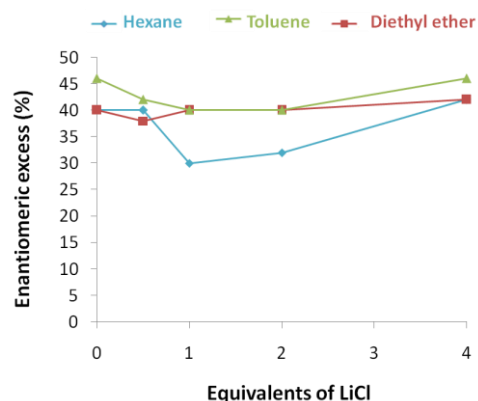
Majewski and co-workers reported how the concentration of the base can affect the enantioselectivity of the reaction of deprotonation of the tropinone with lithium amides,[139] so lower concentrations of the base afforded higher enantioselectivities.

Simpkins performed some competition studies between chiral and achiral lithium amides, concluding that the 1,2-diamines show an enhancement in reactivity.[140]

In this work has been evaluated the behaviour of the base when 0.1, 0.5, 1 and 2 equivalents of the amine are added in hexane, toluene and diethyl ether.

2.3.2.4 Effect of a change in the number of equivalents of chiral amine.

Table 2.6 Influence of the number of equivalents of chiral amine added to the base in hexane, toluene and diethyl ether.

n	Solvent	Conversion (%)			Enantiomeric ratio of silyl enol ether
		Remaining SM 76	Silyl enol ether 77	1,2-addition 83	
2	Hexane	19	81	-	70:30
1		35	29	23	73:27
0.5		28	30	28	66:34
0.1		14	27	41	60:40
2	Toluene	22	78	-	72:28
1		33	38	20	69:31
0.5		14	40	29	65:35
0.1		11	41	39	67:33
2	Diethyl ether	13	87	-	73:37
1		24	52	15	65:35
0.5		16	47	24	57:43
0.1		6	20	50	53:47

The obtained results of the deprotonation with different equivalents of the chiral amine are highlighted in **Table 2.6**.

Regardless of the solvent, when two equivalents of the amine are used to form the base the reaction exclusively undergoes the silyl enol ether (**77**). If the number of equivalents of amine are reduced by half, the conversion to the silyl enol ether notably decreases due to the formation of the *n*-butyl addition product (**83**).

There are two possible explanations for that addition product. One possibility is that the monoamido-bisalkyl lithium amide

"(TMEDA)·LiMg(PEA)^{n}Bu$_2$" (**84**) affords the 1,2-addition product, as well as the deprotonation. Another possibility is that an equilibrium process is taking place, an equilibrium where the monoamido-bisalkyl species disproportionates to the bisamido-monoalkyl (**80**) and trialkyllithium magnesiate (**55**) (**Scheme 2.15**).

(TMEDA)·LiMg(PEA)^{n}Bu$_2$ ⇌ 0.5 (TMEDA)·LiMg(PEA)$_2$^{n}Bu + 0.5 (TMEDA)·LiMg^{n}Bu$_3$

84 **80** **55**
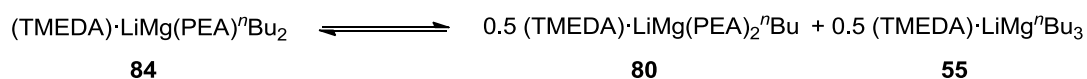
Scheme 2.15 Disproportionation equilibrium of the lithium magnesiate "(TMEDA)·LiMg(PEA)^{n}Bu$_2$" (**84**).

Figure 2.6 represents the conversion of the reaction in hexane. When the number of equivalents of the amine in hexane decreases to one, the conversion to the silyl enol ether (**77**) diminishes to 29%. There is competition between the formation of the silyl enol ether and the 1,2-addition product (**83**), whose chromatographic yield is 21%. This yield becomes greater the number of equivalents of chiral amine is lowered, however, the conversion to the silyl enol ether remains at 30% even when just 0.1 equivalents is added.
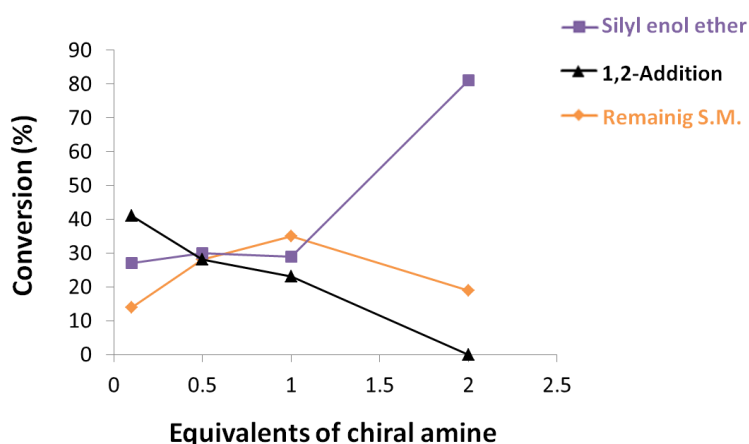
Figure 2.6 Conversion of the reaction in function of the number of equivalents of chiral amine in hexane.

A similar behaviour can be found when the reaction is performed in toluene (**Figure 2.7**). The formation of the 1,2-addition product (**83**) increases when the

amount of chiral amine disminishes. Akin to the case of hexane, the conversion to the silyl enol ether remains the same no matter if 1, 0.5 or 0.1 equivalents of chiral amine were added. In fact, when only 0.1 equivalents of PEA(H) were added, the conversion to the silyl enol ether is 41% and the conversion to the 1,2-addition product is 39%.
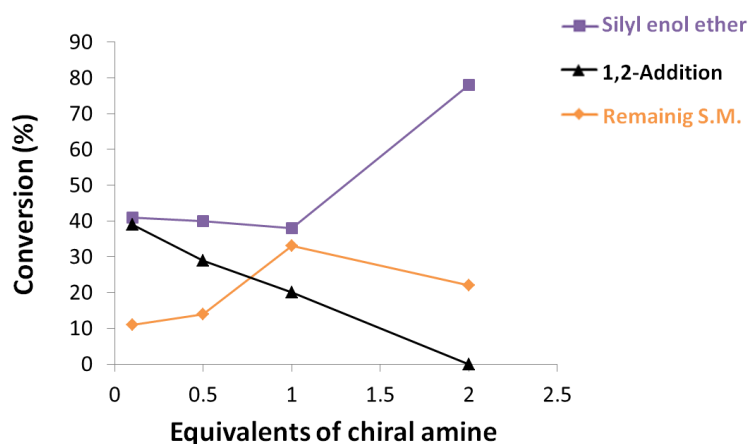
Figure 2.7 Conversion of the reaction in function of the number of equivalents of chiral amine in toluene.

However, when the reaction is performed in diethyl ether (**Figure 2.8**) the conversion to the silyl enol ether diminishes and the formation of **83** when the amount of chiral amine is decreased. The conversion to **83** is 50% when only 0.1 equivalents of amine are added.
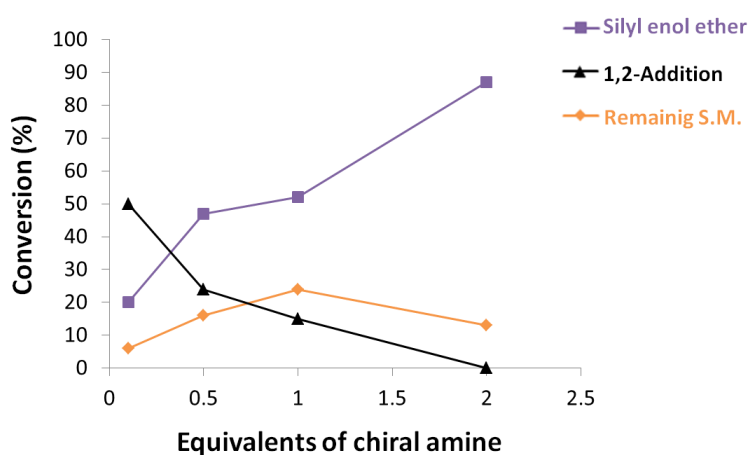
Figure 2.8 Conversion of the reaction in function of the number of equivalents of chiral amine in diethyl ether.

Figure 2.9 shows the enantiomeric excess of the silyl enol ether **77** in different solvents.

When diethyl ether is the bulk solvent of the reaction, the enantiomeric excess decreases as the concentration of **57**-(H) is reduced, being only 6% when 0.1 equivalents are added.
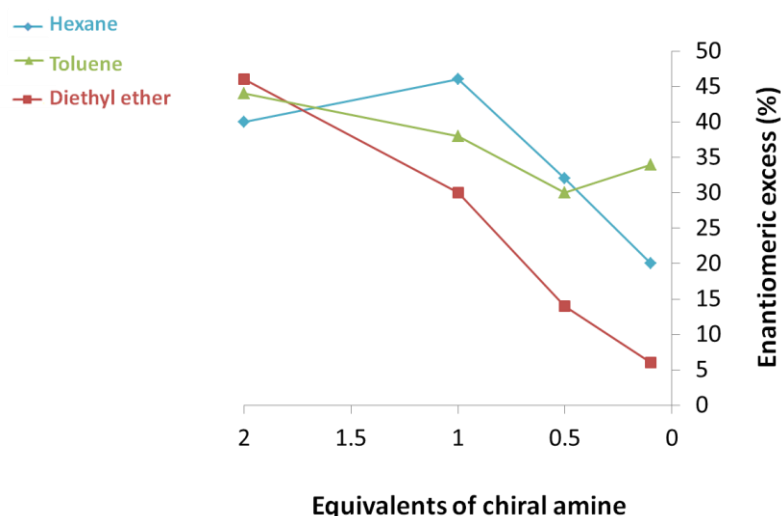
Figure 2.9 Enantiomeric excess of the silyl enol ether in different solvents.

The most remarkable fact is that, in non-coordinating solvents, the enantiomeric excess does not decrease as much as it could be expected when the number of equivalents of PEA(H) is reduced; in fact, the enantiomeric excess remains almost stable when 1, 0.5 or 0.1 equivalents of PEA(H) are added in toluene.

In summary, when 1 or less equivalents of chiral amine are employed in hexane or toluene, the conversion to the silyl enol ether remains stable and, more importantly, the enantiomeric excess does not decrease significantly, being the lowest value 20% when the reaction is carried out in hexane with 0.1 equivalents of PEA(H) (**57**-(H)).

Scheme 2.16 shows the species present in solution when 1 or less equivalents of PEA(H) are used (with **80** being susceptible to undergo an equilibrium process indicated in **Scheme 2.15**). As shown in paragraph 2.3.1, when

alkyllithium magnesiates are employed as bases versus prochiral ketones, the major product is the 1,2-addition product but the deprotonation of the ketone also occurs to some extent. However, the enantiomeric ratio of that silyl enol ether is 50:50.

$$(\text{TMEDA}) \cdot \text{LiMg}^n\text{Bu}_3 + \textbf{n} \text{ PEA(H)} \longrightarrow \textbf{n} \text{ (TMEDA}) \cdot \text{LiMg(PEA)}^n\text{Bu}_2 + \textbf{(1-n)} \text{ (TMEDA}) \cdot \text{LiMg}^n\text{Bu}_3$$

55   **57-(H)**   **80**   **55**
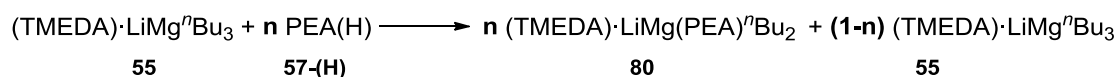
Scheme 2.16 Species present in solution when 1 or less equivalents of chiral amine are employed in the reaction.

These results indicate that the amido-containing species **80** reacts as deprotonating agent faster than **55**. If the alkyl substituent was bulky enough to avoid nucleophilic addition, the asymmetric deprotonation of ketones could in theory be performed with *catalytic* amounts of chiral amine. Therefore, paragraph 2.3.2.5 shows the results of the deprotonation of **76** employing bulky diorganomagnesium compounds.

2.3.2.5 Catalytic asymmetric deprotonation of the 4-*tert*-butylcyclohexanone.

Koga presented a catalytic deprotonation of 4-substituted cyclohexanones with a chiral diamine (**Scheme 2.17**).[141] NMR spectroscopic studies showed that lithium-hydrogen interchange between an achiral tridentate lithium amide (Li-**86**) and a chiral bidentate amine (**85**) occurs rapidly in THF, favouring the formation of the bidentate lithium amide so it was possible to deprotonate the prochiral ketone in presence of stoichiometric quantities of achiral amine and catalytic amounts of the chiral amine with enantiomeric exccess up to 80%.
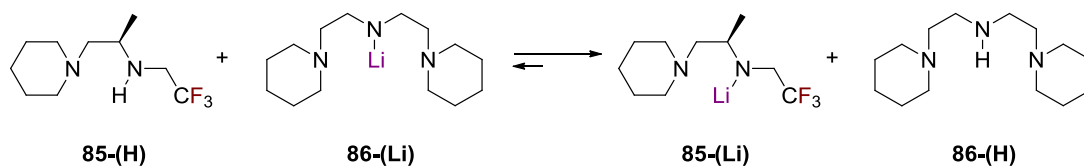
Scheme 2.17 Lithium-hydrogen interchange between a bidentate amine (**86**) and an tridentate lithium amide (Li-(**85**)).

Studies of the asymmetric catalytic deprotonation of the 4-*tert*-butylcyclohexanone (**76**) will be detailed below.

With the aim of improving the obtained results during the catalytic deprotonation, a series of experiments with different magnesium derivatives were reacted with 0.1 equivalent of the chiral amine in presence of TMEDA (**5**) (**Table 2.7**).

Table 2.7 Conversion and enantiomeric ratio values for the catalytic deprotonation of the 4-*tert*-butylcyclohexanone (**76**) with different magnesium derivatives and addition of LiCl (**13**).

		n = 0		n = 1	
	R$_2$Mg	**Conv. (%)**	**E. ratio**	**Conv. (%)**	**E. ratio**
88	^{t}Bu$_2$Mg	71	53 : 47	58	53 : 47
89	Np$_2$Mg	81	58 : 42	68	58 : 42
90	Ph$_2$Mg	51	58 : 42	25	55 : 45
91	*p*-Tol$_2$Mg	48	56 : 44	33	60 : 40
92	(CH$_2$SiMe$_3$)$_2$Mg	32	55 : 45	30	54 : 46

Moreover, reactions were carried out by adding one equivalent of lithium chloride to evaluate if the addition of salts affects the reactivity or selectivity of the process.

Table 2.7 shows the results obtained for the catalytic deprotonation of 4-*tert*-butylcyclohexanone (**76**) into the silyl enol ether (**77**) and the enantiomeric ratio of this product.

To avoid the formation of **83**, *tert*-butyllithium (**87**) has been employed instead of *n*-butyllithium (**22**) and magnesium derivatives have been replaced for bulkier organometallic reagents. Di-*n*-butylmagnesium (**24**) has been replaced by a series of dialkylmagnesium compounds that were synthesised by shifting the Schlenk equilibrium towards the formation of the dialkylmagnesium by addition of dioxane to the media. The synthetic procedure is detailed in page 160.

The use of bulkier substrates improves the conversion of the ketone **76** into the silyl enol ether **77**, giving conversions up to 80% when the dineopentylmagnesium (**89**) is employed. There is a direct correlation between the bulkiness of the alkyl group and the conversion to the silyl enol ether (**77**), as the bulkier the group, the higher the conversion.

However, the enantiomeric excess found for **77** is not ideal. When **89** is employed to form the bimetallic base, the enantiomeric excess of the product is 16%. Even though the conversion to the alcohol **83** has been minimised, the alkyllithium magnesiate seems to be acting as a deprotonating agent, decreasing the enantioselectivity of the process.

Furthermore, the consequence of adding lithium chloride (**13**) has been studied to see how it affects the reactivity of the catalytic process. As it can be seen in **Table 2.7**, the presence of this salt in the reaction media has a detrimental effect in the formation of the silyl enol ether while the enantioselectivity does not seem to be affected by **13**.

Coming back to stoichiometric reactions, and inspired by the work of Mongin and co-workers,[106] the combination of the chiral lithium amide LiPEA with an

organometallic reagents other than $^{n}Bu_2Mg$ could lead in theory to better enantioselectivities for the process.

The next paragraph highlights the work involving the deprotonation of the 4-*tert*-butylcyclohexanone (**76**) with different "ate" complexes formed by combination of LiPEA with a second metal reagent.

2.3.2.6 Evaluation of adding different metal reagents to LiPEA

The formation of the "ate" complex is performed in THF solution to avoid problems with solubilities.

LiPEA is combined with salts such us $CoBr_2$ (**93**), $MgBr_2$ (**94**) or $ZnCl_2$ (**95**) in order to form a complex with formula [M(PEA)X·LiX] through a salt metathesis approach, and also with organometallic reagents such as Me_2Zn (**96**) or $^{i}Bu_3Al$ (**98**) to form a bimetallic complex through co-complexation reactions. The results of the deprotonation of **76** with these complexes in THF at ambient temperature are highlighted in **Table 2.8**.

In the absence of any other metallic centre, the deprotonation of **76** with LiPEA in THF at ambient temperature yields **77** in 76%. The conversion of the reaction dramatically decreases when inorganic salts are combined with LiPEA. On the other hand, the conversion is improved when the bimetallic complex is formed by co-complexation of LiPEA with a second organometallic reagent like Me_2Zn (**96**), $^{t}Bu_2Zn$ (**97**) or $(CH_2SiMe_3)_2Mg$ (**100**).

Table 2.8 Outcome of adding different reagents to chiral LiPEA in the asymmetric deprotonation of **76** at 0°C for 1 hour.

	R$_x$M	Conv. (%)	R. Ratio
	-	76	60 : 40
93	CoBr$_2$	4	-
94	MgBr$_2$	0	-
95	ZnCl$_2$	25	65 : 35
96	Me$_2$Zn	99	58 : 42
97	^{t}BuZn	98	60 : 40
98	^{i}Bu$_3$Al	78	60 : 40
99	Me$_3$Al	89	64 : 36
24	^{n}Bu$_2$Mg	83	70 : 30
100	(Me$_3$SiCH$_2$)$_2$Mg	96	74 : 26
101	(Me$_3$SiCH$_2$)$_2$Mn	99	72 : 29

Figure 2.10 represents the values for the enantiomeric excesses for every reaction. The addition on CoBr$_2$ (**93**) and MgBr$_2$ (**94**) inhibits the reaction so the enantiomeric excess is indicated as zero. Although the addition of **96** or **97** improved the conversion of the reaction, the enantiomeric excess has not been enhanced. The addition of aluminium reagents enhances the outcome of the process; however, the less bulky Me$_3$Al (**99**) produces the best results. The addition of magnesium (**100**) and manganese (**101**) reagents bearing trimethylsilylmethyl groups show the best results, as the enantiomeric excess is increased to 46% when the complex is used as a base is [LiPEA + (Me$_3$SiCH$_2$)$_2$Mg].
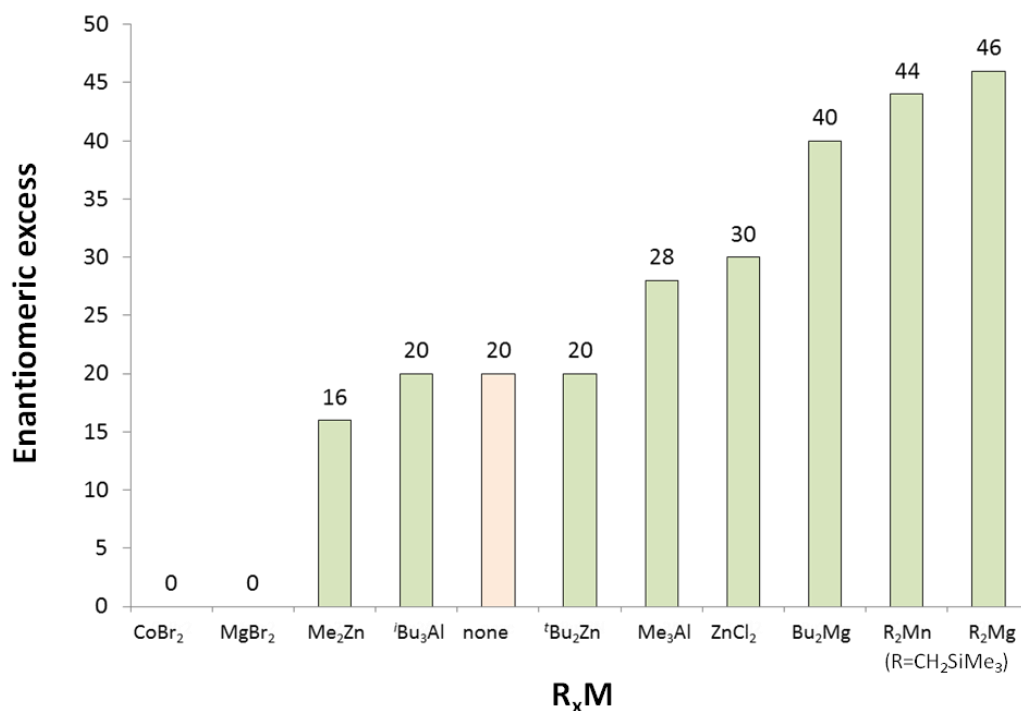
Figure 2.10 Enantiomeric excess of the silyl enol ether upon adding different ragents to
LiPEA in the asymmetric deprotonation of **76** at 0°C for 1 hour.

It should be noted that, for completeness, the deprotonation of 4-*tert*-butylcyclohexanone with [LiPEA + (Me$_3$SiCH$_2$)$_2$Mg] has been performed in hexane, toluene and diethyl ether, showing lower conversions (23%, 2% and 40% respectively) and enantiomeric excesses up to 32%, in the case of diethyl ether.

101 is extremely air sensitive and it needs to be synthesised from its magnesium counterpart. **100** is also very air sensitive but it can be synthesised with high purity and been isolated as a white solid in the glove box. It was decided to study the behaviour of the complex formed by LiPEA (which can also be isolated as a solid and stored in the glove box) and **100** in D$_8$-THF solution.

2.3.3 Solution NMR spectroscopic studies

^{1}H NMR spectroscopic solution studies of a 1:1 mixture of LiPEA and (Me$_3$SiCH$_2$)$_2$Mg (**100**) have been performed in D$_8$-THF at 343K (**Figure 2.11**).

The spectrum shows two resonances around 3.53 and 3.69 ppm that belongs to chiral amine $N(CH(Ph)(Me))_2$. The fact that there are two different resonances does not imply that there are two different amido-containing species, as they could belong to diastereotopic protons present in one organometallic reagent.
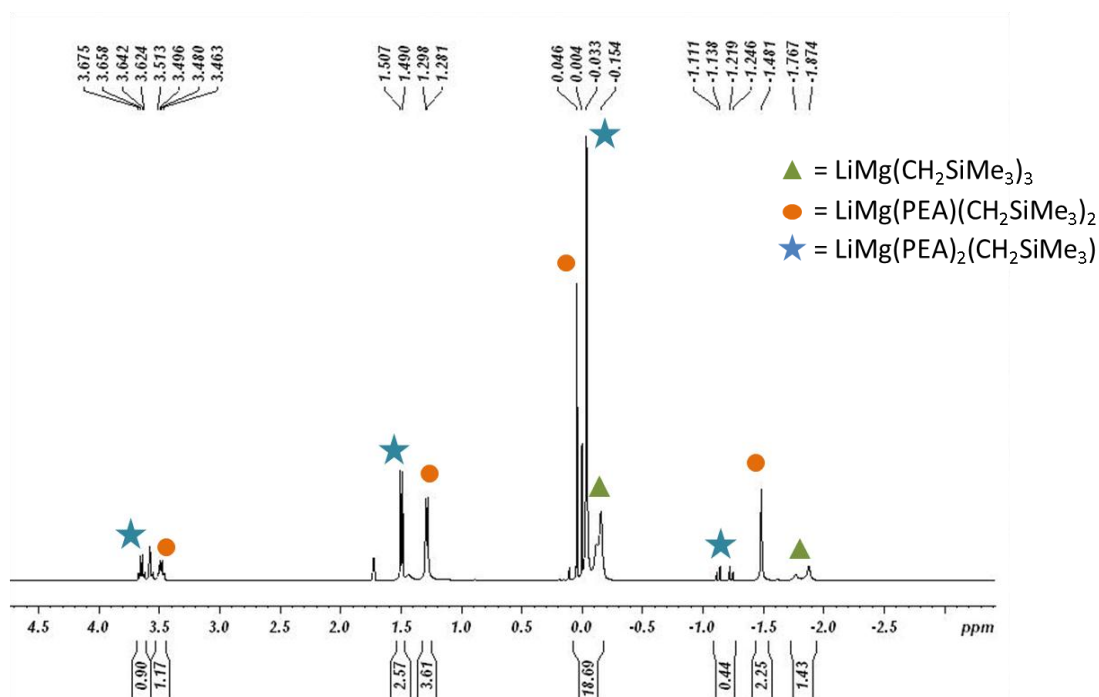
Figure 2.11 ^{1}H NMR spectrum of an equimolar mixture of LiPEA + $(Me_3SiCH_2)_2Mg$ (**100**) in D_8-THF.

To find out whether the signals belong to one or two molecules, ^{1}H DOSY experiment has been carried out. DOSY experiments (paragraph 1.3.6.2) can estimate the molecular weight of a species in solution. In this experiment no internal standards had been added to the solution as the aim here was to simply ascertain whether two species or not were present.
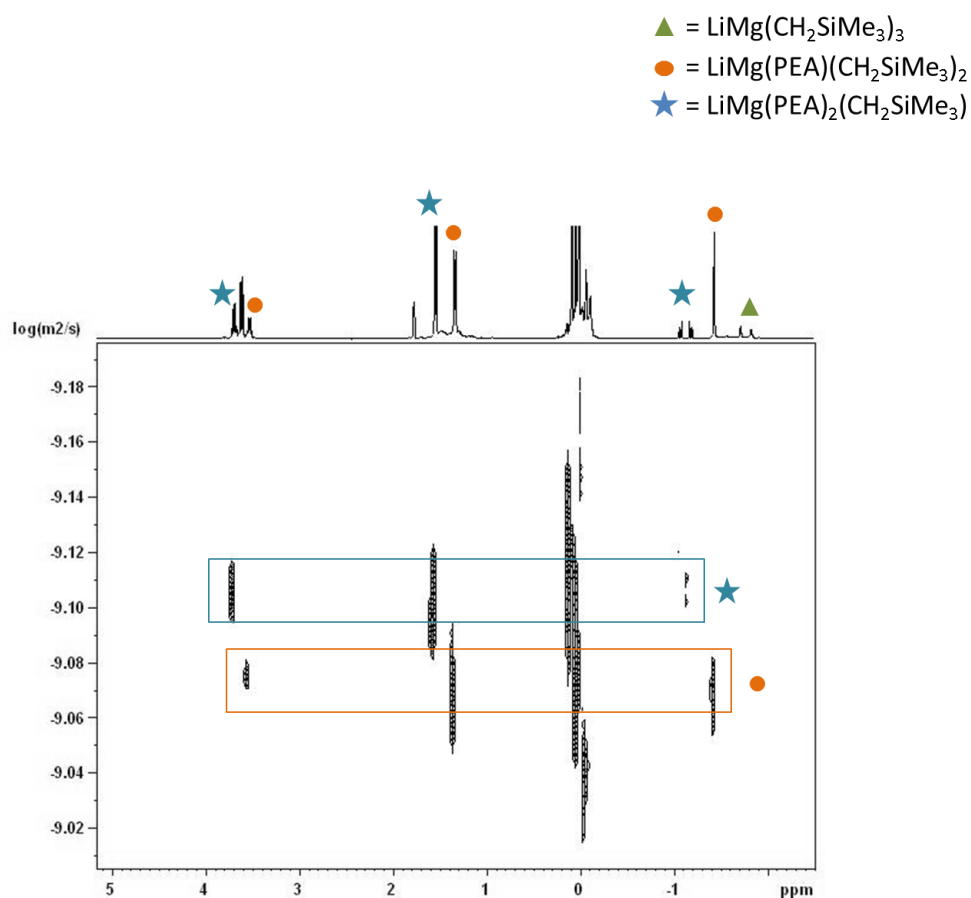
Figure 2.12 ^{1}H DOSY spectrum of an equimolar mixture of LiPEA + $(Me_3SiCH_2)_2Mg$ (**100**) in D_8-THF.

Figure 2.12 shows the ^{1}H DOSY spectrum performed for the 1:1 mixture of LiPEA and **100**. The resonances at 3.53 and 3.69 ppm present different diffusion coefficient and they could be related to another two sets of resonances that could belong to the methyl group of PEA (**57**) (at 1.50 and 1.29 ppm respectively) and the alkyl chain.

In an attempt to find out which of the species present in the equilibrium is the active species, the bis-amido complex $[LiMg(PEA)_2(CH_2SiMe_3)]$ has been employed on the deprotonation of the 4-*tert*-butylcyclohexanone, affording identical enantiomeric ratio than when the 1:1 mixture was employed (74:26).

2.4   Conclusions and future work

The enantioselective deprotonation of 4-*tert*-butylcyclohexanone with bimetallic bases at non-cryogenic temperatures has been studied in this chapter.

A series of complexes formed by the combination of the lithium amide LiPEA and a second organometallic reagent have been studied as deprotonation agents.

When LiPEA is combined with an inorganic salt to form a complex with formula [M(PEA)X·LiX], the conversion of the reaction is decreased or even inhibited. On the other hand, when LiPEA is co-complexed with an organometallic reagent to prepare a complex with formula [LiM(PEA)R_y], the conversion of the reaction and also the selectivity of the process is improved.

Solvent effects have also been evaluated. Coordinating solvents such us tetrahydrofuran or diethyl ether provide better results than non-coordinating solvents.

For the system that has been studied in this chapter, the addition of lithium chloride to the reaction does not seem to affect both, the conversion or the enantioselectivity of the process.

It has been shown that the treatment of prochiral ketones with bimetallic reagents can lead to deprotonation or 1,2-addition products. The employment of catalytic amounts of the chiral amine, induces the nucleophilic addition to be the major product. Changing the alkyl groups of the bimetallic bases to bulkier substituents, the deprotonation can be enhanced from 26% to 81% (conversions obtained respectively when ^{n}Bu$_2$Mg (**24**) or Np$_2$Mg (**89**) were employed). The highest enantiomeric excess found when the chiral amine was added in catalytic amounts was 16% showing that there was catalytic turn over.

In an attempt to improve these results, different chiral amines could be examined. Considering that the lithium amide needs to show the right bulkiness in order to be able to co-complex with a second organometallic reagent,[142] the

employment of bulkier substituents in the amine would probably lead to higher enantiomeric excesses.[100]

2.5 Experimental

2.5.1 Representative experimental procedure for deprotonation reactions.

All the reactions were performed in triplicate to ensure the reproducibility of the data. Progression of the reaction was monitored by gas chromatography and purification of products was carried out by flash chromatography. Characterisation of products is detailed below.

(4-*tert*-butylcyclohexen-1-enyloxy)trimethylsilane (76)

^{1}H NMR (400 MHz, 300 K, CDCl$_3$): δ 0.19 (9H, s, CH_3, TMS), 0.88 (9H, s, CH_3, ^{t}Bu), 1.20 (3H, br, CH_2 and CH cyclohexene ring), 1.76 (2H, br, CH_2, cyclohexene ring), 2.09 (2H, br, CH_2, cyclohexene ring), 4.84 (1H, d, CH double bond cyclohexene ring).

Achiral GC analysis: Chirasil-DEX CB column 30m x 0.25mm x 0.25μm. H$_2$ carrier gas (45 cm sec^{-1}); Split ratio 75:1; Temperature gradient: 90°C, 0.5 min; 45°C min-1; 220°C, 6 min. t$_R$=3.69 min.

Chiral G.C. analysis: (**i**) CP Chirasil-DEX CB column 30m x 0.25mm x 0.25μm; (**ii**) carrier gas, H$_2$ (45 cm sec^{-1}); (**iii**) injector/detector temperature, 250°C; (**iv**) initial oven temperature: 70°C; (**v**) temperature gradient, 70-130°C, 1.5°C min^{-1}; 130°C, 1 min; 130-200°C, 20°C min^{-1} ; 200°C, 1 min; (**vi**) final oven temperature, 200°C (**vii**) detection method, FID.

t$_R$(*S*) = 31.75 min, **t$_R$(*R*)**= 32.11 min.

4-(*tert*-butyl)-1-butylcyclohexanol (83)

^{1}H NMR (500 MHz, 300 K, CDCl$_3$): δ 0.87 (9H, s, CH_3, tBu), 0.91 (3H, t, CH_3, Bu), 1.09 (1H, s, OH), 1.30 (6H, br, CH_2, Bu and 3H, cyclohexane ring), 1.40 (2H, br, CH_2, cyclohexane ring), 1.58 (2H, br,

CH_2, cyclohexane ring), 1.65 (2H, dd, CH_2, cyclohexane ring).

Achiral GC analysis: Chirasil-DEX CB column 30m x 0.25mm x 0.25μm. H2 carrier gas (45 cm x sec-1); Split ratio 75:1; Temperature gradient: 90°C, 0.5 min; 45°C x min^{-1}; 220°C, 6 min. t_R=3.76 min.

2.5.1.1 Evaluation of the donor in affecting the outcome of the enantioselective deprotonation.
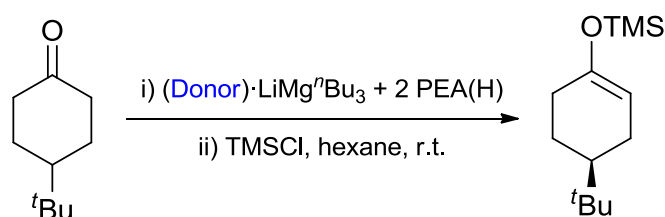
To a flame-dried and Ar-purged Schlenk flask, ^{n}BuLi (1.6 M in hexanes, 0.67 mL, 1.0 mmol) was added and dissolved in anhydrous hexane (5 mL). ^{n}Bu$_2$Mg (1 M in heptane, 1 mL, 1.0 mmol) was then added and solution became turbid solution. 1 mmol of the donor (either (*R,R*)-TMCDA, TMEDA, PMDETA or TMPDA) was added and then 2 mmol of bis[(*R*)-1-phenylethyl]amine (0.46 mL, 2.0 mmol) was added to form a yellow suspension that was stirred for 1 hour. 4-*tert*-butylcyclohexanone (0.152 g, 1.0 mmol) was added to the mixture, and the resulting suspension was allowed to stir for 1 hour. TMSCl (0.25 mL, 2.0 mmol) was added and regular sampling and analysis by gas chromatography monitored the progress of the reaction.

2.5.1.2 Evaluation of the bulk solvent employed during the deprotonation.
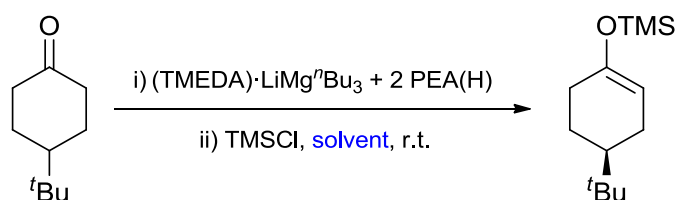
To a flame-dried and Ar-purged Schlenk flask, ^{n}BuLi (1.6 M in hexanes, 0.67 mL, 1.0 mmol) was added and dissolved in 5 ml of anhydrous solvent (either hexane, toluene, diethylether, tetrahydrofuran or methylcyclohexane)

^{n}Bu$_2$Mg (1 M in heptane, 1 mL, 1.0 mmol) was added and solution became a turbid solution. 1 mmol of the donor (either (*R,R*)-TMCDA, TMEDA, PMDETA or TMPDA) was added and then 2 mmol of bis[(*R*)-1-phenylethyl]amine (0.46 mL, 2.0 mmol) was added to form a yellow suspension that was stirred for 1 hour. 4-*tert*-butylcyclohexanone (0.152 g, 1.0 mmol) was added to the mixture, and the resulting suspension was allowed to stir for 1 hour. TMSCl (0.25 mL, 2.0 mmol) was added and regular sampling and analysis by gas chromatography monitored the progress of the reaction. 4-*tert*-butylcyclohexanone (0.152 g, 1.0 mmol) was added to the mixture, and the resulting suspension was allowed to stir for 1 hour. TMSCl (0.25 mL, 2.0 mmol) was added and regular sampling and analysis by gas chromatography monitored the progress of the reaction.

2.5.1.3 Evaluation of the effect of the addition of lithium chloride

To a flame-dried and Ar-purged Schlenk flask, ^{n}BuLi (1.6 M in hexanes, 0.67 mL, 1.0 mmol) was added and dissolved in 5 ml of anhydrous solvent (either hexane, toluene, diethylether, tetrahydrofuran or methylcyclohexane) ^{n}Bu$_2$Mg (1 M in heptane, 1 mL, 1.0 mmol) was added and solution becomes a turbid solution. 1 mmol of the donor (either (*R,R*)-TMCDA, TMEDA, PMDETA or TMPDA) was added and then 2 mmol of bis[(*R*)-1-phenylethyl]amine (0.46 mL, 2.0 mmol) was added to form a yellow suspension that was stirred for 1 hour. LiCl (either 0.1, 0.5, 1 or 2 mmol) was incorporated to the mixture and 4-*tert*-butylcyclohexanone (0.152 g, 1.0 mmol) was added to the mixture, and the resulting suspension was allowed to stir for 1 hour. TMSCl (0.25 mL, 2.0 mmol) was added and regular sampling and analysis by gas chromatography monitored the progress of the reaction.

2.5.1.4 Effect of a change in the number of equivalents of chiral amine.
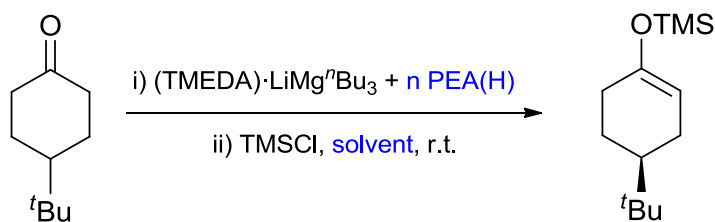
To a flame-dried and Ar-purged Schlenk flask, ^{n}BuLi (1.6 M in hexanes, 0.67 mL, 1.0 mmol) was added and dissolved in 5 ml of anhydrous solvent (either hexane, toluene, diethylether, tetrahydrofuran or methylcyclohexane) ^{n}Bu$_2$Mg (1 M in heptane, 1 mL, 1.0 mmol) was added and solution becomes a turbid solution. 1 mmol of the donor (either (R,R)-TMCDA, TMEDA, PMDETA or TMPDA) was added. Bis[(R)-1-phenylethyl]amine (0.1, 0.5, 1 or 2 mmol) was added and and 4-*tert*-butylcyclohexanone (0.152 g, 1.0 mmol) was added to the mixture, and the resulting suspension was allowed to stir for 1 hour. TMSCl (0.25 mL, 2.0 mmol) was added and regular sampling and analysis by gas chromatography monitored the progress of the reaction.

2.5.1.5 Catalytic asymmetric deprotonation of the 4-*tert*-butylcyclohexanone.
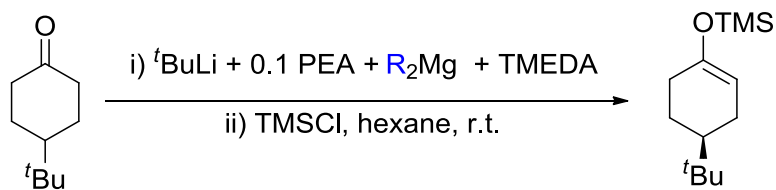
To a flame-dried and Ar-purged Schlenk flask, ^{t}BuLi (1.7 M in pentane, 0.59 mL, 1.0 mmol) was added and dissolved in 5 mL of anhydrous hexane. 1 mmol of R$_2$Mg (R$_2$Mg=^{t}Bu$_2$Mg, Np$_2$Mg, Ph$_2$Mg, (p-tol)$_2$Mg, (CH$_2$Si(CH$_3$)$_3$)$_2$Mg) was added and solution becomes a turbid solution. Bis[(R)-1-phenylethyl]amine (0.023 mL, 0.1 mmol) was added and, after stirring for 30 minutes, 1 mmol of TMEDA was added to form a yellow suspension. 4-*tert*-butylcyclohexanone (0.152 g, 1.0 mmol) was added to the mixture, and the

resulting suspension was allowed to stir for 1 hour. TMSCl (0.25 mL, 2.0 mmol) was added and regular sampling and analysis by gas chromatography monitored the progress of the reaction.
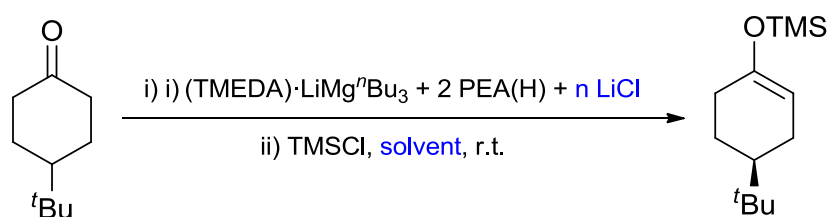
2.5.1.6 Catalytic asymmetric deprotonation in presence of LiCl.
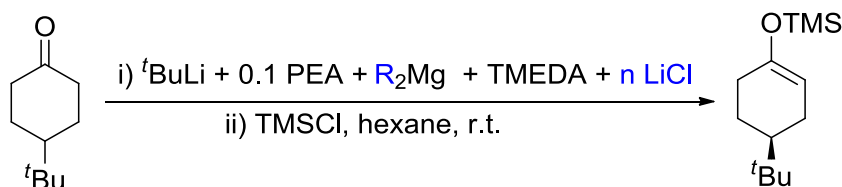
To a flame-dried and Ar-purged Schlenk flask, ^{n}BuLi (1.6 M in hexanes, 0.67 mL, 1.0 mmol) was added and dissolved in 5 mL of anhydrous solvent (either hexane, toluene or diethyl ether). 1 mmol of R_2Mg ($R_2Mg={}^tBu_2Mg$, Np_2Mg, Ph_2Mg, $(p\text{-tol})_2Mg$, $(CH_2Si(CH_3)_3)_2Mg$) was added and solution becomes a turbid solution. Bis[(R)-1-phenylethyl]amine (0.23 mL, 1.0 mmol) was added and, after stirring for 30 minutes, 1 mmol of TMEDA was added to form a yellow suspension. LiCl (either 0.1, 0.5, 1 or 2 equivalents) was incorporated to the mixture and 4-*tert*-butylcyclohexanone (0.152 g, 1.0 mmol) was added to the mixture, and the resulting suspension was allowed to stir for 1 hour. TMSCl (0.25 mL, 2.0 mmol) was added and regular sampling and analysis by gas chromatography monitored the progress of the reaction.

Chapter 3. Structural and reactivity insights of chiral sodium magnesiates

3.1 Summary

Closely related to Chapter 2, this chapter summarises the chemistry obtained when the chiral amide (+)-bis[(*R*)-1-phenylethyl]amide (**57**) is incorporated within sodium magnesiates.

Depending on the reaction conditions, three different crystal structures have been obtained when NaMg^{n}Bu$_3$ (**102**) is reacted with two equivalents of **57**.

Firstly, the unsolvated magnesiate [NaMg(PEA)$_2$^{n}Bu]$_\infty$ (**103**) was obtained when the reaction was performed in hydrocarbon solvent in absence of any donors.

Secondly, the addition of one equivalent of TMEDA to the reaction afforded the crystallisation of [TMEDA·Na(PEA)$_2$Mg^{n}Bu] (**104**).

Finally, the third structure was obtained from a reaction involving **103** which was carefully exposed to air. The new species, an oxygen-containing molecule, [NaMg(PEA)$_4$O] (**105**) was isolated.

When only one equivalent of **57**-(H) was reacted with the bimetallic mixture NaMg^{n}Bu$_3$ (**102**), in the presence of TMEDA, the disproportionation product [TMEDA·Na(PEA)$_2$Mg^{n}Bu] (**104**) was formed.

This species has been studied and characterised in solution by ^{1}H, ^{13}C and 2D DOSY experiments, in order to gain an insight about their aggregation state in solution.

A study of the reactivity of these bases in the asymmetric deprotonation of prochiral ketones in toluene and THF solution has been carried out showing a remarkable enhancement of the enantioselectivity when the monometallic reagents were combined.

3.2 Introduction

Chapter 1 discussed the utility of the lithium magnesiate reagents. However, although the lighter alkali metal has traditionally been the choice of synthetic chemists, a new generation of magnesiates incorporating sodium as a counterpart has been explored in the past decades.

The work of Weiss and co-workers was pioneering in sodium magnesiate complexes. They published the structures of two homoleptic sodium magnesiates, [(PMDETA·Na)$_2$MgPh$_4$] (**106**) and Na$_2$[Mg(C≡C^{t}Bu)$_3$(TMEDA)$_2$]$_2$ (**107**),[143] which are structurally related to lithium magnesiates **34** and **39** described in Chapter 1 (**Table 1.2**).

Hevia and Mulvey *et al.* studied the solid state structures of homoleptic *n*-butylsodium magnesiates stabilised by the bidentate ligand DABCO (diazabicyclo(2,2,2)octane, (**108**)), which form a complex coordinated by toluene [[Na$_2$(DABCO)$_3$(toluene)]$^{2+}$(MgBu$_4$)$^{2-}$]$_\infty$ (**109**).[144] The solid-state structure of **109** shows interstitial [MgBu$_4$]$^{2-}$ dianions within a three-dimensional dicationic network. They also studied the possible equilibrium processes that may be taking place in solution when both, lower and higher order magnesiates, are synthesised.

Unlike lithium magnesiates, there are only a few examples of the employment of sodium magnesiates in synthesis.[145]

Screttas and Micha-Screttas performed the addition of magnesiates with electrophiles like benzophenone (**110**), finding that the main product was the reduction reaction (**111**) over the addition reaction (**112**) to benzophenone (**Scheme 3.1**).[146] Richey Jr. and co-workers found that the ratio of addition to reduction can be increased by adding alkali-metal salts (like sodium methoxide) to dialkylmagnesium reagents.[147]
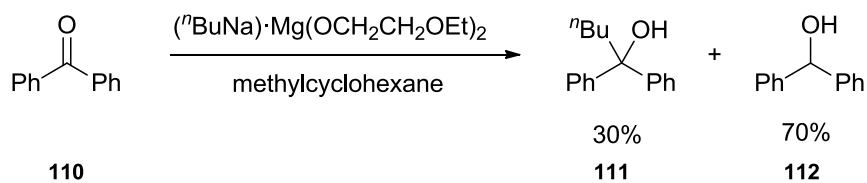
Scheme 3.1 Treatment of benzophenone with a sodium magnesiate.

Wu and co-workers showed how sodium magnesiates supported by the ligand TBBP (2,2′-dihydroxy-3,3′,5,5′-tetra-*tert*-butyl-1,1′-diphenyl, (**113**)) can initiate the polymerization of L-lactide (**114**) (**Scheme 3.2**).[148]
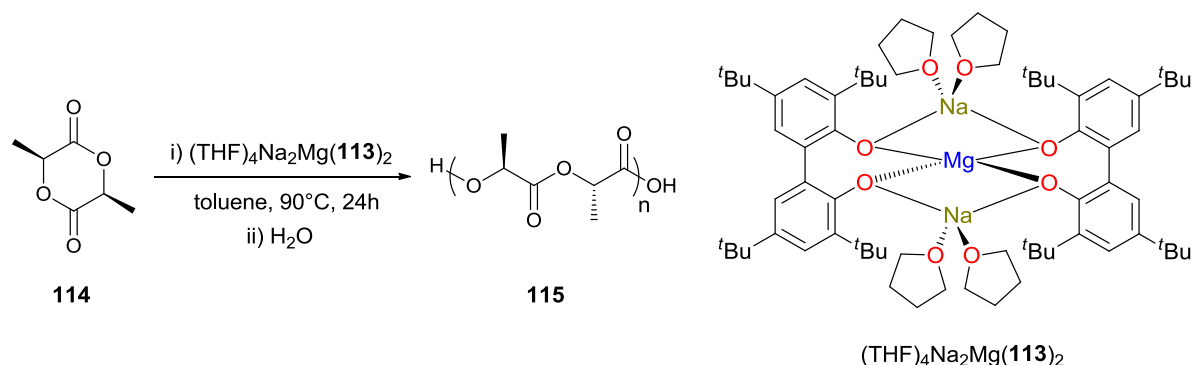
Scheme 3.2 Wu's ring opening polymerisation performed with sodium-magnesium bimetallic complexes.

3.2.1 Inverse crowns

The finding that the regioselective non-methyl deprotonation of toluene (**116**) was possible using sodium magnesiates was a significant advance.[149]

When toluene is reacted with a complex formed by the combination of the *n*-butyl derivatives of sodium and magnesium reagents and three equivalents of TMP(H) (**79**-(H)), instead of leading to the resonance-stabilised benzyl carbanion, dideprotonation at the 2 and 5 position ensued (**117**).

Surprisingly, the positions of dideprotonation can be tuned by changing the organomagnesium reagent, i.e., when trimethylsilylmethyl magnesium complex (**100**) is used to build the bimetallic base, the dideprotonation occurs in 3 and 5 positions (**118**).[150]
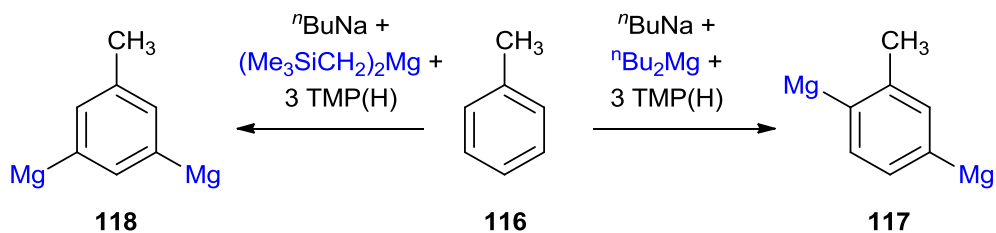
Scheme 3.3 Dimetalation of toluene in 2,5-positions (**117**) or 3,5-positions (**118**).

That deprotonation occurs through a cyclic intermediate commonly called "inverse crown". That name refers to the "crown ether" complexes, which encapsulate a Lewis acid in a crown composed by a Lewis base. Therefore, inverse crown complexes are able to cleave and capture a Lewis base with a ring usually formed by metal amido complexes.

The macrocyclic motif also appears during the deprotonation of benzene when $[Na_4Mg_2TMP_6(C_6H_4)]$ (**119**) is formed.[149] Another dramatic example of this protocol is the tetrametalation of the ferrocene (and analogous metallocenes) by a mixture of tri-*n*-butylsodium magnesiate (**102**) and three equivalents of diisopropylamine, DA(H) (**73**-(H)) (**Figure 3.1**).[151, 152]
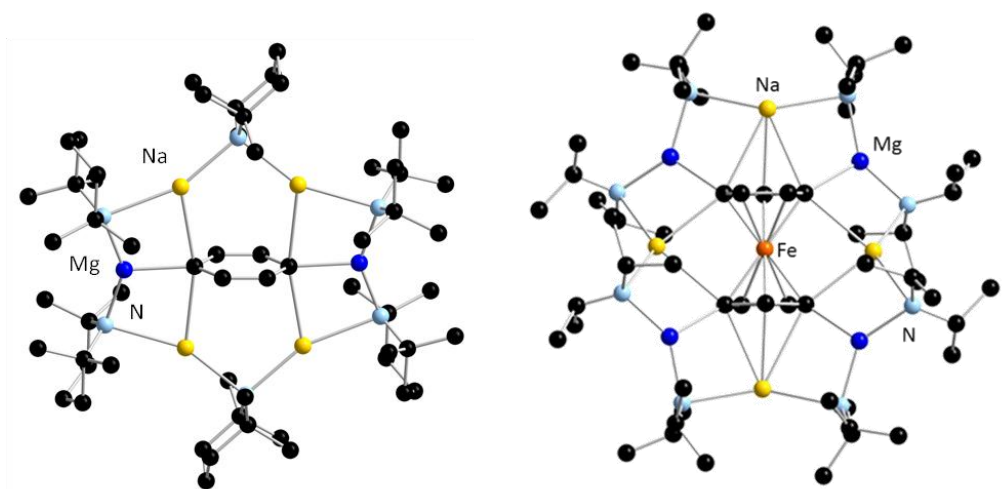
Figure 3.1 Molecular structure of deprotonation of benzene (left) and the deprotonation of ferrocene (right) by the mixture "NaMg(DA)$_3$".

Fifteen years after the pioneering deprotonation of toluene, the significance of the reaction was discovered as other publications revealed the generality and utility of the inverse crown concept. It turned out that the bimetallic mixture $Na_4Mg_2TMP_6{}^nBu_2$ (**120**) is capable of deprotonating a wide scope of aromatic substrates, but the key point was the selectivity of those deprotonations.[153]

That regioselectivity is dictated by both, the electronics and the structure of the aromatic "guest" of the inverse crown.

The directing groups (DG) on arenes can be classed as strong or weak *ortho* directors.[154, 155] Strong directors coordinate well to the metal and are normally electron withdrawing groups, hence acidify the *ortho* position of the arene. Weak directors generally only have the first of these effects.

When reacted with **120**, it seems that all strong directors are deprotonated at the *ortho/meta* positions, whilst some weak directors are deprotonated at the *meta/meta'* positions, although the steric effects may also be at play for the weak directors (e.g. anilines) whereby the *ortho* sites are protected by the alkyl substituent (**Scheme 3.4**).
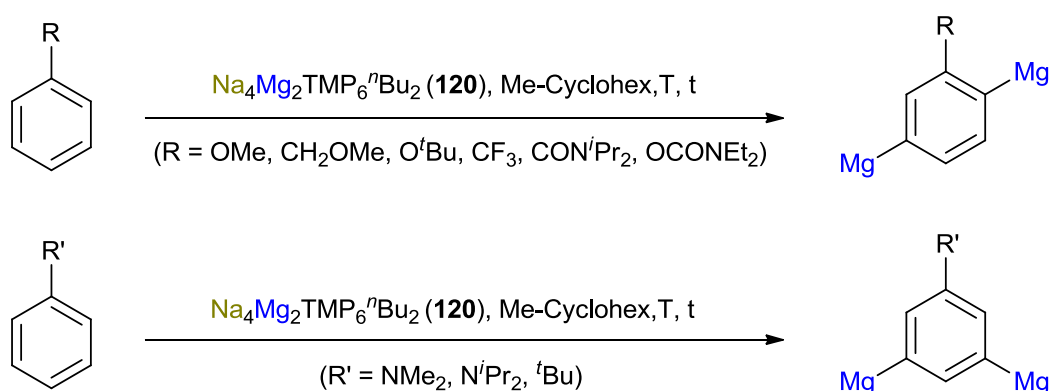
Scheme 3.4 Deprotonation of aromatic compounds with $Na_4Mg_2TMP_6{}^nBu_2$ (**120**).

3.2.1.1 Pre-inverse crowns

For several years there was lack of knowledge about the structure of the active species that perform these special deprotonations. The stoichiometry of the

reactions performed to date seemed to indicate that it was necessary the presence of three equivalents of amine in order to synthesise the base but this is now known not to be the case. For the case of the TMP, the third equivalent does not react and the active species is a heteroleptic sodium magnesiate bearing amido and alkyl groups.[156]

The stoichiometry of the reaction was improved and it was found that the optimised reaction conditions were found when an equimolar mixture of NaTMP (Na-**79**) and $NaMgTMP_2{}^nBu$ (**121**) were reacted in hydrocarbon solvent (**Scheme 3.5**). NMR spectroscopic analysis in *cyc*-C_6D_{12} showed how that mixture afforded a system in which two *n*-butyl-containing species are in dynamic equilibrium (using ^1H EXSY experiment). By ^1H DOSY analysis, the molecular weight could be estimated and it is in agreement with the species $Na_2MgTMP_3{}^nBu$ (**122**) and $Na_4Mg_2TMP_6{}^nBu_2$ (**123**).[157]

$$NaTMP + NaMgTMP_2{}^nBu \longrightarrow Na_2MgTMP_3{}^nBu \rightleftharpoons 1/2\ Na_4Mg_2TMP_6{}^nBu_2$$

Scheme 3.5 Equilibrium between $Na_2MgTMP_3{}^nBu$ (**122**) and $Na_4Mg_2TMP_6{}^nBu_2$ (**123**) in *cyc*-C_6D_{12}.

This pre-inverse crown compexes has also been employed as a deprotonating reagent with N-heterocyclic carbenes (**Scheme 3.6**).[158] Remarkably, magnesiation of IPr (**124**) occurs at the *para*-position of an aryl substituent, sodiation occurs at the abnormal C4 position, and a dative bond occurs between normal C2 and sodium, all within a 20 atom ring structure accommodating two IPr^{2-}.
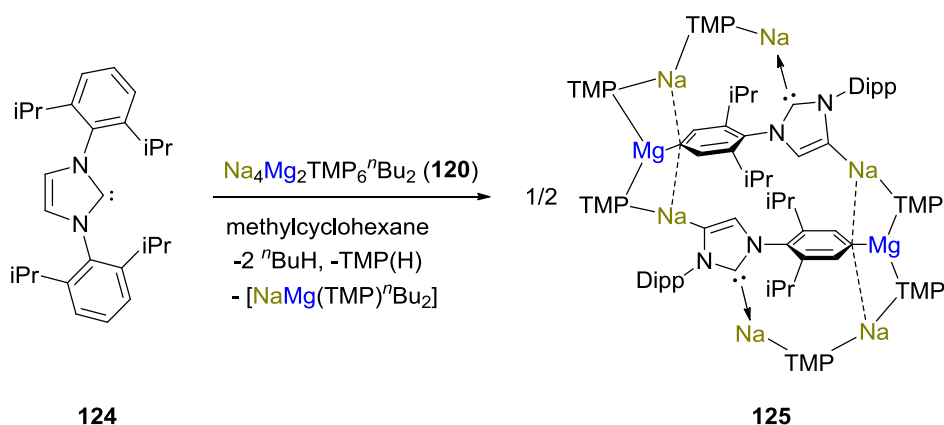
Scheme 3.6 Template metalation of IPr (**124**) with $Na_4Mg_2TMP_6{}^nBu_2$ (**120**).

3.2.1.2 Eight-membered ring inverse crowns

Bimetallic alkali-metal magnesiates have proven to be highly reactive with aromatic substrates. However, a series of macrocyclic complexes have been found, hence proving that they are able to incorporate within their core an anionic ligand different than arene molecules.

In 1998, homoleptic lithium magnesiate $LiMg(HMDS)_3$ (**126**) (HMDS=bis(trimethylsilyl)amide), **127**) was synthesised by Mulvey and co-workers. In one of the attempts to reproduce it, an oxygen-contaminated complex with formula $[Li_2Mg_2(HMDS)_4(O_2)_x(O)_y]$ (**128**) was encountered.[86] Far from being simply an impurity, this macrocyclic lithium magnesiate was the first in a new series of complexes to be formed, which are now termed "inverse crown ethers".

As alluded to earlier, inverse crown ethers owe their name to their inverse relationship to that of conventional crown ether complexes.[159] In conventional crown ether complexes, the Lewis base plays host to an electron-poor metal cation guest, but in inverse crown ether complexes, the Lewis acidic metal centres play host to an anionic Lewis basic oxide (**Figure 3.2**).

Crown ether   **Inverse crown ether**
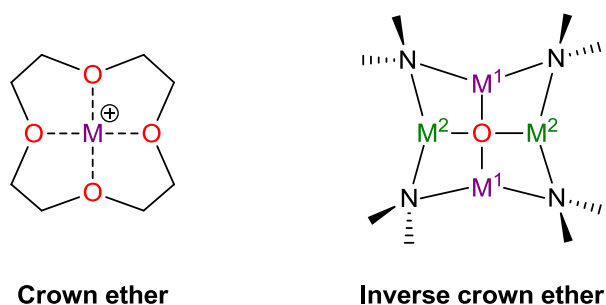
Figure 3.2 Generalised structures of crown ether complexes (left) and inverse crown ether complexes (right).

The sodium congener of the first inverse crown, $[Na_2Mg_2(HMDS)_4O]$ (**129**),[87] was found by Mulvey. Kennedy also published a similar structure containing TMP (**130**)[160] as the anionic ligand instead of HMDS.

Mulvey and co-workers focused on sodium magnesiates and so reacted together $NaMg^nBu_3$ (**102**) with 3 equivalents of diisopropylamine (**73**-(H)) in toluene under reflux, they found a molecular hydride with formula $[Na_2Mg_2{}^iPr_4(\mu\text{-}H)_2\cdot(tol)_2]$ (**132**) (**Scheme 3.7**).[161]
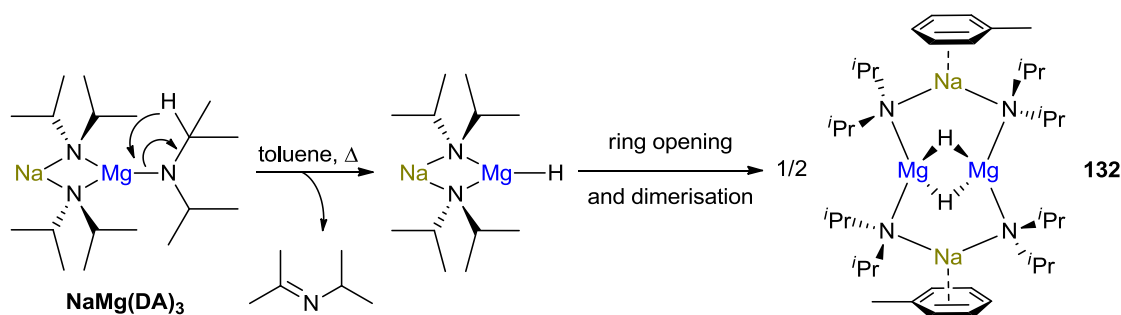
Scheme 3.7 synthesis of $[Na_2Mg_2{}^iPr_4(\mu\text{-}H)_2]$ (**132**) through an intramolecular β-hydride transfer pathway.

The suggested reaction pathway involves an intramolecular β-hydride elimination from the bimetallic amide $NaMg(DA)_3$ (**131**) resulting in the loss of imine. The steric crowding around the magnesium atom would be reduced so it would be likely dimerisation would occur (**Scheme 3.7**). Hydride **132** crystallised as a dimer with a molecule of toluene coordinated to every sodium atom. Mulvey found that when the reaction is performed in hexane in

presence of bis(benzene)chromium (**133**) it is possible to isolate a solvent-free polymer which propagates through a Na···C interaction.[162]

Chapter 1 described the sodium magnesiate described by Mulvey *et al.* containing *n*-butoxide groups (**Figure 1.9**)[85]. In this example, the crown is composed by Na and Mg atoms alternating with alkyl groups.

3.2.2 Donor-stabilised sodium magnesiates

A common feature in the reactions described above, it is that all complexes were prepared in the absence of any donor solvent, which could coordinate the less Lewis acidic metal and form monomeric units.

The isolation of the sodium magnesiate (TMEDA)·Na(μ-TMP)(μ-^{n}Bu)Mg(TMP) (**134**) in 2004 gave some insights into the structure of the pre-inverse crowns.[156] Prior to its discovery, it was thought that the active species able to deprotonate the arene molecules was the putative "NaMg(TMP)$_3$", formed by reaction of NaMg^{n}Bu$_3$ with 3 equivalents of TMP(H). However, isolation of **134** showed how only two of the butyl carbanions had been consumed to form butane. Reflux conditions did not encourage the coordination of a third equivalent of TMP, presumably for steric reasons.
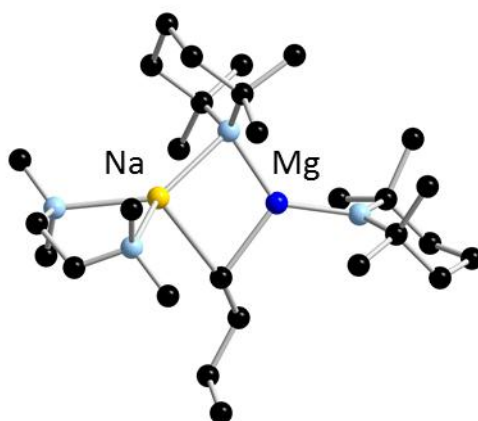
Figure 3.3 Molecular structure of (TMEDA)·Na(μ-TMP)(μ-^{n}Bu)Mg(TMP) (**134**).

Sodium magnesiate **134** not only gave insight into the structures of pre-inverse crowns, but also proved to be an excellent reagent for performing monodeprotonations on arene molecules. Reaction studies proved that **134** could successfully monodeprotonate benzene,[156] furan[163, 164] and also toluene in *meta*-position.[165]

Reaction of an excess of **134** with benzene, afford a dimagnesiated benzene in 1,4-positions (**135**),[166] the same resactivity that was found when the pre-inverse crown was used.[149]
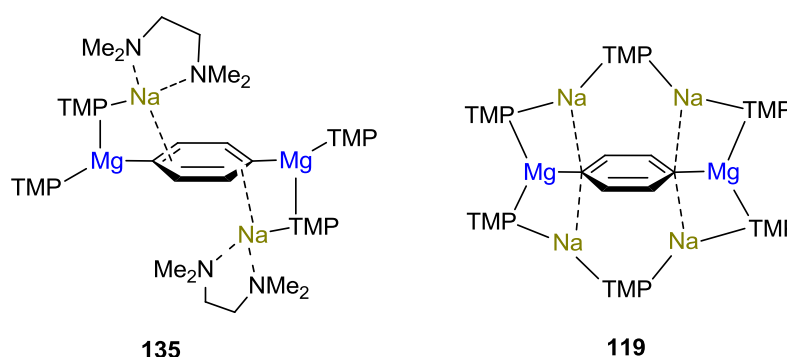
Figure 3.4 Dideprotonation of benzene by sodium magnesiates.

Another interesting application of a heteroleptic sodium magnesiate stabilise by TMEDA when (TMEDA)·Na(TMP)(CH$_2$SiMe$_3$)Mg(TMP) (**136**) is reacted with tetrahydrofuran (**Scheme 3.8**).[167]

The THF ring breaks into two parts, and the fragments are captured in separate crystalline complexes. Analogous to the dideprotonation of benzene, C4 fragments ultimately appear as bimetallated butadiene ions and oxide fragments occupy guest positions in bimetallic, inverse crown ethers.
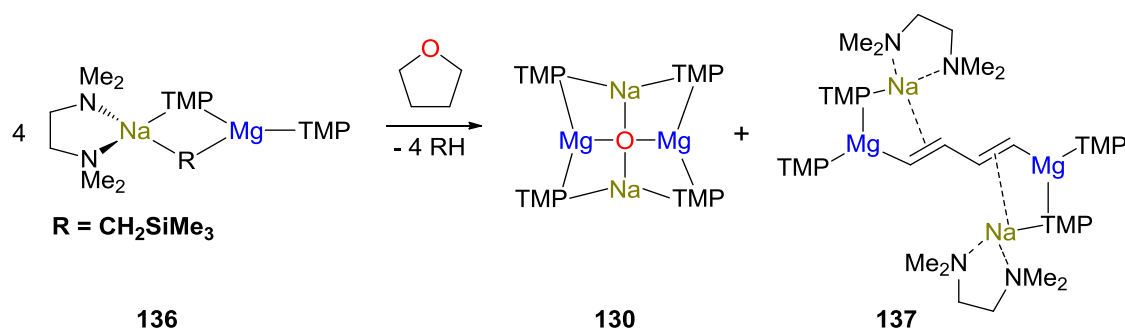
Scheme 3.8 Reaction of (TMEDA)·Na(TMP)(CH$_2$SiMe$_3$)Mg(TMP) with tetrahydrofuran.

The sodium magnesiate containing the fragment of butadiene (**137**) is structurally related to **135**. This reactivity has not been achieved with pre-inverse crowns or indeed in the absence of ancillary ligands.

3.2.2.1 Chiral sodium magnesiates

The first chiral sodium magnesiate crystallographically characterised was ((−)-sparteine)·Na(μ-TMP)(μ-^{n}Bu)Mg(TMP) (**138**) (**Figure 3.6**).[80]

(−)-Sparteine (**60**) is a natural product, a lupinalkaloid extracted from the Scotch broom plant. Its structure can be described as a tetracyclic skeleton composed of two quinolizidine rings condensed forming a central bispidine ring (**Figure 3.5**). Free (−)-sparteine exists with the A, C and D rings in a chair conformation, while B adopts a boat conformation but the exclusive appearance on complexation with the Lewis acid metal centre is that all rings adopt a chair conformation to be able to act as bidentate ligand.[168]
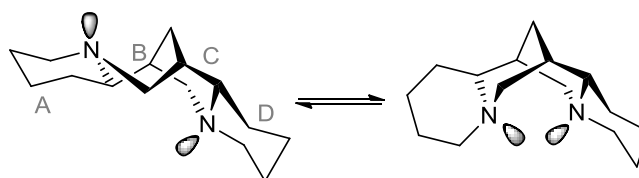
Figure 3.5 Conformational equilibrium of (−)-sparteine (**60**).

Sodium magnesiate **138** constitutes the first example of a chiral sodium magnesiate and it is structurally related to the synthetically important TMEDA derivative **134**.
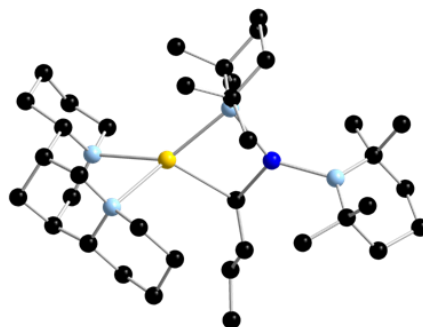
Figure 3.6 X-ray structure of ((–)-sparteine)·Na(μ-TMP)(μ-^{n}Bu)Mg(TMP) (**138**).

O´Hara and co-workers described the polymeric sodium magnesiate (*R,R*)-TMCDA·Mg^{n}Bu(NaHMDS)$_2$ (**139**) that incorporated chiral ligand (R,R)-TMCDA (**4**) in the structure (**Figure 3.7**).[65] This complex was described as an inverse magnesiate as the ancillary ligand binds to the magnesium atoms and they seem to act as a Lewis base solvating the NaHMDS (Sodium bis(trimethylsilyl)amide, Na-(**127**)) dimers.
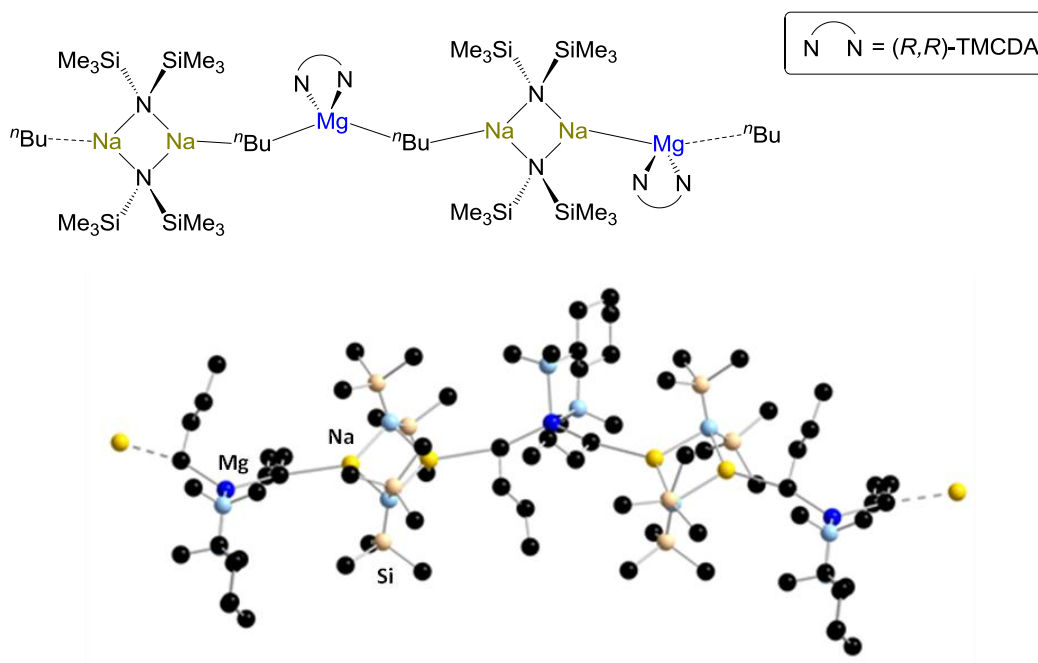
Figure 3.7 Chem Draw and X-ray structure of (R,R)-TMCDA· Mg^{n}Bu(NaHMDS)$_2$ (**139**).

3.2.3 Trisamido sodium magnesiates

As explained *vide supra*, heteroleptic sodium magnesiate **134** has been proven to crystallise constantly as a heteroleptic alkylamido magnesiate. This occurs even though three equivalents of amine were added. However, changing the stoichiometry of the reaction by adding an excess of the ancillary ligand, it was possible to get a (tris)amido sodium magnesiate (**140**).[163]
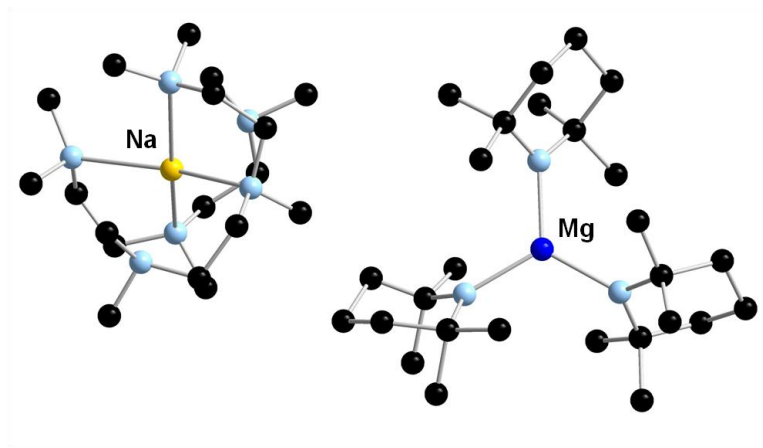
Figure 3.8 Molecular structure of [(PMDETA)Na]$^+$[Mg(TMP$_3$]$^-$ (**140**).

A similar solvent separated ion pair structure was found by O´Hara and co-workers. In this case, the amine of choice was HMDS(H) and the sodium atom was stabilised by TMEDA (**141**) or (*R,R*)-TMCDA (**142**).

The [Mg(amide)$_3$]$^-$ motif is identical whether TMP or HMDS were employed as the magnesium atoms adopt an almost perfect trigonal structure in both cases.

The cationic part of the molecule is obviously different as three different ligands have been used [TMEDA, PMDETA and (R,R)-TMCDA]. For the case of the tridentate ligand PMDETA, the two equivalents of the donor do not chelate to the sodium atoms symmetrically so they instead form two short and one longer Na–N bonds with each Na atom.

Both heteroleptic alkylamido sodium magnesiates crystallise as contacted ion pair complexes and the tris(amido) magnesiate crystallise as a solvent separated ion pair. However, this is highly dependent on the stoichiometry of the reaction and the steric demand of the amine (**Figure 3.9**).
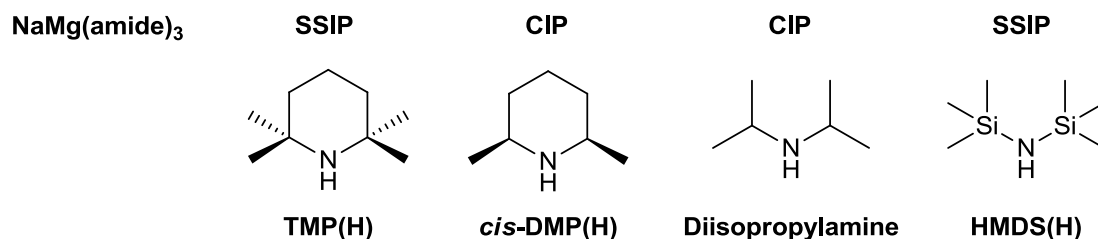
Figure 3.9 ChemDraw representation for amines found in trisamido sodium magnesiates. (CIP=Contacted ion pair, SSIP=Solvent separated ion pair).

There are two examples in the literature of contacted ion pairs with general formula (TMEDA)NaMg(amide)$_3$. Mulvey *et al.* published the structure of the sodium magnesiate containing three equivalents of diisopropylamide (**131**)[169] while O´Hara and co-workers studied the behaviour of the amide *cis*-DMP (*cis*-2,6-dimethylpiperidide, (**143**)).[170] In both examples, sodium magnesiates crystallise as discrete monomers where magnesium has a trigonal planar conformation and the sodium atom adopts a tetrahedral conformation.

Therefore, the results seem to indicate that there is a relationship between the steric bulk of the amido group and the nature of the bimetallic compound, being more likely to find SSIP when bulky amines are employed.

3.3 Results and discussion

In order to expand the knowledge of the chemistry of sodium magnesiates, reactivity of NaMg^{n}Bu$_3$ (**102**) with the chiral amine PEA(H) (**Figure 3.10**) was studied. The reactivity of these complexes in the deprotonation of prochiral ketones will be highlighted *vide infra* (page 103).

57-(H)
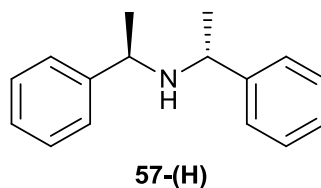
Figure 3.10 ChemDraw representation of the chiral amine PEA(H) ((+)-Bis-[(*R*)-1-phenylethyl]amine).

3.3.1 Synthesis

Three new magnesiates have been synthesised in this chapter (**Scheme 3.9**).

The deprotonation reaction of two equivalents of PEA(H) in hexane by the bimetallic mixture $NaMg^nBu_3$ (**102**) affords a thick white solid which after work up was found to be the heteroleptic sodium magnesiate $[NaMg(PEA)_2{}^nBu]_\infty$ (**103**) in 81% of yield.

Addition of one equivalent of TMEDA solubilises the solid immediately to produce a sodium magnesiate with the formula $[(TMEDA)\cdot NaMg(PEA)_2{}^nBu]$ (**104**) in 88% of yield.

Exposure of **103** to air afforded a new complex, the inverse crown ether $[Na_2Mg_2(PEA)_4O]$ (**105**).
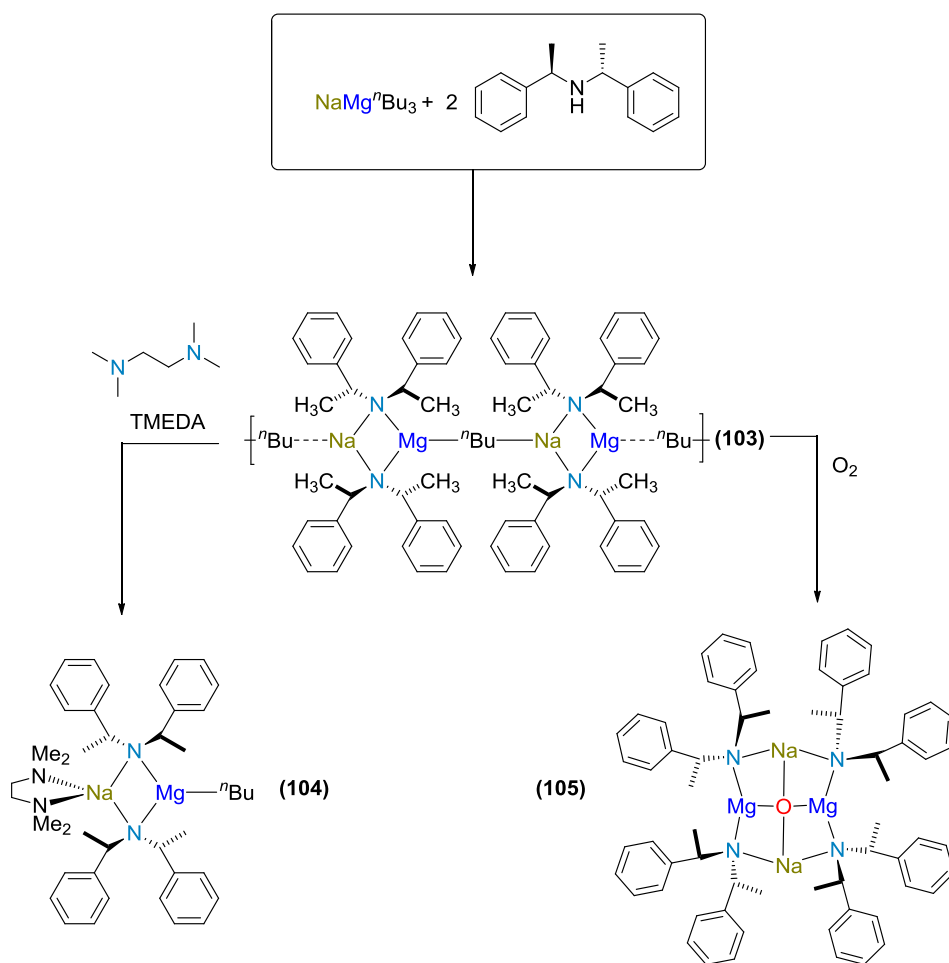
Scheme 3.9 Synthesis of chiral sodium magnesiates **103**, **104** and **105**.

3.3.2   Solid state molecular structures

3.3.2.1 [Na(μ-PEA)$_2$Mg^{n}Bu]$_\infty$ (103)

Crystallisation of **103** was achieved by suspending 1 mmol of the solid in 5 mL of dried hexane. 0.7 mL of dried toluene was added while heating and the solid completely dissolved. The solution was allowed to cool down slowly in a hot water bath overnight and a crop of crystals suitable for X-ray crystallography were obtained (69 %).

Sodium magnesiate **103** was found to be a one-dimensional polymeric chain that propagates through a Na$\cdots$C interaction and crystallises in the space group P4$_3$ (**Figure 3.11**). The two metallic centres are linked to each other by two chiral amines and the butyl chain bonded to the magnesium atoms acts as a bridge between adjacent [NaMg(PEA)$_2$^{n}Bu] units.

Both metallic centres adopt a trigonal planar arrangement. The bridge angle Na1-C33-Mg1 is tending towards linearity (162.5(8)°).
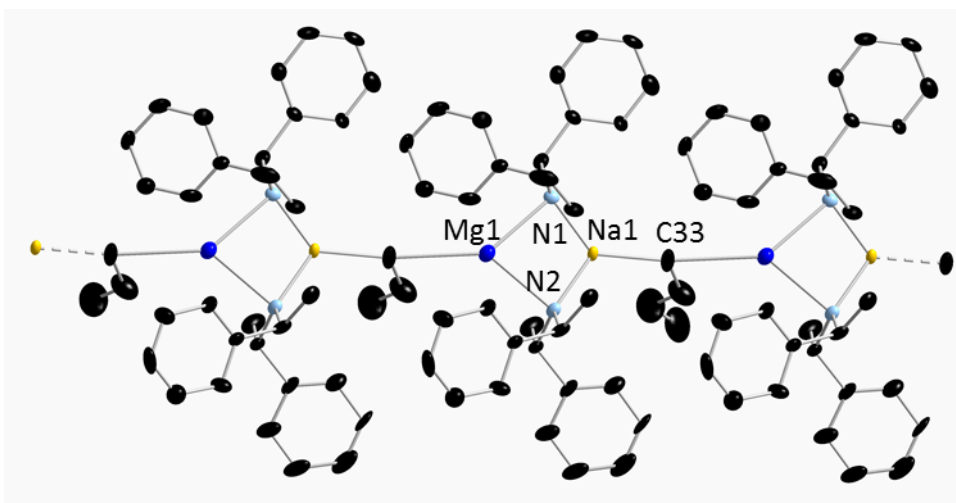
Figure 3.11 Molecular structure of **103**. All hydrogen atoms are omitted for clarity. Selected bond lengths (Å) and angles (°): Na(1)-N(2), 2.533(7); Na(1)-N(1) 2.523(7); Mg(1)-N(1), 2.070(1); Mg(1)-N(2), 2.061(7); Mg(1)-C(33), 2.182(18); Na(1)-C(33), 2.882(18); Na(1)-N(1)-Mg(1), 83.4(2); N(1)-Mg(1)-N(2), 109.5(3); N(1)-Na(1)-N(2), 83.7(2); Na(1)-C(33)-Mg(1), 162.5(8). Symmetry transformations

used to generate equivalent atoms: #1 x,y-1,z   #2 x,y+1,z. Ellipsoids showed at 30% of probability level.

This complex is closely related to the sodium magnesiate recently described by O'Hara and co-workers, [Na(HMDS)$_2$Mg(^{n}Bu)]$_\infty$ (**144**).[65] The conformation of **103** resembles the conformation of **144** and their values for bond lengths and angles are very similar (**Table 3.1**).

Table 3.1 Bond lengths (Å) and angles (°) of **103** and **144.**

Bond lenghts (Å) and angles (°)	103	144
Na-N1	2.523(7)	2.486(2)
Mg-N1	2.070(1)	2.077(2)
Na-N2	2.533(7)	2.451(2)
Mg-N2	2.061(7)	2.063(2)
Na-C	2.82(2)	2.781(2)
Mg-C	2.18(2)	2.155(2)
N(1)-Na(1)-N(2)	83.7(2)	84.16(6)
N(1)-Mg(1)-N(2)	109.5(3)	106.13(7)

3.3.2.2 [(TMEDA)·Na(μ-PEA)$_2$Mg^{n}Bu] (104)

Crystallisation of **104** was achieved in dried methylcyclohexane. The homoleptic mixture NaMg^{n}Bu$_3$ was reacted with two equivalents of PEA(H) and one equivalent of TMEDA. The white suspension was gently heated to afford a colourless solution that, after being cooled down slowly, afforded a crop of colourless crystals (66 % yield).

Compound **104** is a monomeric sodium magnesiate which crystallises in the space group P 4$_3$ 2$_1$ 2.

Unfortunately, a large amount of unresolved disorder adversely affects the precision of the *n*-butyl group and therefore precludes discussion of any geometrical parameters, although its connectivity is unequivocal.
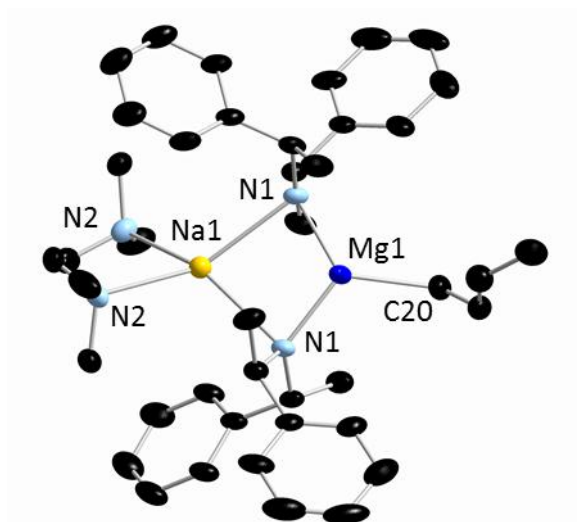
Figure 3.12 Molecular structure of **104**. All hydrogen atoms are omitted for clarity. Disorder in the butyl chain prevents talking about bond distances and angles. Symmetry transformations used to generate equivalent atoms: y,x,-z+2. Ellipsoids showed at 30% of probability level.

The addition of one molar equivalent of TMEDA affords a monomeric unit where two chiral amides bridge the two metallic centres and the magnesium atom adopts a trigonal planar arrangement binding to a terminal *n*-butyl group which, in absence of donor solvents, links monomeric units. Ancillary ligand TMEDA coordinates the sodium atom, which adopts a tetrahedral disposition.

Sodium magnesiate **104** resembles the heteroleptic monomer published by O'Hara and co-workers, $(Et_2O)\cdot NaMg\{\{N(SiMe_3)_2\}_2{}^tBu$ (**145**). The chiral amide **57** (PEA) seems to be a good mimic of the HMDS anion as in both cases the two metallic centres are bridged by two amides and magnesium atoms bears a terminal alkyl group.

TMEDA seems to be especially effective in order to get crystallisation when coordinating sodium magnesiates.[169-174] Crystallisation of the chiral sodium magnesiate coordinated by tetrahydrofuran was unsuccessful. Having a look at the crystallographic data base (CCDC), only a few sodium magnesiates

stabilised by THF can be found.[148, 175-177] Mulvey and co-workers performed the reaction of *n*-butylsodium, di-*n*-butylmagnesium and three equivalents of an amine (TMP(H) or DA(H)) in presence of THF. The reaction resulted in an unexpected but reproducible bimetallic compound with formula [(NaMg(amide)O(THF))$_6$].[175]

Complexes with formula MM'(amide)$_2$(alkyl) can crystallise with the metals bridged by two amido groups and one terminal alkyl group (in that case, the formula could be represented as M(μ-amide)$_2$M'(alkyl), **Figure 3.13 a**) or they can have one terminal amido group and the two metallic centres being bridged by one amido and one alkyl group (M(μ-amide)(μ-alkyl)M'(amide), (**Figure 3.13 b**).

That difference in the conformation is highly dependent on the nature of the amido group. In that way, all the complexes with this formula bearing HMDS[128, 129, 178] or DA[179-182] anions are with a conformation as M(μ-amide)$_2$M'(alkyl). On the other hand, all the complexes bearing bulkier TMP anions adopt the conformation M(μ-amide)(μ-alkyl)M'(amide).[80, 156, 164, 165, 183-185]
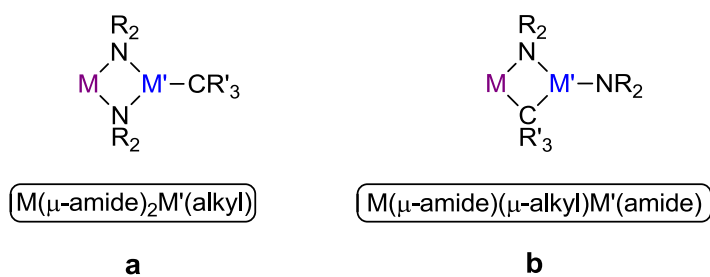
Figure 3.13 Conformations found in heteroleptic sodium magnesiates.

It seems likely that the structural similarities of the complexes that contain PEA and HMDS are due to similar steric hindrance of the amido groups so the reactivity of these new species will be studied.

3.3.2.3 Na₂Mg₂(PEA)₄O (105)

Crystallisation of **105** was achieved by reacting *n*-butylsodium, di-*n*-butylmagnesium and two equivalents of PEA(H) in 5 mL of dried hexane. After fifteen minutes, a white solid precipitates. A drying tube containing calcium chloride is inserted into the Schlenk tube and the reaction is stirred for two hours. The suspension turns from white to pale yellow. 10 mL of dried toluene were added while heating and the suspension turns to a dark orange solution which is allowed to cool down slowly in a hot water bath. A crop of needles suitable for X-ray crystallography were obtained (21 %).
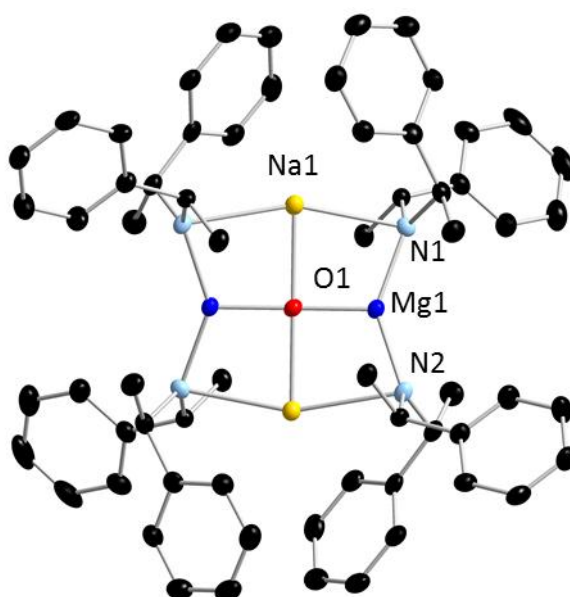
Figure 3.14 Molecular structure of **105**. All hydrogen atoms are omitted for clarity. Selected bond lengths (Å) and angles (°): Mg1-O1, 1.865(1); Mg1-N1, 2.016(4); Mg1-N2, 2.022(4); Mg1···Na1, 2.970(2); Na1-O1, 2.312(2); Na1-N1, 2.595(4); Na1-N2, 2.595(4); Na1-N1-Mg1, 79.1(1); Na1-N2-Mg1, 79.0(1); N1-Mg1-N2, 142.7(2); N1-Na1-N2, 159.6(1); Mg1-O1-Mg1', 178.7(3); Na1-O1-Na1', 179.8(3); Mg1-O1-Na1, 90.01(6). Symmetry transformations used to generate equivalent atoms: -x+1,y,-z. Ellipsoids showed at 30% of probability level.

Compound **105**, which crystallises in the C 2 space group, shows how these bimetallic species can act as oxygen scavengers and it represents the first chiral example of an inverse crown ether (

Figure 3.14).

The structure can be defined as a heterobimetallic macrocycle a dicationic $(N_4Na_2Mg_2)^{2+}$ ring framework that encapsulates a dianionic $(O)^{2-}$. Sodium and magnesium atoms are linked by PEA anions, Na-N distances being 2.595(4) Å
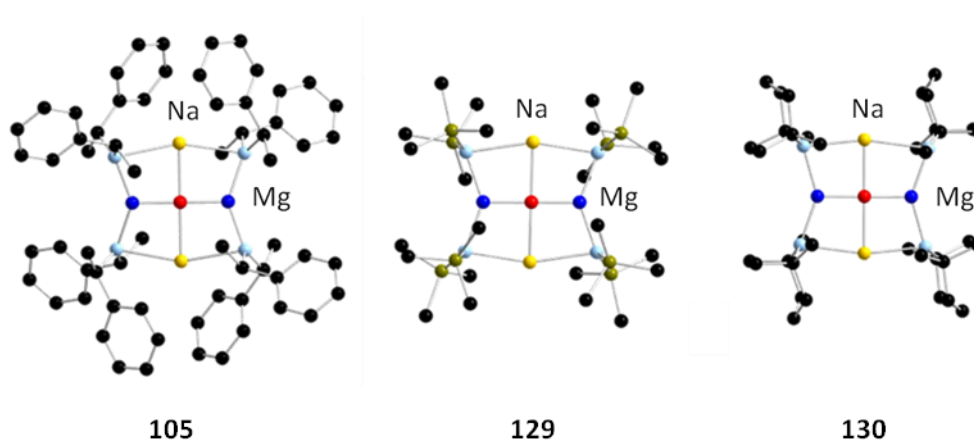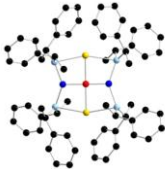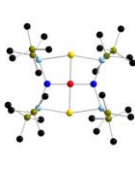
Figure 3.15 Molecular X-ray structure of **105, 129** and **130.**

 In the literature can be found two analogues to this inverse crown ether which contain the same metals linked by different amides such us HMDS (**129**)[87] and TMP (**130**)[160] (**Figure 3.15**).

Table 3.2 shows selected geometry parameters for **105** and a comparison with its analogues.

Table 3.2 Selected parameters of Na-Mg inverse Crown ethers.

	PEA (**105**)	HMDS (**129**)	TMP (**130**)
Na-N	2.595(4) 2.595(4)	2.549(1) 2.595(1)	2.445(3) 2.572(3)
Mg-N	2.016(4) 2.022(4)	2.049(1) 2.055(1)	2.032(2) 2.063(2)
Na-O	2.312(2)	2.3278(7)	2.241(1)
Mg-O	1.865(1)	1.8575(4)	1.8673(9)
N1-Na-N2	159.6(1)	156.8(2)	166.57(9)
N1-Mg-N2	142.7(2)	141.6(5)	144.5(1)
Na-N1-Mg	79.1(1)	78.76(4)	79.84(9)
Na-N2-Mg	79.0(1)	79.86(4)	77.93(8)

From the comparison of bond lengths shown in **Table 3.2**, it appears that the steric bulk of the amido component influences the molecular structure of the inverse crowns. In general terms, bond distances and angles of molecule **105** are more similar to the inverse crown described previously when HMDS was employed and this perhaps could be an indicative that the steric hindrance of PEA is closer to HMDS than TMP.

Perhaps one of the main differences of these three complexes is the disposition on the plane of the metals and the anions (**Figure 3.16**).

For the TMP-containing compound (**130**) the ring and its guest are coplanar. Magnesium, nitrogen and oxygen atoms of compound **129** ($Na_2Mg_2HMDS_4O$) are coplanar, while one sodium atom is above and the other below the plane. The ring core of the sodium magnesiate **105** is composed by the four metallic centres and the oxygen atom in the same plane, while two alternating nitrogen atoms are below and two are above the plane.
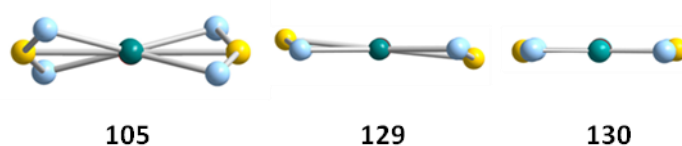
Figure 3.16 Frontal representation of ring core of inverse crown ethers (Na$_2$Mg$_2$(PEA)$_4$O) (**105**), (Na$_2$Mg$_2$HMDS$_4$O) (**129**) and (Na$_2$Mg$_2$TMP$_4$O) (**130**).

3.3.3   Solution NMR spectroscopic studies

^{1}H and ^{13}C NMR studies of compounds **103**, **104** and **105** were performed in deuterated toluene solution.

Table 3.3 shows the ^{1}H NMR resonances for products **103**, **104** and **105**. As a first conclusion, it seems evident that none of the products have separated into their starting materials. As expected, the values for these resonances appear more downfield than those for NaPEA, but more upfield than the signals of [n]BuMgPEA.

Table 3.3 Chemical shifts of NaPEA, [n]BuMgPEA and sodium magnesiates **103**, **104** and **105**.

Standard	CH$_3$ (PEA)	CH (PEA)	Ph (PEA)
NaPEA	1.110 - 1.491	3.682 - 3.729	6.978 - 7.272
[n]**BuMgPEA**	1.657 - 1.662	3.939 - 3.986	6.907 - 7.366
103	1.129 - 1.146	3.714 - 3.760	7.000 - 7.230
104	1.549 - 1.566	3.923 - 3.973	7.079 - 7.432
105	1.645 - 1.662	3.765 - 3.814	6.998 - 7.300

The ^{1}H NMR spectrum of the magnesium derivative appears to be particularly complex, probably due to equilibrium processes taking place in solution, a phenomenon which has been encountered in other alkylamido magnesium compounds.[186]

Stalke recently stated: "*Determination of the aggregation and solvation numbers of organometallic complexes in solution is an important task to increase insight in reaction mechanisms. Thus knowing which aggregates are*

formed during a reaction is of high interest to develop better selectivity and higher yields".[187]

Stalke and co-workers showed in this publication that the addition of one internal reference, which could be the solvent itself if the signal does not overlap with the complex, together with an external calibration is sufficient to get a good approximation of the molecular weight.

In this study, based on the correlation of the diffusion coefficient and the molecular weight, internal calibration curves were created to predict the molecular weight of the "polymer" in deuterated toluene solution.

[1]H DOSY studies of polymer **103** have been performed in deuterated toluene to have an insight into the aggregation state of the polymer in this solvent. [1]H DOSY studies of this polymer in deuterated tetrahydrofuran have also been carried out, as reactivity studies in tetrahydrofuran will be evaluated later on.

3.3.3.1 ^{1}H DOSY studies in D_8-tol

Polymer **103** and the internal standards 1,2,3,4-tetraphenylnaphthalene (TPhN), 1-phenylnaphthalene (PhN), and tetramethylsilane (TMS) were dissolved in deuterated toluene and ^{1}H DOSY studies were carried out.

Figure 3.17 shows the two-dimensional spectrum in which can be found four sets of signals with different diffusion coefficient (along the Y-axes). Resonances for compound **103** remain together so the arene solvent does not seem to separate the bimetallic mixture into its corresponding starting materials.
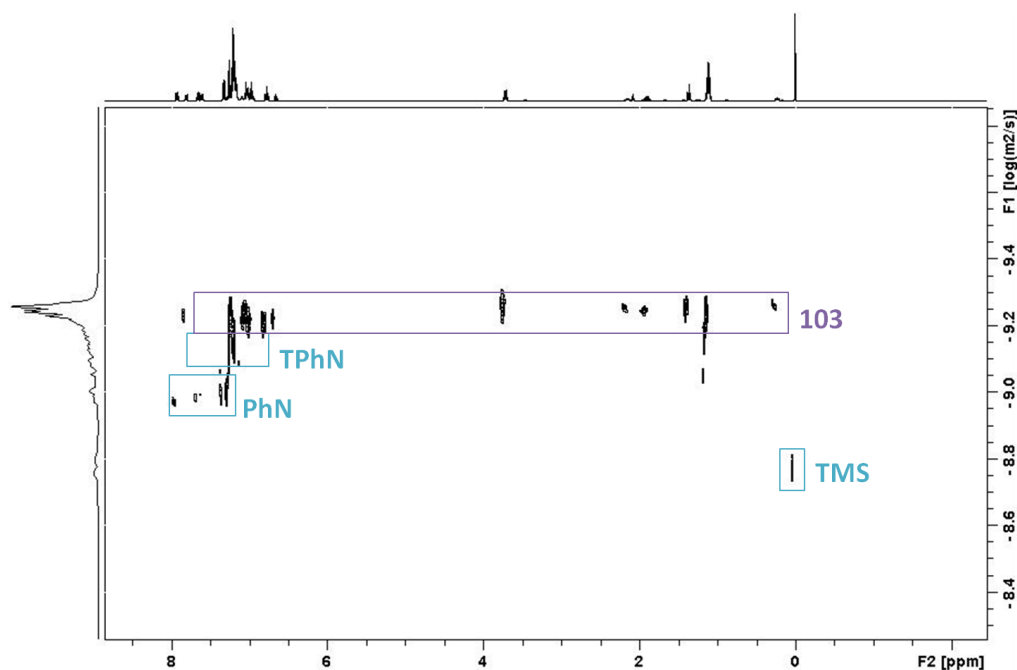
Figure 3.17 ^{1}H DOSY spectrum for **103** in D$_8$-tol.

The logarithm of the diffusion coeffient of the internal standards can be represented versus the logarithm of their molecular weights (**Figure 3.18**).

These data are related by the correlation curve log D = −0.673 log FW − 7.444 (R^2 = 0.999). By extrapolation of the data for the average coefficient diffusion of polymer **103** (average D=5.60x10^{-10}) can be estimated that the average molecular weight of this compound is 485 g/mol (**Table 3.4**).

The molecular weight for the monomeric unit [NaMg(PEA)$_2${^{n}}Bu] is 552 g/mol so the error associated to this value is 13%. This is a high value so the composition of compound **103** in deuterated toluene solution cannot be estimated, but the analysis of this data suggests that the polymeric constitution of this magnesiate is not retained in solution.

Future studies will focus on repeating this experiment in an attempt at unraveling how **103** behaves in D$_8$-toluene solution.

$$y = -0.673x - 7.444$$
$$R^2 = 0.999$$
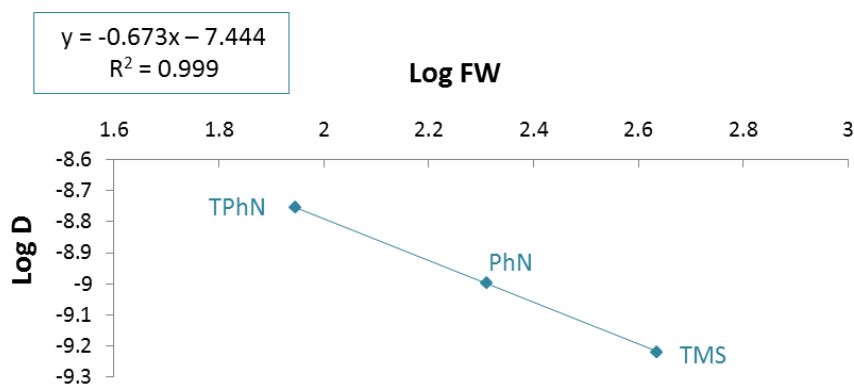
Figure 3.18 Calibration curve for the internal standards added to perform DOSY experiment of **103** in in D_8-toluene.

Table 3.4 Data of ^{1}H DOSY experiment of **103** in D_8-toluene.

Standard	D (av)	Log FW	Log D	FW
TPhN	6.04×10^{-10}	2.64	-9.22	432.5
PhN	1.01×10^{-9}	2.31	-9.00	204.3
TMS	1.76×10^{-9}	1.94	-8.75	88.2
103	5.60×10^{-10}	2.68	-9.25	**484.9**

3.3.3.2 ^{1}H DOSY studies in D_8-THF

Following the same procedure, polymer **103** and the internal standards 1,2,3,4-tetraphenylnaphthalene (TPhN), 1-phenylnaphthalene (PhN), and tetramethylsilane (TMS) were dissolved in deuterated tetrahydrofuran and ^{1}H DOSY studies were carried out.
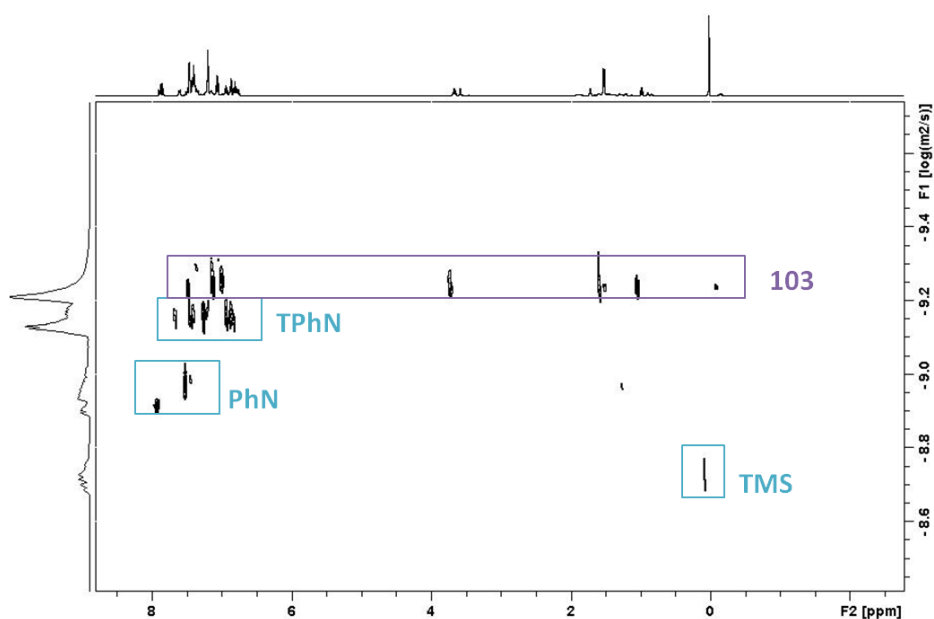
Figure 3.19 ^{1}H DOSY spectrum of **103** in D8-THF.

Figure 3.19 shows the two-dimensional spectrum in which can be found four sets of signals with different diffusion coefficient (along the Y-axes).

Table 3.5 shows the data of the diffusion coefficient and molecular weights of the internal standards and **103** in D_8-THF. These data are related by the correlation curve $\log D = -0.593 \log FW - 7.571$ ($R^2 = 0.996$) (**Figure 3.20**). By extrapolation of the data for the average coefficient diffusion of polymer **103** (average $D=5.88 \times 10^{-10}$) can be estimated that the average molecular weight of this compound is 629 g/mol.

It seems likely that one -or several- molecule of deuterated tetrahydrofuran coordinates to the sodium centre breaking the polymeric structure. The monomer [$(D_8$-THF)$\cdot$NaMg(PEA)$_2{}^n$Bu] would have a molecular weight of 632 g/mol and therefore, an associated error to the experimental value of 0.5%.

Table 3.5 Data of ^{1}H DOSY experiment for **103** in D_8-THF.

Standard	D (av)	Log FW	Log D	FW
TPhN	7.20×10^{-10}	2.64	-9.14	432.5
PhN	1.19×10^{-9}	2.31	-8.93	204.3
TMS	1.85×10^{-9}	1.94	-8.73	88.2
103	5.88×10^{-10}	2.80	-9.23	**629.4**

$$y = -0.593x - 7.5709$$
$$R^2 = 0.9956$$
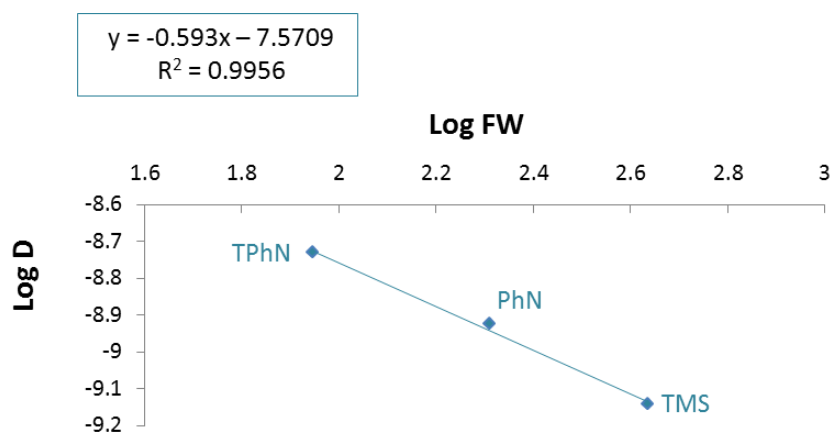
Figure 3.20 Calibration curve for the internal standards added to perform DOSY experiment of **103** D8-THF.

3.3.4 Disproportionation in magnesiates

Reaction of the homoleptic mixture NaMg^{n}Bu$_3$ with one molar equivalent of PEA(H) (**57**-(H)) in hexane affords a pink oil which, on addition of one equivalent of TMEDA, forms a white suspension. Crystallisation of this solid was achieved by heating the mixture and letting it cool down slowly. Suitable crystals for X-ray crystallographic analysis were formed and found that the white power was the bisamido sodium magnesiate **104** (**Scheme 3.10**).

The formation of this compound instead of the expected monoamido-sodium magnesiate may be as a result of an equilibrium process where the monoamido-bisalkyl sodium magnesiate disproportionates into the bisamido-monoalkyl magnesiate and the homoleptic tri-*n*-butylsodium magnesiate (**Scheme 3.10**).
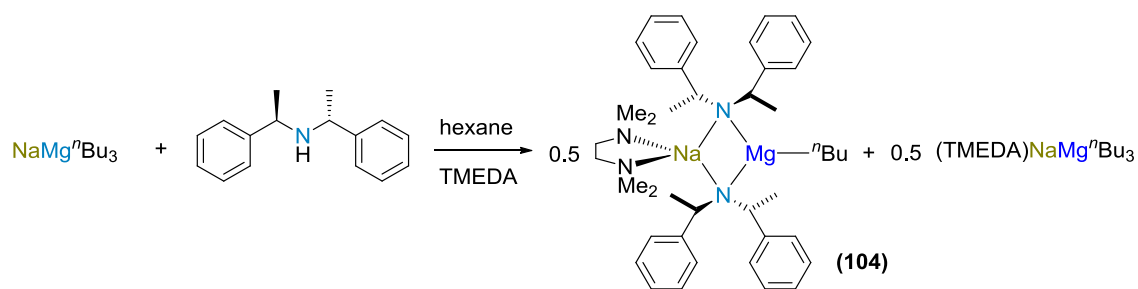
Scheme 3.10 Disproportionation process during the reaction of NaMg^{n}Bu$_3$ and one molar equivalent of PEA(H) in hydrocarbon solvent.

A similar equilibrium was described in Chapter 2 for the lithium magnesiate LiMg(PEA)(CH$_2$SiMe$_3$)$_2$, when solution studies seemed to indicate that two species were present (**Scheme 2.15**).

Disproportionation processes are common in organometallic chemistry.[170,] [188,] [189] One of the most important disproportionation processes is the reaction described by Schlenk where heteroleptic alkyl or aryl magnesium halide complexes (with general formula RMgX) disproportionate into their homoleptic component parts (**Scheme 3.11**).[190]
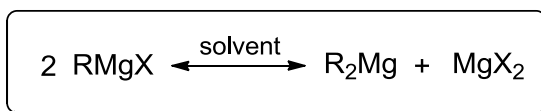
Scheme 3.11 Schlenk equilibrium

This equilibrium is highly influenced by the solvent (amongst other factors such as temperature or concentration). In the presence of monoethers, as they coordinate the magnesium atom of the alkyl (or aryl) magnesium halide, the equilibrium is shifted to the left side of the equation. In contrast, when dioxane is added to the solution, this bidentate donor binds to the magnesium halide forming a white precipitate and shifting the equilibrium towards the right side.[191]

NMR studies of the bimetallic sodium-magnesium system represented in **Scheme 3.10** have been performed in deuterated toluene, to avoid precipitation of the products.

^{1}H NMR spectrum of the in-situ reaction of an equimolar mixture of ^{n}BuNa, ^{n}Bu$_2$Mg and **78** shows two different signals for the proton N(CH(Me)Ph)$_2$ of the chiral amine at 3.77 and 4.03 ppm. When this spectrum is compared with the ^{1}H NMR spectrum of the unsolvated **103** in deuterated toluene, can be appreciated how the signal at 3.77 ppm appears to correspond to this bisamido-monoalkyl compound (**103**).

Three species are present in equilibrium: the monoamido species [NaMg(PEA)^{n}Bu$_2$], the "polymer" **103** and homoleptic NaMg^{n}Bu$_3$.

The ^{1}H NMR spectrum shown in **Figure 3.21** highlights how the bisamido magnesiate **103** is present as a minor product.
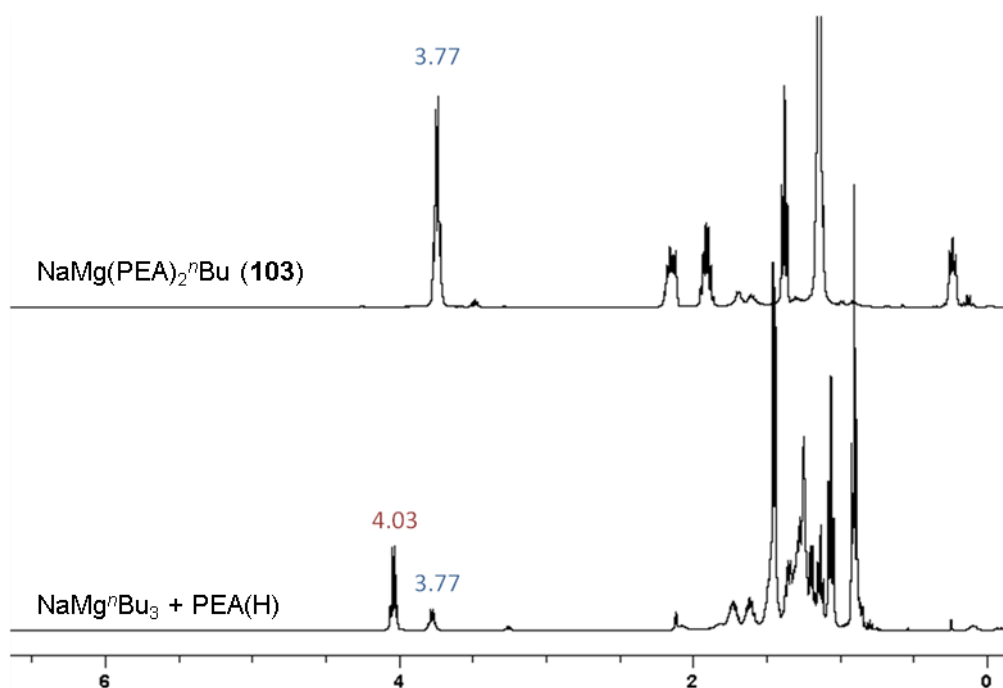
Figure 3.21 ^{1}H NMR spectra in D$_8$-toluene of sodium magnesiate **103** (top) and a mixture of NaMg^{n}Bu$_3$ + PEA(H) (bottom).

Apart from the previously discussed Grignard reagents, solvents can also induce disproportionation processes in different magnesium systems.[65, 163, 186, 192, 193]

^{1}H NMR studies of the reaction in presence of TMEDA were performed (**Figure 3.22**) to evaluate the effect of this bidentate donor during the disproportionation process.

Figure 3.22 b shows the ^{1}H spectrum in D8-toluene of a equimolar mixture of NaMg^{n}Bu$_3$, PEA(H) and TMEDA.

The quadruplet present at 3.953 ppm belongs to the proton N(CH(Me)Ph)$_2$ of the amine present in the monomer **104** (**Figure 3.22 b**). There are also resonances for the butyl chains of the compound (TMEDA)NaMg^{n}Bu$_3$. Therefore, the equilibrium is totally shifted to the right side of the equation (**Scheme 3.10**) when one equivalent of TMEDA is added to the solution.
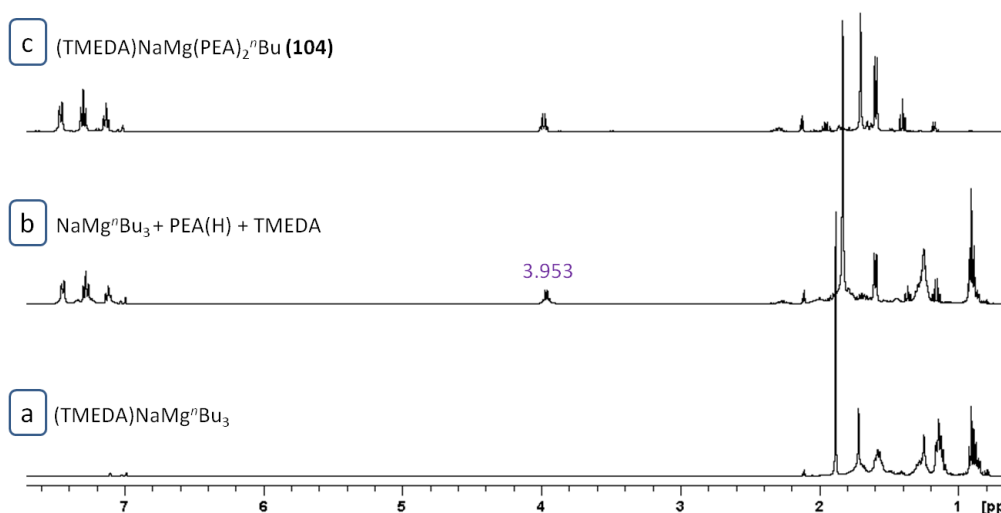
Figure 3.22 Comparison of the ^{1}H NMR specta of (TMEDA)NaMg^{n}Bu$_3$, **146 (a)**, the in-situ mixture of NaMg^{n}Bu$_3$ + PEA(H) + TMEDA (**b**) and the monomer (TMEDA)NaMg(PEA)$_2$^{n}Bu, **137 (c)**.

Scheme 3.12 shows the postulated equilibrium processes that may be happening during the synthesis of "(TMEDA)NaMg(PEA)^{n}Bu$_2$".
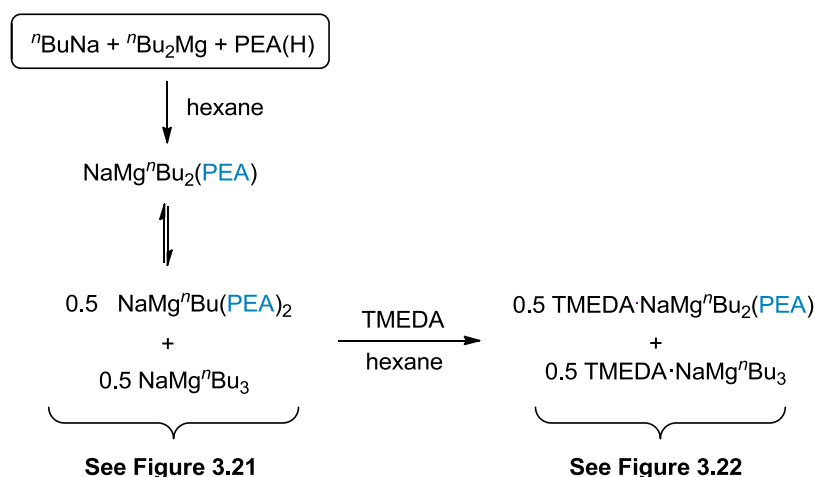
Scheme 3.12 Postulated disproportionation equilibrium of the mixture $NaMg^nBu_3$ + PEA(H) before and after the addition of TMEDA.

Garden related the disproportionation process in zincate chemistry with the steric bulk and also the basicity of the amido group,[194] with the tendency to induce disproportionation being inversely proportional to the bulkiness and basicity of the amido group.

But disproportionation processes seems to be more likely in monoamido bisalkyl magnesiate chemistry than with the respective zinc chemistry. While the TMP-containing sodium zincates (TMEDA)·NaZn(TMP)$^tBu_2$[195] or (TMEDA)·NaZn(TMP)(CH$_2$SiMe$_3$)$_2$[196] have been characterised and remain stable in solution, the sodium magnesiate "(TMEDA)NaMg(TMP)$^nBu_2$" has never been characterised as it disproportionates into the synthetically important (TMEDA)·NaMg(TMP)$_2^nBu$ (**134**) and (TMEDA)·NaMg$^nBu_3$.[156] The difference on the nature of the alkyl group could be an important factor to promote or avoid disproportionaton; however, a search in the CCDC revealed that no monoamido-bisalkyl magnesiate species have been characterised.

Chiral amide **57** may not be bulky -or basic- enough to facilitate the isolation of the monoamido sodium magnesiate, but curiously, it was found to be too bulky to allow the formation of the the trisamido-sodium magnesiate "NaMg(PEA)$_3$". Reaction of NaMg$^nBu_3$ with three equivalents of **57** at ambient temperature

invariably lead to the bisamido complex **103** or complex **104** when TMEDA was present.

Once the synthetic pathways were explored, complexes **103** and **104** were tested as bases for the deprotonation of 4-*tert*-butylcyclohexanone (**76**).

3.3.5 Organic transformations

As a first approach, deprotonation of cyclohexanone **76** with the monometallic counterparts of the chiral sodium magnesiates **103** and **104** were studied (**Scheme 3.13**).

The reaction of **76** with NaPEA in THF at -78°C for 1 hour and subsequent quench with SiMe$_3$Cl, affords the corresponding silyl enol ether in quantitative yield but with no enantiomeric excess. On the other hand, no conversion was achieved with the magnesium derivative ^{n}BuMgPEA it only undergoes a reaction with 48% yield, but the product of this reaction is the addition of the butyl chain to the carbonylic carbon not the desired deprotonation.
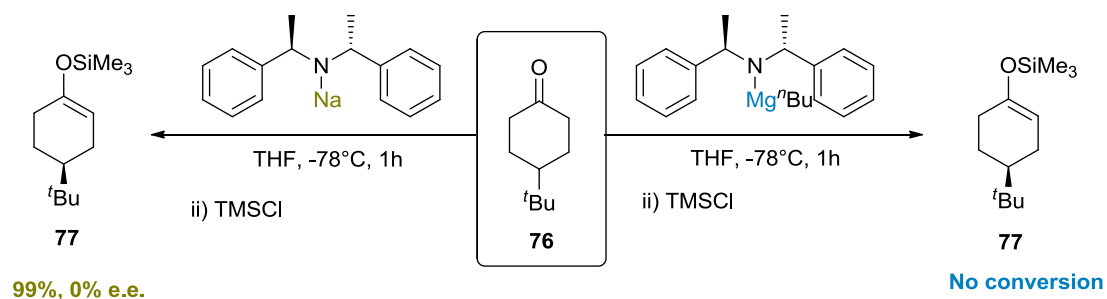
Scheme 3.13 Deprotonation of 4-*tert*-butylcyclohexanone (**76**) by monometallic reagents.

Tetrahydrofuran is probably one of the most utilised solvent to carry out organic transformations with organometallic compounds as it forms strong complexes with metals[197] and it is more basic than other ether such us diethyl ether,[198] hence the reactions in which polymer **103** used were performed in this solvent. To preserve the coordination of TMEDA to the sodium centre, the reactions in which the monomer **104** was involved were perfomed in toluene, as

the ¹H NMR analysis of **104** in D$_8$-THF shows only signals for free TMEDA (**Figure 3.23**).
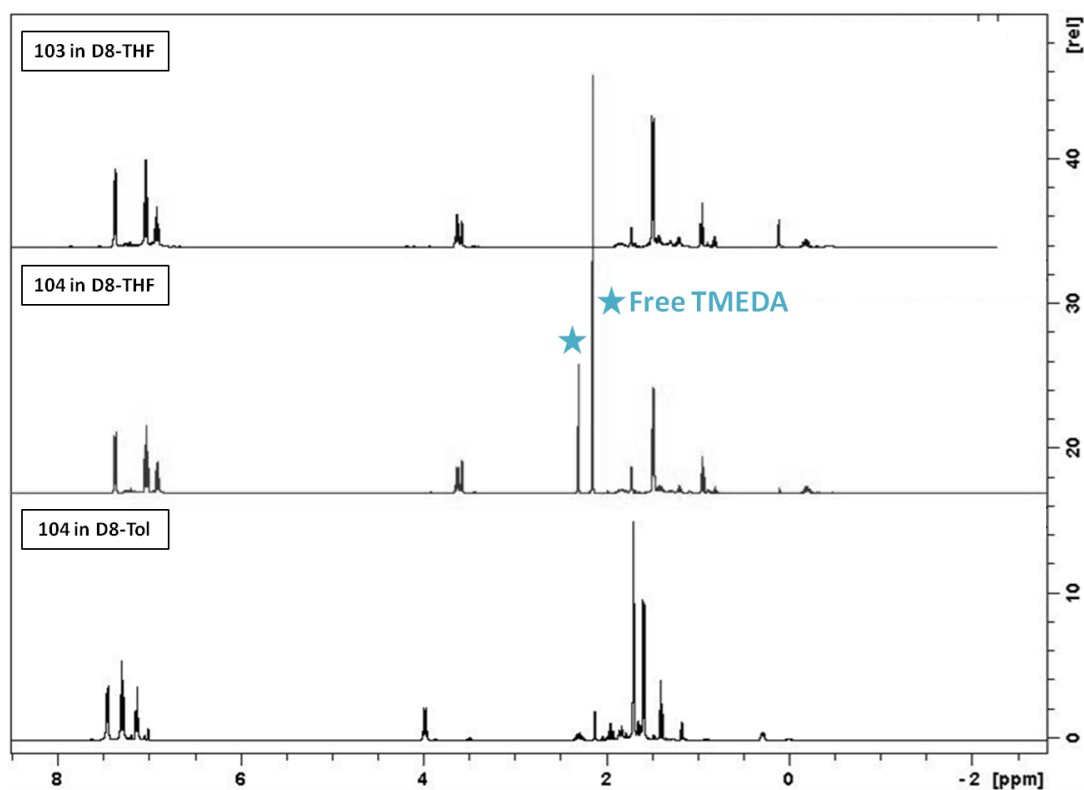
Figure 3.23 ¹H NMR spectra of **103** in D$_8$-THF and **104** in D$_8$-THF and D$_8$-Tol.

When using PEA, as the only magnesiate stable in solution is the bisamido-monoalkyl sodium magnesiate, the reactions were performed using a 1:2 ratio of the base and the ketone (**Scheme 3.14**).
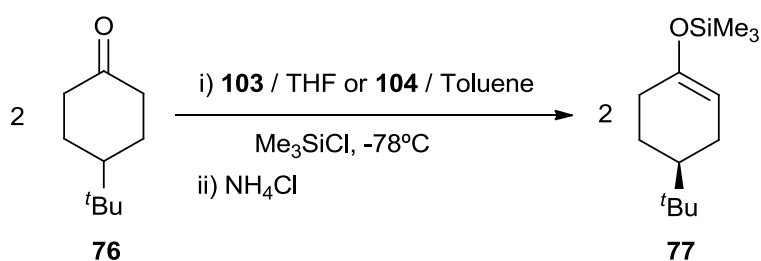
Scheme 3.14 Asymmetric deprotonation of the prochiral ketone **76** using sodium magnesiates.

Time (h)	Conversion (%)	
	103	104
0.5	87	58
1	90	63
2	92	69
3	98	73
8	98	78
24	99	78
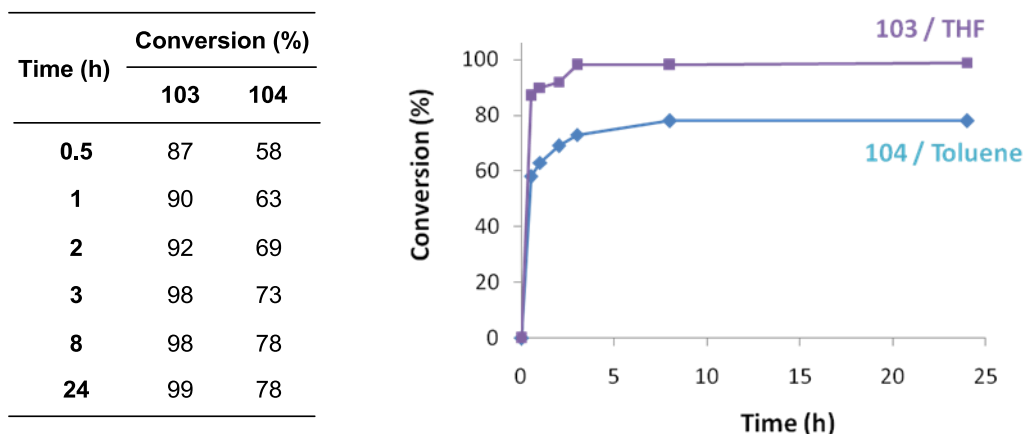
Figure 3.24 Conversion of the deprotonation reactions performed using **103** and **104** as bases.

Figure 3.24 represents the conversion of ketone to silyl enol ether versus time. The conversion of the reaction is lower when TMEDA-stabilised magnesiate **104** was used. This could be rationalised as the first step for this reaction could be the coordination of the sodium centre to the oxygen atom of the carbonyl group of the ketone. The presence of the bidentate ligand would cause an important steric hindrance so this coordination would be less effective than when THF is used as a donor.

Enantioselectivity of the process does not seem to be affected by the donor as the enantiomeric ratio found when THF or TMEDA were employed were 85:15 and 87:13 respectively.

The reactions were performed with internal quench method, as this had an impressive effect over the speed of the process. In external quench conditions, the conversion of the reaction with **103** was only 11%, while this result was found to be 87% with internal quench (**Table 3.6**).

The conversion to the silyl enol ether **77** is slightly lower when external quench conditions and when LiCl are employed but the enantiomeric excess dramatically decreases. LiCl causes the opposite effect when the reaction is performed with the lithium amide LiPEA as Simpkins found that the

employment of this salt with external quench improved the enantiomeric excess from 63% (IQ) or 23% (EQ) to 83%.[114]

Table 3.6 Progress of the reaction when **103**/THF was used with different quench methods.

	Conversion (%)		
	IQ	EQ	EQ + LiCl
0.5	87	11	58
1	90	13	63
2	92	17	69
3	98	26	73
8	98	65	78
24	99	93	78
e. r.[a]	70	64	32

[a]Values of enantioselectivities after 24 hours of reaction.

Table 3.7 summarises the results obtained for the synthesis of **77** employing different organometallic compounds bearing the same chiral centre. In all the cases the reaction has been performed in THF at −78°C. The reaction time is 1 hour for LiPEA,[136] LiMg(PEA)(CH$_2$SiMe$_3$)$_2$[127] and NaMg(PEA)$_2$^{n}Bu. In the case of Mg(PEA)$_2$[125] the authors only reported data for reaction time of 16 hours (**Table 3.7**).

In terms of conversion, sodium magnesiates are the most efficient reagents as the yield achieved after 1 hour of reaction is 90%. This value is increased when Mg(PEA)$_2$ but the monometallic reagent, not only needs longer reaction times but also the reaction is not as atom efficient as two equivalents of the chiral amine are needed for every mol of ketone.

As expected, the sodium-containing compound reacts faster than the complexes of lithium. However, this seems to be detrimental in terms of the

enantioselectivity of the process as the enantiomeric excess of the silyl enol ether is the lowest when $NaMg(PEA)_2{}^nBu$ is used.

Table 3.7 Comparison of the progress of the reaction employing different organometallic compounds in THF at −78°C.

	$LiPEA^{a, c}$	$Mg(PEA)_2{}^b$	$LiMg(PEA)(CH_2SiMe_3)_2{}^a$	$NaMg(PEA)_2{}^nBu^a$
Conversion	73%	93%	72%	90%
enantiomeric excess	69%	86%	86%	70%

[a] Reaction time = 1 hour
[b] Reaction time = 16 hours
[c] Enantiomeric excess is 84% when EQ+LiCl conditions are employed.

3.4 Experimental

3.4.1 Synthesis of 103,$[Na(μ\text{-}PEA)_2Mg^nBu]_∞$

^nBuNa (1 mmol, 0.08 g) was suspended in 5 mL of dried hexane and placed in an ultrasonic bath for 10 minutes. $^nBu_2Mg$ (1 mmol, 1 mL of 1 M solution in heptanes) was added and a white solid is formed. Addition of PEA(H) (2 mmol, 0.46 mL) and stirring for three hours afforded to a white precipitate (0.45 g, 81%). Addition of 0.7 mL of toluene while heating gives a clear solution which is allowed to cool down in a hot water bath to give **103** in crystalline material suitable for X-ray crystallographic analysis. (0.38 g, 69%).

^{1}H NMR (400.13 MHz, 300 K, D8-THF): δ −0.32-−0.14 (2H, br, CH_2-Mg) 0.80-0.84 (3H, t, $^3J_{HH}$=7.2 Hz, CH_3, Bu), 0.94-0.98 (2H, br, CH_2, Bu), 1.22-1.23 (12 H, d, $^2J_{HH}$=7.2, CH_3, PEA), 1.72-1.85 (2H, br, CH_2, Bu), 3.61-3.66 (4H, q, $^4J_{HH}$=, CH, PEA), 6.91-6.94 (4H, CH_{para}, PEA), 7.03-7.07 (8H, $CH_{2(meta)}$, PEA), 7.37-7.39 (8H, $CH_{2(ortho)}$, PEA). ^{13}C{^{1}H} NMR (100.62 MHz, 300 K, D8-THF): δ 14.9 (CH_3, Bu), 16.4 (Mg-CH_2, Bu), 29.1 (CH_3, PEA), 33.2 (CH_2, Bu), 34.8 (CH_2, Bu), 62.3 (CH, PEA), 124.6 (CH_{para}, PEA), 127.5 (CH_{meta}, PEA), 128.6 (CH_{ortho}), 155.2 (C_{ipso}, PEA).

^{1}H NMR (400.13 MHz, 300 K, D8-toluene): δ 0.21-0.25 (2H, br, CH_2-Mg), 1.13-1.15 (12 H, d, $^3J_{HH}$=6.7, CH_3, PEA), 1.36-1.39 (3H, t, $^3J_{HH}$=7.2 Hz, CH_3, Bu), 1.86-1.94 (2H, br, CH_2, Bu), 2.11-2.17 (2H, br, CH_2, Bu), 3.71-3.77 (4H, q, $^3J_{HH}$=6.7, CH, PEA), 7.00-7.23 (10H, br, Ph, PEA). ^{13}C{^{1}H} NMR (100.62 MHz, 300 K, D8-toluene): δ 14.4 (CH_3, Bu), 14.7 (Mg-CH_2, Bu), 24.7 (CH_3, PEA), 32.7 (CH_2, Bu), 33.7 (CH_2, Bu), 59.2 (CH, PEA), 126.5 (CH_{para}, PEA), 127.0 (CH_{meta}, PEA), 129.2 (CH_{ortho}), 151.3 (C$_{ipso}$, PEA).

Elemental Microanalysis calculated for **103**; C, 78.21; H, 8.24; N, 5.07%; found: C, 75.59; H, 9.15; N, 8.72%.

3.4.2   Synthesis of 104, [TMEDA]·Na(μ-PEA$_2$)Mg^{n}Bu

^{n}BuNa (1 mmol, 0.08 g) was suspended in 5 mL of methylcyclohexane and placed in an ultrasonic bath for 10 minutes. ^{n}Bu$_2$Mg (1 mmol, 1 mL of 1 M solution in heptanes) was added and a white solid is formed. Addition of PEA(H) (2 mmol, 0.46 mL) and stirring for three hours afforded clear solution. Addition of TMEDA (1 mmol, 0.15 mL) afforded a white precipitate which was redissolved by gently heating. Cooling slowly in a hot water bath affords a crop of needles suitable for X-ray crystallographic analysis. (0.44 g, 66%).

The reaction can be carried out in hexane in order to isolate **104** as a white solid to improve the yield (0.59g, 88%).

^{1}H NMR (400.13 MHz, 300 K, D8-toluene): δ 0.24-0.28 (2H, br, CH_2-Mg) 1.35-1.38 (3H, t, $^3J_{HH}$=7.6 Hz, CH_3, Bu), 1.55-1.57 (12 H, d, $^3J_{HH}$=, CH_3, PEA), 1.59-1.62 (2H, CH_2, TMEDA) 1.67 (12H, CH_3, TMEDA), 1.55-1.57 (12H, CH_3, TMEDA), 1.80-1.82 (2H, CH_2, TMEDA), 1.87-1.96 (2H, br, CH_2, Bu), 2.20-2.24 (2H, br, CH_2, Bu), 3.92-3.97 (4H, q, $^4J_{HH}$=, CH, PEA), 7.08-7.12 (4H, CH_{para}, PEA), 7.24-7.28 (8H, C$H_{2(meta)}$, PEA), 7.41-7.43 (8H, C$H_{2(ortho)}$, PEA). ^{13}C{^{1}H} NMR (100.62 MHz, 300 K, D8-toluene): δ 14.7 (CH_3, Bu), 15.0 (Mg-CH_2, Bu), 27.8 (CH_3, PEA), 32.7 (CH_2, Bu), 33.7 (CH_2, Bu), 45.8 (CH_3, TMEDA), 57.3 (CH_2, TMEDA), 60.5 (CH, PEA), 126.1 (CH_{para}, PEA), 127.4 (CH_{meta}, PEA), 128.5 (CH_{ortho}), 151.5 (C$_{ipso}$, PEA).

Elemental Microanalysis calculated for **104**; C, 75.41; H, 9.24; N, 8.37%; found: C, 73.85; H, 9.12; N, 8.54%.

3.4.3   Synthesis of 105, Na$_2$Mg$_2$(PEA)$_4$O

*n*BuNa (4 mmol, 0.08 g) was suspended in 5 mL of dried hexane and placed in an ultrasonic bath for 10 minutes. *n*Bu$_2$Mg (4 mmol, 1 mL of 1 M solution in heptanes) was added and a white solid is formed. Addition of PEA(H) (8 mmol, 1.84 mL) and stirring for three hours afforded a white precipitate. A drying tube was placed in the Schlenk tube for 4 hours, and the suspension becomes pale yellow. Addition of 10 mL of toluene afforded a dark orange solution which is allowed to cool down slowly in a hot water bath, affording colourless needles suitable for X-ray diffraction. (0.41 g, 21%).

^{1}H NMR (400.13 MHz, 343 K, d8-toluene): δ 1.64-1.66 (6H, CH$_3$, PEA), 3.77-3.81 (2H, CH, PEA), 6.99-7.30 (10H, Ph, PEA + residual signal for D8-tol).

The relatively low solubility of **105** over prolonged periods of time in D$_8$-toluene solution precluded the collection of its ^{13}C{^{1}H} spectrum.

Elemental Microanalysis calculated for **105**; C, 78.21; H, 7.38; N, 5.72%; found: C, 72.25; H, 8.12; N, 4.46%.

3.4.4   Representative experimental procedure for deprotonation reactions

3.4.4.1 Asymmetric deprotonation of 76 with [NaMg(PEA)$_2$*n*Bu] in THF
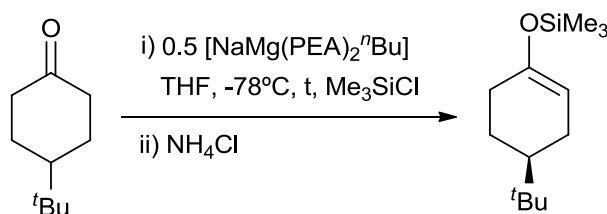
To a flame-dried and Ar-purged Schlenk flask, [NaMg(PEA)$_2$*n*Bu] (**104**) (0.276 g, 0.5 mmol) was added and dissolved in anhydrous tetrahydrofuran (5 mL). Solution was cooled down to –78°C, then freshly distilled TMSCl (1.2 mmol, 0.15 mL) were added and the reaction was stirred for 10 minutes. 4-*tert*-butylcyclohexanone (0.152 g, 1.0 mmol) was added and reaction was allowed

to stir. Regular sampling quenching with NH$_4$Cl solution and analysis by gas chromatography monitored the progress of the reaction.

3.4.4.2 Asymmetric deprotonation of 76 with [(TMEDA)·NaMg(PEA)$_2$^{n}Bu] in Toluene
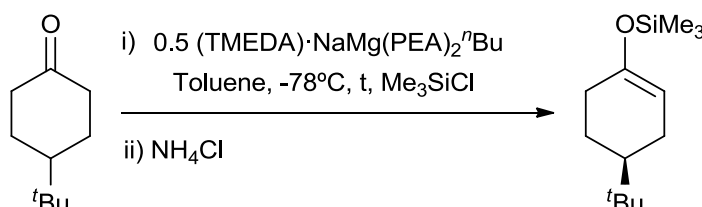
To a flame-dried and Ar-purged Schlenk flask, (TMEDA)NaMg(PEA)$_2$^{n}Bu (**104**) (0.334 g, 0.5 mmol) was added and dissolved in anhydrous toluene (5 mL). Solution was cooled down at −78°C, then freshly distilled TMSCl (1.2 mmol, 0.15 mL) were added and the reaction was stirred for 10 minutes. 4-*tert*-butylcyclohexanone (0.152 g, 1.0 mmol) was added and reaction was allowed to stir. Regular sampling quenching with NH$_4$Cl solution and analysis by gas chromatography monitored the progress of the reaction.

Characterisation of products is detailed below.

(4-*tert*-butylcyclohexen-1-enyloxy)trimethylsilane (76)

^{1}H NMR (400 MHz, 300 K, CDCl$_3$): δ 0.19 (9H, s, CH$_3$, TMS), 0.88 (9H, s, CH$_3$, ^{t}Bu), 1.20 (3H, br, C*H$_2$* and C*H* cyclohexene ring), 1.76 (2H, br, CH$_2$, cyclohexene ring), 2.09 (2H, br, CH$_2$, cyclohexene ring), 4.84 (1H, d, CH double bond cyclohexene ring).

Achiral GC analysis: Chirasil-DEX CB column 30m x 0.25mm x 0.25μm. H$_2$ carrier gas (45 cm sec^{-1}); Split ratio 75:1; Temperature gradient: 90°C, 0.5 min; 45 ºC min-1; 220°C, 6 min. t$_R$=3.69 min.

Chiral G.C. analysis: (**i**) CP Chirasil-DEX CB column 30m x 0.25mm x 0.25μm; (**ii**) carrier gas, H$_2$ (45 cm sec^{-1}); (**iii**) injector/detector temperature, 250°C; (**iv**) initial oven temperature: 70°C; (**v**) temperature gradient, 70–130°C, 1.5°C min^{-1}; 130°C, 1 min; 130-200°C, 20°C min^{-1} ; 200°C, 1 min; (**vi**) final oven

temperature, 200°C (**vii**) detection method, FID.

$t_R(S)$ = 31.75 min, $t_R(R)$ = 32.11 min

3.5 Conclusions and future work

Three new sodium magnesiates have been crystallographically characterised in this chapter.

Compound **103** was found to crystallise as a monodimensional polymer composed by [NaMg(PEA)$_2$^{n}Bu] units that are linked through a Mg···C interaction but in solution state this structure does not seem to be retained.

When TMEDA is present, the monomeric magnesiate (TMEDA)NaMg(PEA)$_2$^{n}Bu (**104**) can be synthesised and the isolation of the mono or trisamido-sodium magnesiate have not been possible.

These sodium magnesiates proved to be more reactive than the lithium or magnesium reagents during the deprotonation of the 4-*tert*-butylcyclohexanone. However, the enantioselectivities were not ideal.

The chiral inverse crown ether **105** has been rationally synthesised and characterised in this work.

O'Hara and co-workers showed that sodium magnesiates can have very different behaviour from potassium magnesiates[157] so in the future this work can be continued exploring the chemistry of the chiral amide (+)-Bis-[(*R*)-1-phenylethyl]amide with larger metals.

In addition, chiral sodium magnesiates can be employed to perform organic transformations such us rearrangement of epoxides to allylic alcohols or enantioselective reactions of tricarbonyl (η6-arene)-chromium complexes.[100]

Chapter 4. Introduction to homo and heteroleptic lithium zincates

4.1 Summary

This chapter focuses on the synthesis of chiral homoleptic and heteroleptic lithium zincates and their applications in enantioselective addition reactions to ketones.

Two new lithium zincates have been fully characterised. Compound **147**, TMEDA·Li(μ-PEA)ZnMe$_2$ is a heteroleptic bimetallic compound (contacted ion pair) prepared by combining LiPEA, Me$_2$Zn (**96**) and TMEDA.

The synthesis of a lithium zincate was tried incorporating ^{t}Bu$_2$Zn (**97**), instead of Me$_2$Zn. However, the product crystallised was a product of an intramolecular deprotonation (**148**) where the zinc atom is linked to the chiral amine by the nitrogen atoms and also by a zinc-carbon bond.

Compound **149**, (R,R)-TMCDA·Li(μ-Me)$_2$ZnMe, is a contacted ion pair as well, but in this case it is a homoleptic monomer LiZnMe$_3$ where the chiral ancillary ligand (R,R)-TMCDA completes the coordination sphere of the lithium atom.

The alkyl addition of **147** and **149** to ketones has been studied, proving the importance of the solvent in these kind of reactions.

Solution characterisation studies of these complexes have been carried out in an attempt to relate the structure in solution with the observed reactivity.

4.2 Introduction

4.2.1 Addition of dialkylzinc reagents to ketones and aldehydes

Addition of organometallic reagents to a carbonyl group is an efficient method to form new carbon-carbon bonds.[199, 200] Although organolithium and Grignard reagents have been widely employed as alkylating reagents in many transformations,[132, 201] organozinc complexes have proven to give great results for the nucleophilic addition to aldehydes and ketones.[202-204]

The first asymmetric addition of a diorganozinc reagent to aldehydes was performed by Noguni *et al.* with moderate enantioselectivity.[205]

Two years later, Noyori and co-workers performed enantioselective addition of ZnR_2 to aldehydes with good enantiomeric excess.[206] The employment of the chiral subtituent DAIB (1*R*, 2*S*, 3*R*, 4*S*)-3-Dimethylamino-1, 7, 7-trimethylbyciclo[2, 2, 1]heptan-2-ol, **150**) allowed them to perform reactions with enantioselectivities up to 98%. However, this reaction offered poor conversions for the addition reaction to ketones (**Scheme 4.1**).

Fu *et al.* improved the reaction conditions of this conversion by adding an excess of MeOH to the zinc reagent.[207] The presence of methoxide increases the Lewis acidity of the zinc centre and the fact that diphenylzinc (β-hydrogen atoms) is employed also helps to increase the stability of the process.

Since then, numerous groups have reported successful enantioselective addition reactions with different chiral ligands.[202-204]
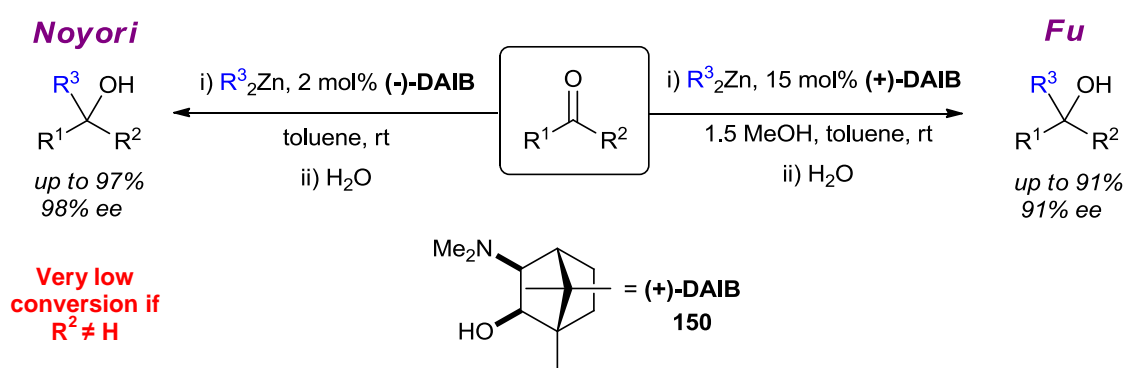
Scheme 4.1. Addition of dialkylzinc to aldehydes and ketones.

Wolf and co-workers performed the asymmetric addition of organozinc reagents to ketones, finding out that only catalytic amounts of TMEDA are needed to successfully promote the reaction to yields of up to 99%.[208]

Hevia and co-workers investigated the solid state chemistry of the reaction intermediates obtained for the addition reaction across 2,2,2-trifluoroacetophenone of diorganozinc reagents (R_2Zn where R=Me, Et, ^tBu, CH_2SiMe_3) stabilised with TMEDA.[209, 210] They showed that the addition of the alkyl group is the only product of the reaction when Me_2Zn or Et_2Zn were employed. However, for bulkier substituents such as *tert*-butyl group, the reduction of the ketone also occurs. **Figure 4.1** shows the tetranuclear intermediate of the reduction of a ketone by $^tBu_2Zn$.
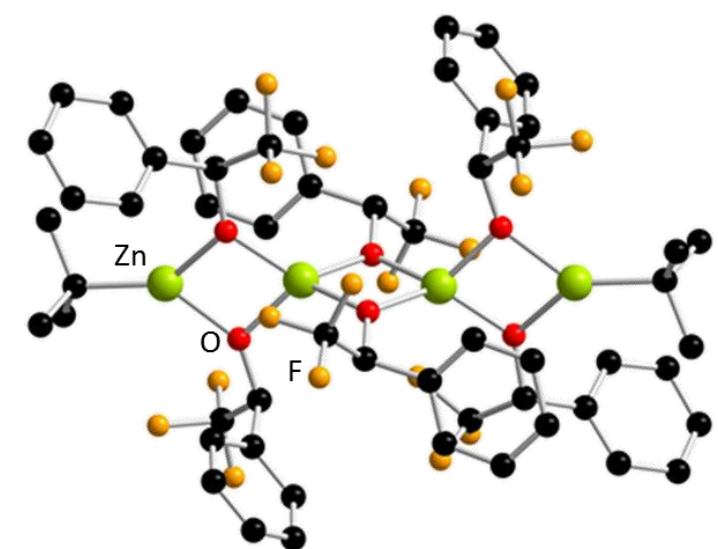
Figure 4.1 Crystal structure of $[(^tBu)_2Zn_4\{OC(CF_3)(H)Ph\}_6]$.

4.2.2 Alkali metal zincates

As indicated in **Chapter 1**, the concept of "ate" complex was first discussed by Wittig in 1959;[5] however, the first bimetallic compound ever reported was by Wanklyn in 1858 when he published the synthesis of the zincate $NaZnEt_3$.[211]

Zincates share properties with organozinc reagents as they function under mild conditions and they are functional group tolerant, but the "anion-enhanced" zinc atom of the bimetallic compound makes them more reactive.[212]

As an example, Kondo described the metalation of different aromatic compounds by employing a lithium zincate obtained by co-complexation of LiTMP and $^tBu_2Zn$ (**Scheme 4.2**).[213] The metalation proved to be unsuccessful when attempted with $^tBu_2Zn$ or if it was carried out in a stepwise manner, that is first LiTMP and then $^tBu_2Zn$. The combination of two monometallic species seems to be a requisite for the reaction to be completed.
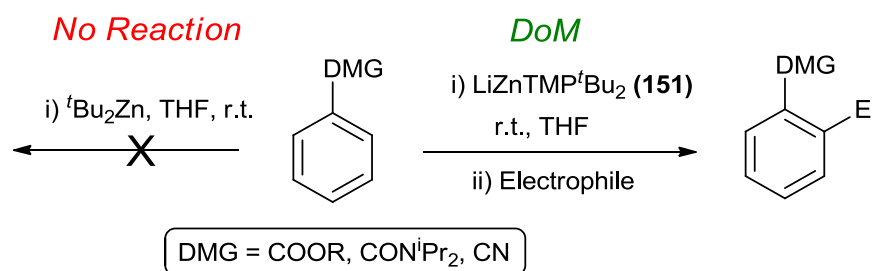
Scheme 4.2 Scheme of the metalation of aromatic substrates with a lithium zincate.

The crystal structure of zincate **151** was published by Mulvey and co-workers (**Figure 4.2**).[214] Compound **151** is a contacted ion pair zincate where the Zn atom is trigonal planar and contacts the lithium atom primarly by a N of TMP. To complete the coordination sphere of lithium, there is a weaker interaction with a methyl group (C10) so a five-membered ring (LiNZnCC) is formed.[215]
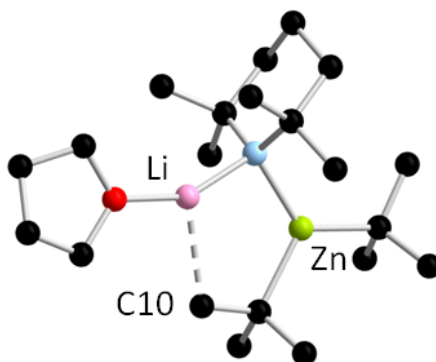
Figure 4.2. X-ray structure of **151.**

Hevia and co-workers showed the reactivity of (**151**) across pyrazine. They found that when one equivalent is treated with two molar equivalents of **151**, a selective two-fold deprotonation at the 2,5-positions of the heterocycle takes place in quantitative yield (**Scheme 4.3**).[216]

However, when pyrazine is treated with the homoleptic zincate (PMDETA)·LiZn^{t}Bu$_3$ (**152**), the reaction procees with 1,2-addition of the *tert*-butyl group of the zincate.

This is an excellent example of how the modification of the bimetallic base by simply replacing an alkyl group with an amido group can dramatically change its reactivity.
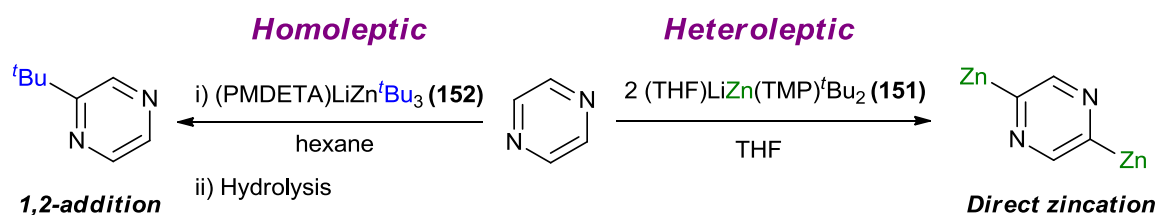
Scheme 4.3 Scheme of the reaction of pyrazine with homoleptic and heteroleptic lithium zincates.

Homoleptic lithium zincates LiZnPh$_3$ and Li$_2$ZnPh$_4$ have been evaluated by Hevia and co-workers as arylating reagents towards acridine.[217]

Lithium zincate [(TMEDA)·Li(μ-^{n}Bu)(μ-TMP)Zn(^{n}Bu)] (**155**) crystallises as a contacted ion pair and Mulvey and co-workers showed that it is capable of deprotonating ferrocene.[218] This is another example of an alkali-metal mediated zincation as LiTMP or ^{n}Bu$_2$Zn are not strong enough bases on their own to deprotonate ferrocene even in presence of donor solvents.

Sodium zincates have also proven to be very reactive towards the metalation of organic substrates.[188, 219-227] Perhaps the most striking example is the controlled deprotonation of tetrahydrofuran by a sodium zincate.[196] Very closely related to **151**, the bimetallic compound formed by combination of NaTMP and

bis(trimethylsilylmethyl)zinc in presence of TMEDA (**153**) is able to deprotonate cyclic ethers (**154**) (**Figure 4.3**).
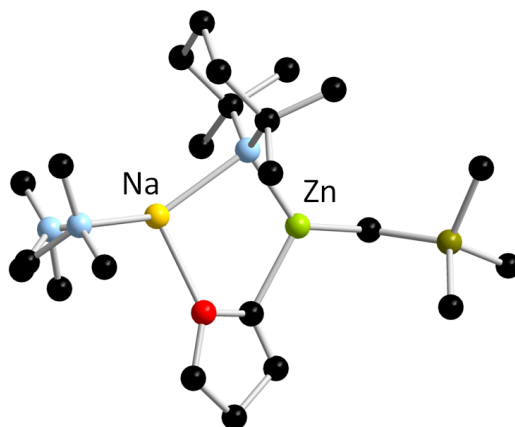
Figure 4.3 X-ray structure of [(TMEDA)·Na(μ-TMP)(μ-C$_4$H$_7$O)Zn(CH$_2$SiMe$_3$)] (**154**).

The conformation in the solid state of alkali-metal zincates is usually dictated by the solvent.[228] Stalke *et al.* studied the aggregation of the homoleptic zincate [LiZnMe$_3$] coordinated by either, PMDETA or diglyme (**156**).[75] Under identical reaction conditions, the adduct formed when PMDETA is present is a contacted ion pair with formula [(PMDETA)Li(μ-Me)$_2$ZnMe] (**157**), whereas the presence of diglyme gives the solvent separated ion pair [(diglyme)$_2$Li]$^+$[ZnMe$_3$]$^-$ (**158**).

Lower-order zincate bearing the same anionic groups was characterised by Hevia *et al* (**159**).[229] When coordinated to TMEDA molecules, it crystallises as a contacted ion pair with a chain arrangement. The nature of **158** is unexpected as only zincates with bulky substituents (SiMe$_3$, aryl[230, 231]) had been found to crystallise as solvent-separated ion pairs prior to this report.

Westerhausen characterised lithium zincates containing both, methyl and bulky group as CH(SiMe$_3$)Ph, showing that all the compounds crystallised as SSIP.[232]

4.2.3 Chiral zincates

Hevia and co-workers described the first chiral amido zincate [TMEDA·NaZn(^{t}Bu)$_2$(N(CH$_2$Ph)(CH(CH$_3$)Ph))] (**160**), bearing a chiral amide closely related to PEA (**57**).[179] Also, this publication shows a new reactivity of the heteroleptic alkylamido-zincate **153**, as found to undergo transamination reactions when reacted with different amines, which are able to replace the TMP anion in the bimetallic moiety.

Inspired by the results of Mulvey[152, 218, 233] and Knochel[234] on the deprotonation of ferrocene by bimetallic bases, Mongin performed asymmetric transformation employing chiral zincates.[106]

They studied the behaviour of a series of lithium zincates containing the chiral amine PEA (**57**) and different alkyl anions, such as methyl, ethyl, *n*-butyl or *tert*-butyl groups. As **Table 4.1** highlights, they obtained enantioselectivities up to 80% and quantitative conversions when an equimolar mixture of the base and the substrate are reacted at 0°C.

Table 4.1 Selected data for the deprotonation of substituted ferrocenes by chiral lithium zincates.

Lithium zincate	Yield (%)	Enantiomeric excess (%)
LiZn(PEA)Me$_2$	93	61
Li$_2$Zn(PEA)$_2$Me$_2$	99	65
LiZn(PEA)^{n}Bu$_2$	99	53
Li$_2$Zn(PEA)$_2$^{n}Bu$_2$	95	56
Li$_2$Zn(PEA)$_2$Me$_2$[a]	97	80

[a]Reaction performed at 0°C.

4.3 Results and discussion

Two new chiral lithium zincates have been synthesised and structurally characterised in this chapter; the heteroleptic TMEDA·Li(μ-PEA)(μ-Me)ZnMe (**147**) and the homoleptic (R,R)-TMCDA·LiZnMe$_3$ (**149**).

An unexpected intramolecular deprotonation reaction takes place when LiPEA is reacted with TMEDA·^{t}Bu$_2$Zn in hydrocarbon solvent under reflux.

Also, the reactivity in nucleophilic addition reactions of ketones has been studied.

4.3.1 Heteroleptic lithium zincates

4.3.1.1 Use of dimethylzinc, Me$_2$Zn

For the synthesis of **147**, equimolar quantities of TMEDA and Me$_2$Zn were reacted in hexane. This solution is transferred by cannula to a suspension of LiPEA in hexane to yield a slightly turbid solution. Gently heating affords a colourless solution which, upon slowly cooling down, affords **147** as colourless crystals suitable for X-ray diffraction studies (**Figure 4.4**).
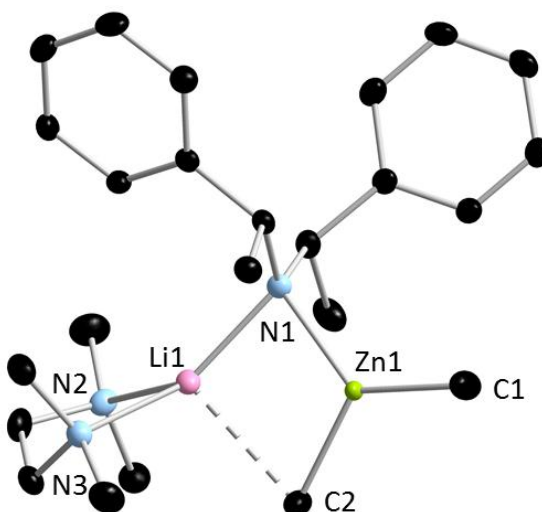
Figure 4.4. Molecular structure of **147**. Hydrogen atoms are omitted for clarity. Selected bond lengths (Å) and angles (°): Zn1-C1, 1.993(3); Zn1-C2, 2.028(3); Zn1-N1, 2.052(2); Zn(1)···Li(1), 2.694(4); Li1-N1, 2.052(4); Li1-N2, 2.226(5); Li1-

N3, 2.177(5); Li1⋯C2, 2.521(6); C1-Zn1-C2, 123.7(1); C1-Zn1-N1, 126.1(1); C2-Zn1-N1, 110.1(1); N1-Li1-N2, 128.2(2); N1-Li1-N3, 134.9(2); N2-Li1-N3, 85.5(2); N1-Li1-C2, 93.5(2); N3-Li1-C2, 100.7(2); N2-Li1-C2, 111.6(2). Ellipsoids showed at 30% of probability level.

Lithium zincate **147** crystallises in the monoclinic system in the space group P 1 2$_1$ 1. Its conformation in the solid state can be described as a contacted ion pair whereby the two metallic centres are bridged by the amido and one alkyl group, forming a four elements [LiNZnC] four membered ring. This ring is closed by a Li1⋯C2 weak interaction. The Li1⋯C2 bond length (2.521(6) Å) is long when compared with Li-C distances of organolithium compounds such as MeLi. (mean C-Li bond distance, 2.31 Å).[235]

Zinc atom presents a trigonal planar conformation (sum of angles 359.9°) and the Zn1-C1 and Zn1-C2 bond distances are presumably different as carbon C1 is a terminal carbon. Therefore, Zn1-C1 distance is 1.993(3) Å while Zn1-C2 distance is 2.028(3) Å.

Complex **147** is structurally related to other lithium zincates present in the literature, such as compounds (THF)·Li(μ-TMP)Zn^{t}Bu$_2$ (**151**)[214] or (TMEDA)·Li(μ-*cis*-DMP)Zn^{t}Bu$_2$ (**161**).[236] These zincates present a secondary "agostic" Li⋯C contact with bond lengths of 2.721(7) Å and 2.410(6) Å respectively.

4.3.1.2 Use of di-*tert*-butylzinc, ^{t}Bu$_2$Zn

To expand the knowledge of the reactivity of LiPEA and ^{t}Bu$_2$Zn, a mixture of an equimolar mixture of LiPEA, ^{t}Bu$_2$Zn and TMEDA was reacted in hexane. The mixture affords a white solid which can be redissolved by the addition of toluene while heating. The Schlenk tube containing this mixture was stored at −35°C and the solution afforded a crop of crystals suitable for X-ray diffraction studies.

Lithium zincate **148** is the product of an unexpected reaction, as one phenyl ring of the chiral amide **57** has lost one proton due to an intramolecular deprotonation with the concomitant loss of one *tert*-butyl group. The asymmetric cell of **148** contains two different molecules with different metrics so both will be discussed separately (**Figure 4.5** and **Figure 4.6**).
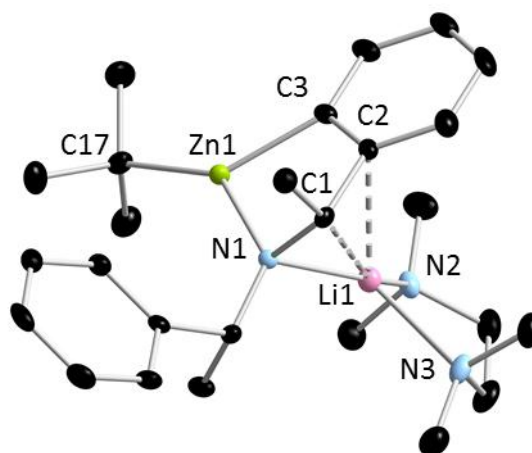
Figure 4.5 Molecular structure of **148**. First molecule in the unit cell. All hydrogen atoms are omitted for clarity. Selected bond lengths (Å) and angles (°): Zn(1)-N(1), 1.998(3); Zn(1)-C(17), 2.006(4); Zn(1)-C(3), 2.011(4); N(1)-Li(1), 2.042(6); Li(1)-N(2), 2.067(7); Li(1)-N(3), 2.137(7); Li(1)-C(1), 2.431(7); Li(1)-C(2), 2.491(8); Li(1)···C3, 2.801(1); N(1)-Zn(1)-C(17), 137.5(1); N(1)-Zn(1)-C(3), 84.9(1); C(17)-Zn(1)-C(3), 137.0(2); N(1)-Li(1)-N(2), 142.8(4); N(1)-Li(1)-N(3), 122.9(3); N(2)-Li(1)-N(3), 88.4(3); N(1)-Li(1)-C(1), 37.2(2); N(2)-Li(1)-C(1), 157.7(4); N(3)-Li(1)-C(1), 107.3(3); N(1)-Li(1)-C(2), 63.9(2); N(2)-Li(1)-C(2), 122.2(3); N(3)-Li(1)-C(2), 117.8(3); C(1)-Li(1)-C(2), 36.3(2). Ellipsoids showed at 30% of probability level.

In the first molecule the zinc atom has a trigonal conformation (sum of angles 359.4°) and the lithium atom presents two long distance contacts Li(1)···C(1), 2.431(7) and Li(1)···C(2), 2.491(8). However, the lithium atom in the second molecule of the unit cell presents three long distance contacts (Li(2)···C(28), 2.465(7) Å; Li(2)···C(27), 2.515(7) Å and Li(2)···C(29), 2.523(7) Å). The first molecule does not present that third contact, as the Li(1)-C(3) is notably

longer than Li(2)-C(29) (2.801(1) Å and 2.523(7) Å respectively). The bond lengths and angles involving the zinc atom are comparable in both molecules.
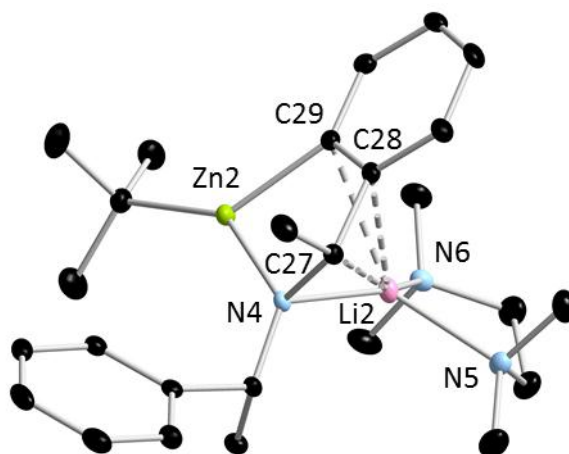
Figure 4.6 Molecular structure of **148**. Second molecule in the unit cell. All hydrogen atoms are omitted for clarity. Selected bond lengths (Å) and angles (°): Zn(2)-N(4), 1.999(3); Zn(2)-C(43), 2.011(4); Zn(2)-C(29), 2.024(4); Li(2)-N(5), 2.073(7); Li(2)-N(4), 2.088(7); Li(2)-N(6), 2.114(7); Li(2)-C(28), 2.465(7); Li(2)-C(27), 2.515(7); Li(2)-C(29), 2.523(7); N(4)-Zn(2)-C(43), 141.2(1); N(4)-Zn(2)-C(29), 84.5(1); C(43)-Zn(2)-C(29), 134.2(2); N(5)-Li(2)-N(4), 122.0(3); N(5)-Li(2)-N(6), 87.3(3); N(4)-Li(2)-N(6), 142.5(3); N(5)-Li(2)-C(28), 114.0(3); N(4)-Li(2)-C(28), 63.9(2); N(6)-Li(2)-C(28), 128.7(3); N(5)-Li(2)-C(27), 106.8(3); N(4)-Li(2)-C(27), 35.8(2); N(6)-Li(2)-C(27), 162.2(3); C(28)-Li(2)-C(27), 35.60(14); N(5)-Li(2)-C(29), 140.0(3); N(4)-Li(2)-C(29), 71.1(2); N(6)-Li(2)-C(29), 102.4(3); C(28)-Li(2)-C(29), 32.7(2); C(27)-Li(2)-C(29), 59.9(2). Ellipsoids showed at 30% of probability level.

^{1}H NMR analysis of a solution of **148** showed that the crystals did not correspond to a pure product. However, this result was achieved at the end of this PhD so future work is needed in order to assess the reproducibility of the reaction.

Spectroscopic studies of the mixture [LiPEA + ^{t}Bu$_2$Zn] were performed in order to find out if the monometallic species co-complex in absence of donor solvents (**Figure 4.7**).

Di-*tert*-butylzinc is very volatile so the sample was prepared in an NMR-tube inside the glove-box. 0.1 mmol of freshly prepared ^{t}Bu$_2$Zn[237] and 0.1 mmol of LiPEA were dissolved in 0.5 mL of C$_6$D$_6$ in order to compare the values with the published data for LiPEA.

Henderson and co-workers published the solid state structure of LiPEA in absence of donor solvents.[238] They found that LiPEA crystallises as a trimer but the trimeric and the monomeric conformations are in equilibrium in deuterated benzene solution.

Figure 4.7 shows the spectra of a pure sample of LiPEA (**a**), a pure sample of ^{t}Bu$_2$Zn (**b**) and a mixture of [LiPEA + ^{t}Bu$_2$Zn] (**c**).
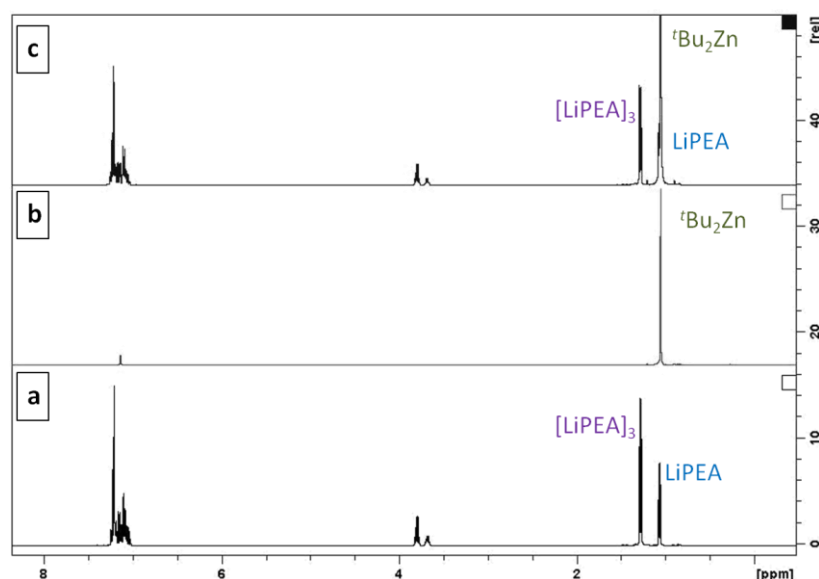
Figure 4.7 ^{1}H NMR spectra of pure LiPEA (**a**), a pure sample of ^{t}Bu$_2$Zn (**b**) and a mixture of [LiPEA + ^{t}Bu$_2$Zn] (**c**) in C$_6$D$_6$.

In agreement with the published data, ^{1}H NMR spectrum of a pure sample of LiPEA shows two sets of resonances. Concentration studies carried out by Henderson showed that the monomer exists in lower concentration.

^{1}H NMR spectrum of the sample of ^{t}Bu$_2$Zn shows one singlet at 1.07 ppm. That signal also appears in the spectrum of the mixture [LiPEA + ^{t}Bu$_2$Zn] but it is overlapped by the doublet of the monomeric LiPEA. In order to get better understanding, a ^{1}H DOSY experiment of the mixture was carried out (**Figure 4.8**).

The ^{t}Bu$_2$Zn signals appear with different diffusion coefficient than those for LiPEA, proving that the monometallic species do not co-complex in solution.
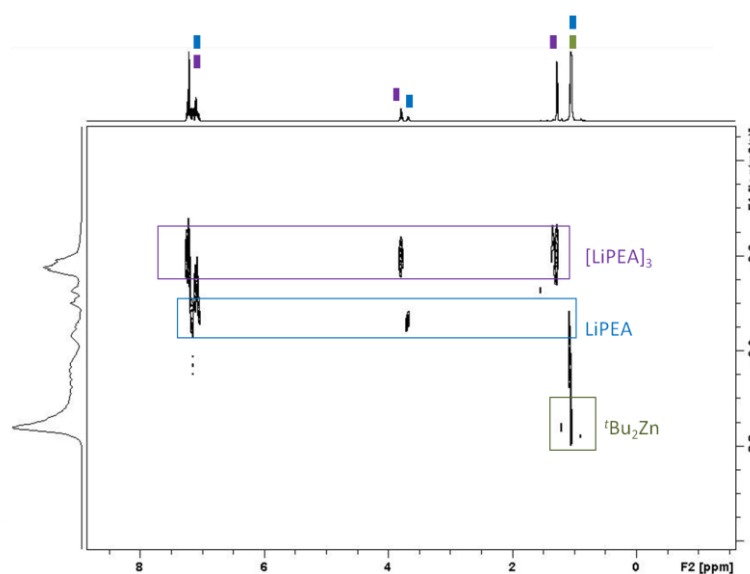
Figure 4.8 ^{1}H DOSY NMR spectrum of an equimolar mixture of LiPEA and ^{t}Bu$_2$Zn.

^{1}H-NMR studies of an equimolar mixture of the lithium amide LiPEA and Et$_2$Zn were performed and they showed that the mixture co-complex in the absence of donors and the product is soluble in arene solvents.

4.3.1.3 Organic transformations

When **162** is reacted with the lithium zincate in toluene, in presence or absence of TMEDA, the nucleophilic alkyl addition takes place but two more products are found in the reaction; the reduction of **162** to the alcohol 2,2,2-trifluoro-1-phenylethanol (**163**) and the addition of the chiral amine to the carbonylic carbon (**164**).

Lithium zincate **147** has been employed in nucleophilic addition reactions with ketones to evaluate its effectiveness as an alkylating agent.

Preliminary studies focus on a study with 2, 2, 2-trifluoroacetophenone (**162**) as it is a ketone that has been studied previously.[208, 209] It does not contain protons in α-position to the carbonyl group and the presence of the three fluorine atoms, creates an inductive effect that facilitates the nucleophilic addition over the carbonylic carbon.

As well as **147**, different lithium zincates formed by combination of LiPEA and R$_2$Zn (R=Et, ^{t}Bu) and different reaction conditions have been evaluated (**Table 4.2**).

Table 4.2 Nucleophilic addition reaction using chiral lithium zincates.

Solvent	R$_2$Zn		
	Me$_2$Zn	**Et$_2$Zn**	**^{t}Bu$_2$Zn**
Toluene^a	Insoluble mixture	35%	No co-complexation
Toluene/TMEDA^a	5%	11%	messy
THF	68%	93%	11%
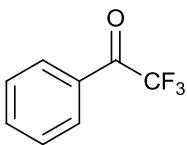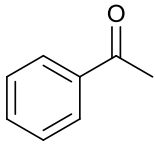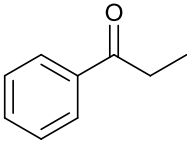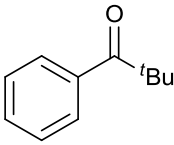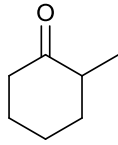
^{a}Reactions carried out in these solvents also afford the reduction product and the addition of the amido group as byproducts.

As **Table 4.2** shows, when the reaction is performed in THF, the only product is the addition of the alkyl chain. However, all the dialkyl reagents afford the racemic product.

The addition reaction to **162** proved to be faster when Et$_2$Zn was involved. However, the study of (TMEDA)Li(μ-PEA)(μ-Me)ZnMe (**147**) provided us structural insights into screening of the reaction between **147** and a series of ketones in THF have been performed. Et$_2$Zn was employed for the reaction with acetophenone (**18**), as the addition product using **147** would not be chiral.

Table 4.3 highlights the results obtained for these reactions. Ketones **162** and **166** do not have protons in the α-position of the carbonylic carbon. The conversion for the addition of the methyl group was 63% and 69% respectively but again no enantiomeric excess was found.

Table 4.3 Reaction scope for the reaction of a series of ketones with a chiral lithium zincate.

Ketone	R"$_2$Zn	Conversion	e. ratio
162	Me$_2$Zn	63%	51:49
18	Et$_2$Zn	0 %[a]	-
165	Me$_2$Zn	0 %[a]	-
166	Me$_2$Zn	69%	50:50
167	Me$_2$Zn	0 %[a]	-

[a]The reaction was quenched with TMSCl before the addition of NH$_4$Cl and GC analysis showed that quantitative deprotonation had taken place.

Ketones **18**, **165** and **167** did not give any conversions over the addition reaction. As they have acidic protons, they are susceptible to deprotonation

so the reactions were repeated quenching with 1.2 molar equivalents of TMSCl prior to the addition of NH_4Cl. Gas chromatographic analysis of the organic product showed that the quantitative deprotonation of the ketones had occurred.

At this point, spectroscopic studies of the lithium zincate **147** in D_8-THF solution were performed.

0.1 mmol of **147** were dissolved in 0.5 mL of D_8-THF. ^1H DOSY experiment of the mixture shows that at least three different species are present in solution. TMEDA has been totally replaced by THF and, more importantly, the methyl and PEA groups do not seem to belong to the same molecule.

The resonances for the PEA-containing species correspond to the resonances of LiPEA in deuterated THF. However, the singlet of the methyl group is slightly more shielded that the resonance of Me_2Zn in D_8-THF (-0.89 ppm).[239]

Perhaps, a methyl-containing bimetallic species is present in solution as the ^7Li NMR spectrum shows two resonances. The first resonance at 2.56 ppm corresponds to LiPEA and there is another resonance at 2.08 ppm that has not been possible to identify.
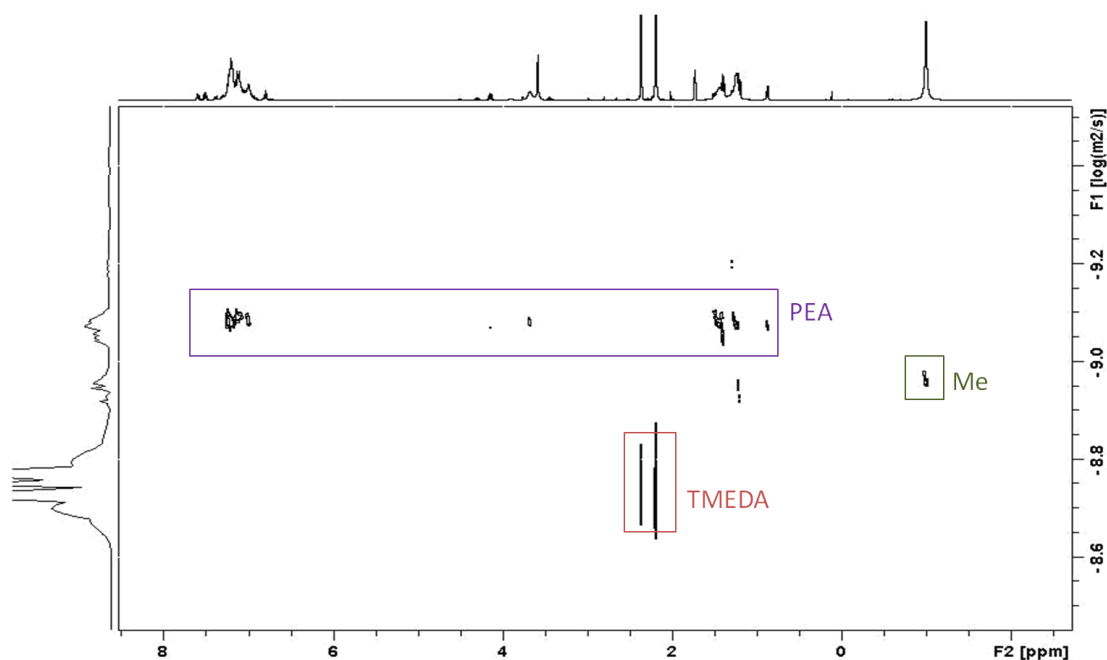
Figure 4.9 ^{1}H DOSY spectrum of **147** in D_8-THF solution.

The methyl-containing complex would undergo nucleophilic addition over the ketones, but if the ketone has protons susceptible to react with a base, lithium amide LiPEA would react so quickly that no nucleophilic addition occurs.

When the reaction is performed in toluene, the base retains its bimetallic conformation but this seems to render the base non-selective. Homoleptic lithium zincates.

4.3.2 Homoleptic lithium zincates

In order to compare the reactivity of heteroleptic and homoleptic chiral lithium magnesiates, a homoleptic lithium zincate has been synthesised.

Reaction in hexane of an equimolar mixture of methyllithium, dimethylzinc and the chiral ligand (*R,R*)-TMCDA affords a fine white suspension. Gently heating, followed by storage at –35°C, results in the crystallization of a crop of needles suitable for X-ray diffraction (**149**).
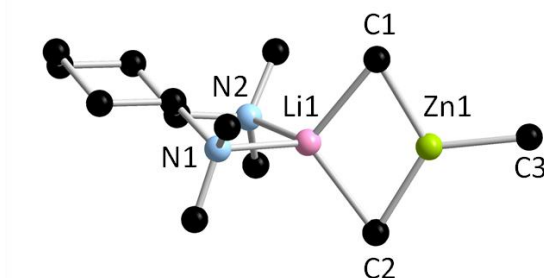
Figure 4.10 Molecular structure of (*R,R*)-TMCDA·LiZnMe$_3$, **149**. Hydrogen atoms are omitted for clarity.

Lithium zincate **149** is a homoleptic monomer where the two metallic centres are bridged by two methyl groups. The zinc atom completes its coordination sphere with one terminal methyl group while the lithium atom coordinates to the two nitrogen atoms of the bidentate ligand (*R,R*)-TMCDA.

Unfortunately, the lithium atom presents disorder so it is not possible to discuss the bond distances and angles.

Complex **149** is a contacted ion pair, structurally related to the lithium zincate **157** described by Stalke *et al.*, [(PMDETA)·Li(μ-Me)$_2$ZnMe].[75] It is not surprising that **149** crystallises as a CIP as zincates bearing methyl anions present this arrangement, except for the previously discussed zincate stabilised by diglyme, complex **158** ([(diglyme)$_2$Li]$^+$[ZnMe$_3$]$^-$).

^{1}H NMR spectrum in deuterated toluene (**Figure 4.11**) shows only one singlet for the methyl groups which integrates to 9 protons so an equilibrium exchange in solution must be taking place in solution that makes the three methyl groups (two bridging, one terminal) becoming equivalent.

The two distinct the signals for the protons of the $-CH_3$ groups of the TMCDA ligand implies that it remains coordinated to the lithium atom, as the signals for the free ligand are equivalent (**Figure 4.11**).
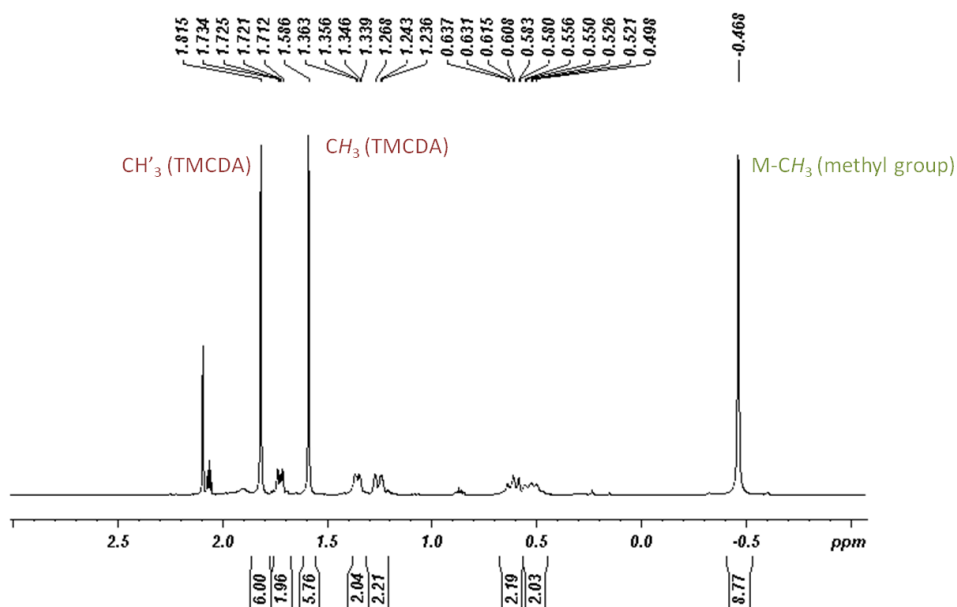
Figure 4.11 ^{1}H NMR spectrum of **149** in D_8-toluene.

Compound **149** appears to retain its bimetallic nature in D_8-toluene solution and the ^{7}Li NMR spectrum shows only one signal, highlighting the purity of the sample.

Table 4.4 Reaction scope of the reaction of a series of ketones with a homoleptic chiral lithium zincate.

Ketone	Conversion	e. ratio
162	99%	50:50
165	47%	56:44
166	99%	53:47
167	20%	60:40

Lithium zincate **149** has been employed as an alkylating reagent for ketones (**Table 4.4**).

The reaction with this homoleptic complex is more selective than the reaction performed with heteroleptic lithium zincate as it does not appear to reduce the ketones to the corresponding alcohol. However, reaction with ketones **165** and **167** affords the addition product to some extent but also the deprotonation of the protons in α-position to the carbonyl group.

For ketones **162** and **166** the reaction is completed after one hour, but the obtained alcohol is the racemic product.

4.4 Experimental

4.4.1 Synthesis of 147, (TMEDA)·Li(μ-PEA)ZnMe$_2$

Me$_2$Zn (0.5 mL of 2 M solution in heptanes) was dissolved in 5 mL of dried hexane in an oven-dried Schlenk tube. TMEDA (1 mmol, 0.15 mL) was added and the solution was stirred for 10 minutes.

In a separate Schlenk tube, ^{n}BuLi (1 mmol, 0.67 mL, 1.6 M solution in hexanes) and PEA(H) (1 mmol, 0.23 mL) were reacted in 5 mL of dried hexane. After 1 hour of stirring, a white suspension has been formed.

The solution of TMEDA·ZnMe$_2$ was transferred to the LiPEA suspension via cannula. The suspension was stirred for two hours. Gently heating affords a solution which was cooled down slowly in a hot water bath. The reaction affords a crop of cube-like crystals suitable for X-ray diffraction studies (0.15 g, 34%).

^{1}H NMR (400.13 MHz, 300 K, D$_8$-Tol): δ -0.38 (6H, s, M-CH_3, Me), 1.37-1.38 (6H, d, $^2J_{HH}$=6.4 Hz, CH_3, PEA), 1.68-1.71 (2H, br, CH_2, TMEDA), 1.89 (12H, s, CH_3, TMEDA), 1.99-2.01 (2H, br, CH$_2$, TMEDA), 3.98-4.03 (4H, q, $^4J_{HH}$=6.4 , CH, PEA), 7.11-7.23 (10H, br, Ph, PEA). ^{13}C{^{1}H} NMR (100.62 MHz, 300 K, D$_8$-Tol): δ 27.0 (*C*H$_3$, Me), 46.6 (*C*H$_3$, PEA), 32.7 (*C*H$_2$, Bu), 55.6 (*C*H$_3$, TMEDA), 57.5 (*C*H$_2$, TMEDA), 60.8 (*C*H, PEA), 126.0 (*C*H$_{para}$, PEA), 128.0 (*C*H$_{meta}$, PEA), 128.1 (*C*H$_{ortho}$), 137.5 (*C*$_{ipso}$, PEA). ^{7}Li NMR (155.50 MHz, 300 K, D$_8$-Tol): δ 1.46.

4.4.2 Synthesis of 148, (TMEDA)·Li(μ-PEA)(μ-Ph)Zn^{t}Bu

The synthesis of ^{t}Bu$_2$Zn is described in page 161.

^{t}Bu$_2$Zn (1 mL of 1 M solution in hexane) was transferred via cannula to an oven-dried Schlenk tube. TMEDA (1 mmol, 0.15 mL) was added and the solution was stirred for 10 minutes.

In a separate Schlenk tube, ^{n}BuLi (1 mmol, 0.67 mL, 1.6 M solution in hexanes) and PEA(H) (1 mmol, 0.23 mL) were reacted in 5 mL of dried hexane. After 1 hour of stirring, a white suspension has been formed.

The solution of TMEDA·Zn^{t}Bu$_2$ was transferred to the LiPEA suspension via cannula. The suspension was stirred for 2 hours. Vigorously heating and addition of toluene while heating, affords a pale-yellow solution. The Schlenk flask was transferred to a freezer operating at –35°C. After three days, a crop of crystals suitable for X-ray diffraction studies were found. (0.07 g, 16%).

NMR of the sample showed that **148** was not a pure sample. This result could not be repeated by the end of this 36 months so further work is necessary.

4.4.3   Synthesis of 149, [(*R,R*)-TMCDA]·Li(μ-Me)$_2$ZnMe

MeLi (0.625 mL, 1 mmol of 1.6 M solution in diethyl ether) was dissolved in 5 mL of dried hexane in an oven-dried Schlenk tube. A turbid solution si formed. 1 mmol of Me$_2$Zn (0.5 mL of 2 M solution in heptanes) were added and then (*R,R*)-TMCDA (1 mmol, 0.19 mL). Addition of toluene while heating gave a colourless solution. The solution was transferred to a freezer (-35°C) affording colourless crystals after 24 hours. (0.17 g, 61%).

^{1}H NMR (400.13 MHz, 300 K, C$_6$D$_{12}$): δ –0.47 (9H, s, M-CH_3, Me), 0.50-0.58 (2H, m, γ-CH_2, (*R,R*)-TMCDA), 0.61-0.64 (4H, m, β-CH_2, (*R,R*)-TMCDA), 1.24-1.27 (4H, m, γ'-CH_2, (*R,R*)-TMCDA), 1.34-1.35 (4H, m, β'-CH_2, (*R,R*)-TMCDA), 1.59 (12H, s, N-CH_3, (*R,R*)-TMCDA), 1.72-1.73 (2H, br, CH, TMCDA), 1.81 (12H, s, N-CH_3 and α-CH, (*R,R*)-TMCDA). ^{13}C{^{1}H} NMR (100.62 MHz, 300 K, C$_6$D$_{12}$): δ –8.0 (M-CH_3, Me), 21.8 (γ-CH_2, (*R,R*)-TMCDA), 25.2 (β-CH_2, (*R,R*)-TMCDA), 36.9 (N-CH3, (*R,R*)-TMCDA), 44.4 (N-CH3, (*R,R*)-TMCDA), 64.1 (α-CH, (*R,R*)-TMCDA). ^{7}Li NMR (155.50 MHz, 300 K, C6D12): δ 1.40.

4.4.4   Experimental procedure for the nucleophilic addition reaction to ketones.

0.5 mmol of the bases **147** or **149** were synthetised according to the experimental procedure in the appropriate solvent. Solution was cooled down to –78°C with a dry ice/acetone bath and 0.5 mmol of the ketone was added.

Once the base was formed, a solution of the ketone in 1 mL of solvent was added. Solution was stirred for one hour and quenched with NH$_4$Cl. Progression of the reaction was followed by gas chromatography.

4.5 Conclusions and future work

Two new crystals structures have been fully characterised in this work. Firstly, complex TMEDA·Li(μ-PEA)ZnMe$_2$ (**147**) is a heteroleptic bimetallic compound which contains one unit of the chiral amide **57**, (+)-Bis-[(*R*)-1-phenylethyl]amide. This monomer was tested as an alkylating reagent for ketones, it was shown to maintain its bimetallic entity in hydrocarbon solvents and it works as well as a reducing reagent with the addition of the amido group being another byproduct of the reaction.

In tetrahydrofuran solution, the base does not retain its bimetallic nature.

The synthesis of a different lithium zincate was attempted, using ^{t}Bu$_2$Zn, instead of Me$_2$Zn. However, the product that crystallised was a product of an intramolecular deprotonation (**148**) where the zinc atom is linked to the chiral amine by the nitrogen atoms and also by a Zn-C bond. Future work should focus on zincate **148** in order to ensure its reproducibility.

The other zincate fully characterised was compound **149**, (*R,R*)-TMCDA·Li(μ-Me)$_2$ZnMe. Complex **149** is a homoleptic monomer that comprises a LiZnMe$_3$ framework, with the chiral ancillary ligand (*R,R*)-TMCDA finishing the coordination sphere of the lithium atom. The alkyl addition to ketones with this monomer is successful although the enantiomeric excess is relatively low.

As a future work, nucleophilic addition reactions of **147** and **149** to less reactive organic substrates, such us imines, should be studied.

Chapter 5.   Structural insights of chiral mixed alkali metal amides

5.1 Summary

The chapter describes the synthesis, characterisation and reactivity studies of a series of mixed alkali-metal complexes, containing the chiral amide (+)-bis[(*R*)-1-phenylethyl]amide (**57**).

Three different mixed metal chiral amides have been characterised. Mixed lithium-sodium amide [LiNa(PEA)$_2$]$_2$ (**168**) can be synthesised from hydrocarbon solution. This amide crystallises as an eight-membered ring, with the metallic centres alternating and bridged to each other through an amido nitrogen atom.

In presence of tetrahydrofuran, the dimeric structure of **168** breaks into a monomer with formula [(THF)$_2$LiNaPEA$_2$] (**169**). Two chiral amides bridge the lithium and sodium atoms, which are each coordinated by one molecule of THF.

Closely related to **168**, another donor-free complex has been structurally characterised. The mixed lithium-potassium amide [LiK(PEA)$_2$]$_2$ (**170**) mimics the coordination of its sodium counterpart forming a dimeric ring with the lithium atoms coordinated to two amido groups in a linear arrangement.

Due to their low solubility in hydrocarbon solvents, these complexes have been studied in deuterated tetrahydrofuran solution. ^{1}H, ^{7}Li and ^{13}C NMR spectroscopic analysis have been performed and also two-dimensional ^{1}H DOSY experiments.

A preliminary study on the reactivity of these amides as initiators for asymmetric rearrangement of epoxides has been performed in order to compare their activity with the published data for the lithium amide LiPEA.

5.2 Introduction

5.2.1 Alkali-metal amides

Alkali-metal amides are the metal-amido derivatives that have been most widely studied and employed for synthesis, particularly lithium amide complexes.[100] A short summary of key structural features will be covered here.

5.2.1.1 Lithium amides

The most commonly used achiral lithium amides are LDA (lithium diisopropylamide, Li-**73**), LiTMP (lithium 2,2,6,6-tetramethylpiperidide, Li-**79**) and LiHMDS (lithium hexamethyldisilazide, Li-**127**) (**Figure 5.1**). Below, a brief review of the solid state structural chemistry is detailed.
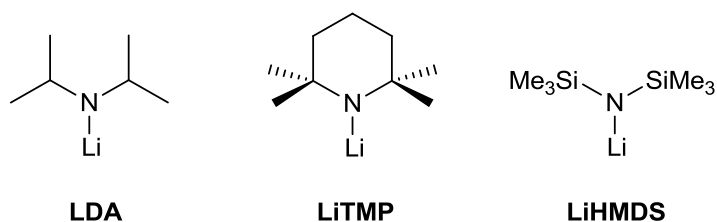
Figure 5.1 ChemDraw representation of LDA, LiTMP and LiHMDS.

LiHMDS is composed of (LiN)$_3$ units, forming a six-membered trimeric planar ring, where each lithium centre is coordinated to two nitrogen atoms (**Figure 5.2**).[240]

When the amide is substituted for the markedly more bulky 2,2,6,6-tetramethylpiperidide (**79**), it would perhaps be expected that a decrease in the aggregation state would occur. However, when crystallised at ambient temperature, the LiTMP molecular structure is actually an *eight*-membered tetrameric ring where the lithium and nitrogen atoms tend towards linearity, resulting in a structure which can be considered as a tertanuclear pseudo-dimer (**Figure 5.2**).[241] The use of low temperatures favours the crystallisation of a cyclotrimeric structure that resembles the LiHMDS arrangement.[242]
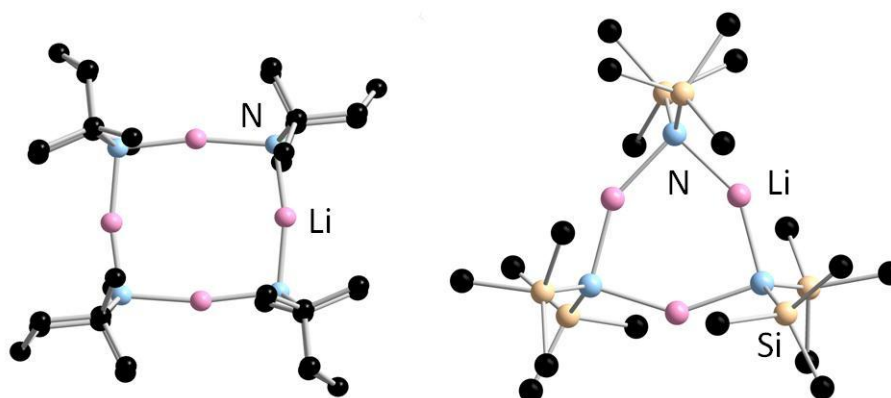
Figure 5.2 X-ray structures of [LiTMP]$_4$ (left)[241] and [LiHMDS]$_3$ (right)[240].

Lithium diisopropylamide crystallises as a polymeric chain.[243] Looking at the structure along the *b*-axis it bears resemblance to the LiTMP structure; an eight-membered tetrameric ring but in this case the tetramer is not planar but undergoes a rotation of 360° along the *c*-axis every four monomers of lithium amide (**Figure 5.3**). Viewing from the *c*-axis, it can be easily appreciated how the structure is formed by one helical single strand of [Li-N-Li-N] with the isopropyl groups projecting outwards.
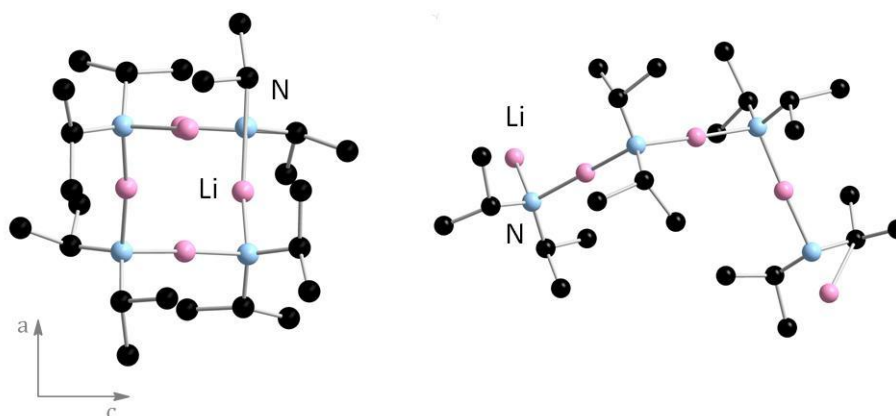
Figure 5.3 X-ray structures of LDA along *b*-axis (left) and along the *c*-axis (right). H atoms omitted for clarity.

5.2.1.2 Chiral lithium amides

The interest in chiral lithium amides started in the 1990s and over the past years a number of structures have been characterised. Chirality in lithium amides increases the number of possible structures, especially when there are chelating groups present.[244] Three known structures containing the chiral amine PEA(H) ((+)-(*R*)-bis-(1-phenylethyl)amine) have been published (**Figure 5.4**).
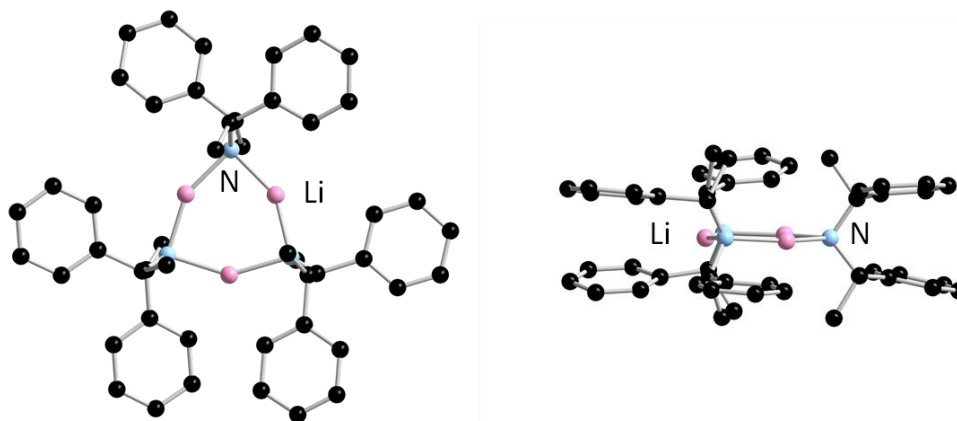
Figure 5.4 X-ray structure of LiPEA.

LiPEA in non-coordinating solvents crystallises as a cyclic trimer where the lithium and nitrogen atoms form a six membered "shield-shaped" planar ring and three phenyl rings that are situated above the plane and three are located below (**Figure 5.4**).[238] This amide was crystallised from THF/hexane and characterised as a dimer with every lithium atom solvated by one molecule of THF.[245]

The only structure of this chiral amide with an amine donor was published by Andrews and co-workers (**Figure 5.5**).[246] By reacting LiPEA and PMDETA in hexane/toluene solution, they crystallised a monomer [(PMDETA)·Li(PEA)] (**174**).
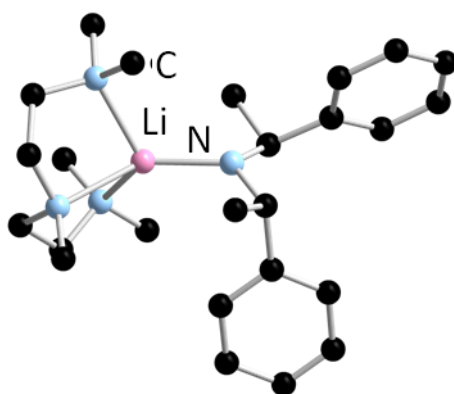
Figure 5.5 X-ray structure of (PMDETA)·LiPEA (**174**).

In the same publication, Andrews and co-workers characterised a sodium enamide stabilised by PMDETA that is formed from the reorganization of the sodium amide, with concomitant loss of a molecule of styrene and hydrogen (**Scheme 5.1**).
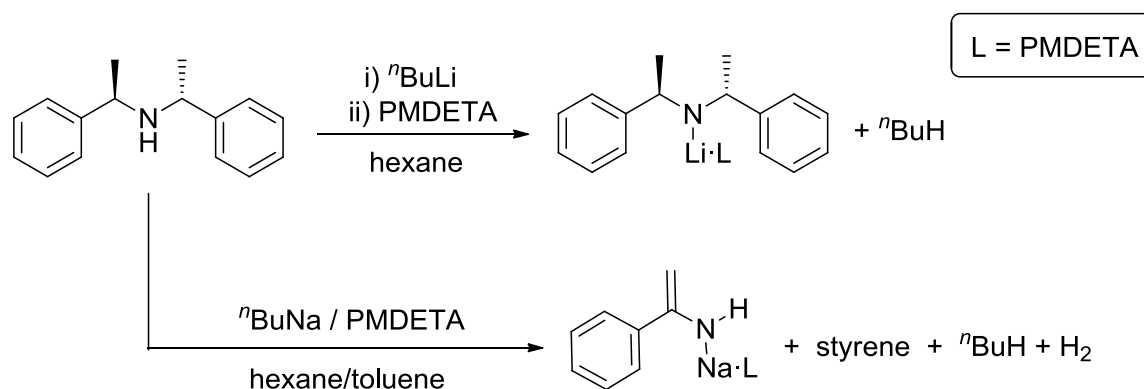
Scheme 5.1 Synthesis of the amide (PMDETA)·LiPEA (**174**) and the enamide [PhC(NCH$_2$)N(H)Na·PMDETA] (**175**).

Andrews, Blair and co-workers showed that the lithium derivate of the chiral amine (*S*)-α-(methylbenzyl)benzylamine, structurally related to PEA(H), can be isolated. The use of heavier alkali metal such as sodium or potassium undergoes the generation and isolation of the corresponding aza-allyl complexes.[247]

5.2.2 Mixed alkali-metal compounds

Mixtures of organolithium compounds and alkali metal alkoxides MO-R (M=Na, K, Rb, Cs) are known to be more reactive than the separate reagents. This formed complexes, commonly known as "Schlosser bases" or "Superbases", are extremely strong bases; they readily react with many organic compounds and thus represent useful tools in organic synthesis.[248-252] Accordingly, the complex "LiC-KOR" (an equimolar mixture of ^{n}BuLi and KO^{t}Bu) shows an intermediate reactivity between the monometallic species ^{n}BuLi (less reactive) and ^{n}BuK (more reactive).

Strohmann and co-workers recently published the structure of the intermediate of the metalation of benzene by the mixture LiC-KOR.[253] They crystallised a heterometallic Li_2K_4 cluster that contains phenyl anions and *tert*-butoxide, $[(PhK)_4(PhLi)(^tBuOLi)(THF)_6(C_6H_6)_2]$ (**176**). This aggregate displays superbasic behavior as it is capable of deprotonating toluene.

5.2.3 Mixed alkali-metal amides

The work of O'Shea *et al.* focused their attention on heterometallic amides and they described a method for performing benzylic metalation in *ortho*-, *meta*- and *para*-substituted toluenes using the mixture LiTMP/KO^{t}Bu.[254]

Mulvey and Robertson[255] recently reviewed the structural chemistry of three commonly employed amides: DA(H) (diisopropylamine, **73**-(H)), TMP(H) (2,2,6,6-tetramethylpiperidine, **79**-(H)) and HMDS(H) (bis(trimethylsilyl)amine, **127**-(H)).

They included the characterisation of a series of mixed Li/Na, Na/K and Li/K amides of the aforementioned amines, showing how metal amides can adopt a wide variety of conformations, depending on solvation, steric and electronic factors.[99, 256-258]

5.2.3.1 Chiral concepts in mixed alkali metal compounds

To the best of our knowledge, no structural characterization of a mixed alkali-metal chiral amide has been made.

Solution studies of a lithium-sodium bidentate amide have been performed together with reactivity studies for the deprotonation of epoxides to undergo the correspondent chiral alcohol.[259, 260]

i)

$M^1=M^2=Li$, ee=70%
$M^1=M^2=Na$, ee=37%
$M^1=Na$, $M^2=Li$, ee=10%

ii) Hydrolysis

Et$_2$O
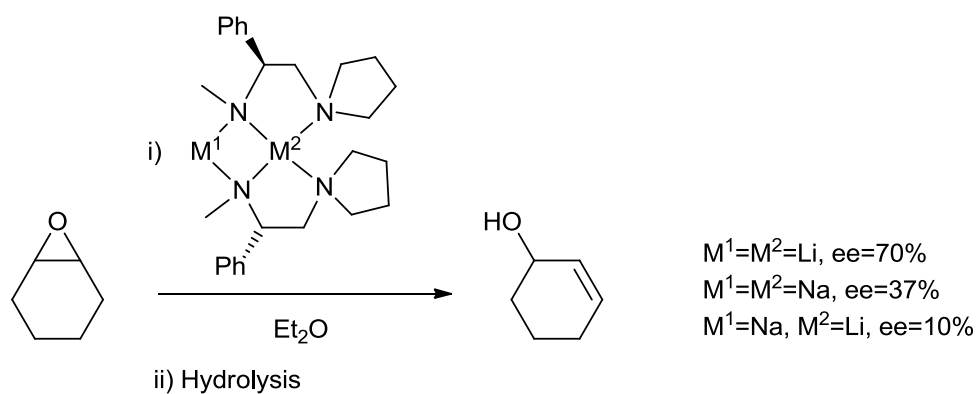
Scheme 5.2 Deprotonation of cyclohexene oxide by a chiral metal-amide.

The authors evaluated the homometallic lithium and sodium amides, and also the mixed lithium-sodium amide, as deprotonating reagents of cyclohexene oxide.

The change in the enantioselectivity of the process is dramatic when the sodium is incorporated in the system as it drops from 70% of enantiomeric excess to 37% for the sodium amide and 10% for the mixed lithium-sodium amide.

A study of the structural insights of a series of chiral metal amides has been performed in this work.

5.3 Results and discussion

5.3.1 Solid state molecular structures

5.3.1.1 Mixed lithium-sodium amide [LiNa(PEA)₂]₂

With the aim of synthesizing a complex bearing two different amido groups, the chiral lithium amide LiPEA was reacted with the sodium amide NaHMDS (Na-(**127**)) in hexane. Addition of toluene while heating afforded a solution which, upon cooling down, resulted in a crop of crystals of complex **168** (

Figure 5.6).

This complex could be achieved by a rational method, reacting an equimolar mixture of *n*-butyllithium and *n*-butylsodium with two equivalents of PEA(H).
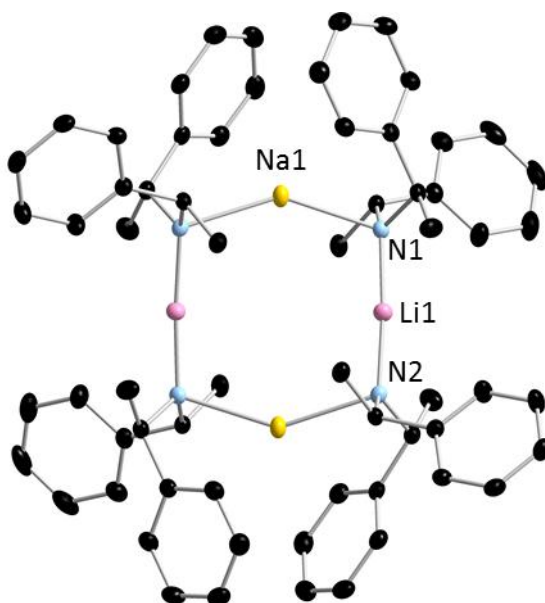
Figure 5.6. Molecular structure of **168**. Hydrogen atoms are omitted for clarity. Selected bond lengths (Å) and angles (°): Li1-N1, 1.930(3); Li1-N2 1.932(3); Li1···Na1 3.495(3); N1-Na1, 2.426(2); N2-Na1, 2.422(2); N1-Li1-N2, 175.7(2); Li1-N1-Na1, 107.1(1); Li1-N2-Na1, 106.2(1); N1-Na1-N2, 144.9(6). Symmetry transformations used to generate equivalent atoms: -x+1,y,-z+2. Ellipsoids showed at 30% of probability level.

Amide **168** crystallises in the space group C2 and it can be described as a cyclic structure with an eight-membered ring as its core motif and all the phenyl groups of the amide directed away from the ring. This ring is composed of metal-nitrogen bonds, the metals alternating between lithium and sodium. It can be considered a dimeric structure of two units of [LiNaPEA$_2$]. Eight-membered rings are a common feature in organometallic chemistry;[86][261, 262]

A vast number of inverse crown ethers have been described, and it is a common feature that the Lewis acidic ring bears two different metallic centres (and four metals in total). The rings formed by the eight constituent atoms appears to be the perfect sized cavity to host small Lewis bases such as hydride, oxide or hydroxide anions.[160, 161, 178, 263, 264]

Closely related to them, O'Hara published an inverse crown ether with a homoleptic ring, the solvent-separated complex [Na$_4$(μ-HMDS)$_4$(μ$_4$-OH)]$^-$[Na$_2$(μ-HMDS){(−)-sparteine}$_2$]$^+$ (**171**). The anionic part of this structure is composed by a tetrameric ring of NaHMDS that encapsulates a hydroxide anion. Other unsolvated mixed lithium-sodium amides have been crystallographically described.[265]

While tetrameric [LiTMP]$_4$ is isostructural to **168**, the mixed Li/Na derivative crystallises as a polymeric chain. Considering the structural parameters, the mean of the Li-N bond distance in **168** is 1.931 Å, slightly shorter than the mean of the Li-N bond distance of the monometallic trimer [LiPEA]$_3$, 1.977 Å.[238] [LiPEA]$_3$ has a non-crystallographic D$_3$ symmetry and the lithium atoms and the Li-N bond distances are not equivalent, while all the Li-N bond distances of **168** are equivalent.

5.3.1.2 Mixed lithium-sodium amide [(THF)$_2$LiNa(PEA)$_2$]

If the synthesis of the mixed lithium-sodium amide is performed in the presence of tetrahydrofuran, the dimer structure breaks into a monomer with formula [(THF)$_2$LiNa(PEA)$_2$], **169** (**Figure 5.7**).
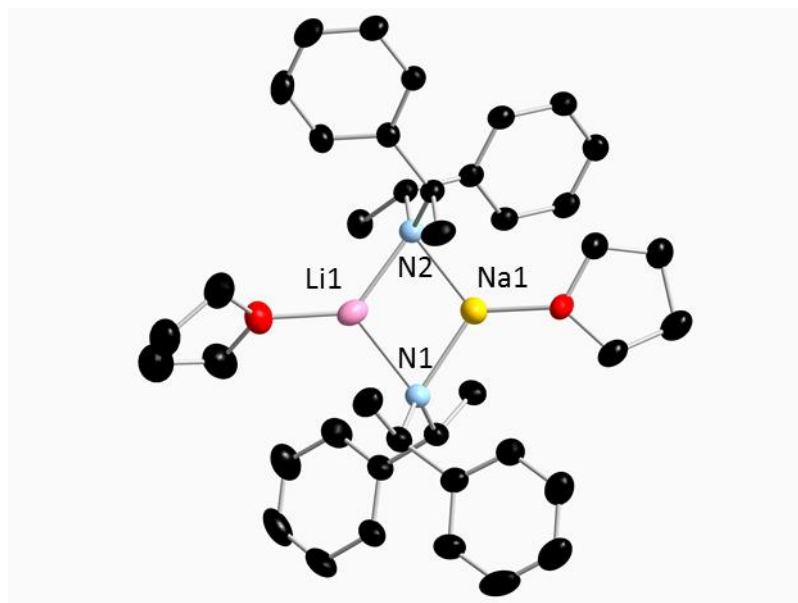
Figure 5.7 Molecular structure of **169**. Hydrogen atoms are omitted for clarity.

Ellipsoids showed at 30% of probability level.

Amide **169** crystallises in the space group P 2_1 2_1 2_1 with each metal coordinated to two bridging amido groups and one molecule of THF. Unfortunately, the lithium and sodium atoms exchange positions so there is mutual substitution disorder in the THF·Li and THF·Na moieties, rendering it impossible to discuss the bond distances and angles.

Compound **169** is isostructural to the dimeric lithium amide [THF·LiPEA]$_2$ (**172**)[245] and both crystallise in the same space group as the latter has a lack of symmetry and the lithium and nitrogen atoms are inequivalent.

There are also structural similarities with the mixed-metal complex (THF)$_3$LiNa(HMDS)$_2$. Once again, the chiral amide PEA (**57**) mimics the way that the bis(trimethylsilyl)amide behaves. For other different amides, a ladder rearrangement is the most frequent conformation.[266, 267]

5.3.1.3 Mixed lithium-potassium amide [LiK(PEA)₂]₂

To expand the knowledge of the alkali-metal derivatives of the chiral amide ((+)-bis-[(*R*)-1-phenylethyl]amide, an unsolvated mixed lithium-potassium amide has been characterised (**Figure 5.8**).
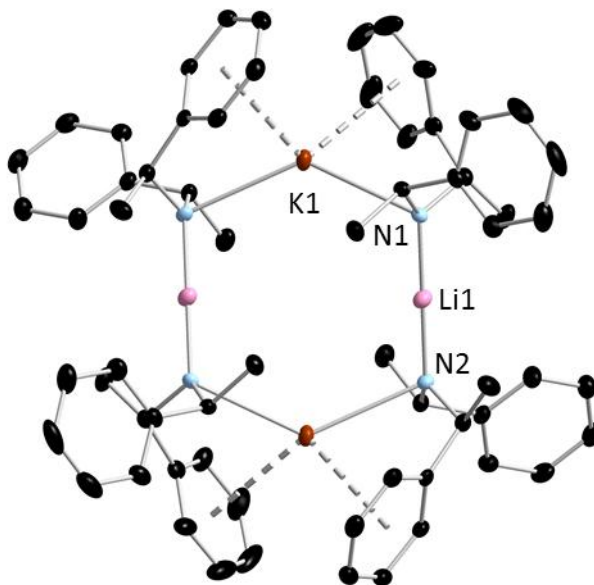
Figure 5.8 Molecular structure of **170**. Hydrogen atoms are omitted for clarity. Selected bond lengths (Å) and angles (°): Li(1)-N(1), 1.909(6); Li(1)-N(2), 1.900(6); K(1)-N(1), 2.907(3); K(1)-N(2), 2.873(2); Li(1)···K(1), 3.940(6); N(1)-Li(1)-N(2), 178.1(3); N(1)-K(2)-N(2), 130.05(7); Li(1)-N(1)-K(2), 110.7(2); Li(1)-N(2)-K(2), 109.6(2). Symmetry transformations used to generate equivalent atoms: -x+1,y,-z+2

Dimeric amide [LiK(PEA)₂]₂ (**170**) crystallises in the space group C2 and shows the same conformation as its sodium counterpart. Lithium and potassium atoms are two-coordinated and the lithium-nitrogen bonds are close to linearity (N1-Li1-N2 angle, 178.1°).

Potassium's coordination sphere is completed by an interaction with one of the phenyl rings of each amide. The distances between the potassium atom

and the phenyl ring are 2.975 and 3.015 Å which are comparable to the bond distances found by O'Hara and co-workers when they characterised a potassium magnesiate $(PMDETA) \cdot K(\mu-NPh_2)Mg(THF)(NPh_2)_2$.[268] This structure showed a similar π-K$\cdots$C$_{aryl}$ interaction between the potassium atom and one phenyl ring of each amide (K-centroid distance, 3.031 Å.)

Synthesis of **170** from the deprotonation of the chiral amine wih Me_3SiCH_2Li and Me_3SiCH_2K was unsuccessful. However, it could be isolated through a disproportionation of the reaction of LiPEA and KHMDS (potassium bis(trimethylsilyl)amide) in hexane/toluene.

Table 5.1 Comparison of bond lengths and angles of $[LiNa(PEA)_2]_2$ (**168**) and $[LiK(PEA)_2]_2$ (**170**).

Bond distances (Å) and angles (°)	$[LiNa(PEA)_2]_2$ **168**	$[LiK(PEA)_2]_2$ **170**
Li(1)-N(1)	1.930(3)	1.909(6)
Li(1)-N(2)	1.932(3)	1.900(6)
M(1)-N(1)	2.426(2)	2.907(3)
M(1)-N(2)	2.422(2)	2.873(2)
Li(1)$\cdots$M(2)	3.495(3)	3.940(6)
N(1)-Li(1)-N(2)	175.7(2)	178.1(3)
N(1)-M(1)-N(2)	144.9(6)	130.0(7)
Li(1)-N(1)-K(2)	107.1(1)	110.7(2)
Li(1)-N(2)-K(2)	106.2(1)	109.5(2)

Table 5.1 compares a selected data for chiral amides **168** and **170**.

Amide **170** has shorter Li-N bond distances and narrower N(1)-M-N(2) angles than the sodium-containing amide, with the lithium being in an almost linear rearrangement in both structures.

The crystal structure of another unsolvated lithium-potassium amide, $[LiK(HMDS)_2]$ (**173**), was published by Henderson and co-workers. Amide **173** crystallises as a polymeric chain with lithium and potassium atoms alternating and bonded though the nitrogen atoms of the amido group.[269]

5.3.2   Solution NMR spectroscopic studies

Solution studies of complexes **168-170** have been performed. Due to their low solubility in hydrocarbon solvents, the solution studies of complexes **168** and **170** have been performed in deuterated tetrahydrofuran (**Table 5.2**).

Almost no variation of the signals for the phenyl and the CH groups of the amide is observed. However, the signals of the methyl groups for KPEA are significantly upfield when compared with the resonances of the rest of amides. For the monometallic amides NaPEA and KPEA, that signal is a doublet indicating that dynamic processes are at play. However, in the ^{1}H NMR spectrum of LiPEA recorded at 300K, the doublet merges into only one broad singlet. Similarly, the resonance for the protons of the CH_3 of the heterometallic species **168** and **170** apprear as two broad signals.

Table 5.2 ^{1}H and ^{7}Li NMR spectroscopic data for LiPEA, LiNa(PEA)$_2$ (**168**), NaPEA, LiK(PEA)$_2$ (**170**), KPEA in D$_8$-THF.

	Ph	CH	CH$_3$	^{7}Li
LiPEA	7.06-7.26	3.57-3.61	1.44	2.56
LiNaPEA$_2$	6.98-7.18	3.57-3.61	1.27-1.44	2.53
NaPEA	6.94-7.16	3.57-3.61	1.20-1.22	
LiKPEA$_2$	6.98-7.41	3.56-3.61	1.21-1.44	2.37
KPEA	6.90-7.15	3.53-3.59	1.18-120	

The ^{1}H NMR spectrum of LiNa(PEA)$_2$ is very similar to the spectra of the monometallic species. Perhaps, the presence of an excess of donor solvent makes the dimeric amide to break into the monometallic amides LiPEA and NaPEA.

Two-dimensional ^{1}H DOSY experiment of **168** in D$_8$-THF solution was carried out (**Figure 5.9**).
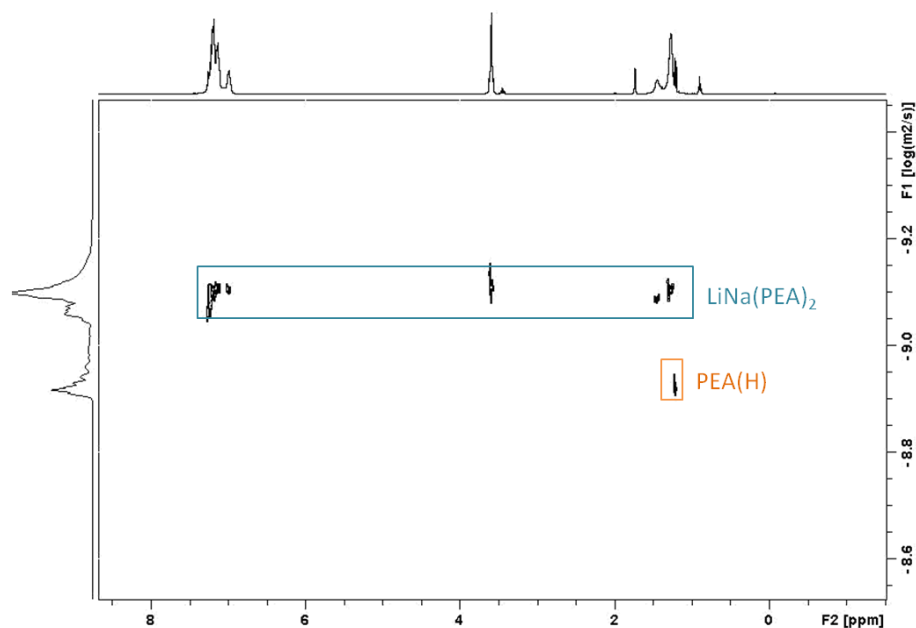
Figure 5.9 ^{1}H DOSY NMR spectrum of **168** in D_8-THF.

Apart for a small signal of free amine, **Figure 5.9** shows only one single species in solution. Therefore, a multinuclear (and probably monomeric) entity of the base remains in solution.

^{7}Li NMR spectra show a clean signal for LiPEA, $LiNaPEA_2$ and $LiKPEA_2$. As expected, the presence of a heavier alkali metal in the structure shifts the resonance upfield.

^{1}H and ^{13}C NMR studies of complex **169** were performed in deuterated benzene and the resonances of the prontos that belong to THF show that this donor keeps coordinated to the metals in solution.

5.3.3 Organic transformations

The rearrangement of epoxides was discussed in the paragraph **2.2.2.1**, as one of the main applications of chiral lithium amides. In this chapter, a series of alkali metal and mixed alkali metal amides have been synthesised and applied as bases for the asymmetric rearrangements of epoxides to chiral alcohols (**Table 5.3**).

Table 5.3 Scope of the reaction of rearrangement of epoxides with chiral alkali-metal amides.

Base	Temperature (°C)	Conversion (%)	E. Ratio
LiPEA	Reflux	65	68:32
	r.t.	0	-
NaPEA	-78 to r.t.	50	47:53
	-78	0	-
LiNaPEA$_2$	-78 to r.t.	65	57:43
	-78	0	-
LiKPEA$_2$	-78 to r.t.	72	47:53
	-78	0	-

Asymmetric rearrangement of epoxides has been chosen as a target to test the reactivity of the metal amides because the monometallic LiPEA need reflux conditions to be able to deprotonate the epoxide **61** i.e., when the reaction is performed at ambient temperature, no deprotonation takes place.

NaPEA, LiNaPEA$_2$ (**168**) and LiKPEA$_2$ (**170**) have been evaluated as bases. The potassium amide KPEA was not considered due to its high instability.

The reactions were performed in THF at –78°C. At cryogenic temperatures, the reaction did not take place with any of the bases. However, when the epoxide is added at –78°C and the reaction is warmed up to 0°C, the conversion of the reaction is 50%, 65% and 72% for NaPEA, LiNaPEA$_2$ and LiKPEA$_2$ respectively.

The higher polarity of the metal-nitrogen bond of these amides compared with the lithium-nitrogen bond of LiPEA makes them more reactive so they can work at comparatively low temperatures.

On the other hand, the enantioselectivity of the reactions is only modest; being the mixed lithium-sodium amide is the species that affords the highest enantioselectivity (14% of enantiomeric excess).

5.4 Experimental

5.4.1 Synthesis of 168, LiNaPEA$_2$

1 mmol of ^{n}BuNa (0.08g) was suspended in 5 mL of dried hexane and placed in an ultrasonic bath for ten minutes. 1 mmol of freshly titrated ^{n}BuLi (0.67 mL, 1.6M solution in hexanes) was added and suspension was stirred for five minutes. 2 mmol (0.46 mL) of PEA(H) are added and a thick white suspension was formed. Toluene was added while heating until a solution was formed. Solution was allowed to cool down in a hot water bath. The reaction affords a crop of cube-like crystals suitable for X-ray diffraction studies (0.27 g, 57%).

^{1}H NMR (400.13 MHz, 343 K, D8-toluene): δ 1.28 (6H, br, CH$_3$, PEA), 3.68-3.73 (2H, br, CH, PEA), 6.99-7.24 (10H, Ph, PEA + residual signal for D8-tol). ^{13}C{^{1}H} NMR (100.62 MHz, 343 K, D8-toluene): δ 26.9 (*C*H$_3$, PEA), 61.1 (*C*H, PEA), 126.0 (*C*H$_{para}$, PEA), 126.1 (*C*H$_{meta}$, PEA), 129.2 (*C*H$_{ortho}$), 152.0 (*C*$_{ipso}$, PEA). ^{7}Li NMR (155.47 MHz, 343 K, D8-toluene, reference of LiCl in D$_2$O): δ 2.48.

Elemental Microanalysis calculated for **168**; C, 80.30; H, 7.62; N, 5.66%; found: C, 79.6; H, 7.82; N, 5.87%.

5.4.2 Synthesis of 169, (THF)$_2$LiNaPEA$_2$

1 mmol of ^{n}BuNa (0.08g) was suspended in 5 mL of dried hexane and placed in an ultrasonic bath for ten minutes. 1 mmol of freshly titrated ^{n}BuLi (0.67 mL, 1.6M solution in hexanes) was added and suspension was stirred for five minutes. 2 mmol (0.46 mL) of PEA(H) are added and a thick white suspension was formed. THF was added dropwise until a solution was formed. Solution was allowed to cool down in the bench overnight. After that period, a crop of crystals suitable for X-ray diffraction studies appear (0.53g, 86%).

^{1}H NMR (400.13 MHz, 300 K, C_6D_6): δ 1.29-1.32 (8H, br, OCH$_2$CH_2, THF), 1.63-1.65 (12H, d, $^2J_{HH}$=6.8 Hz, CH_3, PEA), 3.31-3.38 (4H, q, $^4J_{HH}$=6.8 Hz, CH, PEA), 7.11-7.45 (10H, Ph, PEA + residual signal for C_6D_6).

^{13}C{^{1}H} NMR (100.62 MHz, 300 K, C_6D_6): 24.8 (OCH2CH2, THF), 26.4 (CH$_3$, PEA), 61.0 (CH, PEA), 67.6 (OCH2CH2, THF), 124.8 (CH$_{para}$, PEA), 126.2 (CH$_{meta}$, PEA), 128.0 (CH$_{ortho}$), 153.1 (C_{ipso}, PEA).

^{7}Li NMR (155.47 MHz, 343 K, D8-THF, reference of LiCl in D_2O): δ 2.31

5.4.3 Synthesis of 170, LiKPEA$_2$

4 mmol of PEA(H) (0.23 mL) are dissolved in 5 mL of hexane. 4 mmol of ^{n}BuLi are added and the solution was stirred for one hour. A white suspension was formed. 4 mmol of KHMDS (0.796 g) are added via solid addition tube and suspension was stirred overnight. Toluene was added while heating to the pale-brown suspension until a solution was formed. Solution was allowed to cool down slowly in a hot water bath and a crop of crystals suitable for X-ray diffraction studies was obtained (0.19 g, 24%).

^{1}H NMR (400.13 MHz, 300 K, D$_8$-THF) δ 1.26-1.44 (6H, br, CH$_3$, PEA), 3.56-3.61 (2H, br, CH, PEA), 6.98-7.41 (10H, Ph, PEA + residual signal for D$_8$-toluene). ^{13}C{^{1}H} NMR (100.62 MHz, 300 K, D$_8$-THF): δ 28.7, (CH$_3$, PEA), 62.3 (CH, PEA), 124.6 (CH$_{para}$, PEA), 127.4 (CH$_{meta}$, PEA), 127.5 (CH$_{ortho}$), 154.9 (C_{ipso}, PEA). ^{7}Li NMR (155.47 MHz, 343 K, D8-THF, reference of LiCl in D_2O): δ 2.37.

Due to the extreme air- and moisture-sensitivity of this compound, satisfactory elemental microanalysis data could not be obtained.

5.4.4 Experimental procedure for the asymmetric rearrangement of epoxides.

Cyclohexane oxide (0.5 mmol, 0.05 mL) are dissolved in 5 mL of THF and the solution is cooled down to -78°C. 0.5 mmol the appropriate base were added with help of a solid addition tube and the reaction was stirred for one hour.

The reactions were performed by duplicate. In the first reaction, NH$_4$Cl was added after one hour at -78°C. In the second reaction, the dry ice/acetone

bath is removed after the addition of the base and, after one hour, NH_4Cl was added.

Progression of the reaction is monitored by gas chromatographic analysis.

5.5 Conclusions and future work

To the best of our knowledge, herein, the first three structures containing the chiral amide bis-[(*R*)-1-phenylethyl]amine (PEA(H)) and a heavy alkali metal have been isolated and characterised in solid state and solution.

Mixed lithium-sodium amide $[LiNa(PEA)_2]_2$ (**168**) can be synthesised from the deprotonation of PEA(H) by an organometallic mixture of ^nBuLi and ^nBuNa in a mixture of aliphatic and aromatic solvents. This amide crystallises as a cyclic eight-membered ring, with the metallic centres alternating and bonded with each other through a nitrogen atom.

In presence of tetrahydrofuran, the dimeric structure of **168** breaks into a monomer with formula $[(THF)_2LiNaPEA_2]$ (**169**). Two chiral amides bridge the lithium and sodium atoms, which are coordinated to one molecule of THF each. The coordination of the THF molecules remains in deuterated benzene solution and the bimetallic entity of the base remains in bulk THF.

Closely related to **168**, another donor-free complex has been structurally characterised. The mixed lithium-potassium amide $[LiK(PEA)_2]_2$ (**170**) mimics the coordination of its sodium counterpart forming a dimeric ring with the lithium atoms coordinated to two amido groups in a linear arrangement.

A preliminary study of the reactivity of these chiral amides as deprotonating reagents of the epoxide cyclohexene oxide shows that the three new complexes are more reactive than LiPEA, as they react at low temperatures. However, LiPEA brings the best enantioselectivity as the 14% of enantiomeric excess obtained when $LiNa(PEA)_2$ was used was the highest.

Future lines of research include assessing the stability of the complexes in the presence of multidentate donors, as well as the study of different combinations of heavier alkali metals.

Chapter 6. Experimental section

This chapter will summarise all the experimental procedures which have been carried out during this project, including general experimental techniques and the preparation of starting materials.

6.1 General Experimental Techniques

6.1.1 Inert atmosphere techniques

Reactions performed in this work involved reactants and products which are highly sensitive to the air and the moisture, so all the reactions were undertaken using an inert atmosphere protocol. Standard Schlenk techniques were used and the products and synthesised starting materials were stored in a glove box. Glassware was pre-dried in an oven prior to utilisation.

6.1.1.1 Schlenk techniques

6.1.1.2 Schlenk line

All reactions performed in this research project were carried out using Schlenk apparatus connected to a Schlenk line. The Schlenk line or vacuum glass manifold is composed of two separated glass tubes incorporating a vacuum system and an argon line joined by double taps so it can be switched between vacuum and gas for the manipulation of air-sensitive compounds.

Before starting an experiment, all air and moisture had to be removed from the Schlenk tubes. This was achieved by placing them under vacuum for ten minutes and refilling them with argon; a procedure which was repeated three times as standard practice.

The Schlenk line is attached to a release bubbler to avoid an overpressure in the system.

6.1.1.3 Glove box

The glove box employed in this work was a MBraun MG10, filled with argon.

A glove box is a sealed enclosure that provides a place completely segregated from the outside so the moisture sensitive compounds can be stored and manipulated. The box itself is mainly made from stainless steel, the window from poly carbonate and the gloves from neoprene.

The glove box system works using the principle of gas circulation so the gas permanently circulates between the glove box and the gas purification System. When the adsorbent material of the gas purification system becomes exhausted, is necessary to regenerate the glove box with a regeneration gas. In this case the regeneration gas was 15 % H_2/85% N_2.

6.1.2 Solvent and Liquid Reagent Purification

- Solvents (specifically diethyl ether, THF and hexane) were dried by heating them to reflux in a still containing sodium and benzophenone. A 2.5 L consistency Winchester of the appropriate solvent was charged with 10 grams of potassium hydroxide to assist with pre-drying the solvent. 2L three-necked flask were filled approximately 3/4 full with pre-dried solvent, and 30g of benzophenone and 5 grams of sodium metal (introduced as a wire) were added. Sodium and benzophenone react, forming an intensely blue ketyl radical, which is highly reactive towards water – producing colourless or yellow products, making it a useful self-indicating desiccant. As the indicator is barely soluble in hexane, a small amount of triglyme (triethylene glycol dimethyl ether) is added to help to see the change in the colour.

- TMEDA, PMDETA, TMPDA, SiMe$_3$Cl and solvents not included in the solvent-drying procedure such us pentane, benzene or methylcyclohexane were distilled in presence of calcium hydride and stored in argon-filled flasks in presence of activated 4Å molecular sieves.

- TMP(H) and PEA(H) were dried by adding 4Å molecular sieves.

- Deuterated solvents were degassed using the freeze-pump-thaw methodology to ensure the removal of any dissolved oxygen. This involved freezing the solvent in a liquid nitrogen bath prior to warming up to ambient temperature under vacuum, whereby they were then stored in oven-dried glassware containing 4 Å molecular sieves to prevent contamination by moisture.[270]

6.2 Standardisation of organometallic reagents

A wide variety of methods exist for determining the molarity of organometallic reagents are available, the procedure followed in this work is detailed below.

6.2.1 Standardisation of alkyllithium reagents.

Titration of alkyllithium solutions were performed with menthol/1,10-phenanthroline in THF at 0°C. Colour change: From colourless to purple.[271]

Menthol (1 mmol, 0.156 g accurately weighed out) and a tip of spatula of 1,10-phenanthroline were dissolved in 2 mL of THF in an oven dried 10 mL round bottom flask. Solution was cooled down to 0°C alkyllithium reagent was added dropwise until the colour change is observed.
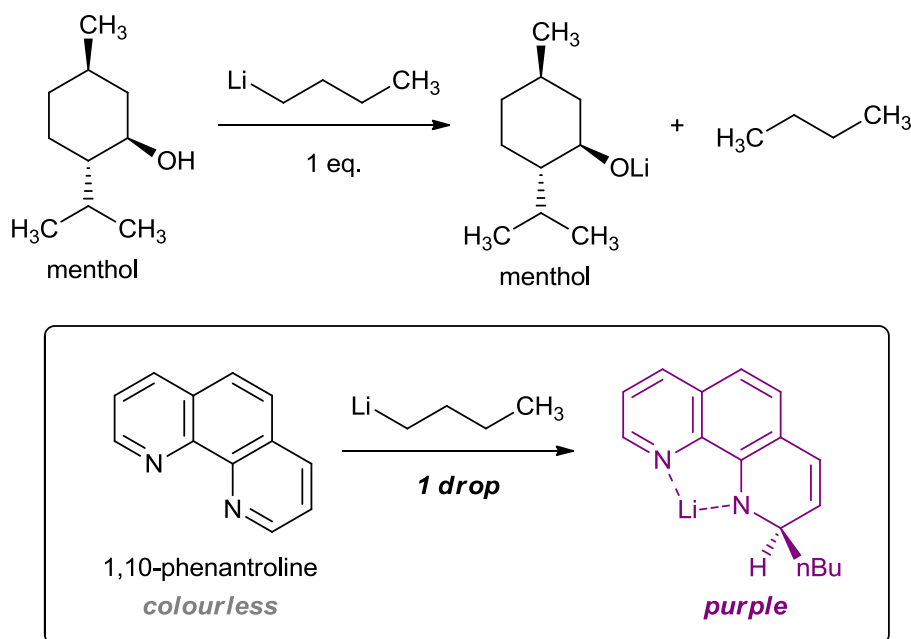
Scheme 6.1 Procedure for the titration of ^{n}BuLi.

6.2.2 Standardisation of Grignard reagents and diorganomagnesium or diorganozinc compounds.

Grignard reagents were titrated with iodine in presence of an excess of LiCl, in THF at 0°C.[272] A sharp colour change from the brown colour of the iodine

solution in THF to a colourless, completely transparent solution at the end point of the titration could be easily observed, indicating the complete consumption of iodine. In the absence of LiCl, the precipitation of mixed magnesium halides takes and the color change cannot be observed.

$$^{n}Bu_2Mg + 2\ I_2 \xrightarrow[\text{exc. LiCl}]{\text{THF}} {}^{n}BuMgI{\cdot}LiCl + I_2 + {}^{n}BuI{\cdot}LiCl \xrightarrow[\text{LiCl}]{\text{THF}} MgI_2{\cdot}LiCl + 2{}^{n}BuI$$

brown solution   *colourless solution*

Scheme 6.2 Procesure for the titration of di-*n*-butylmagnesium.

6.3 Instrumentation

NMR spectroscopy. ^{1}H, ^{13}C NMR and ^{7}Li NMR spectra were recorded on a Bruker DPX 400 MHz or 500 MHz spectrometer. ^{1}H NMR spectra were recorded on a Bruker AV3, AV400 or DRX 500 spectrometer, operating at 400.13, 400.03 or 500.13 MHz respectively. The same instruments, operating at 100.62, 100.60 or 125.77 MHz respectively were used to record ^{13}C. All ^{13}C NMR spectra were proton decoupled.

Gas Chromatography. Gas chromatography was carried out using a Perkin Elmer Clarus 500 Gas Chromatograph.

Achiral G.C. analysis: (i) CP Chirasil-DEX CB column30m x 0.25mm x 0.25μm; (ii) carrier gas, H_2 (45 cm sec^{-1}): (i) injector/detector temperature, 250°C; (ii) Temperature gradient: 90 °C, 0.5 min; 45 °C min^{-1}; 220 °C, 6 min (iii) detection method, FID (flame ionization detector).

Chiral G.C. analysis: (i) CP Chirasil-DEX CB column 30m x 0.25mm x 0.25μm; (ii) carrier gas, H_2 (45 cm sec^{-1}); (iii) injector/detector temperature, 250°C; (iv) initial oven temperature: 70 °C; (v) temperature gradient, 70-130 °C 1.5 °C min^{-1}; 130 °C, 1 min; 130-200 °C 20 °C min^{-1} ; 200 °C, 1 min; (vi) final oven temperature, 200 °C (vii) detection method, FID.

X-ray Diffraction. Crystals suitable for X-ray diffraction were measured on Oxford Diffraction Xcalibur and Gemini diffractometers at 123 K using CuKα and MoKα radiation.

Flash Chromatography. Purification of products was performed by employing silica gel flash chromatography on a Teledyne IscoCombiFlashRf flash chromatography by employing 4 g silica columns and a hexane/ethyl acetate solvent mixture.

Elemental microanalysis. Elemental (C, H, N) analysis was carried out using a Perkin Elmer 2400 elemental analyser. Microanalysis samples were prepared in an argon filled glovebox, and were sealed in an air-tight box prior to removal from the glovebox.

6.4 Preparation of Starting Materials

6.4.1 Preparation of ^{n}BuNa

$$^{t}\text{BuONa} + {}^{n}\text{BuLi} \xrightarrow[\text{0°C}]{\text{hexane}} {}^{t}\text{BuOLi} + {}^{n}\text{BuNa}$$
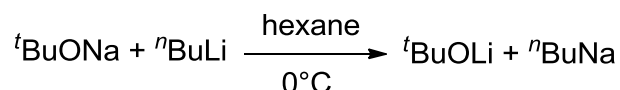
Sodium *tert*-butoxide (3.84 g, 40 mmol) was placed in an oven-dried Schlenk tube inside the glove box, and was suspended in 60 mL of dried hexane under argon atmosphere. The Schlenk tube was then cooled to 0°C in an ice bath and *n*-butyllithium (25 mL, 1.6 M solution in hexanes, 40 mmol) was added dropwise. The off-white suspension was stirred at ambient temperature overnight.

The solid product was isolated using standard Schlenk filtration techniques, and washed with several aliquots of hexane to eliminate the lithium *tert*-butoxide. The product was dried *in vacuo* for at least an hour, prior to being transferred to the glove box. This reaction usually affords ^{n}BuNa in quantitative yields.[273]

6.4.1.1 Preparation of (*R,R*)-TMCDA

Synthesis of (R,R)-1,2-diammoniumcyclohexane mono-(+)-tartrate salt
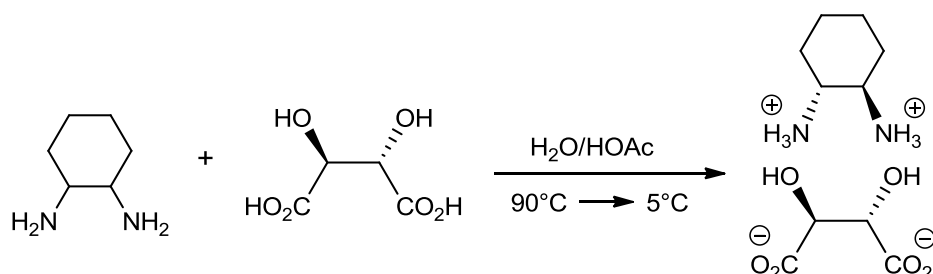
L-(+)-tartaric acid (150 g, 0.99 mol) and distilled water (400 mL) were introduced in a 1-L beaker and the mixture was stirred at ambient temperature until complete dissolution occurred. At that point a mixture of *cis*-and *trans*-1,2-diaminocyclohexane (240 mL, 1.94 mol) was added at a rate such that the reaction temperature just reached 70°C. Glacial acetic acid (100 mL, 1.75 mol) was added to the resulting solution at a rate such that the reaction temperature just reached 90°C. A white precipitate formed immediately upon addition of the acid, and the slurry was vigorously stirred as cooled to ambient temperature over a period of 2 h. The mixture was then cooled to ≤5°C in an ice bath for 2 h and the precipitate was collected by vacuum filtration. The wet cake was washed with 5°C water (100 mL) and then rinsed with methanol (5 x100 mL). The solid was dried by drawing air for 1 h and then dried at 40°C under reduced pressure to yield (R,R)-1,2-diammoniumcyclohexane mono-(+)-tartrate salt as a white solid in quantitative yields.[275]

Synthesis of (*R,R*)-(−)-*N,N,N',N'*-Tetramethyl-*trans*-1,2-cyclohexanediamine
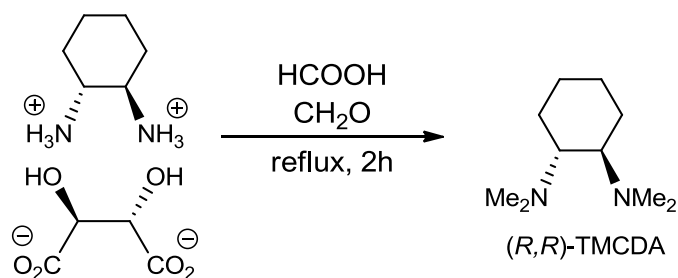
(*R,R*)-1,2-Diammoniumcyclohexane mono-(+)-tartrate (24 g, 0.091 mol) was dissolved in formic acid 85% (36 mL) and formaldehyde 40% (44 mL) was added slowly at ambient temperature. The mixture was refluxed for 2 h. After cooling to ambient temperature, and then to 0°C, the reaction mixture was made basic until pH 12 with solid sodium hydroxide and extracted thoroughly with diethyl ether. The combined organic layers were dried over Na_2SO_4, filtered, and concentrated under reduced pressure. The residue was purified by distillation in a bulb-to-bulb apparatus (b.p. 95°C/vacuum line) to afford a colorless liquid (11.35 g, 74%). Spectral data were in agreement with the literature.[276]

6.4.2 Preparation of dialkylmagnesium derivatives

$$2 \text{ MgRCl} + 1,4\text{-dioxane} \xrightarrow{\text{diethyl ether}} \text{MgR}_2 + [\text{MgCl}_2(\text{dioxane})]\downarrow$$
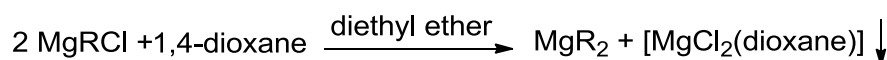
Dialkylmagnesium derivatives were prepared from the Grignard reagent by manipulation of the Schlenk equilibrium via the dioxane precipitation method. A representative experimental procedure for the synthesis of $(Me_3SiCH_2)_2Mg$ is given below.[277]

Magnesium turnings (4.0 g, 165 mmol) were added to a 500 mL round bottom flask equipped with a condenser and addition funnel. 100 mL of diethyl ether were added and the addition funnel was charged with chloromethyltrimethylsilane (19 mL, 136 mmol) and 50 mL of diethyl ether. This solution was added dropwise to the mixture to form the Grignard reagent. The system was heated to reflux for two hours.

The addition funnel was charged with 1,4-dioxane (10 mL, 117 mmol) and 50 mL of diethyl ether. The resulting thick grey suspension was stirred overnight and filtered using standard Schlenk filtration techniques and washed twice with 50 mL of diethyl ether. Solvent was eliminated slowly in vacuo and the solid was washed once again with 4 mL of diethyl ether. Solvent was evacuated affording an off-white solid which was purified by sublimation.

^{1}H NMR (400.03 MHz, 300 K, d$_8$-THF): δ −1.73 (4H, s, C*H*$_2$Si(CH$_3$)$_3$); −0.107 (18H, s, CH$_2$Si(C*H*$_3$)$_3$).

6.4.3 Preparation of di-*tert*-butyl zinc

Dried $ZnCl_2$ (40 mmol, 5.45 g) was transfered into a Schlenk flask under inert atmosphere and dissolve in diethyl ether (80 mL).

The solution was cooled down to 0 °C and *t*BuLi (80 mmol, 48 mL of a 1.7 M solution in pentane) was added dropwise. In order to prevent decomposition, the Schlenk tube was covered with aluminium foil and stirred for 3 h at ambient temperature.
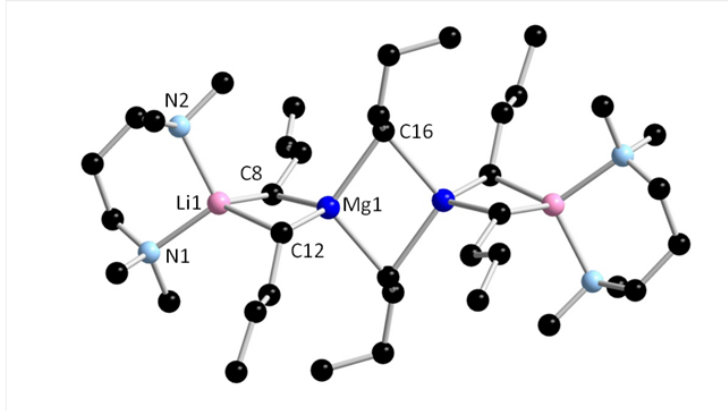
The resultant gray suspension was filtered through Celite and glass wool. Solvent was removed under *vacumm* until ~15 mL of solvent remains.

The colorless solution was transferred to a sublimation apparatus via cannula and then the remaining solvent was removed *in vacuo*. As soon as a white solid begins to form, add chilled *iso*-propanol is added to the cold finger (the temperature of the cold finger should be kept between −20 and −30 °C throughout the sublimation).

Collect the purified product in a glove box and then store at −35°C as a solution in hexane.[278]

^{1}H NMR (400.03 MHz, 300 K, C_6D_6): δ 1.07 ppm.
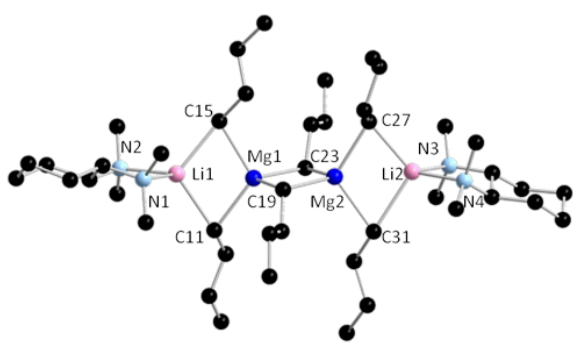
Appendix of crystallographic data

Compound	48
Formula	$C_{38}H_{90}Li_2Mg_2N_4$
Formula weight	665.64
Crystal system	Orthorhombic
Space group	P bca
a [Å]	13.8489(4)
b [Å]	17.5351(6)
c [Å]	19.0192(7)
β [°]	90
V [Å³]	4618.7(3)
Z	2
$\rho_{calcd.}$ [g cm⁻³]	0.890
Absorption coefficient [mm⁻¹]	0.641
T [K]	123(2)
Radiation type, wavelength [Å]	CuKα, 1.54180
θ range for data collection [°]	6.39 to 73.34
Reflections collected	14556
Reflections unique	4547
Data/restraints/parameters	253
R_{INT}	0.0224
Goodness-of-fit on F²	1.023
Final R indexes [I>2s (I)]	R1=0.0501, wR2=0.1387
Final R indexes (all data)	R1=0.0709, wR2=0.1596
Largest diff. peak/hole [e.Å⁻³]	0.206 / -0.203
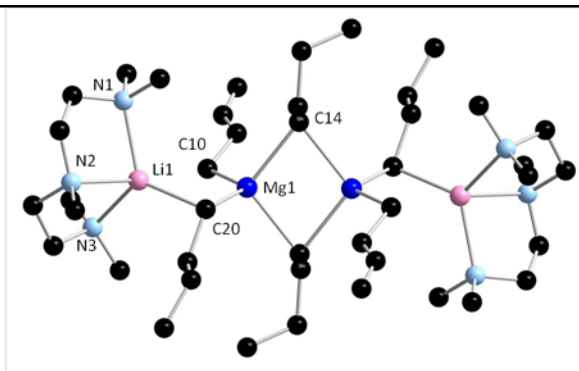
Compound	49
Formula	$C_{42}H_{100}Li_2Mg_2N_6$
Formula weight	751.78
Crystal system	Monoclinic
Space group	P 2_1/n
a [Å]	12.0911(7)
b [Å]	15.5710(7)
c [Å]	13.7974(7)
β [°]	90
V [Å³]	2546.5(2)
Z	2
$\rho_{calcd.}$ [g cm⁻³]	0.980
Absorption coefficient [mm⁻¹]	0.078
T [K]	123(2)
Radiation type, wavelength [Å]	MoKα, 0.71073
θ range for data collection [°]	3.42 to 26.00
Reflections collected	13451
Reflections unique	4986
Data/restraints/parameters	275
R_{INT}	0.0562
Goodness-of-fit on F²	1.023
Final R indexes [I>2s (I)]	R1=0.0706, wR2=0.1839
Final R indexes (all data)	R1=0.1148, wR2=0.2114
Largest diff. peak/hole [e.Å⁻³]	0.558 / -0.278

Compound	**51**
Formula	$C_{44}H_{98}Li_2Mg_2N_4$
Formula weight	745.76
Crystal system	Monoclinic
Space group	P 2_1
a [Å]	9.9060(12)
b [Å]	14.5510(13)
c [Å]	17.7804(17)
β [°]	96.405(11)
V [Å³]	2546.9(5)
Z	2
$\rho_{calcd.}$ [g cm⁻³]	0.972
Absorption coefficient [mm⁻¹]	0.077
T [K]	123(2)
Radiation type, wavelength [Å]	MoKα, 0.71073
θ range for data collection [°]	2.92 to 26.00
Reflections collected	7794
Reflections unique	7794
Data/restraints/parameters	7794 / 34 / 484
R_{INT}	0.0446
Flack parameter	-0.02(6)
Goodness-of-fit on F²	0.940
Final R indexes [I>2s (I)]	R1=0.0714, wR2=0.1625
Final R indexes (all data)	R1=0.1355, wR2=0.1895
Largest diff. peak/hole [e.Å⁻³]	0.270 / -0.273
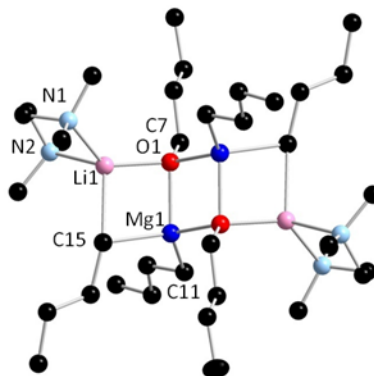
Compound	**55**
Formula	$C_{36}H_{86}Li_2Mg_2N_4O_2$
Formula weight	669.59
Crystal system	Monoclinic
Space group	$P\,2_1/c$
a [Å]	10.0718(2)
b [Å]	13.5833(2)
c [Å]	16.9469(3)
β [°]	95.751(2)
V [Å³]	2306.81(7)
Z	2
$\rho_{calcd.}$ [g cm⁻³]	0.964
Absorption coefficient [mm⁻¹]	0.678
T [K]	123(2)
Radiation type, wavelength [Å]	$CuK\alpha$, 1.54180
θ range for data collection [°]	6.18 to 26.00
Reflections collected	17305
Reflections unique	4601
Data/restraints/parameters	231
R_{INT}	0.0541
Goodness-of-fit on F^2	1.042
Final R indexes [I>2s (I)]	R1=0.0508, wR2=0.1450
Final R indexes (all data)	R1=0.0565, wR2=0.1521
Largest diff. peak/hole [e.Å⁻³]	0.463 / -0.256

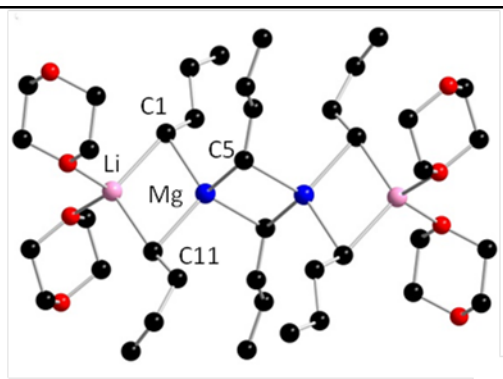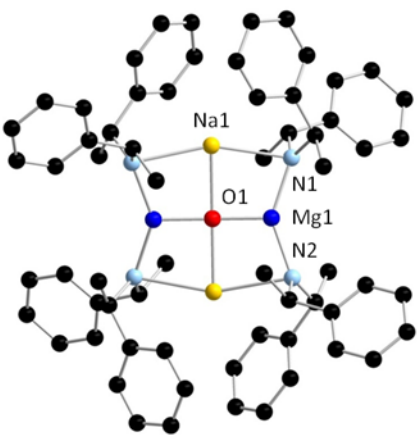| Compound	56
Formula	$C_{19}H_{38}LiMgO_2$
Formula weight	329.74
Crystal system	Monoclinic
Space group	C 2/c
a [Å]	10.5458(8)
b [Å]	22.265(2)
c [Å]	18.0116(12)
β [°]	93.437(7)
V [Å³]	4221.6(6)
Z	8
$\rho_{calcd.}$ [g cm⁻³]	1.038
Absorption coefficient [mm⁻¹]	0.090
T [K]	123(2)
Radiation type, wavelength [Å]	MoKα, 0.71073
θ range for data collection [°]	3.03 to 26.00
Reflections collected	11951
Reflections unique	4082
Data/restraints/parameters	228
R_{INT}	0.0315
Goodness-of-fit on F²	1.103
Final R indexes [I>2s (I)]	R1=0.0924, wR2=0.2420
Final R indexes (all data)	R1=0.1318, wR2=0.2721
Largest diff. peak/hole [e.Å⁻³]	0.486 / -0.476
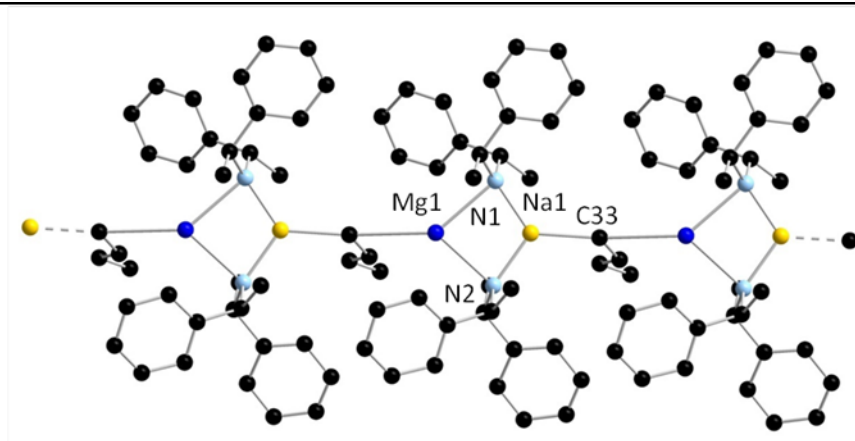
Compound	**103**
Formula	$C_{36}H_{45}MgN_2Na$
Formula weight	553.04
Crystal system	Tetragonal
Space group	$P4_3$
a [Å]	8.0811(4)
b [Å]	8.0811(4)
c [Å]	47.458(2)
β [°]	90
V [Å³]	3099.2(3)
Z	4
$\rho_{calcd.}$ [mg cm⁻³]	1.183
Absorption coefficient [mm⁻¹]	0.098
T [K]	123(2)
Radiation type, wavelength [Å]	CuKα, 1.54180
θ range for data collection [°]	3.046 to 25.999
Reflections collected	24263
Reflections unique	5981
Data/restraints/parameters	5981 / 30 / 378
R_{INT}	0.0909
Flack parameter	0.2(8)
Goodness-of-fit on F²	1.110
Final R indexes [I>2s (I)]	R1 = 0.0986, wR2 = 0.2146
Final R indexes (all data)	R1 = 0.1094, wR2 = 0.2209
Largest diff. peak/hole [e.Å⁻³]	0.291 and -0.395
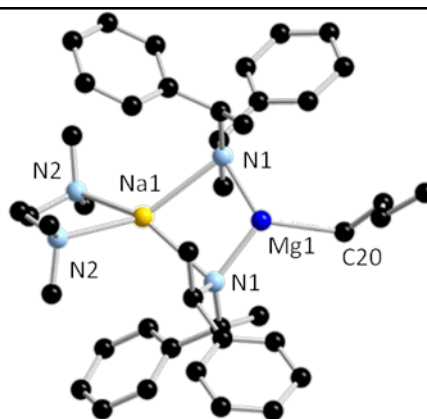
Compound	**104**
Formula	$C_{42}H_{61}MgN_4Na$
Formula weight	669.25
Crystal system	Tetragonal
Space group	P 4_1 2_1 2
a [Å]	10.6428(5)
b [Å]	10.6428(5)
c [Å]	36.260(3)
b [°]	90
V [Å³]	4107.1(4)
Z	4
$\rho_{calcd.}$ [g cm⁻³]	1.082
Absorption coefficient [mm⁻¹]	0.086
T [K]	123(2)
Radiation type, wavelength [Å]	MoKα, 0.71073
θ range for data collection [°]	2.93 to 27.00
Reflections collected	13719
Reflections unique	4460
Data/restraints/parameters	4460 / 26 / 241
R_{INT}	0.0478
Flack parameter	0.2(4)
Goodness-of-fit on F²	1.032
Final *R* indexes [I>2s (I)]	R1 = 0.0554, wR2 = 0.1187
Final *R* indexes (all data)	R1 = 0.1220, wR2 = 0.1466
Largest diff. peak/hole [e.Å⁻³]	0.347 and -0.284

Compound	**105**
Formula	$C_{64}H_{72}Mg_2N_4Na_2O$
Formula weight	1007.86
Crystal system	Monoclinic
Space group	C 1 2 1
a [Å]	26.951(3)
b [Å]	8.0499(6)
c [Å]	13.9314(13)
β [°]	113.030(12)
V [Å³]	2781.6(4)
Z	2
$\rho_{calcd.}$ [g cm⁻³]	1.203
Absorption coefficient [mm⁻¹]	0.884
T [K]	123(2)
Radiation type, wavelength [Å]	CuKα, 1.54180
θ range for data collection [°]	3.45 to 69.99
Reflections collected	7574
Reflections unique	4013
Data/restraints/parameters	4013 / 1 / 350
R_{INT}	0.0540
Flack parameter	-0.02(9)
Goodness-of-fit on F²	0.964
Final R indexes [I>2s (I)]	R1 = 0.0572, wR2 = 0.1286
Final R indexes (all data)	R1 = 0.0795, wR2 = 0.1420
Largest diff. peak/hole [e.Å⁻³]	0.506 and -0.243
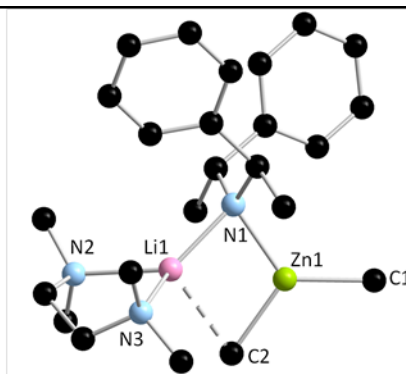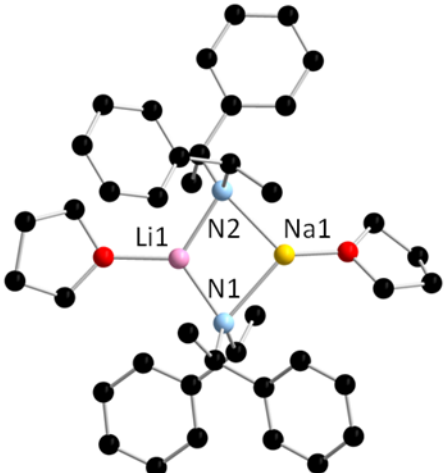
Compound	**147**
Formula	$C_{24}H_{40}LiN_3Zn$
Formula weight	442.9
Crystal system	Monoclinic
Space group	P 1 21 1
a [Å]	9.782(2)
b [Å]	11.5664(14)
c [Å]	12.047(3)
β [°]	112.05(3)
V [Å³]	1263.3(4)
Z	2
$\rho_{calcd.}$ [g cm⁻³]	1.164
Absorption coefficient [mm⁻¹]	1.425
T [K]	123(2)
Radiation type, wavelength [Å]	CuKα, 1.54180
θ range for data collection [°]	6.20 to 89.51
Reflections collected	7395
Reflections unique	7395
Data/restraints/parameters	7395 / 1 / 279
R$_{INT}$	0.0426
Flack parameter	0.2(4)
Goodness-of-fit on F²	1.009
Final R indexes [I>2s (I)]	R1 = 0.0350, wR2 = 0.0768
Final R indexes (all data)	R1 = 0.0424, wR2 = 0.0787
Largest diff. peak/hole [e.Å⁻³]	0.293 and -0.311
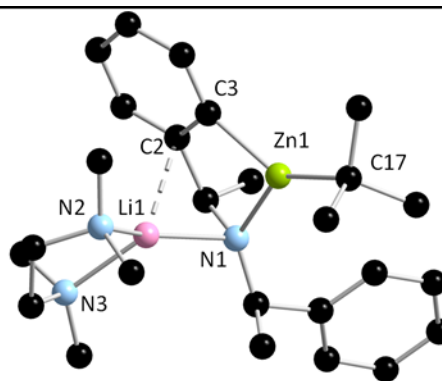
Compound	**148**
Formula	$C_{52}H_{84}Li_2N_6Zn_2$
Formula weight	937.87
Crystal system	Orthorhombic
Space group	$P2_12_12_1$
a [Å]	12.4069(3)
b [Å]	12.7104(3)
c [Å]	34.1158(10)
β [°]	90
V [Å^3]	5379.9(2)
Z	4
$\rho_{calcd.}$ [mg cm^{-3}]	1.158
Absorption coefficient [mm^{-1}]	0.929
T [K]	123(2)
Radiation type, wavelength [Å]	MoKα, 0.71073
θ range for data collection [°]	3.261 to 27.000
Reflections collected	33150
Reflections unique	11739
Data/restraints/parameters	11739 / 0 / 577
R_{INT}	0.0371
Flack parameter	-0.003(4)
Goodness-of-fit on F^2	1.094
Final R indexes [I>2s (I)]	R1 = 0.0413, wR2 = 0.0766
Final R indexes (all data)	R1 = 0.0494, wR2 = 0.0795
Largest diff. peak/hole [e.Å^{-3}]	0.634 and -0.429

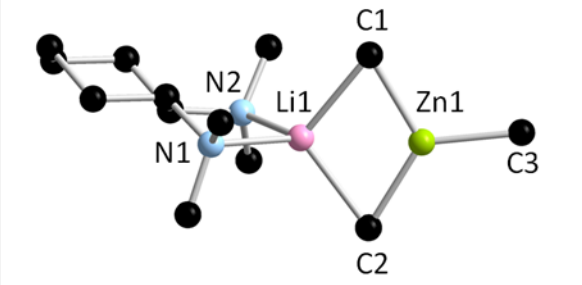| Compound	**149**
Formula	$C_{13}H_{31}LiN_2Zn$
Formula weight	287.71
Crystal system	Monoclinic
Space group	$P2_1$
a [Å]	8.2940(1)
b [Å]	16.6359(2)
c [Å]	12.0707(1)
β [°]	99.6222(11)
V [Å³]	1642.07(3)
Z	4
$\rho_{calcd.}$ [g cm⁻³]	1.164
Absorption coefficient [mm⁻¹]	1.908
T [K]	123(2)
Radiation type, wavelength [Å]	CuKα, 1.54184
θ range for data collection [°]	7.444 to 73.246
Reflections collected	16249
Reflections unique	6326
Data/restraints/parameters	6326 / 19 / 354
R_{INT}	0.0295
Flack parameter	0.04(3)
Goodness-of-fit on F²	1.064
Final R indexes [I>2s (I)]	R1 = 0.0370, wR2 = 0.1046
Final R indexes (all data)	R1 = 0.0381, wR2 = 0.1060
Largest diff. peak/hole [e.Å⁻³]	0.693 and -0.313

Compound	**169**
Formula	$C_{64}H_{72}Li_2N_4Na_2$
Formula weight	957.12
Crystal system	Monoclinic
Space group	C 2
a [Å]	26.160(2)
b [Å]	8.1933(5)
c [Å]	13.7668(11)
β [°]	111.283(9)
V [Å³]	2749.5(3)
Z	2
$\rho_{calcd.}$ [mg cm^{-3}]	1.156
Absorption coefficient [mm^{-1}]	0.639
T [K]	123(2)
Radiation type, wavelength [Å]	MoKα, 0.71073
θ range for data collection [°]	3.44 to 72.73
Reflections collected	12298
Reflections unique	5262
Data/restraints/parameters	5262 / 1 / 375
R_{INT}	0.0313
Flack parameter	0.03(6)
Goodness-of-fit on F²	1.043
Final *R* indexes [I>2s (I)]	R1 = 0.0373, wR2 = 0.0952
Final *R* indexes (all data)	R1 = 0.0411, wR2 = 0.0982

Compound	**170**
Formula	$C_{40}H_{52}LiN_2NaO_2$
Formula weight	622.76
Crystal system	Orthorhombic
Space group	$P2_12_12_1$
a [Å]	9.7253(1)
b [Å]	13.3902(2)
c [Å]	27.8330(4)
b [°]	90
V [Å^3]	3624.52(8)
Z	4
$\rho_{calcd.}$ [mg cm^{-3}]	1.141
Absorption coefficient [mm^{-1}]	0.632
T [K]	123.2
Radiation type, wavelength [Å]	CuKα, 1.54180
θ range for data collection [°]	3.176 to 69.997
Reflections collected	25322
Reflections unique	6797
Data/restraints/parameters	6797 / 406 / 462
R_{INT}	0.0295
Flack parameter	0.04(3)
Goodness-of-fit on F^2	1.029
Final R indexes [I>2s (I)]	R1 = 0.0581, wR2 = 0.1691
Final R indexes (all data)	R1 = 0.0623, wR2 = 0.1752

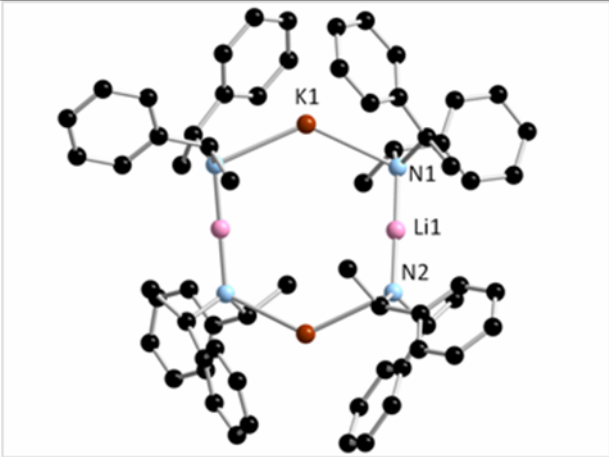| Compound	**171**
Formula	$C_{32}H_{36}KLiN_2$
Formula weight	494.67
Crystal system	Monoclinic
Space group	C2
a [Å]	26.804(2)
b [Å]	8.6314(3)
c [Å]	13.8250(10)
β [°]	115.868(9)
V [Å³]	2878.0(4)
Z	4
$\rho_{calcd.}$ [mg cm⁻³]	1.142
Absorption coefficient [mm⁻¹]	0.206
T [K]	123(2)
Radiation type, wavelength [Å]	CuKα, 1.54180
θ range for data collection [°]	3.044 to 26.992
Reflections collected	9828
Reflections unique	5696
Data/restraints/parameters	5696/1/329
R_{INT}	0.0258
Flack parameter	0.05(2)
Goodness-of-fit on F²	1.017
Final R indexes [I>2s (I)]	R1 = 0.0461, wR2 = 0.0795
Final R indexes (all data)	R1 = 0.0639, wR2 = 0.0873
Largest diff. peak/hole [e.Å⁻³]	0.273 and -0.225

Chapter 7. References

1. J. Clayden, *Organolithiums: Selectivity for Synthesis*, Pergamon, Manchester, 2002.

2. S. R. Harutyunyan, T. den Hartog, K. Geurts, A. J. Minnaard and B. L. Feringa, *Chem. Rev.*, 2008, **108**, 2824.

3. R. W. Hoffmann, *Chem. Soc. Rev.*, 2003, **32**, 225.

4. P. Knochel and P. Jones, *Organozinc Reagents*, Oxford University Press, Oxford, 1999.

5. G. Wittig, F. J. Meyer and G. Lange, *Justus Liebigs Ann. Chem.*, 1951, **571**, 167.

6. A. Krasovskiy and P. Knochel, *Angew. Chem. Int. Ed.*, 2004, **43**, 3333

7. H. Ila, O. Baron, A. J. Wagner and P. Knochel, *Chem. Commun.*, 2006, 583.

8. N. M. Barl, V. Werner, C. Sämann and P. Knochel, *Heterocycles*, 2014, **88**, 827.

9. A. Krasovskiy, V. Krasovskaya and P. Knochel, *Angew. Chem. Int. Ed.*, 2006, **45**, 2958

10. W. Lin, O. Baron and P. Knochel, *Org. Lett*, 2006, **8**, 5674.

11. S. H. Wunderlich, C. J. Rohbogner, A. Unsinn and P. Knochel, *Org. Process Res. Dev.*, 2010, **14**, 339.

12. B. Haag, M. Mosrin, H. Ila, V. Malakhov and P. Knochel, *Angew. Chem. Int. Ed.*, 2011, **50**, 9794

13. P. García-Álvarez, D. V. Graham, E. Hevia, A. R. Kennedy, J. Klett, R. E. Mulvey, C. T. O'Hara and S. Weatherstone, *Angew. Chem. Int. Ed.*, 2008, **47**, 8079.

14. D. R. Armstrong, P. García-Álvarez, A. R. Kennedy, R. E. Mulvey and J. A. Parkinson, *Angew. Chem. Int. Ed.*, 2010, **49**, 3185.

15. M.-L. Hsueh, B.-T. Ko, T. Athar, C.-C. Lin, T.-M. Wu and S.-F. Hsu, *Organometallics*, 2006, **25**, 4144.

16. E. C. Ashby, L.-C. Chao and J. Laemmle, *J. Org. Chem.*, 1974, **39**, 3258.

17. H. G. Richey and B. A. King, *J. Am. Chem. Soc.*, 1982, **104**, 4672.

18. H. G. Richey and J. Farkas, *Organometallics*, 1990, **9**, 1778.

19. M. Hatano, T. Matsumura and K. Ishihara, *Org. Lett.*, 2005, **7**, 573.

20. J. G. Sośnicki, *Tetrahedron Lett.*, 2006, **47**, 6809.

21. R. Noyori, S. Suga, K. Kawai, S. Okada and M. Kitamura, *Pure App. Chem.*, 1988, **60**, 1597.

22. F. Buron, N. Plé, A. Turck and F. Marsais, *Synlett*, 2006, **2006**, 1586.

23. S. Dumouchel, F. Mongin, F. Trécourt and G. Quéguiner, *Tetrahedron Lett.*, 2003, **44**, 2033.

24. S. Dumouchel, F. Mongin, F. Trécourt and G. Quéguiner, *Tetrahedron Lett.*, 2003, **44**, 3877.

25. S. Dumouchel, F. Mongin, F. Trécourt and G. Quéguiner, *Tetrahedron*, 2003, **59**, 8629.

26. K. Fukuhara, Y. Takayama and F. Sato, *J. Am. Chem. Soc.*, 2003, **125**, 6884.

27. T. Iida, T. Wada, K. Tomimoto and T. Mase, *Tetrahedron Lett.*, 2001, **42**, 4841.

28. A. Inoue, K. Kitagawa, H. Shinokubo and K. Oshima, *J. Org. Chem.*, 2001, **66**, 4333.

29. A. Inoue, J. Kondo, H. Shinokubo and K. Oshima, *Chem. Eur. J.*, 2002, **8**, 1730.

30. S. Ito, T. Kubo, N. Morita, Y. Matsui, T. Watanabe, A. Ohta, K. Fujimori, T. Murafuji, Y. Sugihara and A. Tajiri, *Tetrahedron Lett.*, 2004, **45**, 2891.

31. S. Kii, A. Akao, T. Iida, T. Mase and N. Yasuda, *Tetrahedron Lett.*, 2006, **47**, 1877.

32. K. Kitagawa, A. Inoue, H. Shinokubo and K. Oshima, *Angew. Chem. Int. Ed.*, 2000, **39**, 2481.

33. J. Kondo, A. Inoue, H. Shinokubo and K. Oshima, *Angew. Chem. Int. Ed.*, 2001, **40**, 2085.

34. T. Shoji, S. Ito, K. Toyota, T. Iwamoto, M. Yasunami and N. Morita, *Eur. J. Org. Chem.*, 2009, **2009**, 4307.

35. F. D. Therkelsen, M. Rottländer, N. Thorup and E. B. Pedersen, *Org. Lett.*, 2004, **6**, 1991.

36. T. Tsuji, T. Nakamura, H. Yorimitsu, H. Shinokubo and K. Oshima, *Tetrahedron*, 2004, **60**, 973.

37. J. Xu, N. Jain and Z. Sui, *Tetrahedron Lett.*, 2004, **45**, 6399.

38. D. Catel, O. Payen, F. Chevallier, F. Mongin and P. C. Gros, *Tetrahedron*, 2012, **68**, 4018.

39. O. Payen, F. Chevallier, F. Mongin and P. C. Gros, *Tetrahedron: Asymmetry*, 2012, **23**, 1678.

40. J. Francos, P. C. Gros, A. R. Kennedy and C. T. O'Hara, *Organometallics*, 2015, 2550.

41. M. Yasuda, M. Ide, Y. Matsumoto and M. Nakata, *Synlett*, 1997, **1997**, 899.

42. H. Hawad, O. Bayh, C. Hoarau, F. Trécourt, G. Quéguiner and F. Marsais, *Tetrahedron*, 2008, **64**, 3236.

43. H. Awad, F. Mongin, F. Trécourt, G. Quéguiner and F. Marsais, *Tetrahedron Lett.*, 2004, **45**, 7873.

44. H. Awad, F. Mongin, F. Trécourt, G. Quéguiner, F. Marsais, F. Blanco, B. Abarca and R. Ballesteros, *Tetrahedron Lett.*, 2004, **45**, 6697.

45. O. Bayh, H. Awad, F. Mongin, C. Hoarau, L. Bischoff, F. Trécourt, G. Quéguiner, F. Marsais, F. Blanco, B. Abarca and R. Ballesteros, *J. Org. Chem.*, 2005, **70**, 5190.

46. O. Bayh, H. Awad, F. Mongin, C. Hoarau, F. Trécourt, G. Quéguiner, F. Marsais, F. Blanco, B. Abarca and R. Ballesteros, *Tetrahedron*, 2005, **61**, 4779.

47. F. Mongin, A. Bucher, J. P. Bazureau, O. Bayh, H. Awad and F. Trécourt, *Tetrahedron Lett.*, 2005, **46**, 7989.

48. G. Bentabed-Ababsa, F. Blanco, A. Derdour, F. Mongin, F. Trécourt, G. Quéguiner, R. Ballesteros and B. Abarca, *J. Org. Chem.*, 2009, **74**, 163.

49. D. Thoennes and E. Weiss, *Chem. Ber.*, 1978, **111**, 3726.

50. S. Hao, S. Gambarotta and C. Bensimon, *J. Am. Chem. Soc.*, 1992, **114**, 3556.

51. R. S. Hay-Motherwell, G. Wilkinson, B. Hussain and M. B. Hursthouse, *Polyhedron*, 1990, **9**, 931.

52. J. J.H. Edema, S. Gambarotta, F. van Bolhuis, W. J.J. Smeets, A. L. Spek and M. Y. Chiang, *J. Organomet. Chem.*, 1990, **389**, 47.

53. K. Lamm, M. Stollenz, M. Meier, H. Görls and D. Walther, *J. Organomet. Chem.*, 2003, **681**, 24.

54. R. J. Morris and G. S. Girolami, *J. Am. Chem. Soc.*, 1988, **110**, 6245.

55. R. J. Morris and G. S. Girolami, *Organometallics*, 1989, **8**, 1478.

56. R. Wyrwa, H. O. Fröhlich and H. Görls, *Z. Anorg. Allg. Chem.*, 2000, **626**, 819.

57. R. Wyrwa, H.-O. Fröhlich and H. Görls, *J. Organomet. Chem.*, 1995, **491**, 41.

58. T. Greiser, J. Kopf, D. Thoennes and E. Weiss, *Chem. Ber.*, 1981, **114**, 209.

59. B. Schubert and E. Weiss, *Chem. Ber.*, 1984, **117**, 366.

60. K. M. Waggoner and P. P. Power, *Organometallics*, 1992, **11**, 3209.

61. S. E. Baillie, W. Clegg, P. García-Álvarez, E. Hevia, A. R. Kennedy, J. Klett and L. Russo, *Organometallics*, 2012, **31**, 5131.

62. R. Fischer, R. Suxdorf, H. Görls and M. Westerhausen, *Organometallics*, 2012, **31**, 7579.

63. R. E. Mulvey, *Acc Chem Res*, 2009, **42**, 743.

64. S. E. Baillie, T. D. Bluemke, W. Clegg, A. R. Kennedy, J. Klett, L. Russo, M. de Tullio and E. Hevia, *Chem. Commun.*, 2014, **50**, 12859.

65. J. Francos, B. J. Fleming, P. Garcia-Alvarez, A. R. Kennedy, K. Reilly, G. M. Robertson, S. D. Robertson and C. T. O'Hara, *Dalton Trans.*, 2014, **43**, 14424.

66. H. O. Yamamoto, K., *Main Group Metals in Organic Synthesis*, Wiley-VCH: Weinheim, 2004.

67. S. Zaragoza-Calero, J. Francos, A. R. Kennedy and C. T. O'Hara, *Dalton Trans.*, 2015, **44**, 7258.

68. C. Cambridge Structural Database v5.32 (November 2011); Cambridge Crystallographic Data Centre, U.K., 2011.

69.   B. Schubert and E. Weiss, *Chem. Ber.*, 1983, **116**, 3212.

70.   D. R. Armstrong, A. H. Khandelwal, P. R. Raithby, R. Snaith, D. Stalke and D. S. Wright, *Inorg. Chem.*, 1993, **32**, 2132.

71.   G. E. Herberich, B. Schmidt, U. Englert and T. Wagner, *Organometallics*, 1993, **12**, 2891.

72.   A. Lennartson, J. Sundberg, T. Wiklund, G. Hilmersson and M. Håkansson, *Eur. J. Inorg. Chem.*, 2010, **2010**, 3029.

73.   D. R. Armstrong, E. Herd, D. V. Graham, E. Hevia, A. R. Kennedy, W. Clegg and L. Russo, *Dalton Trans.*, 2008, 1323.

74.   D. R. Armstrong, H. S. Emerson, A. Hernan-Gomez, A. R. Kennedy and E. Hevia, *Dalton Trans.*, 2014, **43**, 14229.

75.   S. Merkel, D. Stern, J. Henn and D. Stalke, *Angew. Chem. Int. Ed.*, 2009, **48**, 6350.

76.   J. Gonzalez-Sabin, F. Rebolledo and V. Gotor, *Chem. Soc. Rev.*, 2009, **38**, 1916.

77.   T. Kano, R. Sakamoto, M. Akakura and K. Maruoka, *J. Am. Chem. Soc.*, 2012, **134**, 7516.

78.   J.-C. Kizirian, N. Cabello, L. Pinchard, J.-C. Caille and A. Alexakis, *Tetrahedron*, 2005, **61**, 8939.

79.   A. Cayuelas, L. Serrano, C. Nájera and J. M. Sansano, *Tetrahedron: Asymmetry*, 2014, **25**, 1647.

80.   A. R. Kennedy and C. T. O'Hara, *Dalton Trans.*, 2008, 4975.

81.   P. Garcia-Alvarez, A. R. Kennedy, C. T. O'Hara, K. Reilly and G. M. Robertson, *Dalton Trans.*, 2011, **40**, 5332.

82.   H. D. Flack, *Helv. Chim. Acta*, 2003, **86**, 905.

83.   R. E. Mulvey, *Chemical Society Reviews*, 1991, **20**, 167.

84.   R. E. Mulvey, *Chem. Soc. Rev.*, 1998, **27**, 339.

85.   N. D. R. Barnett, W. Clegg, A. R. Kennedy, R. E. Mulvey and S. Weatherstone, *Chem. Commun.*, 2005, 375.

86.   A. R. Kennedy, R. E. Mulvey and R. B. Rowlings, *J. Am. Chem. Soc.*, 1998, **120**, 7816.

87.   A. R. Kennedy, R. E. Mulvey and R. B. Rowlings, *Angew. Chem. Int. Ed.*, 1998, **37**, 3180.

88.   W. Uhl, K.-W. Klinkhammer, M. Layh and W. Massa, *Chem. Ber.*, 1991, **124**, 279.

89.   A. Fürstner, R. Martin, H. Krause, G. Seidel, R. Goddard and C. W. Lehmann, *J. Am. Chem. Soc.*, 2008, **130**, 8773.

90.   D. Li, I. Keresztes, R. Hopson and P. G. Williard, *Acc. Chem. Res.*, 2008, **42**, 270.

91. A. Macchioni, G. Ciancaleoni, C. Zuccaccia and D. Zuccaccia, *Chem. Soc. Rev.*, 2008, **37**, 479.

92. C. Su, R. Hopson and P. G. Williard, *Eur. J. Inorg. Chem.*, 2013, **2013**, 4136.

93. J.-H. Lamm, P. Niermeier, A. Mix, J. Chmiel, B. Neumann, H.-G. Stammler and N. W. Mitzel, *Angew. Chem. Int. Ed.*, 2014, **53**, 7938.

94. J.-C. Kizirian, *Chem. Rev.*, 2008, **108**, 140.

95. Y. Nishibayashi, Y. Arikawa, K. Ohe and S. Uemura, *J. Org. Chem.*, 1996, **61**, 1172.

96. P. Steffen, C. Unkelbach, M. Christmann, W. Hiller and C. Strohmann, *Angew. Chem. Int. Ed.*, 2013, **52**, 9836.

97. K. B. Wiberg and W. F. Bailey, *J. Am. Chem. Soc.*, 2001, **123**, 8231.

98. H. Nozaki, T. Aratani and T. Toraya, *Tetrahedron Lett.*, 1968, **9**, 4097.

99. M. Lappert, A. Protchenko, P. Power and A. Seeber, *Metal Amide Chemistry*, John Wiley & Sons, Ltd, Chichester, UK, 2009.

100. P. O'Brien, *J. Chem. Soc., Perkin Trans. 1*, 1998, 1439.

101. J. K. Whitesell and S. W. Felman, *J. Org. Chem.*, 1980, **45**, 755.

102. D. Milne and P. J. Murphy, *Chem. Commun.*, 1993, 884.

103. D. Hodgson, *Tetrahedron: Asymmetry*, 1994, **5**, 337.

104. R. A. Ewin, A. M. MacLeod, D. A. Price, N. S. Simpkins and A. P. Watt, *J. Chem. Soc., Perkin Trans. 1*, 1997, 401.

105. S. Gibson, *Chem. Commun.*, 1996, 2757.

106. G. Dayaker, D. Tilly, F. Chevallier, G. Hilmersson, P. C. Gros and F. Mongin, *Eur. J. Org. Chem.*, 2012, **2012**, 6051.

107. R. Shirai, M. Tanaka and K. Koga, *J. Am. Chem. Soc.*, 1986, **108**, 543.

108. C. Cain, R. P. C. Cousins, G. Coumbarides and N. S. Simpkins, *Tetrahedron*, 1990, **46**, 523.

109. M. J. T. Robinson, *Organic stereochemistry*, Oxford University Press, New York, 2000.

110. M. Majewski, *Can. J. Chem.*, 1994, **72**, 1699.

111. K. Aoki and K. Koga, *Tetrahedron Lett.*, 1997, **38**, 2505.

112. K. Koga, *Pure App. Chem.*, 1994, **66**, 1487.

113. J. Busch-Petersen and E. J. Corey, *Tetrahedron Lett.*, 2000, **41**, 6941.

114. N. Simpkins, *Pure App. Chem.*, 1996, **68**, 691.

115. E. J. Corey and A. W. Gross, *Tetrahedron Lett.*, 1984, **25**, 495.

116. B. H. Lipshutz, M. R. Wood and C. W. Lindsley, *Tetrahedron Lett.*, 1995, **36**, 4385.

117. M. Majewski, R. Lazny and P. Nowak, *Tetrahedron Lett.*, 1995, **36**, 5465.

118. M. Toriyama, K. Sugasawa, M. Shindo, N. Tokutake and K. Koga, *Tetrahedron Lett.*, 1997, **38**, 567.

119. K. Sugasawa, M. Shindo, H. Noguchi and K. Koga, *Tetrahedron Lett.*, 1996, **37**, 7377.

120. K. W. Henderson and W. J. Kerr, *Chem. Eur. J.*, 2001, **7**, 3430.

121. J. D. Anderson, P. García García, D. Hayes, K. W. Henderson, W. J. Kerr, J. H. Moir and K. P. Fondekar, *Tetrahedron Lett.*, 2001, **42**, 7111.

122. M. J. Bassindale, J. J. Crawford, K. W. Henderson and W. J. Kerr, *Tetrahedron Lett.*, 2004, **45**, 4175.

123. W. Kerr, M. Middleditch, A. Watson, W. Kerr, M. Middleditch and A. Watson, *Synlett*, 2011, 177.

124. E. L. Carswell, W. J. Kerr, D. McArthur, M. Pažický and A. J. B. Watson, *Tetrahedron*, 2014, **70**, 7344.

125. L. S. Bennie, W. J. Kerr, M. Middleditch and A. J. B. Watson, *Chem. Commun.*, 2011, **47**, 2264.

126. R. E. Mulvey, F. Mongin, M. Uchiyama and Y. Kondo, *Angew. Chem. Int. Ed.*, 2007, **46**, 3802

127. J. Francos, S. Zaragoza-Calero and C. T. O'Hara, *Dalton Trans.*, 2014, **43**, 1408.

128. G. C. Forbes, A. R. Kennedy, R. E. Mulvey, P. J. A. Rodger and R. B. Rowlings, *J. Chem. Soc., Dalton Trans.*, 2001, 1477.

129. P. C. Andrikopoulos, D. R. Armstrong, A. R. Kennedy, R. E. Mulvey, C. T. O'Hara, R. B. Rowlings and S. Weatherstone, *Inorg. Chim. Acta*, 2007, **360**, 1370.

130. N. Haddad, B. Qu, S. Rodriguez, L. van der Veen, D. C. Reeves, N. C. Gonnella, H. Lee, N. Grinberg, S. Ma, D. Krishnamurthy, T. Wunberg and C. H. Senanayake, *Tetrahedron Lett.*, 2011, **52**, 3718.

131. W. Zhang and X. Zhang, *J. Org. Chem.*, 2007, **72**, 1020.

132. C. Vidal, J. García-Álvarez, A. Hernán-Gómez, A. R. Kennedy and E. Hevia, *Angew. Chem. Int. Ed.*, 2014, **53**, 5969.

133. P. Caubere, *Chem. Rev.*, 1993, **93**, 2317.

134. E. Hevia and R. E. Mulvey, *Angew. Chem. Int. Ed.*, 2011, **50**, 6448.

135. D. Seebach, *Angew. Chem.*, 1988, **100**, 1685.

136. B. J. Bunn, N. S. Simpkins, Z. Spavold and M. J. Crimmin, *J. Chem. Soc., Perkin Trans. 1*, 1993, 3113.

137. F. Paté, N. Duguet, H. Oulyadi, A. Harrison-Marchand, C. Fressigné, J.-Y. Valnot, M.-C. Lasne and J. Maddaluno, *J. Org. Chem.*, 2007, **72**, 6982.

138. S. Merkel, Georg-August-Universität Göttingen, December 2009.

139. M. Majewski and F. Wang, *Tetrahedron*, 2002, **58**, 4567.

140. M. R. Prestly and N. S. Simpkins, *Angew. Chem. Int. Ed.*, 2012, **51**, 12068.

141. T. Yamashita, D. Sato, T. Kiyoto, A. Kumar and K. Koga, *Tetrahedron*, 1997, **53**, 16987.

142. P. García-Álvarez, R. E. Mulvey and J. A. Parkinson, *Angew. Chem. Int. Ed.*, 2011, **50**, 9668.

143. M. Geissler, J. Kopf and E. Weiss, *Chem. Ber.*, 1989, **122**, 1395.

144. P. C. Andrikopoulos, D. R. Armstrong, E. Hevia, A. R. Kennedy, R. E. Mulvey and C. T. O'Hara, *Chem. Commun.*, 2005, 1131.

145. F. Mongin and A. Harrison-Marchand, *Chem. Rev.*, 2013, **113**, 7563.

146. C. G. Screttas and M. Micha-Screttas, *J. Organomet. Chem.*, 1986, **316**, 1.

147. H. G. Richey and J. P. DeStephano, *J. Org. Chem.*, 1990, **55**, 3281.

148. L. Wang, J. Zhang, L. Yao, N. Tang and J. Wu, *Inorg. Chem. Commun.*, 2011, **14**, 859.

149. D. R. Armstrong, A. R. Kennedy, R. E. Mulvey and R. B. Rowlings, *Angew. Chem. Int. Ed.*, 1999, **38**, 131.

150. V. L. Blair, L. M. Carrella, W. Clegg, B. Conway, R. W. Harrington, L. M. Hogg, J. Klett, R. E. Mulvey, E. Rentschler and L. Russo, *Angew. Chem. Int. Ed.*, 2008, **47**, 6208.

151. P. C. Andrikopoulos, D. R. Armstrong, W. Clegg, C. J. Gilfillan, E. Hevia, A. R. Kennedy, R. E. Mulvey, C. T. O'Hara, J. A. Parkinson and D. M. Tooke, *J. Am. Chem. Soc.*, 2004, **126**, 11612.

152. W. Clegg, K. W. Henderson, A. R. Kennedy, R. E. Mulvey, C. T. O'Hara, R. B. Rowlings and D. M. Tooke, *Angew. Chem. Int. Ed.*, 2001, **40**, 3902.

153. A. J. Martínez-Martínez, A. R. Kennedy, R. E. Mulvey and C. T. O'Hara, *Science*, 2014, **346**, 834.

154. P. Beak and V. Snieckus, *Acc. Chem. Res.*, 1982, **15**, 306.

155. V. Snieckus, *Chem. Rev.*, 1990, **90**, 879.

156. E. Hevia, D. J. Gallagher, A. R. Kennedy, R. E. Mulvey, C. T. O'Hara and C. Talmard, *Chem. Commun.*, 2004, 2422.

157. A. J. Martinez-Martinez, D. R. Armstrong, B. Conway, B. J. Fleming, J. Klett, A. R. Kennedy, R. E. Mulvey, S. D. Robertson and C. T. O'Hara, *Chem. Sci.*, 2014, **5**, 771.

158. A. J. Martínez-Martínez, M. Á. Fuentes, A. Hernán-Gómez, E. Hevia, A. R. Kennedy, R. E. Mulvey and C. T. O'Hara, *Angew. Chem. Int. Ed.*, 2015, n/a.

159. G. Gokel, *Crown Ethers and Cryptands*, The Royal Society of Chemistry Cambridge, 1991.

160. A. R. Kennedy, J. G. MacLellan and R. E. Mulvey, *Acta Cryst. C*, 2003, **59**, m302.

161. D. J. Gallagher, K. W. Henderson, A. R. Kennedy, C. T. O'Hara, R. E. Mulvey and R. B. Rowlings, *Chem. Commun.*, 2002, 376.

162. D. V. Graham, A. R. Kennedy, R. E. Mulvey and C. T. O'Hara, *Acta Cryst. C*, 2006, **62**, m366.

163. D. V. Graham, E. Hevia, A. R. Kennedy, R. E. Mulvey, C. T. O'Hara and C. Talmard, *Chem. Commun.*, 2006, 417.

164. V. L. Blair, A. R. Kennedy, J. Klett and R. E. Mulvey, *Chem. Commun.*, 2008, 5426.

165. P. C. Andrikopoulos, D. R. Armstrong, D. V. Graham, E. Hevia, A. R. Kennedy, R. E. Mulvey, C. T. O'Hara and C. Talmard, *Angew. Chem.*, 2005, **117**, 3525.

166. D. R. Armstrong, W. Clegg, S. H. Dale, D. V. Graham, E. Hevia, L. M. Hogg, G. W. Honeyman, A. R. Kennedy and R. E. Mulvey, *Chem. Commun.*, 2007, 598.

167. R. E. Mulvey, V. L. Blair, W. Clegg, A. R. Kennedy, J. Klett and L. Russo, *Nat. Chem.*, 2010, **2**, 588.

168. V. Galasso, F. Asaro, F. Berti, B. Kovač, I. Habuš and A. Sacchetti, *Chem. Phys.*, 2003, **294**, 155.

169. E. Hevia, Fiona R. Kenley, Alan R. Kennedy, Robert E. Mulvey and René B. Rowlings, *Eur. J. Inorg. Chem.*, 2003, **2003**, 3347.

170. R. Campbell, B. Conway, G. S. Fairweather, P. Garcia-Alvarez, A. R. Kennedy, J. Klett, R. E. Mulvey, C. T. O'Hara and G. M. Robertson, *Dalton Trans.*, 2010, **39**, 511.

171. V. L. Blair, A. R. Kennedy, R. E. Mulvey and C. T. O'Hara, *Chem. Eur. J.*, 2010, **16**, 8600.

172. R. Forret, A. R. Kennedy, J. Klett, R. E. Mulvey and S. D. Robertson, *Organometallics*, 2010, **29**, 1436.

173. J. Garcia-Alvarez, D. V. Graham, E. Hevia, A. R. Kennedy and R. E. Mulvey, *Dalton Trans.*, 2008, 1481.

174. E. Hevia, K. W. Henderson, A. R. Kennedy and R. E. Mulvey, *Organometallics*, 2006, **25**, 1778.

175. A. M. Drummond, L. T. Gibson, A. R. Kennedy, R. E. Mulvey, C. T. O'Hara, R. B. Rowlings and T. Weightman, *Angew. Chem. Int. Ed.*, 2002, **41**, 2382.

176. A. Hernan-Gomez, T. D. Bradley, A. R. Kennedy, Z. Livingstone, S. D. Robertson and E. Hevia, *Chem. Commun.*, 2013, **49**, 8659.

177. X. Pan, X. Yang, L. Chen, J. Wu and N. Tang, *Inorg. Chem. Commun.*, 2010, **13**, 919.

178. G. C. Forbes, A. R. Kennedy, R. E. Mulvey, R. B. Rowlings, W. Clegg, S. T. Liddle and C. C. Wilson, *Chem. Commun.*, 2000, 1759.

179. D. R. Armstrong, W. Clegg, S. H. Dale, J. Garcia-Alvarez, R. W. Harrington, E. Hevia, G. W. Honeyman, A. R. Kennedy, R. E. Mulvey and C. T. O'Hara, *Chem. Commun.*, 2008, 187.

180. T. Y. Her, C. C. Chang and L. K. Liu, *Inorg. Chem.*, 1992, **31**, 2291.

181. M.-D. Li, C.-C. Chang, Y. Wang and G.-H. Lee, *Organometallics*, 1996, **15**, 2571.

182.   R. E. Mulvey, D. R. Armstrong, B. Conway, E. Crosbie, A. R. Kennedy and S. D. Robertson, *Inorg. Chem.*, 2011, **50**, 12241.

183.   P. Alborés, L. M. Carrella, W. Clegg, P. García-Álvarez, A. R. Kennedy, J. Klett, R. E. Mulvey, E. Rentschler and L. Russo, *Angew. Chem. Int. Ed.*, 2009, **48**, 3317.

184.   L. M. Carrella, W. Clegg, D. V. Graham, L. M. Hogg, A. R. Kennedy, J. Klett, R. E. Mulvey, E. Rentschler and L. Russo, *Angew. Chem. Int. Ed.*, 2007, **46**, 4662.

185.   W. Clegg, B. Conway, P. García-Álvarez, A. R. Kennedy, R. E. Mulvey, L. Russo, J. Sassmannshausen and T. Tuttle, *Chem. Eur. J.*, 2009, **15**, 10702.

186.   K. W. Henderson, R. E. Mulvey and A. E. Dorigo, *J. Organomet. Chem.*, 1996, **518**, 139.

187.   R. Neufeld and D. Stalke, *Chem. Sci.*, 2015, **6**, 3354.

188.   D. R. Armstrong, W. Clegg, S. H. Dale, J. Garcia-Alvarez, R. W. Harrington, E. Hevia, G. W. Honeyman, A. R. Kennedy, R. E. Mulvey and C. T. O'Hara, *Chem. Commun.* , 2008, 187.

189.   K. W. Henderson, G. W. Honeyman, A. R. Kennedy, R. E. Mulvey, J. A. Parkinson and D. C. Sherrington, *Dalton Trans.*, 2003, 1365.

190.   W. Schlenk and W. Schlenk, *Ber. Dtsch. Chem. Ges.*, 1929, **62**, 920.

191.   W. Strohmeier and F. Seifert, *Chem. Ber.*, 1961, **94**, 2356.

192.   A. Torvisco, A. Y. O'Brien and K. Ruhlandt-Senge, *Coord. Chem. Rev.*, 2011, **255**, 1268.

193.   K.-C. Yang, C.-C. Chang, J.-Y. Huang, C.-C. Lin, G.-H. Lee, Y. Wang and M. Y. Chiang, *J. Organomet. Chem.*, 2002, **648**, 176.

194.   J. A. Garden, *Advances in Synthetic, Structural and Reaction Chemistry of Zinc and Zincate Complexes Containing Alkyl and/or Amido Ligands*, 2014, PhD Thesis, University of Strathclyde.

195.   P. C. Andrikopoulos, D. R. Armstrong, H. R. L. Barley, W. Clegg, S. H. Dale, E. Hevia, G. W. Honeyman, A. R. Kennedy and R. E. Mulvey, *J. Am. Chem. Soc.*, 2005, **127**, 6184.

196.   A. R. Kennedy, J. Klett, R. E. Mulvey and D. S. Wright, *Science*, 2009, **326**, 706.

197.   C. Elschenbroich and A. Salzer, *Organometallics : A Concise Introduction*, Wiley-VCH: Weinheim 2nd edn., 1992.

198.   B. L. Lucht and D. B. Collum, *Acc. Chem. Res.*, 1999, **32**, 1035.

199.   E. C. Ashby and J. T. Laemmle, *Chem. Rev.*, 1975, **75**, 521.

200.   S. E. Denmark and J. Fu, *Chem. Rev.*, 2003, **103**, 2763.

201.   M. R. Luderer, W. F. Bailey, M. R. Luderer, J. D. Fair, R. J. Dancer and M. B. Sommer, *Tetrahedron: Asymmetry*, 2009, **20**, 981.

202.   C. M. Binder and B. Singaram, *Org. Prep. Proced. Int.*, 2011, **43**, 139.

203.   L. Pu and H.-B. Yu, *Chem. Rev.*, 2001, **101**, 757.

204. D. J. Ramón and M. Yus, *Angew. Chem. Int. Ed.*, 2004, **43**, 284.

205. N. Oguni and T. Omi, *Tetrahedron Lett.*, 1984, **25**, 2823.

206. M. Kitamura, S. Suga, K. Kawai and R. Noyori, *J. Am. Chem. Soc.*, 1986, **108**, 6071.

207. P. I. Dosa and G. C. Fu, *J. Am. Chem. Soc.*, 1998, **120**, 445.

208. K. Yearick and C. Wolf, *Org. Lett.*, 2008, **10**, 3915.

209. E. Hevia, A. R. Kennedy, J. Klett, Z. Livingstone and M. D. McCall, *Dalton Trans.*, 2010, 520.

210. G. Alvaro, P. Pacioni and D. Savoia, *Chem. Eur. J.*, 1997, **3**, 726.

211. J. A. Wanklyn, *Justus Liebigs Ann. Chem.*, 1858, **107**, 125.

212. M. Uchiyama, M. Kameda, O. Mishima, N. Yokoyama, M. Koike, Y. Kondo and T. Sakamoto, *J. Am. Chem. Soc.*, 1998, **120**, 4934.

213. Y. Kondo, M. Shilai, M. Uchiyama and T. Sakamoto, *J. Am. Chem. Soc.*, 1999, **121**, 3539.

214. W. Clegg, S. H. Dale, E. Hevia, G. W. Honeyman and R. E. Mulvey, *Angew. Chem. Int. Ed.*, 2006, **45**, 2370.

215. M. Uchiyama *et al.* reported a similar X-ray structure for a TMP-Zn-ate prepared under different conditions. See: Uchiyama, M. Uchiyama, Y. Matsumoto, D. Nobuto, T. Furuyama, K. Yamaguchi and K. Morokuma, *J. Am. Chem. Soc.*, 2006, **128**, 8748.

216. S. E. Baillie, V. L. Blair, D. C. Blakemore, D. Hay, A. R. Kennedy, D. C. Pryde and E. Hevia, *Chem. Commun.*, 2012, **48**, 1985.

217. A. Hernán-Gómez, E. Herd, M. Uzelac, T. Cadenbach, A. R. Kennedy, I. Borilovic, G. Aromí and E. Hevia, *Organometallics*, 2015, **34**, 2614.

218. H. R. L. Barley, W. Clegg, S. H. Dale, E. Hevia, G. W. Honeyman, A. R. Kennedy and R. E. Mulvey, *Angew. Chem. Int. Ed.*, 2005, **44**, 6018.

219. E. Hevia, G. W. Honeyman, A. R. Kennedy and R. E. Mulvey, *J. Am. Chem. Soc.*, 2005, **127**, 13106.

220. W. Clegg, S. H. Dale, R. W. Harrington, E. Hevia, G. W. Honeyman and R. E. Mulvey, *Angew. Chem. Int. Ed.*, 2006, **45**, 2374.

221. W. Clegg, S. H. Dale, E. Hevia, L. M. Hogg, G. W. Honeyman, R. E. Mulvey and C. T. O'Hara, *Angew. Chem. Int. Ed.*, 2006, **45**, 6548.

222. D. R. Armstrong, J. Garcia-Alvarez, D. V. Graham, G. W. Honeyman, E. Hevia, A. R. Kennedy and R. E. Mulvey, *Chem. Eur. J.*, 2009, **15**, 3800.

223. J. J. Crawford, B. J. Fleming, A. R. Kennedy, J. Klett, C. T. O'Hara and S. A. Orr, *Chem. Commun.*, 2011, **47**, 3772.

224. J. A. Garden, A. R. Kennedy, R. E. Mulvey and S. D. Robertson, *Dalton Trans.*, 2011, **40**, 11945.

225. D. R. Armstrong, L. Balloch, J. J. Crawford, B. J. Fleming, L. M. Hogg, A. R. Kennedy, J. Klett, R. E. Mulvey, C. T. O'Hara, S. A. Orr and S. D. Robertson, *Chem. Commun.*, 2012, **48**, 1541.

226. E. Hevia, A. R. Kennedy and M. D. McCall, *Dalton Trans.*, 2012, **41**, 98.

227. D. R. Armstrong, S. E. Baillie, V. L. Blair, N. G. Chabloz, J. Diez, J. Garcia-Alvarez, A. R. Kennedy, S. D. Robertson and E. Hevia, *Chem. Sci.*, 2013, **4**, 4259.

228. W. Clegg, D. V. Graham, E. Herd, E. Hevia, A. R. Kennedy, M. D. McCall and L. Russo, *Inorg. Chem.*, 2009, **48**, 5320.

229. D. R. Armstrong, C. Dougan, D. V. Graham, E. Hevia and A. R. Kennedy, *Organometallics*, 2008, **27**, 6063.

230. K. Thiele, H. Görls and W. Seidel, *Z. Anorg. Allg. Chem.*, 1998, **624**, 555.

231. M. Westerhausen, B. Rademacher and W. Schwarz, *Z. Anorg. Allg. Chem.*, 1993, **619**, 675.

232. M. Westerhausen, M. Wieneke, W. Ponikwar, H. Nöth and W. Schwarz, *Organometallics*, 1998, **17**, 1438.

233. W. Clegg, E. Crosbie, S. H. Dale-Black, E. Hevia, G. W. Honeyman, A. R. Kennedy, R. E. Mulvey, D. L. Ramsay and S. D. Robertson, *Organometallics*, 2015, **34**, 2580.

234. A. H. Stoll, P. Mayer and P. Knochel, *Organometallics*, 2007, **26**, 6694.

235. E. Weiss and G. Hencken, *J. Organomet. Chem.*, 1970, **21**, 265.

236. D. R. Armstrong, J. A. Garden, A. R. Kennedy, S. M. Leenhouts, R. E. Mulvey, P. O'Keefe, C. T. O'Hara and A. Steven, *Chem. Eur. J.*, 2013, **19**, 13492.

237. Pure $^{t}Bu_2Zn$ is isolated as a white solid and, due to its high volatility, it is stored in hexane solution at -35°C. Prior to the solubilisation, a sample or 0.1 mmol is inserted in a NMR tube inside the glove box.

238. D. R. Armstrong, K. W. Henderson, A. R. Kennedy, W. J. Kerr, F. S. Mair, J. H. Moir, P. H. Moran and R. Snaith, *J. Chem. Soc., Dalton Trans.*, 1999, 4063.

239. K. Kobayashi, M. Ueno, H. Naka and Y. Kondo, *Chem. Commun.*, 2008, 3780.

240. D. Mootz, *Angew. Chem. Int. Ed.*, 1969, **8**, 378.

241. M. F. Lappert, M. J. Slade, A. Singh, J. L. Atwood, R. D. Rogers and R. Shakir, *J. Am. Chem. Soc.*, 1983, **105**, 302.

242. E. Hevia, A. R. Kennedy, R. E. Mulvey, D. L. Ramsay and S. D. Robertson, *Chem. Eur. J.*, 2013, **19**, 14069.

243. N. D. R. Barnett, R. E. Mulvey, W. Clegg and P. A. O'Neil, *J. Am. Chem. Soc.*, 1991, **113**, 8187.

244. G. Hilmersson, J. e. R. Granander, Z. Rappoport and I. Marek, *The Chemistry of Organolithium Compounds*, John Wiley & Sons Ltd: , Chichester, 2006.

245. A. J. Edwards, S. Hockey, F. S. Mair, P. R. Raithby, R. Snaith and N. S. Simpkins, *J. Org. Chem.*, 1993, **58**, 6942.

246. P. C. Andrews, P. J. Duggan, M. Maguire and P. J. Nichols, *Chem. Commun.*, 2001, 53.

247. P. C. Andrews, V. L. Blair, E. C. Border, A. C. Peatt, J. G. MacLellan and C. D. Thompson, *Organometallics*, 2013, **32**, 7509.

248. M. Blangetti, G. Croce, A. Deagostino, E. Mussano, C. Prandi and P. Venturello, *J. Org. Chem.*, 2011, **76**, 1814.

249. M. Blangetti, A. Deagostino, C. Prandi, S. Tabasso and P. Venturello, *Org. Lett.*, 2009, **11**, 3914.

250. L. Lochmann and D. Lím, *J. Organomet. Chem.*, 1971, **28**, 153.

251. M. Schlosser, *J.Organomet. Chem.*, 1967, **8**, 9.

252. D. Seyferth, *Organometallics*, 2009, **28**, 2.

253. C. Unkelbach, D. F. O'Shea and C. Strohmann, *Angew. Chem. Int. Ed.*, 2014, **53**, 553.

254. P. Fleming and D. F. O'Shea, *J. Am. Chem. Soc.*, 2011, **133**, 1698.

255. R. E. Mulvey and S. D. Robertson, *Angew. Chem. Int. Ed.*, 2013, **52**, 11470.

256. P. G. Williard and M. A. Nichols, *J. Am. Chem. Soc.*, 1991, **113**, 9671.

257. D. R. Armstrong, A. R. Kennedy, R. E. Mulvey and S. D. Robertson, *Chem. Eur. J.*, 2011, **17**, 8820.

258. D. R. Armstrong, A. R. Kennedy, R. E. Mulvey and S. D. Robertson, *Dalton Trans.*, 2013, **42**, 3704.

259. A. Johansson and Ö. Davidsson, *Chem. Eur. J.*, 2001, **7**, 3461.

260. R. Sott, J. Granander, C. Williamson and G. Hilmersson, *Chem. Eur. J.*, 2005, **11**, 4785.

261. S. Sung, D. C. Braddock, A. Armstrong, C. Brennan, D. Sale, A. J. P. White and R. P. Davies, *Chem. Eur. J.*, 2015, **21**, 7179.

262. R. E. Mulvey, *Dalton Trans.*, 2013, **42**, 6676.

263. X.-H. Lu, M.-T. Ma, Y.-M. Yao, Y. Zhang and Q. Shen, *Inorg. Chem. Commun.*, 2010, **13**, 1566.

264. A. R. Kennedy, R. E. Mulvey, B. A. Roberts, R. B. Rowlings and C. L. Raston, *Chem. Commun.*, 1999, 353.

265. N. D. R. Barnett, R. E. Mulvey, W. Clegg and P. A. O'Neil, *Polyhedron*, 1992, **11**, 2809.

266. D. R. Baker, R. E. Mulvey, W. Clegg and P. A. O'Neil, *J. Am. Chem. Soc.*, 1993, **115**, 6472.

267. W. Clegg, K. W. Henderson, L. Horsburgh, F. M. Mackenzie and R. E. Mulvey, *Chem. Eur. J.*, 1998, **4**, 53.

268. B. J. Fleming, P. García-Álvarez, E. Keating, A. R. Kennedy and C. T. O'Hara, *Inorg. Chim. Acta*, 2012, **384**, 154.

269. J. J. Morris, B. C. Noll and K. W. Henderson, *Acta Cryst., E*, 2007, **63**, m2477.

270. D. F. Shriver and M. A. Derezdon, *The Manipulation of Air-Sensitive Compounds*, Wiley and Sons, New York, 2nd ed. edn., 1986.

271. H.-S. Lin and L. A. Paquettea, *Synth. Commun.*, 1994, **24**, 2503.

272. A. Krasovskiy and P. Knochel, *Synthesis*, 2006, 890.

273. C. Schade, W. Bauer and P. Von Ragué Schleyer, *J. Organomet. Chem.*, 1985, **295**, c25.

274. C. Strohmann and V. H. Gessner, *Angew. Chem. Int. Ed.*, 2007, **46**, 8281.

275. J. F. Larrow, E. N. Jacobsen, Y. Gao, Y. Hong, X. Nie and C. M. Zepp, *J. Org. Chem.*, 1994, **59**, 1939.

276. N. Cabello, J.-C. Kizirian, S. Gille, A. Alexakis, G. Bernardinelli, L. Pinchard and J.-C. Caille, *Eur. J. Org. Chem.*, 2005, **2005**, 4835.

277. R. A. Andersen, G. Wilkinson, M. F. Lappert and R. Pearce, in *Inorganic Syntheses*, John Wiley & Sons, Inc., 2007, pp. 262.

278. R. E. Mulvey and J. A. Garden, in *Encyclopedia of Reagents for Organic Synthesis*, John Wiley & Sons, Ltd, 2001.